DESIGN AND REALISATION OF 3D COLLAGEN GEL MODELS FOR THE STUDY OF CONNECTIVE TISSUE REMODELLING AND INTEGRATION IN VITRO

MASSIMO MARENZANA

THESIS SUBMITTED FOR THE DEGREE OF DOCTOR OF PHILOSOPHY, 2003

UNIVERSITY COLLEGE LONDON.
TISSUE REPAIR AND ENGINEERING CENTRE,
INSTITUTE OF ORTHOPAEDICS,
ROYAL NATIONAL ORTHOPAEDICS HOSPITAL,
BROCKLEY HILL, STANMORE,
MIDDLESEX HA7 4LP

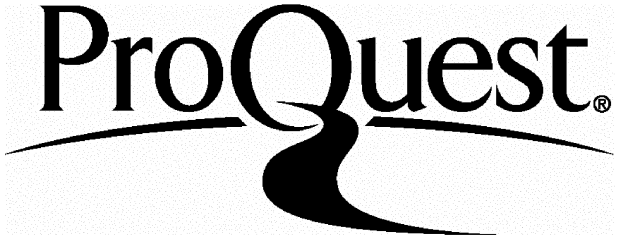

Acknowledgments

I am really grateful to Robert Brown for his great lessons about science and lab work and, principally, for being a friend besides a careful supervisor. Thanks to all the people at the TREC with special mention to Vivek Mudera and Rebecca Porter who first introduced me to the lab world. I would like to mention also Umber, Oksana, and Dimitris for their helpful collaboration. A special thanks to James Phillips for his suggestions and for a lot of proof reading.
Thanks to Padmini Sarathchandra and Mike Kaiser for their precious help in the ultrastructural study.
I also want to thank all the people from other labs who contributed to this work through collaborations. In particular Sandy McRobert and David Pickard in light spectroscopy, Steve Huges, Ying Yang and Alicia El Hay in the development of interface templates and Jan-Herman Kuiper, Danny Kelly and Patrick Prendergast in FE modelling.

An acknowledgment for their help with the graphic of this work goes to the architect-friends Simone Cordara and Enrico Galliani.

I will be forever grateful to my wife Margherita for following me in this adventure and to her parents for hosting me in the completion period and allowing me to work at their place as if I was their son.
Obviously I have to thank my parents for all the opportunity they have given me and for their always ready support.

This study has been supported by the Fifth Framework Programme of the European Commission, "Biomechanichal Interactions in Tisssue Engineering and Surgical Repair (BITES)".

Abstract

Cell spatial remodelling in tensile connective tissue is at the base of fundamental biological processes including tissue morphology, growth adaptation and repair. It is increasingly clear that cell-force generation plays a central role in the remodelling process, however the understanding of how cell generated forces lead to stable 3-dimensional collagenous structures formation is poorly understood.

In order to investigate two different processes occurring during cellular connective tissue remodelling, two models were developed using 3D fibroblast populated collagen lattices (FPCLs):

1) The process of stable structural remodelling of the matrix, was investigated in uniaxially tethered gels in the tensioning Culture Force Monitor (tCFM). The tension retained in the matrix after blocking cell force, by cytoskeletal disrupting agent cytochalasin D, was a measure of the degree of stable structural remodelling.
2) The processes of adhesion formation and integration between interfaces was investigated using an interface model made of a cell-free and a cell-seeded collagen lattice. The mechanical adhesion strength was measured to quantify the cellular remodelling process.

Results showed that the residual matrix tension (RMT) retained in the collagen matrix, after cytochalasin D treatment, increases with culture time. Treatment with TGF-β1 and external cyclical loading seemed to increase RMT by different mechanisms. TGF-β1 by upregulating cell force generation, hence contraction; cyclical loading by increasing the alignment of collagen fibrils, hence accelerating the remodelling process.

Adhesion strength in the interface model increased with culture time and was correlated with cellular migration across the interface zone. The distribution of failure stresses in the interface construct was determined by a computer model

using Finite Element method.

Results are discussed in terms of a mechanism of cell-matrix interaction in collagen lattices. This suggests that cell-matrix interactions are modulated by a constant iterative feed back relation between cell force generation and mechanical properties of the matrix both at microscopic (i.e. fibril packing and alignment) and macroscopic level (i.e. contraction force generation and uniform alignment of cells and matrix throughout the lattices). A computer model using Finite Element (FE) analysis, was developed in order to simulate the process of cell-matrix interaction, following the iterative concept to model the remodelling process. The results suggested a possible mechanism by which randomly orientated tractional forces in the matrix lead to highly aligned structures.

Identifying the mechanisms which regulate the cell-matrix spatial remodelling process can provide strategies to tackle important pathologies such as tissue contractures and tissue adhesions or poor-integration.

The final part of this study presents the development of an optical method, based on elastic scattering spectroscopy (ESS) with the potential of minimally invasive monitoring of tissue formation. Changes in ESS spectra obtained from fibroblast-populated lattices were correlated to cellular remodelling (i.e. contraction) measured as lattice compaction or development of tension. Additionally distinct spectra were obtained for different areas of the interface constructs, indicating the ability of the ESS method to discriminate different structure within the same construct.

This study has presented an interdisciplinary model platform which can be useful for the development of a new generation of complex bioreactors in which tissue formation can be analysed under different simultaneous parameters (e.g. biochemical, mechanical and structural).

Contents

List of Figures

Chapter 1

Chapter 2

Chapter 3

Chapter 4

Chapter 5

Chapter 6

List of Tables

Chapter 4

Chapter 1
Introduction

1.1 Regulation of connective tissue remodelling

Regulation of connective tissue remodelling is a fundamental biological process which determines the continuous adaptation of the body structures to the continuous changes in physical and biochemical environment. Tissue remodelling processes are present during tissue growth, repair, and adaptation to mechanical conditions or changes in body shape (Cowin, 2000). The knowledge and understanding of the mechanisms involved in the regulation of connective tissue remodelling is not complete, especially concerning the contribution of mechanical forces.

Importantly, when the complex regulation mechanisms in tissue remodelling are altered, serious pathologies are known to arise, including burn-scar contracture (Lorenz et al., 2000), breast implant failure due to capsule contracture (Gruber & Jones, 1981), peritoneal adhesion strictures (Liakakos et al., 2001; Sulaiman et al., 2002), Dupuytren's disease (McFarlane, 2002), degenerative arthritis (Edwards, 2000; Pap et al., 2000), age-related skeletal pathologies (Theodorou et al., 2003), and fibrosis disorders of kidney, liver and lung (Boukhalfa et al., 1996; Cohen, 1995; Desmouliere & Gabbiani, 1995; Tuchweber et al., 1999; Yamamoto et al., 1994).

The purpose of the current study was to understand how cellular processes remodel matrix by altering its structural and mechanical

properties. The study was focused on the simplest tissue model in vitro, i.e. fibroblast-populated collagen lattices (FPCLs). The cell-base remodelling of collagen lattices includes a combination of collagen self-assembly processes coordinated by cellular control processes, involving tractional force generation, collagen deposition and degradation.

Although it is well known that the mechanisms of spatial control and material aggregation, termed "3D-remodelling" of an existing fibrillar collagen matrix are the very base of these reorganising processes, they are surprisingly poorly understood. It is difficult to overstate the importance of these processes in normal and pathological soft tissue function. Identification of the mechanism of this spatial reorganisation would represent a major advance in understanding the dynamic mechanical function of tissue and potentially their most intractable pathologies and age-related changes. In addition, it would provide a fundamental input to tissue engineering technologies that are intrinsically based on the control of tissue formation and regeneration processes (Brown, 2002). Relevant aspects of the tissue remodelling process, with particular attention on the effect of mechanical factors, are reviewed in the following sections.

1.1.1 Mechanical tension in connective tissue remodelling processes

Evolution has produced a functional optimisation of our load-bearing tissues in a way which escapes from any definition in conventional mechanics and engineering. Our tissue architecture has evolved under constraints of mechanical functionality and energetic efficiency. This functional structure is partly achieved through a predefined design (held in the genetic memory), partly through continuous adaptation to mechanical inputs. Adaptive design is achieved by interstitial apposition (or removal) of

building material such as collagen (Jeronimidis, 2000a). Mechanical tension is always present to some degree in soft connective tissues, even at rest. In normal healthy conditions, soft connective tissues do not sag, even around relaxed or reduced musculature. The fact that the length of dissected tissues such as blood vessels, nerves, tendons is 25-30% less than their in situ length demonstrates that there is a resting tension that is built in their anatomy. Ligaments are a clear example of maintained tensional connectivity during changes in body shape due to bone growth in childhood or bone resorption with ageing. Skin tension is maintained relatively constant throughout normal mechanically driven processes such as pregnancy, obesity/slimming cycles, wound contraction etc. Function dictates the organisation of the internal collagenous fibres: long rope-like wound fibres in tendons and ligaments hold high tensional stresses while a wickerwork of interlaced fibre bundles hold both tensions and compressive load redistributing it as tension along many tensile components (the fibres, Cowin, 2000).

To date it is not known how cells spatially organise the collagen fibres in different architecture and how they maintain this structural organisation in a permanent tensional homeostasis.

In normal adult connective tissue, cells are shielded from much of the mechanical loading by their surrounding matrix architecture. This implies, in engineering terms, that there are components (e.g. fibre bundles) that due to their geometry and mechanical properties will take most of the load with respect to other components (e.g. cells and compliant proteins in the matrix). A similarity in the field of construction is given by the system man-crane: the crane takes all the stresses and strains due to the external loading while the man conducting it is almost completely shielded from strains.

The close interdependence of matrix remodelling and mechanical stress-shielding is well recognised in bone biology (Wolff, 1870), but its importance in soft tissue has only recently become appreciated. For instance, it is very poorly understood what are the tissue assembly

mechanisms that lead from the basic cell-fibre interaction to the higher structural level in the complex, hierarchical, highly specialised organisation of the different tissues. These concepts apply to formation, growth, adaptation and repair of living tissues.

Another interesting aspect of connective tissue architecture is represented by the subdivision of the load bearing area of tension elements into many sub-elements. An example of this is given by the osteo-tendon/ligament complex. This structure is mechanically very efficient in terms of multiple load patterns, redundancy and hence resistance to crack propagation. Additionally osteo-tendon/ligament junctions are composed of a mixed fibro-cartilage tissue and a gradual continuum transition between tissues, rather than a net change, is present (Woo & Buchwalter, 1988). The virtual absence of connecting structures in favour of a continuum transition represents an additional optimisation in terms of tensile efficiency. In engineering terms, it can be demonstrated that the tensile efficiency of fibrous mechanical structures increases as the weight of fibre terminator decreases, i.e. terminators are increased in number and decreased in size (Jeronimidis, 2000b). How material is deposited and spatially organised during growth (let alone reformed in repair) at these interface sites is not known.

Also little is known about the initiation of the mechanical link between heterogeneous tissues during their formation. Tendon embryogenesis supplies limited indications about the initial assembly of these interfaces. Early stage mesenchymal non-specialised cells migrate into "patches" set in a loose matrix during limb development (Schmidt-Nielsen, 1983). The signal for such cellular packing or condensation of cells is unknown. The forming tissue seems to convert itself into the one-dimensional structure, a tendon precursor, but its formation occurs simultaneously with embryonic bone and muscle. It has been speculated that fibroblasts, aligned by tractional forces, lay down bundles of aligned collagen fibrils that associate to form fine tendons (Cowin, 2000; Eastwood et al., 1998a; Harris et al., 1981).

1.1.2 Connective tissue pathologies related to unbalanced regulation of mechanical tissue tension

Tissue mechanical tension is an essential regulator of tissue functions such as lung alveoli, kidney capsule, granulation tissue contraction and uterine involution (Tomasek et al., 2002).

A number of examples can be found in tissue growth and morphogenesis, in which the regulatory effect of mechanical tension plays a fundamental role. Childhood growth could be regulated by 'threshold external tension' deriving from expanding bone growth plate (Rodriguez et al., 1994). Osseous deficiencies have been improved clinically by application of regulated tension through distraction osteogenesis techniques (Gonzalez et al., 2001).

Epithelial morphogenesis has been explained by a tension-driven remodelling process in which cell proliferation and matrix tension (e.g. the thickness of basal lamina) are tightly linked in a homeostatic regulatory feedback loop (Huang & Ingber, 1999). Failure in this delicate balance may lead to a selection of anchorage independent (hence tension independent) cells with malignant features (Huang & Ingber, 1999).

Burn/scar contractures (Lorenz et al., 2000), breast implant failure due to capsule contracture (Gruber & Jones, 1981), peritoneal adhesion strictures (Liakakos et al., 2001; Sulaiman et al., 2002) and Dupuytren's disease (McFarlane, 2002) are known to develop abnormal tension in connective tissue. These abnormal mechanical conditions cause in turn pathologies connected with reduced mobility and function. The importance of mechano-regulation of connective tissue can become evident when the mechanical dynamic balance is altered or compromised and pathologies develop such as degenerative arthritis (Edwards, 2000; Pap et al., 2000), age-related skeletal pathologies (Theodorou et al., 2003), and fibrosis disorders in kidney, liver and lung (Boukhalfa et al., 1996; Cohen, 1995; Desmouliere & Gabbiani, 1995; Mutsaers et al., 1997; Tuchweber et al., 1999; Yamamoto et al., 1994).

1.1.3 Mechanisms of collagen self-assembly involved in tissue morphogenesis and remodelling processes

The mechanisms of collagen self-assembly play an important role in the understanding of how a tissue is built and maintained (Cowin, 2000). Collagenous fibrous structures are hierarchical structures that stem from the basic structural element constituted by the collagen molecule. One of the best examples of hierarchical structure is the tendon, which has been arbitrarily divided into six distinct levels (Kastelic & Baer, 1980). Tendonous tissues also contain the highest collagen content. The *collagen molecule* can be regarded as the lowest level of the hierarchy (Figure 1-1). It is a right-handed superhelix composed of three (polypeptide) α chains of about 1000 amino acid residues each (α chains are left handed helices (Woodhead-Galloway, 1980). The intra- and interchain bonding (non covalent, e.g. hydrogen bonds, electrostatic and hydrophobic), between specific groups of aminoacids on the chains is essential to the stability of the molecule. The "coil-coiled" structure of the molecule confers high tensile strength (Alberts et al., 2002).

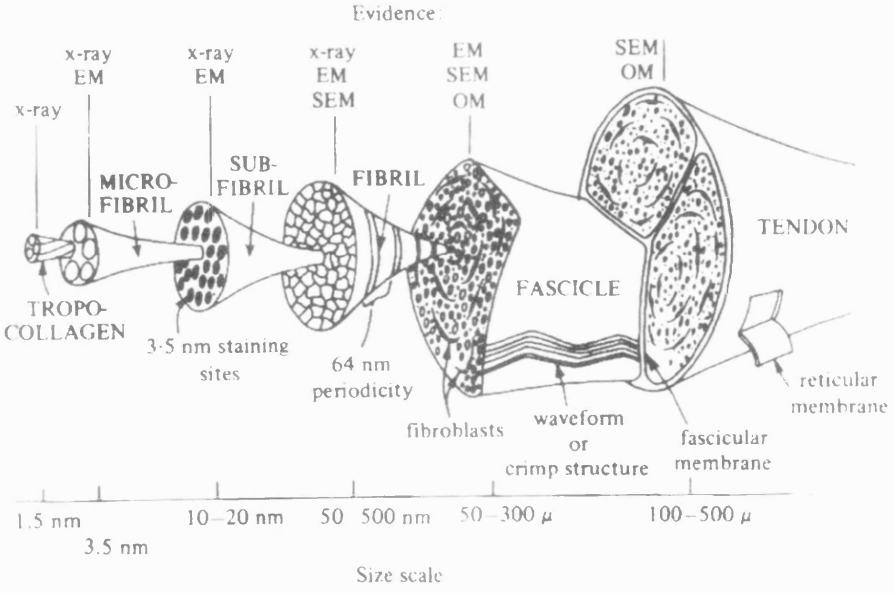

Figure 1-1 Hierarchical structure of a tendon (modified from (Kastelic & Baer, 1980)

Microfibrils are the minimum theoretical level of fibril packing, composed of 5 molecules wound together into a left-handed super-superhelix by electrostatic forces (Woodhead-Galloway, 1980). The microfibril is held together by many hydrophobic interactions and has low mechanical strength. The strength and stability during maturation of the microfibrils are achieved by the development of inter-molecular cross-links. Microfibrils are wound together to form superhelix fibrils. *Fibril* diameters varies widely: in rat tail tendon ranges from 40 to 300 nm. The strength of the fibrils structure is due, in part to a combination of non covalent bonding and covalent crosslinks that form between collagen molecules. However, the detailed patterning of these bonding between hierarchical levels is not well understood. The next hierarchical level in tendon structure is the fascicle, which is composed of bundle of fibrils. Interestingly subunits in tendon and ligaments are organised with no lateral coupling between fascicles. Fascicles can freely slide past each other to impart very specific mechanical properties. Another feature of this hierarchical level (Figure 1-1) is the presence of characteristic crimp patterns in the collagen structure at the level of fibres and fibre bundles. This has been observed only in connective tissue subjected to tensile load (e.g. skin, tendon, ligaments) but not to compressive load (e.g. bone). This pattern allows for limited extension of whole tendon structure at low strains without actual extension of collagen fibrils, which are almost inextensible (Hansen et al., 2002; Silver et al., 1992).

Supramolecular assembly is much less well-understood than molecular self assembly; however the assumption is that it is equivalent to self assembly but at a higher structural level. The role of cells, through cell traction and contraction on the process of higher order assembly is, so far, poorly acknowledged (Eastwood et al., 1998a; Grinnell et al., 1989; Tomasek et al., 2002).

It has been shown (Martin et al., 2000) that, in physiological buffer conditions, the disposition of procollagen molecules can develop long-range liquid crystalline ordering between nematic ordering (i.e. liquid crystals

containing all rod-like molecules lying parallel to one another in layers of equal thickness) and pre-cholesteric ordering (i.e. a liquid crystal containing rod-like molecules lying parallel to one another in each plane but each plane is rotated by a constant angle from the next plane of crystal). This suggests that supra-fibrillar tissue architecture may be determined by the ability of soluble precursor molecules to form liquid crystalline arrays, prior to fibril assembly.

These similarities of collagen solutions to liquid crystals, even at physiological pH, have been exploited to induce fibril alignment in reconstructed collagen matrices by a strong magnetic fields. This technique proved to be effective in aligning cells in the collagen matrix by contact guidance along the magnetically pre-aligned fibrils, demonstrating the importance of collagen fibrillar structures in substrate contact guidance mechanisms during cell-matrix interaction (Guido & Tranquillo, 1993).

Studies on collagen self-assembly in reconstituted collagen lattices (Christiansen et al., 2000) have shown that fibril diameter increased as pH increased (from 5.0 to 8.0) or with addition of glycine. Linear assembly, instead, was promoted by lysine-derived aldehydes (which also showed to increase mechanical stabilisation). Interestingly, the architecture of self-assembly (i.e. lateral or longitudinal) has been correlated with the mechanical properties. Lateral aggregation was shown to influence mechanical properties at small strains but did not correlate to ultimate tensile strength and elastic modulus at high strains (Christiansen et al., 2000). Conversely longitudinal fibril aggregation leads to fibril elongation, which confer higher ultimate mechanical properties at high strains (Christiansen et al., 2000). However, even if some promoting factors have been identified, the mechanisms inducing either lateral or longitudinal aggregation have not been fully unravelled, let alone how this can operate in three-dimensional tissue spatial organisation.

1.1.4 Cellular-based remodelling of fibrillar collagen matrices

The models of collagen molecular/supramolecular self-assembly are unable to account for the local cellular-based remodelling. This consists mainly of the distortion, compression and translocation of fibrils (Roy et al., 1997; Tamariz & Grinnell, 2002) and material apposition or removal (through deposition of new collagen or metalloproteinases for degrading existing structures (Tomasek et al., 2002). On the basis of their investigations using chick tendon, Trelstad and Hayashi (1979) proposed a model to explain the interplay of cell activity and molecular self-assembly during remodelling. The model postulates that cells produce relatively short fibrils of type I collagen within cytoplasmic invaginations that form in the tendon fibroblast membrane. These membranes confine the early fibril aggregates into parallel, orientated structures and allow the fibrils to add to existing bundles, which are themselves held in grooves in the surface of the fibroblasts. The supposition here is that tendon fibroblasts release tropocollagen molecules which are added onto these growing fibrils. In tendon formation and remodelling, such a mechanism would provide means for the cell to control the length and orientation of the fibril bundles as they form.

Neither this model, nor the self assembly theory (section 1.1.3), can account for the development and the effect of tensional forces (Brown et al., 1998; Guidry & Grinnell, 1985; Huang & Ingber, 1999; Silver et al., 2003; Tomasek et al., 2002; Wakatsuki & Elson, 2003). Consolidation of the reorganised collagenous fibrillar network has been shown to depend on contraction through cell force generation on local fibrils. Increased fibril proximity, due to cell traction on the fibrillar network, permits formation of weak non-covalent bonds (e.g. electrostatic, hydrophobic and hydrogen bonds). The higher the number of these non-covalent bonds the higher the stability of the remodelled collagenous fibrillar network (Guidry & Grinnell, 1985). With time collagen-collagen covalent binding interactions develop

increasing the mechanical strength (Huang et al., 1993).

However, how these events can be correlated with the compressive/tensile stresses generated during local cell-matrix interactions is not understood. It is a possibility that the processes of self-assembly (and elongation) of fibres and cell-mediated spatial reorganisation (and coordinated matrix deposition) occur as an orchestrated series of interconnected mechanisms (Tomasek et al., 2002).

The complexity of the spatial/mechanical dimension of connective tissue remodelling is not widely appreciated, perhaps because a clear paradigm for its operation in non-biological systems has not yet been provided. Some similarities can be found in self-repairing smart materials such as cementitious matrices hardened by the release, from interstitial hollow fibres, of liquid phase reparative chemical agents which act as adhesives. Hollow fibres release the reparative chemical agents in response to loading (Dry, 1994). In these smart materials, although the repair response is mechanically activated as for living tissues, there is only one possible cycle for any stimulated area and material can only be added (not removed) in the repair process. Furthermore mechanical interstitial repair is only one of the many events involved in cell-based remodelling.

In all healthy cases of biological remodelling (i.e. growth, expansion and resorption), functioning, load-bearing collagen matrices are spatially expanded/shortened by interstitial addition/removal (respectively) of collagen by resident fibroblasts. It is important to note that tissues grow and reconstruct themselves without ceasing to perform their structural function, e.g. carrying tensile load (Cowin, 2000). However, the process must involve some form of local mechanical unloading (prior to reorganisation), through physical disconnection or uncoupling of the existing collagen fibril structure, prior addition/removal of collagen matrix. In the final stage of the remodelling process, the altered matrix architecture must be reconsolidated, ahead of reapplication of mechanical load (Brown & Byers, 1989). These iterating phases at the cellular level would explain how matrices can change in gross size and shape whilst remaining functionally load bearing, and

retaining the majority of the collagen (Brown & Byers, 1989; Cowin, 2000; Huang & Ingber, 1999; Tomasek et al., 2002).

The architecture of a forming tissue existing at a given time and its mechanical parameters are a unique product of cellular action and matrix properties under specific local constraints. Experimentally, the measurement of spatial remodelling cannot be separated from the force generated by the cells and the external mechanical environment in which the reorganisation is carried out. In other words, in order to understand mechanical factors affecting spatial remodelling, measurement of mechanical properties has to be performed in situ, during tissue formation, minimising changes in the measured structure. This is different from measuring mechanical parameters such as elastic modulus and ultimate strength which involves application of ramps of strain that will alter the structure - especially in the case of newly formed tissues with marked viscoelastic properties (Wakatsuki & Elson, 2003). These mechanical tests cannot normally be performed in situ nor can they be used to follow the dynamic responses. Therefore a system that is able to monitor the dynamic of the forces which govern matrix remodelling would seem to be the best candidate for investigation of remodelling mechanisms.

These are difficult concepts to express in engineering terms because there are no equivalents in the field outside biology. One possible analogy might be seen in the history of the London Millenium Bridge (built in 2000). Its material properties, such as ultimate strength and stiffness modulus, had been carefully evaluated by experts. However it was only after completion that a major unpredictable fault became apparent. A generation of oscillating deformation waves along its structure, caused by the resonance of rhythmic steps of people walking over it (Arup Corporate, 2003). The bridge became unsafe and was closed for strengthening. Bridge engineering is an established branch of civil engineering and before a bridge is built every detail is known in advance and possible fault can be predicted. A similar material resonance phenomenon was famously filmed more than 60 years ago on the Tacoma Bridge in Puget Sound, Washington (Halliday &

Resnick, 1978). In effect, small dynamic forces distorted the structure to destruction.

These examples provide an intuitive parallel of the difficulty of evaluating properties and evolution of a mechanical system, operating outside its "building site", within an environment not fully understood from properties alone.

1.1.5 Fibroblast populated collagen lattice as a model for cell-matrix remodelling

At present, three-dimensional hydrated collagen lattices, containing dispersed fibroblasts, provide a potent model for examining in vitro reciprocal mechanical interactions that occur between the cells and the extracellular matrix (Brown, 2002; Grinnell, 2003; Tomasek et al., 2002). Additionally the collagen matrix remodelling process has been implicated in the matrix morphogenesis which is seen during development growth and tissue repair (Brown, 2002; Grinnell & Ho, 2002; Stopak et al., 1985; Tomasek et al., 2002).

30 years ago Elsdale and Bard described the incorporating of fibroblasts into collagen matrices and reported unique features of motility and growth within a 3D environment not detected in 2D environment (Elsdale & Bard, 1972). One of these features, the ability of the cells to reorganise the collagen matrix into a dense, opaque body (a tenth of its original size) formed the basis for the fibroblast populated collagen lattice (FPCL) model of wound contraction (Hielscher et al., 1997) and contributed to the development of a number of tissue engineering applications and the generation of tissue equivalents (Bell et al., 1979), e.g Apligraf™ (Eaglestein & Falanga, 1998), Dermagraf, etc.

The FPCL contraction model is analogous to the in vivo situation in which cell adhesion occurs three-dimensionally to attachment sites made up

of protein fibrils rather than two-dimensionally along a protein-coated interface.

Immediately after polymerisation, the collagen matrix is highly pliable and cells remodel the matrix as they begin to attach and spread (Eastwood et al., 1996; Grinnell & Lamke, 1984; Tamariz & Grinnell, 2002). Adhesion interactions between binding sites distributed along the cell membrane and fibrils located in proximity of cell edges generates the initial local deformations in the fibrillar network (Roy et al., 1997; Tamariz & Grinnell, 2002). In the subsequent phases, cell spreading and migration, caused by coordinated extension and retraction of cell filipodia, cause larger fibrils translocation (Sawhney & Howard, 2002; Tamariz & Grinnell, 2002). Accumulation of local deformation in the collagenous fibrillar network leads to gradual change of the properties of the network with increase in fibril packing around cellular edges. As fibrillar network deformation and packing increase, the overall mechanical properties of the matrix change. In untethered lattices this process generates a great compaction and compression of fibrils that result in a dense stiffer matrix (large reduction of volume) (Bell et al., 1979; Grinnell & Lamke, 1984). In tethered lattices less compaction occurs but stresses are accumulated in the fibrillar network, producing a reaction force at the global level (as opposed to local ultrastructural level). This causes the tensioned fibrillar network to increase its resistance to cellular traction (through a tension-stiffening mechanism typical of fibre composites). This resistance is perceived by the cell as an increase in stiffness. Net cell migration has been suggested to occur when the fibrillar network becomes sufficiently stiff to resist to cellular traction (Knapp et al., 1999; Roy et al., 1999b; Sawhney & Howard, 2002; Tamariz & Grinnell, 2002).

As global remodelling of the collagen lattices progresses (i.e. reaction forces develops or volume decreases substantially), fibroblasts undergo morphological changes from dendritic (Grinnell et al., 2003) to stellate/bipolar (Eastwood et al., 1996; Porter et al., 1998; Tamariz & Grinnell, 2002; Wakatsuki & Elson, 2003), and cell-matrix interactions

mature from punctate to focal adhesion organization (Tamariz & Grinnell, 2002).

The mechanical configuration (untethered versus tethered) of the matrix has profound phenotypic consequences (i.e. cellular shape and differentiation). Only in tethered cultures, fibroblasts develop prominent actin stress fibres and focal adhesions (Brown et al., 2002; Grinnell, 2000; Grinnell et al., 1999; Tomasek et al., 1992) and can organise a fibronectin matrix (Halliday & Tomasek, 1995; Mochitate et al., 1991). When the tension is released, by untethering the matrix, cells become quiescent within 24 hours and a subpopulation of cells enters apoptosis (Fluck et al., 1998; Grinnell et al., 1999).

Also the response to growth factors appears to be modulated by the mechanical tension that is present in the matrix (Arora et al., 1999; Brown et al., 2002; Grinnell, 2000; Grinnell & Ho, 2002; Shreiber et al., 2001; Tamariz & Grinnell, 2002).

Lysophosphatidic acid (LPA) and platelet derived growth factor (PDGF) have been shown to promote contraction in untethered FPCLs (Clark et al., 1989; Grinnell et al., 1999; Gullberg et al., 1990; Parizi et al., 2000) but only LPA promotes contraction in tethered FPCLs while PDGF inhibits it (Grinnell et al., 1999; Kolodney & Elson, 1993; Shreiber et al., 2001). The differential stimulation of these two growth factors has been suggested to be modulated by the mechanical configuration of FPCLs through different mechano-transduction pathways (Grinnell, 2000). Under this hypothesis, untethered matrix contraction depends on signalling pathways that are important for cell motility (i.e. formation of new extensions), whereas untethered matrix contraction depends on signalling mechanism that are important for cell contractility (i.e. retraction of cell extensions).

Transforming growth factor in the β1 isomeric form (TGF-β1) is the predominant isoform of TGF in adult wounds (85%) (Clark, 1996; Kupper & Ferguson, 1993). It is predominantly synthesised and secreted by platelets

and macrophages (Martin, 1997; Mutsaers et al., 1997) and is a potent mitogen for fibroblasts, increasing their migration, proliferation, extracellular matrix synthesis and remodelling ability. TGF-β1 is one of the several cytokines capable of stimulating the phenotypic transformation of fibroblasts into contractile myofibroblasts (Desmouliere et al., 1993; Jester et al., 1996; Masur et al., 1996). Myofibroblasts have been first identified as a phenotypic modulation of fibroblasts in in vivo wound healing studies (Gabbiani et al., 1971). These cells are characterised by expression of alpha-smooth muscle actin (α-SMA), presence of adhesion fibronexus (equivalent to focal adhesions in vitro) and deposition of extracellular fibronectin. α-SMA has been suggested to be correlated to the increased contractility of myofibroblasts (Hinz et al., 2001). Importantly, it has been shown that TGF-β1 activation of fibroblasts to differentiate into myofibroblasts occurred when cells were in tethered but not in untethered collagen lattices (Arora et al., 1999; Vaughan et al., 2000). The contractile response of TGF-β1 treated fibroblasts has been analysed in untethered and tethered collagen matrices (Grinnell & Ho, 2002). TGF-β1 was shown to have an agonist effect on untethered but not on tethered matrix contraction. On the other hand fibroblasts pre-activated by 5 days in culture in presence of TGF-β1, before the contraction test, contracted similarly tethered or untethered matrices. A recent study (Brown et al., 2002) appears to be in contrast with that of Grinnell et al. (2002), reporting an agonist effect of TGF-β1 treatment on fibroblast contraction in uniaxially tethered gel. This apparent contradiction might be explained by the different doses of agonist TGF-β1 and the different contraction assays which were used in the two studies.

Interestingly, Brown et al. (2002) suggested that, due to the speed of onset of reaction (i.e. force generation by cells) to TGF-β1 and TGF-β3, they might be considered as mechanoregulators of the way in which fibroblasts receive cytomechanical stimuli from the matrix. This modulation would trigger a cascade of cellular secondary downstream responses. This perspective is completely new and distinct from the current view in which

TGF-β1 has a whole range of individual activities (stimulating collagen (Reed et al., 1994; Roberts et al., 1986), proteoglycans and fibronectin production (Borsi et al., 1990), reducing matrix protease expression etc.), which incidentally lead to altered matrix properties.

The identification of specialised contractile fibroblasts (i.e. the myofibroblast) gave rise to a debate concerning the origin of cell-mediated wound contraction. On the one hand, contraction was attributed to myofibroblasts through their ability to contract their actin-myosin contractile system, similarly to muscle cells (but by distinct isoform of myosin, i.e. myosin II). On the other hand wound contraction was thought to occur through cell locomotion. Migration is dependent on integrin mediated cell-matrix attachment (Clark, 1996; Gailit & Clark, 1996; Hynes, 1992). Integrins serve as a dynamic link between the cytoskeletal motile apparatus of the cell and the extracellular matrix (Huttenlocher et al., 1995). Migration leads to generation of tractional forces on the substrate resulting in wound contraction (Eastwood et al., 1994; Guidry et al., 2003; Kupper & Ferguson, 1993). Such traction has been shown using wrinkling sheets experiments (Harris et al., 1980; Pelham & Wang, 1999) or visualisation of collagen fibril translocation in 3D collagen matrices by means of dispersed fiducial markers (Roy et al., 1997; Sawhney & Howard, 2002). Fibroblasts in this case do not change their phenotype into specialised contractile myofibroblasts, but maintain their elongate morphology (Ehrlich, 1988). These fibroblasts are not contractile by nature, and hence rely on cell-matrix attachments and cytoskeletal organisation (sliding actin-myosin elements) for generation of tractional forces (Lauffenburger & Horwitz, 1996; Thoumine & Ott, 1996). More recently the two theories mentioned above have been combined, suggesting that fibroblast generated tractional forces stimulated their transformation into myofibroblast phenotype (Grinnell, 1994; Tomasek et al., 2002). Grinnell (1994) suggested that relaxed tissue were likely to contract through tractional forces whereas stressed tissue would contract via contractile myofibroblasts. Recently Tomasek et al.

(2002) have further elaborated this model suggesting that contraction occurs through a combination of fibroblast-mediated events (consistent with the observation of tractional forces) and myofibroblast-mediated events (consistent with their presence in vivo wound and in vitro collagen matrices under TGF-β1 stimulation and mechanical tension). Therefore an additional phase has been suggested in the collagen matrix remodelling process associated with wound healing (Tomasek et al., 2002). In this phase fibroblasts differentiate in to myofibroblasts, cellular migration is reduced and the force is generated by the muscle-like contraction of the cell cytoskeleton (Tomasek et al., 2002).

Contraction forces, be they through contractile myofibroblasts or through tractional fibroblasts, depend on active myosin-based motors (Kolodney & Elson, 1993; Lauffenburger & Horwitz, 1996).

The mechanism through which such forces are generated, may however, occur differently. Traction exerted by the cell on its matrix can be directly related, but not identical, to intracellularly generated contractile forces, as these can dissipate through cell deformation or disruption of cell-matrix interactions. The matrix, in turn, will also exert an equal and opposite tractional force on the same cell through the same attachments, again a magnitude of this force is dependent on disruption of cell –matrix interactions (Lauffenburger & Horwitz, 1996). Thus, magnitude of cell-generated force alone does not determine cell migration speed. DiMilla et al. (1991) showed that the ratio of contractile force to cell-matrix adhesion strength, contributed to the rate of locomotion biphasically, i.e. intermediary ratios of force to adhesiveness providing the highest migration speed (DiMilla et al., 1991). In order to move the cell forward, contraction (internal forces) and traction (locomotory forces) must be in balance with each other (Huttenlocher et al., 1995). Also both forces must display asymmetry between the front and the rear of the cell, to allow for forward cell movement (Lauffenburger & Horwitz, 1996; Pelham & Wang, 1999; Sheetz, 1994).

The geometry of tethered collagen matrices affects the spatial remodelling of collagen fibrillar network and cell morphology. Two types of configurations have been typically employed: planar and uniaxial tethering.

Planar tethering is obtained by attaching the base of the lattice to a support. This does not allow contraction along the surface of the adherent support but in all other spatial directions. Uniaxial tethering involves the application of mechanical adhesive clamps to two opposed faces of the lattice. This stops not only contraction along the faces of the lattice adhering to the clamps but also along the axis perpendicular to the plane of these faces. Cell morphology varies from mainly bipolar in uniaxially tethered lattices to mainly stellate in planar tethered lattices. The organisation of the fibrillar network varies from planar fibril alignment (parallel to the base of the lattice) to uniaxial alignment (parallel the axis of tethering). Cellular uniaxial alignment has been further characterised and it was shown that the degree and uniformity of alignment is varied by the geometry of the uniaxial configuration Alignment was enhanced by high aspect ratio geometries of the collagen matrices. This mechanism was explained by a computer model (using the finite element method) of the distribution of principal strains in the different geometries. This model showed that different orientation in the principal isostrain lines were generated in the lattices under strain depending on their aspect ratio. Since it was suggested that cells tend to "hide" from strains aligning to isostrain lines as to virtual grid, this explains the different cellular alignment depending on the aspect ratio of the uniaxially tethered lattices (Eastwood, 1996; Eastwood et al., 1998b).

Tethered cultures have been seen as more effective tissue models that untethered cultures since tissues are almost always mechanically tethered (Brown, 2000).

The development of uniaxial culture systems in which isometric tension can be monitored, namely Culture Force Monitors (CFM), has proved an important model for monitoring the development of contraction forces by cells in FPCL (Delvoye et al., 1991; Eastwood et al., 1994; Kasugai

et al., 1990; Kolodney & Wysolmerski, 1992; van de Hulst, 1981). A functional sketch of the CFM is illustrated in Figure 1-2; FPCLs are connected, normally through porous adhering bars (made of polyethylene or vyon) to one fix point and one cantilever beam holding a strain gauge which is the actual force transducer.

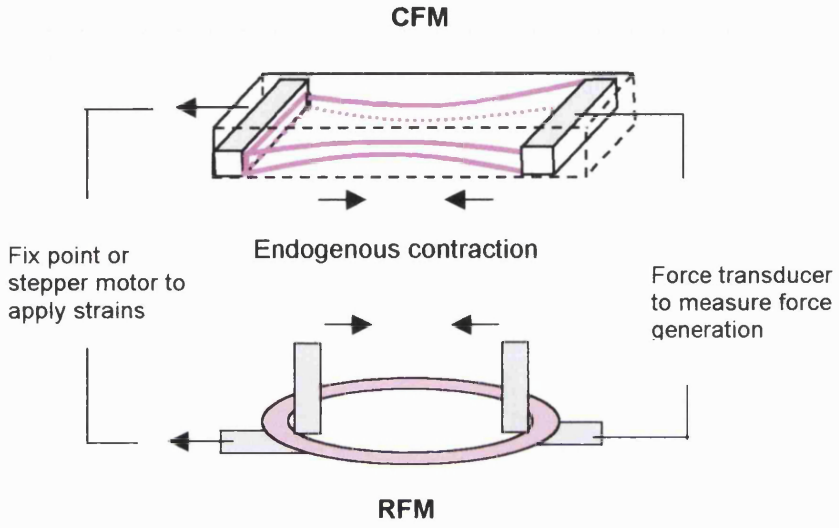

Figure 1-2 Schematic representation of the tensioning-Culture Force Monitor (tCFM) model and the ring force monitor (RFM) model. Lattices in the tCFM are anchored to the mechanical system through attachment bars. The RFM lattices are looped around the anchorage points. In both models endogenous uniaxial tension is developed by cell-mediated isometric contraction and measured by force sensors. Additional external uniaxial load can be applied by precisely displacing the end of the lattices attached to the fix point and allows the measurement of the force response at the other end attached to force sensors.

In order to apply precise, controlled strains to FPCLs an evolution of the CFM, named tCFM, was developed (Eastwood, 1996; Eastwood et al., 1998a). This included a stepper motor, for programmable precision motion, displacing the stage over which the fix point was bolted (and consequently one end of the attached gel). A modification of this system is represented by the ring force monitor (RFM) in which the gel has the form of a ring instead

of a rectangular flat shape (Huang et al., 1993); (Cacou et al., 2000; Wakatsuki et al., 2000). Similarly to the CFM, the ring gel is looped around two posts of which, one is connected to a force transducer, and the other is fixed or connected to stepper motor to apply strains to the construct (Figure 1-2).

Important findings have been achieved uniquely by CFM models. Force generation in 3D collagen matrices was shown to be dependent on actin cytoskeleton integrity (Brown et al., 1996; Eastwood et al., 1994; Kolodney & Wysolmerski, 1992). Contractile forces have been found independent of stress limitations rather than strain limitations (Freyman et al., 2002). Variations in force generation were correlated to different fibroblastic cell types (Eastwood et al., 1996; Zaleskas et al., 2001) or subpopulation of fibroblasts (from the same tissue) selected via different isolation methods (Eastwood et al., 1996). Force upregulation has been correlated to presence of growth factors, such as fetal calf serum (FCS) and TGF-β1 and TGF-β3 (Brown et al., 2002; Gonzalez et al., 2001; Zaleskas et al., 2001) and α–SMA expression in fibroblasts (Zaleskas et al., 2001).

Previous studies examining the effects of precise uniaxial cyclical mechanical loading has demonstrated the ability to increase cells and fibrils alignment (Eastwood et al., 1998b). Importantly mechanisms of tensional homeostasis, identified in the tCFM model, showed the existence of cellular mechano-adaptation processes in 3D matrices (Brown et al., 1998). The mechanical responses of fibroblasts to precise loading showed that cell had the tendency to re-establish an homeostatic level of tension, which had been established after the initial contraction (Brown et al., 1998). Furthermore cyclical loading was shown to cause increase in collagen production (Parsons, 2000) and downregulation in the synthesis of matrix metalloproteinases (MMPs) (Prajapati et al., 2000a; Prajapati et al., 2000b). In this respect, adding contact guidance (i.e. orientated fibronectin mats) aligned perpendicularly to the axis of cyclical loading produced an opposite response locally to the mats with increase in MMPs expression (Mudera et

al., 2000).

In summary, it is clear that the combined influence of local (i.e. fibril packing and alignment, local stiffness gradients, etc.) and global parameters (i.e. volume reduction, macroscopic force generation, external mechanical loading) can give rise to a tremendous variation in the physical environment to which fibroblasts respond.

1.1.6 Fibroblast populated collagen lattices as templates for tissue engineered constructs

The potential of fibroblast populated collagen lattices (FPCLs) as templates for tissue equivalents was apparent since the early times when the 3D culture system was introduced (Bell et al., 1979; Harris et al., 1981). This intuition marked the rise of a new science of tissue engineering which can be defined as "the application of engineering principles to new biology, for the purposes of constructing body tissues" (Brown, 2002). Advances in tissue engineering have led to clinical applications of tissue equivalents (based on FPCLs) such as skin replacement (Bell et al., 1981a)- and there are promising applications for other tissues including tendon (Awad et al., 2000; Lamberti & Wezeman, 2002; Young et al., 1998), ligament (Bellows et al., 1982; Dunn et al., 1995; Goulet et al., 2000; Huang et al., 1993) and blood vessels (Nerem, 2000; Niklason & Langer, 2001).

The ability of the cells to profoundly remodel collagen lattices through contraction is an important characteristic that on the one hand allows the study of cell-matrix interaction and on the other hand guides cell to reorganise the fibrillar collagen network into engineered tissue patterns. It has been shown that cell and fibril alignment can be controlled by appropriate combination of mechanical loading and matrix geometry (Eastwood et al., 1998b; Huang et al., 1993; Theodorou et al., 2003). This is likely to be caused by a contact guidance mechanism which is generated by

the endogenous tension that develops during uniaxial isometric contraction (Tranquillo, 1999).

One of the main goals of tissue engineering is to gain control over tissue regeneration which, in cellular terms, implies a control over cell proliferation and differentiation and, consequently, determines the modulation of the rate of synthesis and deposition of new matrix, and remodelling. Uniaxial configuration of FPCLs has the advantage of inducing controlled cell orientation and fibrils alignment along the principal axis. The effect of long term culture (up to 12 weeks) of collagen gels tethered uniaxially (at the two ends of the matrix) showed to stimulate resident fibroblasts to heavily remodel the matrix, turning it into a highly anisotropic meshwork of aligned collagen bundles with periodic undulation resembling the structure of tendon or ligaments in vivo (Huang et al., 1993). Furthermore the stiffness modulus was reported to increase dramatically (30 times higher) after 12 weeks in culture (Huang et al., 1993). Nevertheless, the modulus of the reconstituted ligament resulted 2 to 3 orders of magnitude lower than the original tissue.

Dynamic mechanical conditioning has been shown to improve the mechanical strength and the histological organisation of tissue-engineered blood vessels in form of RFM model (Seliktar et al., 2000). Additionally long term culture on uniaxially cyclical traction machine (Langelier et al., 1999) showed to be effective in increasing stiffness and histological organisation of bioartificial ligaments (Goulet et al., 2000).

Many other culture systems and biodegradable substrates have been used for tendon or ligament and blood vessel tissue engineering (Brown, 2002; Griffith & Naughton, 2002). None of these models, however, achieved tissue properties comparable to the native tissue which could enable their clinical use. Clearly, a more in depth knowledge of the remodelling processes that govern the tissue reorganisation into target cell-matrix architectures is required.

1.1.7 Stable structural matrix remodelling in fibroblasts populated collagen lattices

For many years the focus of research on 3D hydrated collagen lattices, contracted by resident cells has aimed to identify factors affecting cell contraction, such as cytoskeletal motor proteins, e.g. myosin light chain phosphorylation (Kolodney & Elson, 1993); signalling pathways, e.g. small G protein Rho, small G protein Rac etc. (Grinnell, 2000); adhesion proteins expression, e.g. integrins (Sethi et al., 2002; Tamariz & Grinnell, 2002; Tomasek & Akiyama, 1992).

Considerable progress has been made in understanding the cellular processes and intracellular/cytoskeletal signals involved (Grinnell, 2003; Tomasek et al., 2002). Yet, until recently this did not include changes at the collagenous fibrillar network level which could explain stable, structural remodelling of fibrillar collagen networks (as opposed to cell-mediated 'contraction').

However, this process has been recently identified independently in a number of models (Grinnell & Ho, 2002; Sawhney & Howard, 2002; Wakatsuki & Elson, 2003; Wakatsuki et al., 2000). These studies used the cytoskeletal actin disrupting agent, cytochalasin D (CD), to block cell force generation and over prolonged period this was found to leave a substantial change in the properties of the collagenous network. Stable structural matrix alteration was alternatively measured as engineering material stiffness (Wakatsuki & Elson, 2003), stored elastic energy, also called "actin-independent contraction" (Grinnell & Ho, 2002), fibril displacement and alignment in straps (Sawhney & Howard, 2002), fibril displacement in relation to single cell forces (Roy et al., 1997).

A possible mechanism inducing stable structural remodelling was first elaborated by Tomasek et al. (2002) as an explanation of the wound contracture process. They hypothesised that the permanent shortening generated by proto-myofibroblasts would start in a later phase of the wound contraction in presence of TGF-β1 and, importantly, mechanical tension. At

this point contraction of cytoskeletal stress-fibres would result in shortening and bundling of the surrounding collagen network. The new organisation of collagen fibres is then stabilised by newly synthesised matrix. This process, named "slip and ratchet", generates new local covalently bonded matrix organisation. It is hypothesised that reorganisation would be exquisitely local to the cell and affect only a small area (probably 4 to 8 times the cell size) containing a few other neighbour cells and matrix. Repeating incrementally this process, fibroblasts can lock a tension in the matrix (that is revealed macroscopically as shortening and stiffening of the lattice) in an interstitial, stepwise manner (Tomasek et al., 2002).

The slip and ratchet theory, though, leaves still many fundamental questions unanswered. For instance, at which point the process of local reorganisation of the matrix stops? How the state of cell-matrix homeostasis is reached? And how tensional homeostasis is maintained while the matrix is actively being remodelled? Finally what is the role of growth factors and/or externally applied mechanical load to the matrix in the structural remodelling process of the matrix?

Answering these questions is of fundamental importance for the general understanding of cell mechano-chemical-regulation of the cell-matrix remodelling mechanisms which constitute tissue morphogenesis in growth, adaptation, repair and even neoplastic tissue development.

Tomasek et al. (2002) hypothesised also the existence of a mechanism of contracture in vitro in the CFM model. The hypothesis, illustrated in Figure 1-3, is that fibroblasts first generate tractional forces (measured on the tCFM) during spreading and contraction, later they maintain this force (tensional homeostasis) through cytoskeletal contraction onto stable cell-collagen adhesion and eventually stabilise the contracted matrix producing a stably structural remodelled matrix. The existence and magnitude of this 3D remodelling would be measured as residual tension in the presence of excess cytochalasin D (CD). In this condition cell force generation is known to be blocked, which causes the component of tension retained by the cells to be eliminated, leaving the remaining component of tension retained in the

matrix.

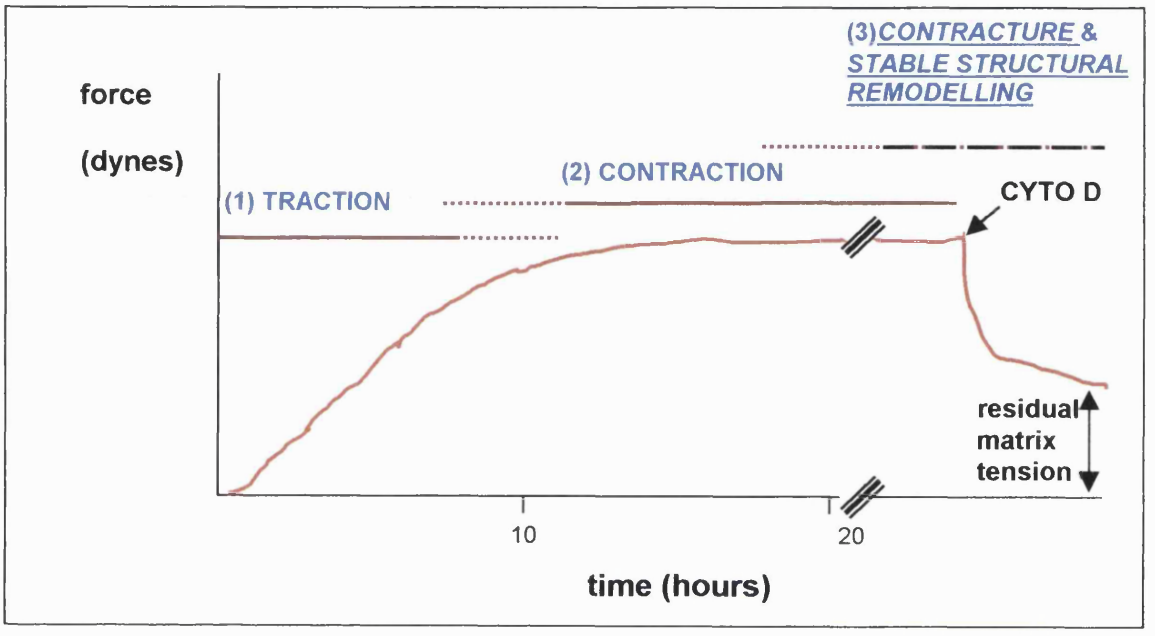

Figure 1-3 Schematic force-time plot representing the three phases of force generation in the culture force monitor. Uncertainty and overlap between the end of one phase and the start of the next is indicated by the dotted sections of the bars. Addition of cytochalasin D shortly after force plateau is reached in the contraction phase resulting in a total loss of force (Kolodney et al. 1992, Eastwood et al. 1994). By contrast addition of cytochalasin D (CYTO D, arrow) much later in the putative contracture/stable structural remodelling phase results in residual tension remaining in the matrix (double arrow). The residual tension is due to stable structural remodelling-shortening of the collagen network, as would be expected with contracture (figure modified from Tomasek et al. 2002).

In the stable structural remodelling phase fibroblasts have been hypothesised to deposit new collagen which increases the process of fibril covalent crosslinking, consolidating the remodelled collagenous fibrillar network (Tomasek et al., 2002). This process has been suggested to be tension controlled and depends on the isometric tension generated by the cells (which also contributes reducing total volume, closing the distance

between adjacent fibrils, hence favouring inter-fibril bonding). Cellular contraction, in turn, is known to depend on the combination of many factors such as cell density, presence of serum, and growth factors.

It is conceivable that the mechanism of contracture is valid as a general paradigm for the process of stable structural remodelling by fibroblasts in collagen matrices. Recently subpopulations of fibroblasts from muscoloskeletal tissue types (i.e. tendon, ligament, meniscus, cartilage, bone) have been shown to express α-SMA independently of injury conditions (Spector, 2001). The increase in cell contractility enabled by α-SMA has been suggested as a mechanism by which fibroblasts can regulate the mechanical/tensional properties of the tissue in which they reside (Spector, 2001).

1.2 Cell-matrix structural remodelling in the integration of tissue interfaces

Previous research in tissue engineering has focused on production of a variety of tissues and organs, as diverse as cartilage, skin, cornea, artery, nerve, bladder and liver. Further in most cases model systems have been developed for 3-dimensional support and culture of cell populations on a biodegradable support matrix (Brown, 2000). However, the vast majority of work has concentrated on relatively homogeneous single tissue entities. While the engineering of tissue interfaces has been very poorly investigated so far. Despite this , it is an area of major importance to surgical tissue reconstruction and repair biology.

Interfaces between tissues layers (particularly where adjacent tissues are injured or diseased) represent a major difficulty in surgical repair, therefore there is a need for new techniques in order to offer new avenues for effective reconstruction. Examples of relevant tissue interfaces are the

osteochondral, ligament-bone, tendon sheath or nerve/fascia. These interfaces can be classified in two groups: fixed (anastomoses) and gliding interfaces. It is critical to connective tissue function how they mechanically 'connect' to adjacent parts of the system. In the area of tissue repair and graft implantation an obvious example is the new interface formed between the implant and the original tissues. Normally, a strong, fixed anastomosis is needed (e.g. through integration between the cut ends of a tendon) but in some instances it is essential for function that a non-adhesive or gliding interface is achieved (e.g. between tendon and its surrounding sheath or fascia). It can be realistically envisaged that many surgical repairs could be significantly improved if interfaces could be pre-engineered into a new tissue construct. Excellent examples are tendon or ligament constructs, where a major problem of post surgical repair is to achieve good ligament-ligament anastomosis (particularly without producing damaging local adhesions).

Little work has been done in the area of connective tissue integration and mechanical linkage at interface sites and little is known about the mechanism involved in this processes. To our knowledge there are no reports of 3D culture models to support the engineered formation of bi-functional constructs. Simple constructs where living tendon is encouraged to mechanically integrate into a collagen gel have been made and tested (Cacou et al., 1996). In that work the adhesion (expressed as force over area) was measured after one week of cultivation and was shown to be cell-mediated through cell emigration (though not cell proliferation) from the tendon. The actual cellular action mechanism, though, was not elucidated. Tissue engineered cartilage discs and ring explants composites, joined by press-fit and sutures, have been shown to increase their integration in bioreactor tissue culture (Reindel et al., 1995). Integration and adhesive strength have been tested between two cartilage explants joined by apposition and compression in a specially designed chamber (Reindel et al., 1995). This group correlated the adhesive strength, duration in culture and collagen deposition (DiMicco & Sah, 2001). Cartilage explants, interfaced

through a layer of fibrin glue and incubated partly in vitro and partly in vivo (Peretti et al., 1999; Silverman et al., 2000) increased in adhesive strength and matrix deposition with time. Although some correlation between matrix deposition has been found in these works, neither the type of connection nor the mechanism by which mechanical bridges are generated within the interface have been yet fully understood.

Attempts to engineer osteochondral constructs in vitro have used either sutures (Schaefer et al., 2000) or fibrin sealant (Gao et al., 2001)to link bone and cartilage elements. Different cells sources were employed, from chondrocytes and osteoblasts (Schaefer et al., 2000) to selectively differentiated mesenchymal stem cells (Gao et al., 2001). Schaefer et al. (2000) conducted the only the investigation entirely in vitro, but neither of the two works reported measurement of the mechanical adhesion between the parts composing the constructs(Schaefer et al., 2000). Further in vivo studies have demonstrated only the ability of osteochondral constructs to fill defects and integrate with the surrounding host tissue (Schaefer et al., 2002; Schreiber et al., 1999; Solchaga et al., 2002).

The hypothesis under test, here, is that the formation and strengthening of interfaces assembled in 3D collagen-based constructs is governed by similar principles governing the 3D spatial remodelling identified in FPCLs. The mechanical adhesion strength of the interface would be a measure of the goodness of the integration and, indirectly, would quantify the cellular remodelling at the interface of 3D integrating models. Matrix remodelling has been associated with cell locomotion and migration that causes a distortion of the collagenous network. It is hypothesised that cell migration across the interface, or locomotion along it, would generate local deformations in adjacent collagen fibrillar networks. Cells and fibrils translocation might result in "collagen bridges" made of long bridging fibrils assembled along the cell migration pathway.

1.3 Optical measurement of 3D spatial remodelling of engineered connective tissue

Analysis of the formation and the organisation of new connective tissue formed in tissue-engineered constructs is a major requirement in tissue engineering, both for tissue bioreactor technology (Sacks et al., 1997) and in vivo assessment of implanted constructs. Minimally / non-invasive optical techniques are attractive because they allow real time monitoring of tissue structure eliminating the need to alter the experimental setup or special processing (such as fixation and thin dissection).

Many optical techniques have been used to detect tissue architecture and composition. These included use of small angle light scattering (Bowes et al., 1999; Ferdman & Yannas, 1993; Sacks et al., 1997; Waldman et al., 1999; Wilkes & Wilkes, 1974) polarised light imaging (Anderson, 1991; Dickey et al., 1998), and birefringence measurement, which is also based on light polarisation (Guido & Tranquillo, 1993; Sankaran & Walsh, 1998). These techniques, excluding Anderson's method (1991) that was based on specular reflection, involved the use of forward scattering of light through thin (up to ~100 μm thick) tissue sections. Hence they do not allow minimally invasive monitoring of tissue because tissue fixation and specific preparation is required.

A range of spectroscopic techniques have been investigated for tissue diagnostic, all of which have one basic principle in common. That is, the specific optical spectrum of a tissue sample contains information about biochemical composition and/or the structure of the tissue.

Laser-induced fluorescence spectroscopy (LIFS) has been investigated with and without the aid of exogenous drugs that target malignant tissue. When LIFS (usually with UV excitation) is used to detect intrinsic tissue fluorescence, or autofluorescence, as the diagnostic marker (Andersson-Engels et al., 1990; Romer et al., 1995), it becomes minimally invasive although concerns may arise when significant fluences of UV illumination are used. LIFS is useful in determining information about biochemical

component of tissue but provides poor tissue structural details. Results of LIFS in diagnostic studies demonstrated levels of reliability from very good (>90% reliability) to what is probably unacceptable (<80% reliability) (Mourant et al., 1996). Some authors noted that it is difficult to separate changes in fluorophore concentration from variations in the detected spectral intensity due to scattering effects caused by changes in the epithelial cellular structure (Bottiroli et al., 1995; Schomacker et al., 1992).

Near infrared (NIR) (Cope & Delpy, 1988; Nilsson et al., 1997) and infrared (IR) (Wong et al., 1993) spectroscopy have been used for identification of relevant tissue parameters such as oxygenation and concentration of absorbing chromophores such as haemoglobin. IR techniques, can be challenged in in vivo applications by the absorption of the water, which overlaps many of the relevant bimolecular vibrational modes. NIR spectral range, instead works in the so called "diagnostic and therapeutic window" in which water absorbance is highly reduced.

Raman spectroscopy (RS) (Frank et al., 1994; Wang et al., 2000), is less affected by water absorption since it can be done with visible or near-IR excitation wavelengths. The Raman-shifted scattered light is still at wavelength where water is essentially transparent. RS method has shown the capability to identify malignancy condition in breast tissue (Frank et al., 1994) and carcinoma (Nijssen et al., 2002). Changes in Raman shifted wavelength have been also correlated to molecular changes in rat tail tendon under strain in vitro. However, the effective RS signal is weak and requires complicated setups and expensive equipment for generation of effective signal collection and processing.

Elastic scattering spectroscopy (ESS) (also called diffusive reflectance spectroscopy) has been extensively investigated for its potential as diagnostic tool (Mourant et al., 1995; Mourant et al., 1996; Mourant et al., 1998; Wallace et al., 2000).

The purpose of this study is to use this technique to develop a method for the monitoring of engineered connective tissue formation.

The main advantages of ESS are:

- the broad range of wavelengths used in ESS has been shown to carry many wavelength-dependent tissue structural information.
- ESS is mainly used in backscattering configuration (i.e. light is collected at the surface level where it has been delivered), which is suitable for optical using setups fibre optics (Figure 1-4). This allows in vivo minimally invasive endoscopic use of this method.
- ESS is generally cheaper than other optical techniques since standard spectrometers for detection and Xenon lamps are used for illumination. In contrast expensive lasers and/or complicated setups are used in other types of spectroscopic analysis (such as NIR, IR and RS).

The main disadvantage of ESS is:

- the difficulty in the interpretation of the information about the tissue contained in the broad spectra.

Figure 1-4 illustrates the principle behind elastic scattering spectroscopy (ESS). Light is flashed onto a tissue area through a fine fibre optic. The light that is elastically scattered from the tissue is collected in the same fibre optic and analysed by a spectrometer. The spectra obtained contain information about tissue composition (biochemical components) and tissue structure architecture that are unique to that tissue area (hence the name "spectral signature" of a given tissue).

The intensity and wavelength dependence of elastic scatter spectrum depends on several light transport properties. The likelihood of scattering is generally quantified as the scattering coefficient μ_s which has units of inverse length. It is in fact the inverse of the average distance light travels between scattering events. A complete description of the scattering properties of a tissue requires knowledge of the angular scattering probability distribution, often written as $P(\theta)$, where the deflection angle, θ, ranges from 0 to π. Physically $P(\theta)$ is the probability of that when a photon is scattered it is deflected by an angle θ. When scattering centres are not

spherical in shape the angular scattering probability is in principle $P(\theta,\phi)$, where ϕ is the azimuthal angle ranging from 0 to 2π. The last essential parameter affecting light transport properties of a medium is the absorption coefficient μ_a which quantifies the decrease in light intensity when light is absorbed.

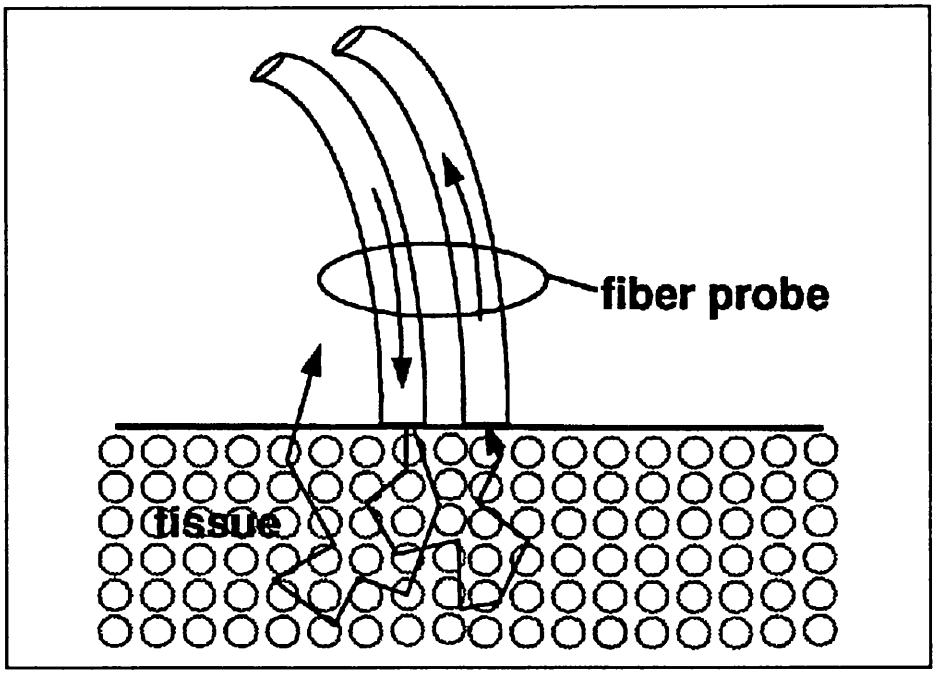

Figure 1-4 Diagramatic representation of the geometry of the fibre probe, used in optical contact with the tissue. Light is shed into the tissue from the light delivery fibre optic. Light undergoes interaction with tissue involving scattering and absorption. The small portion of light, that is scattered back to the surface (and in proximity to the fibre probe), is collected by the collection fibre optic. This is connected to a spectrometer that generates a spectrum for the collected light. The spectrum carries information about the structures and the composition of the tissue.

When scattering coefficient μ_s, absorption coefficient μ_a, and angular scattering probability $P(\theta)$ are all known, the transport of light through tissue can be calculated using the transport equation (Case & Zwefel, 1967). This equation, however, can only be solved analytically for special

geometries and consequently approximations are often used. The most common approximation is the diffusion equation, which holds when the light collection is well-separated from light delivery, typically a few centimetres (Farrell et al., 1992; Haskell et al., 1994). In this approximation the light transport properties can be described by μ_a and the reduced scattering coefficient $\mu_s' = \mu_s (1-g)$, where $g = \langle \cos\theta \rangle$. The anisotropy parameter g is 0 when scattering from an object is equally likely in the forward and backward directions and is near 1 when scattering is primarily forward directed.

In tissues, most light scattering is forward directed, that is the deflection angle θ is on average quite small. The identity of the morphological features that scatter light is uncertain and its investigation is an active area of research. Several structures have been proposed including cell nuclei, mitochondria, lysosomes, striation in collagen fibrils, membranes and other macromolecular aggregates (Figure 1-5).

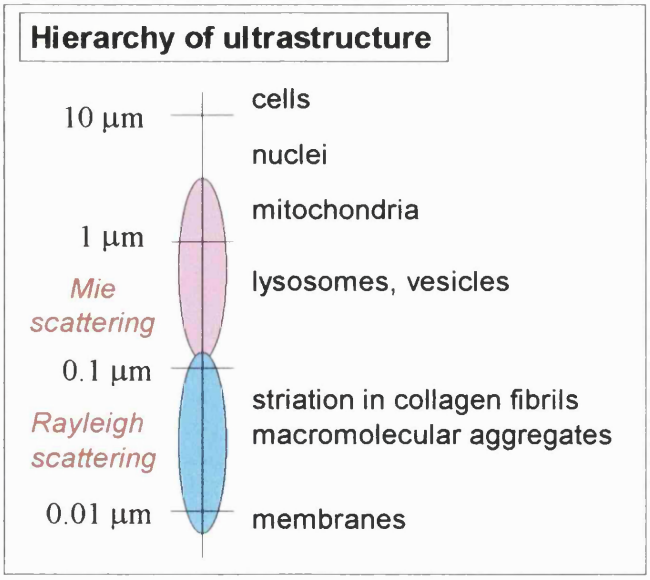

Figure 1-5 Diagramatical representation of the range of tissue ultrastructure which affects light scattering in the range of visible and infrared wavelengths. Scattering of light by structures having the same size scale as the photon wavelength is described by Mie theory. Scattering of light by structures much smaller than the photon wavelength is called the Rayleigh limit of Mie scattering.

The size, shape and refractive index of tissue and cellular structural features determine how light is scattered. For instance the relationship between μ_s and size of scatterers having spherical shape can be derived from Mie theory:

$$\mu_s = \rho_s \sigma_s = \rho_s Q_s A$$

where Q_s is the efficiency of scattering which relates the cross-sectional area of scattering σ_s to the true geometrical section area of the particle $A = \pi a^2$ and ρ_s is the scatter number density (related to particle volume fraction). Mie solution is limited to perfectly spherical particles with size on the order of visible to near IR wavelengths. Below this size the Rayleigh scattering theory applies (Figure 1-5) in which wavelength dependence on scattering properties is proportional to $1/\lambda^4$ (Saidi & Jaques, 1995).

Due to the complexity of tissue ESS spectra are normally fitted to these theoretical relationships and validated by measurements on tissue phantoms having a well defined particle sizes with spherical shapes and known density (Hielscher et al., 1997; Mourant et al., 1996). The shape and refractive index also strongly influence the angular dependence of the scattering at each wavelength. Depending of the geometry of the optical system, light intensity might strongly depend on $P(\theta)$ and consequently on details of tissue structure. When light source and collection are adjacent (Canpolat & Mourant, 2000)- as in the setup used in this study - and especially if they overlap (Canpolat & Mourant, 2001) the intensity of collected light correlates with the probability of high angle scattering events. As separation between the small area of light delivery and the small area of light collection is increased, the dependencies of the collected light on the probability of large scattering events and on the details of $P(\theta)$ decreases (Mourant et al., 1996). In fact at larger separations, (centimetres) only μ_s' and μ_a are needed to predict light collection and the diffusion approximation becomes valid (Saidi & Jaques, 1995).

The system used in this study adopted a small source-detector separation because that is the geometry providing the greatest sensitivity to

details of light scattering properties (Mourant et al., 1996). Interestingly the size distribution of refractive-index structure variations in epithelial cells was found to include particles with effective radii from smaller than a few hundred nanometers to ~2 μm. The number of scattering particles with the size of macromolecules is orders or magnitude higher than the number of particles with the size of organelles (Mourant et al., 2002). Additionally for fibroblasts, less than 40% of the scattered light at any angle was determined to have been scattered from the nucleus (Mourant et al., 2000). This implies that light scattering is likely to be sensitive to structures smaller than cell nuclei. Both experimental and modelling work indicate that small internal structures have a strong influence on the scattering pattern above 40° (Drezek et al., 1999; Mourant et al., 2000). Consequently a decreased source-detector separation may increase the relative contribution of small structures to the measured ESS spectrum. A further advantage of small distances between light delivery and detection is that the measurements can be made using fibre optics enclosed in small diameter probes (diameter < 1 mm). These are suitable for measurements of small areas of tissue, therefore increasing definition and specificity. Alternatively this geometry can be used for endoscopic (therefore minimally invasive) use for in vivo diagnostic purposes.

Quantification of morphological and biochemical properties has been mainly based on quantification of light transport properties. Alternative to quantify μ_s' or μ_a and the properties of the angular dependent scattering function have been used. These involved direct determination of effective size of scattering structures and the concentration of such structures. Two approaches have been taken. One approach is based on observations of interesting optical patterns generated by the propagation of polarised light. Polarised fibre optic and imaging measurements of cell suspensions provided information about the scattering structures (Hielscher et al., 1997). The other method involves the subtraction of the polarised components of the reflected light, parallel and perpendicular to the incident polarised light,

from the total reflected light. When the subtraction is performed as a function of wavelength, the resulting spectrum can be fit to a theoretical expression for scattering from spheres. Backman et al. (1999) have assumed that this spectral response was due to backscattering from nuclei and they reported that the distribution of cell-nucleus sizes obtained was in agreement with microscopic measurements of nuclear size.

An important tool for developing and understanding ESS is the Monte Carlo simulation of light transport (Groenhuis et al., 1983; Wang & Jaques, 1995). In the Monte Carlo simulation a photon is injected into a scattering medium and then propagated through the medium based on the knowledge of μ_s, μ_a and $P(\theta,\phi)$ for the scattering medium. Photon propagation is then simulated for, typically, millions of photons. If scattering centres are assumed spherical, all ϕ are equally likely and $P(\theta)$ can be calculated using Mie theory (Bohren & Huffman, 1983). Henyey-Greenstein phase functions are sometimes used because of their simple analytical form. However their validity is limited to non polarized light and spherical particles. Computational code is now available for other shapes of scattering centres such as ellipsoids of revolution or other particles. This seems more appropriated to simulate light scattering from physical structures in epithelial cells that do not scatter light like spherical scatterers (Canpolat & Mourant, 2001).

Monte Carlo simulations are particularly useful for determining features of light transport that are not easily measured, such as the depth to which light penetrated into tissue before being collected, the length of the path the light travelled in tissue, and the polarisation of light within the tissue. A deeper depth can be probed when the collected light is polarised perpendicularly to the incident light polarisation. Regardless of polarisation, the depth probed decreases with decreasing fibre separation (Meglinsky & Matcher, 2001). Monte Carlo simulation also makes clear that the distance that photons travel in tissue is much greater than the depth they probe (Gandjbakhche et al., 1999; Mourant et al., 1997). Finally when source and

detector are in close proximity, e.g. 200 or 250 μm apart, the collected photons undergo significantly more high-angle scattering events than do photons that entered the tissue, but were not collected (Canpolat & Mourant, 2000; Mourant et al., 1996).

1.4 Aims of the study

The aim of this study was to understand certain mechanical and biochemical factors that govern the spatial and structural remodelling of connective tissue by resident fibroblasts. The regulation of connective tissue remodelling is at the base of fundamental physiological processes such as tissue morphogenesis, growth, repair and turnover. Increase in the understanding of tissue mechano-regulation might be useful to tackle pathologies caused by their abnormal regulation which are still poorly understood. These include fibrosis disorders, burn-scar contractures, degenerative arthritis and age-related skeletal pathologies.

The focus of this investigation was the interactions between cells and three-dimensional collagenous fibrillar matrices. This substrate was adopted for several reasons including: (i) collagen is the basic building component of connective tissue (Alberts et al., 2002); (ii) collagenous substrates have been studied extensively in the last 30 years (Bell et al., 1981b; Grinnell, 2003); (iii) collagen type I lattices are known to be rapidly remodelled by resident fibroblasts (Bell et al., 1979; Eastwood et al., 1994; Grinnell & Lamke, 1984).

To this end two aspects of the cellular matrix remodelling process were analysed in vitro from a structural and mechanical viewpoint: (i) the stable structural matrix remodelling caused by cell-mediated matrix shortening and (ii) the cell-driven remodelling process and mechanical strengthening

process at tissue interfaces. In order to identify basic processes governing the cell-mediated spatial reorganisation of the collagen matrices, a computer model based on the Finite Element model was developed. Finally, optical method was investigated for its potential to monitor the development of tissue structural changes caused by the cell-mediated remodelling process.

1.4.1 Structural matrix remodelling process

Previous studies have shown that cell-matrix interaction in collagen lattices causes large spatial reorganisation of the collagenous fibrillar network (Bell et al., 1979; Bellows et al., 1982; Eastwood et al., 1996; Elsdale & Bard, 1972; Grinnell & Lamke, 1984; Harris et al., 1981). This process is strictly dependent on the ability of fibroblasts to generate forces onto the matrix that has been correlated to the presence of an intact actin cytoskeleton (Eastwood et al., 1994; Kolodney & Wysolmerski, 1992; Roy et al., 1999a; Tomasek et al., 1992; Wakatsuki & Elson, 2003). However, recent studies showed that, after periods in culture (> 48 hours), even if cell force generation was blocked by cytoskeletal disruption with cytochalasin D (CD) the mechanical properties of collagen lattices were altered compared to cell-free lattices (Wakatsuki et al., 2000). Grinnell and Ho (2002) showed that contraction upon release of stressed lattices was reduced but not abolished when cell force generation was blocked by CD treatment (this phenomenon was named "actin independent contraction").

The hypothesis of this study is that fibroblast-mediated contraction generates stable structural shortening of the collagen lattice, which results in a tension, measurable on the tCFM, that is retained in the lattice after removal of the cell tensile component e.g. by cytoskeletal disruption with cytochalasin D.

This study tested the existence and temporal evolution of the stable structural remodelling, measured as retained matrix tension after blocking cell force generation by cytoskeletal disruption with cytochalasin D.

At a fixed time point (24 hours) then the effect of selected treatments

known to increase the remodelling process were tested (for their potential to increase the residual matrix tension accumulation). Two treatments were tested in this study: TGF-β1 and external mechanical loading. TGF-β1 is a well-known growth factor which has been shown to upregulate collagen production (Desmouliere & Gabbiani, 1994; Reed et al., 1994; Roberts et al., 1986; Sarkissian & Lafyatis, 1998), downregulate the expression of matrix metalloproteinases (MMPs) (Chegini, 1997) and increase cell-mediated contraction (Goulet et al., 2000; Montesano & Orci, 1988). Grinnell and Ho (2002) recently showed that actin independent contraction was significantly increased by TGF-β1 treatment.

In the current study the hypothesis is that the combination of increased levels of contraction forces and collagen deposition can enhance stable structural remodelling. The mechanism hypothesised is that the reorganised collagen fibrillar network is consolidated by collagen deposition which favours new covalent bonds between pre-existing fibrils.

The second treatment, i.e. external uniaxial mechanical loading has been shown to stimulate collagen production (Berry et al., 2003; Parsons, 2000) but not cell-mediated contraction (Brown et al., 1998; Eastwood et al., 1998b; Parsons, 2000; Prajapati et al., 2000a). For this treatment the mechanism hypothesised is that the consolidation of the remodelled collagen fibrillar network is increased by collagen deposition. However, the mechanism of reorganisation is different, not due to generation of strong cellular forces, but to uniaxial pattern of strain which increases the reorganisation of the collagenous fibrillar network into aligned structures.

External load and changes in forces were applied and measured using the tCFM.

1.4.2 Cell-driven remodelling process and mechanical strengthening of tissue interfaces

Cell migration across collagen matrices is well documented (Cacou et al., 1996; Gosiewska et al., 2001; Greiling & Clark, 1997; Knapp et al., 1999; Murray & Spector, 2001; Young et al., 1998). Increase in adhesion strength with culture time has been measured in in vitro assembled tissue interfaces. Some investigators correlated this strengthening process with collagen deposition between opposing layers of cartilage tissue (DiMicco & Sah, 2001) and with cell migration, from tendon explants into a surrounding collagen lattices (Cacou et al., 1996). It is also known that cell locomotion causes tractional forces which are able to deform and remodel the collagenous fibrillar network (Porter et al., 1998; Roy et al., 1997; Stopak & Harris, 1982; Tamariz & Grinnell, 2002; Wakatsuki & Elson, 2003).

The hypothesis under investigation is that cell migration across collagenous interfaces, or locomotion along them, generates interstitial remodelling of the interfaces which results in increased mechanical adhesion strength in the interface.

In order to test this hypothesis, 3D collagen-based interface templates were developed in which the mechanical adhesion strength could be precisely quantified. The interface templates comprised the two simplest components, one being a cell-free collagen lattice and the other a cell-seeded lattice. The objective was to identify, through this technique, the basic cellular processes which increase of the measured adhesion strength such as migration and/or local remodelling.

Adhesion strength was tested by a purpose built testing device (derived from the tCFM) by which strain ramps were applied and stresses were measured.

1.4.3 Optical measurement of collagen gel based constructs by elastic scattering spectroscopy

Optical methods have been used extensively in biology and medicine to determine structural properties of tissue (Anderson, 1991; Bowes et al., 1999; de Vries et al., 2000; Ferdman & Yannas, 1993; Sacks et al., 1997; Wang et al., 2000; Wilkes & Wilkes, 1974), quantify biochemical concentrations in blood (Andersson-Engels et al., 1990; Edwards et al., 1993) and distinguish between benign and malignant tissue (Bigio et al., 2000; Perelman et al., 1998; Wallace et al., 2000).

Elastics scattering spectroscopy has been shown to provide promising results in cancer diagnosis (Mourant et al., 1995; Mourant et al., 1996; Wallace et al., 2000) and is particularly attractive for being minimally-invasive, low cost and scalable (Bigio et al., 1993).

The objective here was to develop an optical method, based on elastic scattering spectroscopy for minimally-invasive, real-time, measurement of structural remodelling in soft connective tissue.

The hypothesis under test is that the information contained in the ESS spectra can be correlated to the structural changes in 3D hydrated collagen lattices due to fibroblast-mediated remodelling. The cell-lattice system, here, is used as the simplest possible model system (i.e. cells, collagen fibrils, water) to identify the structural and chemical factors which govern the spectral signatures.

This application has the potential to be extended to a wide range of applications in tissue bioreactor technology and connective tissue pathologies

The ESS spectra were acquired and analysed using an optical setup previously described (Bigio et al., 2000).

Chapter 2

Material and methods

2.1 Devices used for mechanical measurements of force and generation of strains

2.1.1 Culture force monitor (CFM)

The culture force monitor is a device in which the contraction force generated in a uniaxially tethered collagen lattice can be precisely detected (resolution of 1 dyne or 10-5 N). The device used in this work is in principle the same as the CFM previously described by Eastwood et al. (1994).

The core of the device is the force sensor, which is made of a copper beryllium (Cu/Be) beam (0.15mm thick) coupled with a strain gauge (Measurement Group UK, UK). Calibration of force transducer is described in Chapter 3.

The measuring setup was based on a fix point attached to a moving x-y stage (Figure 2-1, left side) and on the force sensor (Figure 2-1, right side) clamped to a static reference point in respect to the moving x-y stage. Lattices floating in purpose built culture chambers were placed on the x-y stage and anchored to the fix point and the force sensor. Anchorage was made by stainless steel suture wire (0.35mm in diameter) shaped in form of A, called "A-frames", connecting the attachment bars (which are integrated with the two ends of the lattice) to metal hooks placed on the fix point and on the force sensor. Attachment bars to form a physical connection to the

collagen lattice were fabricated with layers of polyethylene mesh sheets (10 holes per inch type, HeeBee Designs, UK) sutured together by thin stainless steel wire. These bars were sterilised and placed in the chamber at the time of gel casting (i.e. gel in liquid phase). After gelation bars became integrated with the lattice.

"A-frames" were inserted among the layers composing the bars and secured with the thin stainless steel wire before bars were positioned in the culture chambers. Sterilisation of bars and "A-frames" were performed by immersion in 70% ethanol solution overnight.

Attachment bars had sufficient buoyancy to support the mass of the wire "A-frames". Since the attachment bars then floated in the culture medium, an efficient, near friction-free bearing surface was produced.

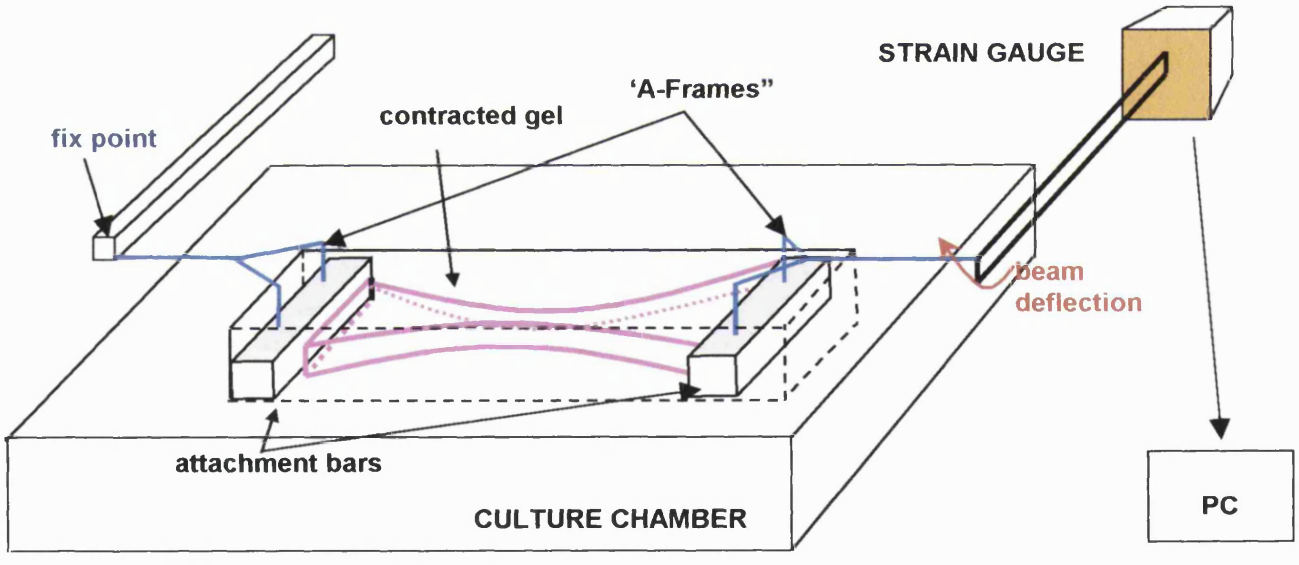

Figure 2-1 Diagrammatic representation of the culture force monitor (CFM).

The data acquisition part of the CFM was replaced. Signal from the amplifier, attached to the force transducer, was acquired by a new data acquisition card (National Instruments, USA) and displayed in real time

and recorded by a PC running LabVIEW 6.0 (National Instruments, USA). Data were collected at 1000 points per second and recorded at a rate of 1 point per second. This provided a large increase in the signal to noise ratio compared to the previous digital to analog converter.
The format of the acquired data file was suitable for post-processing in Microsoft Excel spreadsheets. A purpose written macro for Excel allowed to automatically produce a force generation graph with the time resolution desired (minute unit). This provided further smoothing to the 1 second data set, which further reduced noise.

The major improvement was constituted by the new user-friendly interface which allowed easy setting/resetting of the acquisition and easy data processing. Calibration factors could be inserted direct and real force displayed in real time (see appendix A for details). This allowed an easy monitoring of the force development and possibility to readily interact with the system (e.g. in drug dose studies) depending on the cell-mediated force response.

A number of CFMs using the old data acquisition card (Bytronics, UK) were maintained and interfaced with LabVIEW (a different bespoke application was written) to provide the same real time environment and the user-friendly interface for all the machines in use.

The new data acquisition interface software allowed to acquire multiple outputs from multiple force transducer in parallel on one PC (this was for both software versions for both data acquisition cards).

2.1.2 Tensioning culture force monitor (tCFM)

The tensioning culture force monitor (tCFM) was essentially a CFM in which the stage, and the fix point set on it, could be displaced along the axis of the force measurement. The device used in this work is in principle the same as the tCFM previously described by Eastwood et al. (1998).

Strain was applied to cultures by moving a linear table (to which the

CFM stage was screwed) by a stepper-motor (Parker, Germany) controlled with a microdrive (Parker, Germany). The stepping motor drives a precision ground leadscrew with a pitch of 0.508 mm that is attached to the linear table via a recirculating ball nut. The microdrive was used at a resolution of 4000 pulses per revolution of the microstepping motor. This, in conjunction with the precision ground leadscrew enabled a positional accuracy of 0.127 μm to be achieved. The culture chamber is attached to the tCFM exactly in the same way as for the CFM. The control of the microstepping motor is achieved by the programming of the microdrive in a dedicated language (called X-ware, Parker) via a PC. The connection was made by a serial cable and commands were inputed through an MSDOS shell.

2.1.3 Interface adhesion measuring device (IAMD)

Mechanical integration of engineered tissue interface constructs was assessed by subjecting them to a single-lap shear test to failure using a purpose built Interface Adhesion Measuring Device (IAMD). IAMD design was based on the tCFM, i.e. a linear table displaced by a stepper motor. However both the stepper-motor (SY561T, Parker, Germany) and the microdrive (XL25i, Parker, Germany) were different. This is because less precision on the strain was needed in this ultimate strength measuring device. The force sensor was essentially the same as in the CFM but the thickness of the copper beryllium beam was varied to increase the force range (0.15mm to 0.4mm thick).

The principal difference lies in the position of the force sensor that was mounted vertically on a static reference point to the moving x-y stage. A similar design concept was recently published (Freyman et al., 2001). The aim of this new design was to allow the use of non buoyant attachment bars (i.e. made in non floating materials) but to avoid friction against the bottom of the culture chamber. This was achieved by lifting vertically the force sensor once the attachment bar was anchored to it.

Connection of the two components of the interface were made by attachment bars and A-frames similar to the ones used for CFM. Material of attachment bars was changed to polystyrene when materials different from collagen lattices were employed for the interface components.

2.2 Culture chambers used for collagen gel casting

2.2.1 CFM culture chambers

Traditional CFM culture chambers (Figure 2-2-B), made of silicon elastomer and a polymethylpentene petri dish (Eastwood et al., 1994), were replaced with new culture chambers (Figure 2-2-A) fabricated from Derlin™ blocks (Intertech Ltd, UK) with the same casting area as the previous chambers (i.e. 75 × 25 × 15 mm, external dimensions were 100 × 100 × 20 mm). This channel was essentially hydrophobic in nature (Derlin™ material) to inhibit cell and gel attachment.

The main advantage of the new design was the fact that they were constructed from one block of material avoiding junctions and gaps. A fine gap was present in the previous design between the dish and the elastomer. This gap was traditionally "sealed" with a layer of collagen pre-set before casting the actual experiments. This technique took longer to setup and was less experimentally solid. Leakage of the liquid gel into the gap between dish and elastomer sometimes occurred, leading to loss of the experiment.

The main disadvantage was that Derlin™ material was not transparent and therefore did not allow direct visualisation of the lattices under the microscope (as it was possible previously with petri dishes).
However, this requirement was not needed in the current experimentation and a more reliable design without the possibility of direct microscopic observations was preferred. In the future it is possible to modify the design of the culture chambers installing microscopy windows (made with microscopy glass coverslips) on the bottom of the chambers to allow direct

confocal microscopy on CFM lattices.

Chambers allowing uniaxial tethering without the need of external anchorage of the attachment bars were also employed (Figure 2-2-C and D). The H-shape had 2 vertical lines in the H with size 35 × 7.5 × 15 mm (Figure 2-2-D), which were used to position the attachment bars (made of sizes that would fit into these recesses). The central part of the H had two levels: the bottom level had the same casting area as the CFM mould minus the space occupied by the bars (i.e. 60 × 25 × 5 mm). The upper level occupied the entire volume (i.e. 60 × 35 × 10 mm) and formed a unique rectangular volume with the vertical sides of the H (total upper volume (i.e. 75 × 35 × 5 mm).

This shape was designed to allow uniaxially tethered contraction in the culture chambers without measuring the force when attachment bars were plugged in their recesses. However it could be used for force measurements in the CFM when bars were unplugged and floated above the 5 mm step. This allowed to run CFM equivalent contraction experiment but in a more sterile environment (closed Petri dish with no external connections), hence longer-term experiments. It was also possible to anchor the gels and test force generation at a later stage. A smaller version of the H mould was designed and realised (Figure 2-2-D) to increase the experimental rate and to save cells and materials. In this, the aspect ratio of the casting channel (i.e. 3:1) was maintained (size 33 × 13 × 5 mm) but the gel volume reduced from 5 to 2 ml. While the longer chamber was made with the elastomer and petri dish combination, the small size chamber was fabricated from Derlin™ blocks (Intertech Ltd, UK).

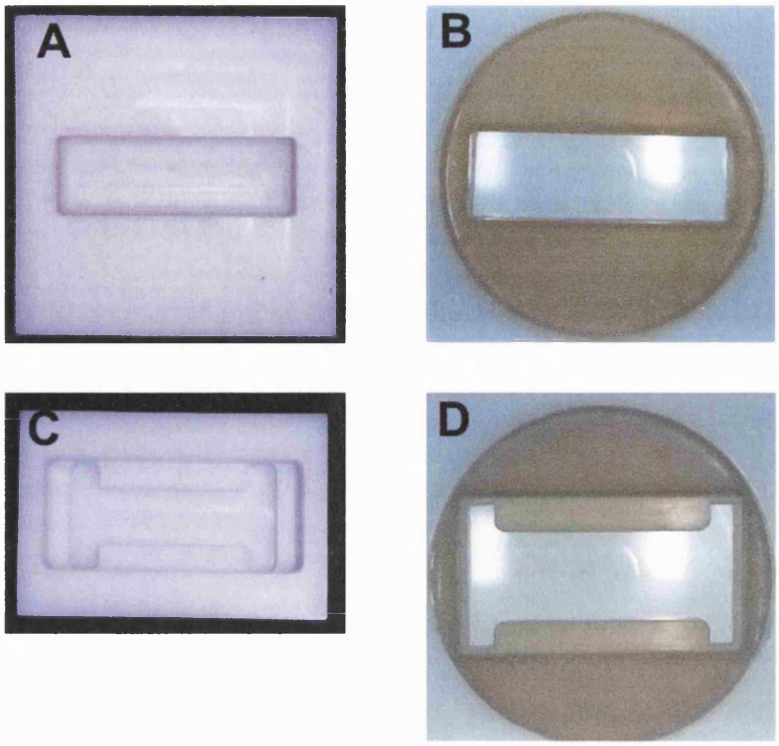

Figure 2-2 Culture chambers used in the current study to generate uniaxial contraction in FPCLs. (A) new culture chambers fabricated from DerlinTM blocks and (B) traditional CFM culture chambers made of silicon elastomer and a polymethylpentene petri dish had the same casting area (i.e. 75 X 25 X 15 mm). (D) H-mould chamber fabricated by the silicon elastomer technique (casting area was the same as the CFM chamber. C) A smaller version of the H-mould (33 X 13 X 5 mm).

2.2.2 Culture chambers for the generation of collagen-gel-based tissue interfaces

The evolution of the interface model led to the development of different conception culture chambers. For the *fracture* model the silicon elastomer of the H-moulds were customised with equally spaced grooves along the edges of the central canal (Figure 2-3). This allowed insertion of 2 transverse stainless steel barriers which divided the central channel into 3 separate compartments which could not become linked until barriers were removed.

Common stainless steel razor blades (Bic, France) were used as barriers. These were joined together onto a central holder which maintained them at a constant distance (same as the grooves relative distance) and allowed easy handling.

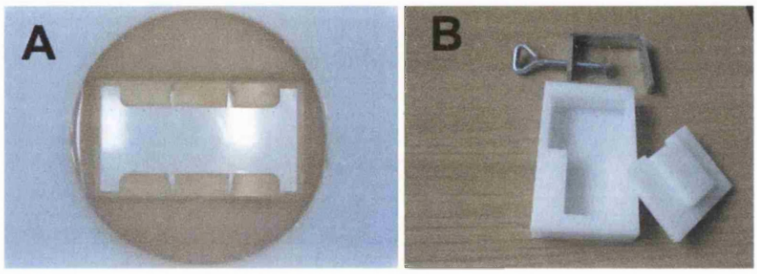

Figure 2-3 Culture chambers for the generation of collagen-gel-based tissue interfaces. (A) fracture model and (B) wrapping model culture chambers.

For the interface model called the *wrapping* model a culture chamber of new conception was designed and realised in order perform vertical casting and subsequent horizontal culturing and mechanical testing (Figure 2-3-B). The culture chamber and the fitting cover were fabricated from Derlin™ blocks (Intertech Ltd, UK). The wrapping model and functionality of this culture chamber have been dealt in great detail in chapter 6.

2.3 Collagen lattice preparation

2.3.1 Collagen gel standard buffering method

A collagen gel mixture composed of 2 ml of acid soluble collagen type I (2.20 mg/ml in 0.6% acetic acid, First Link, UK) and 0.250 ml of 10X DMEM (Gibco Life Technologies, UK) was neutralized by a fixed amount of 5M NaOH. NaOH quantity was standardised empirically by a prior quality control of gelation to identify optimal NaOH concentration for each batch. Batch variability caused the amount of NaOH to range between 48 and 52

µl. Single batches of native rat tail acid soluble collagen normally amounted to around 2 litres (stored in 100 ml bottles at 4 ° C).

2.3.2 Preparation of soluble bovine collagen

Acid soluble calf skin collagen type I (Sigma, UK) was diluted in 0.1 M acetic acid to obtain a 2 mg/ml collagen solution. The solution was stirred for 8 hours at room temperature to allow complete solution. Subsequently the collagen solution was sterilised by transferring to a glass bottle the bottom of which was layered with chloroform (10% of the total collagen solution). The solution was allowed to sit overnight at 4°C overnight. The top layer containing the collagen solution was then aseptically removed and stored in universals at 4°C. The standard buffering procedure was followed to neutralise the gel solution.

2.3.3 Setup of CFM collagen lattices

Fibroblast populated collagen lattices (FPCLs) were prepared similarly as previously described for the CFM experiments (Brown et al., 2002; Eastwood et al., 1994; Eastwood et al., 1998). While still in liquid form, 5 ml of neutralised collagen gel were mixed with a 0.5 ml suspension of 5×10^6 fibroblasts (i.e. concentration of 1 million cells / ml). The rest of the gel was used to pre-coat two attachment bars. These were placed along the short sides of the casting mould. The collagen-cell suspension was then poured into the mould and incubated in a 37°C in a 5% CO_2 humidified incubator for 20 minutes. Finally the gelled lattice was topped with 20 ml of complete DMEM (for definition of culture medium see section 2.5.1).

2.3.4 Setup of round gels in multiwell plates

Collagen lattices were cast in circular wells within multiwell plates for studies in which force measurement was not required.

After gelation, two typical configuration were employed:

1. Unloaded configuration
2. Stressed configuration

Unloaded configuration preparation: after gelation (20 minutes), culture medium was added to wells and gels were gently released, with the help of a needle, from the bottom of the wells (also called free floating configuration) and allowed to contract free from external constraints.

Stressed configuration preparation: after gelation (20 minutes), culture medium was added to wells but gels were left attached to the bottom of the wells that did not allow contraction (also called restrained configuration).

2.4 Drug administration technique

Chemicals were applied to the gels in the culture chamber on the CFM (or tCFM) via directly spraying through a 1 ml syringe fitted with a fine needle. Air was then pumped through the syringe and needle to ensure that all the reagent was added to the experiment (total volume of reagent added was 200 μl). However this method involved some mechanical disturbance of the system caused by opening the incubators doors and physically removing the lid of the culture dish. In the majority of the experiments these disturbance was negligible as tested by repeated door opening and closing without administering the drug. However occasionally it caused non-negligible disturbances and in these cases the experiments were rejected.

2.5 Culture medium and chemicals

2.5.1 Standard complete culture medium

Cells were cultivated in standard complete DMEM consisting of Dulbecco's Modified Eagle's Medium (DMEM) supplemented with 10% (v/v) Fetal Calf Serum (FCS, First Link, UK), glutamine (2mmol/L, Gibco Life Technologies, UK), penicillin/streptomycin (1,000 U/ml/100 mg/ml, Gibco

Life Technologies, UK) 50 μg/ml ascorbic acid (Sigma, UK).

2.5.2 Preparation of treatments

The following treatments were used:

- cytochalasin D (Sigma, UK)
- TGF-β1 (Sigma, UK)

20 μl cytochalasin D aliquots were prepared by diluting in DMSO (Sigma, UK) the amount of cytochalasin needed to obtain final concentrations ranging from 2 to 20 μg/m in a volume of 20 ml. Aliquots were stored at –20 ° C until use.

20 μl TGF-β1 aliquots were prepared by diluting in Phosphate Buffer Solution (PBS, Gibco Life Technologies, UK) the amount of TGF-β1 needed to obtain a final concentration of 12 ng/ml in a volume of 20 ml. Aliquots were stored at –20 °C until use.

2.6 Cell culture

2.6.1 Cell isolation and culture

Routine cell culture was carried out in 225 cm^2 plastic flasks (Corning, USA) filled with 30 ml of complete DMEM. At confluence cells were harvested from flasks and replated in new ones. When cells had to be harvested from flasks, culture medium was removed and 2 washes in phosphate buffer solution (PBS, Gibco Life Technologies, UK) were performed. PBS was then removed and 7 ml of 10% trypsin-EDTA (Gibco Life Technologies, UK) solution (in PBS) were added to cultures. Flasks were then incubated at 37 ° C for 10 minutes, after which time 13 ml complete DMEM were added. The flask contents were transferred to universal tubes and spun for 5 minutes at 400 G. Supernatant was removed and pellets were suspended in complete DMEM. Cells were then counted in standard haematocytometers, pelleted again and suspended again in complete DMEM at the required concentration. Cells were replated at a

density not less than 3000 cells /cm^2.

Fibroblasts were isolated from tissue samples by two techniques: collagenase digestion of tissue or direct plating of tissue explants. Briefly, for both techniques tissue samples were washed twice in PBS and accurately chopped in small cubes (~2 mm^3). These were either plated in 25 cm^2 flasks or digested. The former were placed on the bottom of the flasks, incubated in dry incubators at 37°C for 30 minutes and then topped with 10 ml of complete DMEM and cultured for a period of 2-4 weeks. When the cells migrating out of tissue explants had reached 80% confluence, flasks were washed with PBS and explants carefully removed using Pasteur glass pipettes. From this point onwards cell culture proceeded as routine. Collagenase medium was made with 2 mg/ml collagenase (Sigma, UK) dissolved in complete DMEM. Tissue cubes were transferred in universal tubes filled with 10 ml collagenase solution. A quantity of about 2 grams of tissue was used for each 10 ml of collagenase solution. Tubes were incubated for 30 minutes at 37°C on a roller device. Tubes were then centrifuged and pellets were resuspended in complete DMEM and plated on 75 cm^2 flasks. From this point onwards cell culture proceeded as routine. Cells were sometimes frozen at low passage numbers and cryopreserved in liquid nitrogen until needed. In this case cells were harvested from flasks and resuspended at a concentration of 1 million cells/ml in freezing medium. This consisted of 70% (v/v) Leibovitz L-15 medium (Gibco Life Technologies, UK), 20% (v/v) FCS (First Link, UK), 10% (v/v) DMSO (Sigma, UK), glutamine (2mmol/L, Gibco Life Technologies, UK), penicillin/streptomycin (1,000 U/ml/100 mg/ml, Gibco Life Technologies, UK). 1 ml of cell suspension was poured into cryotubes and frozen down. When needed frozen cells were rapidly thawed, poured into universal tubes filled with warmed complete DMEM and centrifuged. The supernatant was removed and the cells were suspended in new complete DMEM and plated onto 75 cm^2 flasks. At this point culture proceeded as routine.

The list of cell types used in this study follows below

2.6.1.1 Rat tendon fibroblasts isolation

Rat tendon fibroblasts (RTF) were isolated from 12 months old rat Achilles' tendons by collagenase digestion. RTF were used for experiments between passage numbers 5 and 8.

2.6.1.2 Bovine tendon fibroblasts isolation

Bovine tendon fibroblasts (BTF) were isolated from adult calf Achilles' tendons by collagenase digestion. BTF were used for experiments between passage numbers 5 and 8.

2.6.1.3 Human dermal fibroblasts isolation

Human dermal fibroblasts (HDF) were cultured from explants of normal skin taken directly from the operating theatre. HDF were used for experiments between passage numbers 5 and 7.

2.6.1.4 Rat tendon repair cell isolation

In order to collect tendon repair cells, fibronectin mats were implanted in rat tendons following a method previously described (Zavahir et al., 2001). Briefly, orientated fibronectin mats were placed into a partial tenotomy window injury in rat extensor digitorum longus tendons. Fibres in the mats were aligned parallel to the tendon and held in place by a 10/0 Ethilon suture placed in the middle. Animals were sacrificed at 3 days and tendons harvested. Fibronectin mats were removed from tendons and placed in multiwell plates (one per well). Cells migrated out of the mats and grew to confluence in one week, after which cells were trypsinised and replated in bigger flasks. Cells were then cultured in standard complete medium and used by passage 5-6.

2.6.1.5 Human bone marrow fibroblasts

Human bone marrow fibroblasts (hBMF) were kindly donated from Prof. Alicia El Haj (Keele University). hBMF were isolated (in Keele) from bone marrow aspiration following published protocols. hBMF were then

expanded in culture in our laboratory using DMEM D2964 (Sigma, UK) supplemented with the same supplements described above for standard complete medium plus 1% non essential amino acid medium (Sigma, UK).

2.6.1.6 C_2C_{12}, rat transformed myoblast cell line

C_2C_{12}, rat transformed myoblast cell line, were kindly donated from Dr. Umber Cheema (Institute of Orthopaedics, UCL) and cultured with standard culture media used for tendon fibroblasts cultures. C_2C_{12} were used for experiments between passage numbers 9 and 13.

2.7 Microscopy and Staining techniques

2.7.1 Collagen lattices fixation

All collagen lattices were fixed using the same method, independently from the type of staining and microscopy adopted. Lattices were fixed in 2.5% glutaraldehyde (V/V) (Agar Scientific Ltd., Essex, England) in 0.1 M Sodium Cacodylate buffer for 2 hours. CFM lattices were maintained under uniaxial tension during fixation in order to avoid structural changes due to shrinking.

For alpha smooth muscle actin staining, formal saline was used in place of the standard fixative. Lattices were maintained in formal saline for 24 hours.

When fixation time had elapsed samples were washed in in 0.1 M Sodium Cacodylate buffer and stored in the same buffer until use or further processing.

2.7.2 Toluidine blue stain for phase contrast microscopy

1% toluidine blue stain solution was prepared by dissolving 1g of toluidine blue powder (Raymond A Lamb, UK) and 1 g of di-sodium tetraborate (Borax), (VWR International, UK) in 100 ml distilled water. The

solution was then filtered through a Whatman no.1 filter paper.

Fixed lattices were stained by removing 0.1 M Sodium Cacodylate buffer buffer from the Petri dish containing the samples and pouring toluidine blue stain drop wise till the surface of the sample was covered. After 1 minute the sample was washed several times with PBS until traces of colour were removed from non cellular areas. Lattices were then conserved in buffer until examined under phase microscopy.
Thanks to be transparency of the collagen lattices cells could be visualised by phase contrast microscopy also without stain.

2.7.3 Fluorescent and Confocal microscopy

2.7.3.1 Fluorescent CellTracker™ dye

Fluorescent CellTracker™ green (5-chloromethylfluorescein diacetate, Molecular Probes Europe, Leiden, NL) was used to track cells under fluorescence microscopy. A 10 mM stock solution of CellTracker reagent was prepared by dilution in DMSO (Sigma, UK). This was further diluted in complete medium to a final concentration of 15 μM. Collagen lattice were incubated for 1 hour with CellTracker loaded medium, after which medium was removed. After a PBS wash, fresh new complete medium was added. Fluorescence was maintained in cell cytoplasm for prolonged periods of time (observed up to 10 days). Cells were imaged on standard inverted fluorescence microscopes or confocal microscopes (CLSM) with blue excitation light (440nm) (green emission). Images from confocal microscopy obtained from different focal planes in the samples were composed in 3D projection images.

2.7.3.2 Alpha smooth muscle actin stain

Gels were fixed rapidly by immersion in formal saline and left for 24 hours. They were then washed 3 times in PBS and stored in PBS at 4 ° C until stained. Pieces of collagen lattices were cut with a scalpel and soaked in ice-cold methanol with shaking for 1 hour to permeabilise cells. Samples

were then washed with several changes of PBS for 1 hour again on shaker, followed by incubation overnight in a 24 well plate with 500 µl of primary antibody; mouse monoclonal anti a-smooth muscle actin antibody (Sigma, UK) used at 1 in 1000 dilution. Following this, samples were washed with PBS on shaker for 40 minutes. Samples were transferred to a fresh 24 well plate and incubated with 500 µl secondary antibody. FITC conjugated rabbit anti-mouse monoclonal antibody (Sigma, UK) at 1 in 400 dilution + Hoescht nuclear stain (Sigma, UK) at 1 in 1000 dilution. Incubation in the dark on orbital shaker lasted 1 hour, after which time samples were kept in the dark in PBS for 40 minutes to 1hr.

The pieces of gel were placed on a glass slide and held firmly by coverslips. Confocal scanning laser microscopy (CLSM, Leika, Germany) was performed with dual excitation lights, i.e. UV laser (340nm) and blue light (420nm). Separately acquired fluorescent images were superimposed. Images obtained from different focal planes in the samples were composed in 3D projection images.

2.7.4 Scanning Electron microscopy

Fixed lattices were washed twice in buffer and the secondary fixation with 1% osmium tetroxide (Agar Scientific Ltd., UK) in 0.1 M Sodium Cacodylate buffer was carried out for one hour at room temperature. The specimens were washed with 0.1 M sodium cacodylate buffer.

A piece of collagen lattice (10 X 5 X full thickness) was cut with a scalpel and snap frozen by placing it into liquid nitrogen for 2 minutes. As it was removed the specimen was immediately fractured. The fractured sample was placed onto a carbon adhesive disc (Agar, UK). The disc was placed in the Joel JJM 5500LV scanning electron microscope in the low vacuum mode. The microscope was degassed starting at 130 Pa, dropping pressure in increments of 10 Pa until the vacuum of 20 Pa was obtained. Specimens were then removed from the vacuum chamber of the microscope and placed in an Emitech K550 sputter coater and coated with

gold/palladium (60/40) for 2 minutes. Finally, the sample was viewed in the scanning electron microscope in the high vacuum mode.

2.7.5 Transmission Electron microscopy

Fixed lattices were washed twice in buffer and the secondary fixation with 1% osmium tetroxide (Agar Scientific Ltd., UK) in 0.1 M Sodium Cacodylate buffer was carried out for one hour at room temperature.
The specimens were washed with 0.1 M Sodium Cacodylate buffer and dehydrated with acetone, infiltrated with 1:1 acetone: araldite CY212 resin overnight in the specimen rotator. After two changes of fresh resin, for a minimum of three hours each, samples were embedded in araldite CY212 resin and blocks were polymerised at 60°C for 18 hours.

Semi-thin (1μm) sections were cut on a Reichert-Jung Ultracut E ultramicrotome and floated onto distilled water and collected on glass slides. Sections were stained with 1% toluidine blue in borax in order to select suitable areas for TEM. Ultra-thin sections were cut using a Diatome diamond knife, floated onto distilled water, collected on copper grids and stained with 2% uranyl acetate and lead citrate for 15 minutes in each solution. The stained sections were viewed on a Philips CM12 electron microscope. All the EM reagents were purchased from Agar Scientific Ltd., UK.

2.8 Setup of the optical system for elastic scattering spectroscopy

The elastic scattering spectroscopy (ESS) system consisted of an optical probe connected both to a light source and a spectrometer, which are both controlled by a PC that is also used as data acquisition and elaboration device (Figure 2-4). The optical probe is made of two optic fibres: one that

delivers white light (short pulses ~35 ms) from a xenon-arc lamp (EG&G), and another one that collects the spectrum of the backscattered light, which is analysed by the spectrometer (a modified version of a spectrometer manufactured by Ocean Optics, Dunedin, FL) which employs a linear charge-coupled device (CCD) array for detection. The 400 μm light delivery fibre and the 200 μm collection fibre are configured in the probe to have a fibre centre separation of ~350um. This configuration restricts the volume of material that is sampled but has been shown (Mourant et al., 1996) maximises the sensitivity of the collected signal to high angle scattering events and thus to the effects of scattering from cellular structures and matrix ultrastructural features.

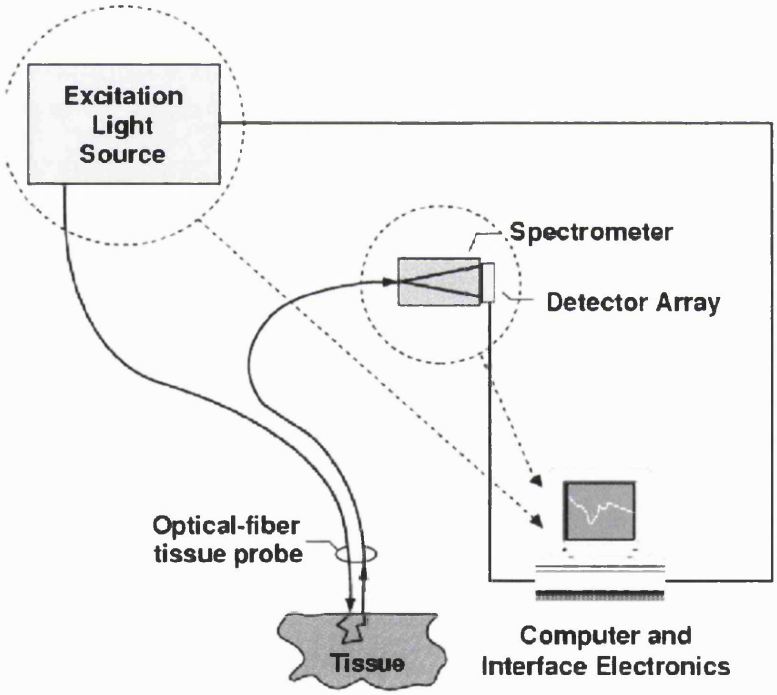

Figure 2-4 Optical system: schematic diagram of the system showing the light source, spectrometer, and representation of the scattering of light from FPCLs (regarded as the tissue under testing).

The wavelength range of the system was from 300 to 900 nm, but the range used for these studies was 320 to 820 nm, which covers the near-UV-

visible part of the electromagnetic spectrum.

The experimental system consisted of an optical probe in contact with the surface of a collagen gel seeded with cells.

The entire measurement process, i.e. activating the spectrometer, triggering the arc lamp, reading the detector array with an analog/digital (A/D) converter etc. is computer controlled by a laptop PC. Typical data acquisition and display time is less than 1 s for each site measurement.

For the optical measurement of CFM lattices a special setup was manufactured in order to allow to insert the probe from the bottom of the culture chamber. This was because it was observed that the lattice tends to sink gradually as compaction increases. The probe height, though, could not be adjusted to be in touch with the lattice surface, as this would cause perturbation of the force reading.

The special CFM setup involved the perforation of the bottom of the chamber whose casting surface was maintained smooth by a glass coverlip laid on the top of the hole. The bottom side of the perforation was glued with a sealing rubber gasket through which the probe was inserted. After gelation the lattice was floated and the coverslip moved away from the hole by a needle. Finally the probe was pushed up till contact with the lower surface of lattice was made. Additionally x-y stage was modified to provide a space for the optical probe.

Chapter 3

Methods development

3.1 Machine Operations

3.1.1 Calibration of the Culture Force Monitor (CFM)

The CFM was calibrated against known dead weights, which ranged between 0.5g and 30 mg (i.e. 29 to 490 dynes). Brand new force transducers were left to thermally soak for a period of 24 hours in the incubator, which were running in standard mode (37 °C, 95% humidity and 5% CO_2). After the initial 24 hours period had expired transducers were thermally conditioned and ready for calibration (a small thermal drift of about 10 dynes was observed). For recalibration of transducer in use (therefore already inside incubators) thermal soaking was not necessary.

Force transducers were positioned horizontally (along the flat side of the beam) and data recording was run for 5 min. Data recording was then stopped to add a calibration weight and then restarted and run for 5 minutes. This procedure was repeated for each weight.

Figure 3-1 shows two typical calibration curves displaying the force generated by the known calibration weights versus the digitalized voltage output from the force transducer. Both calibrations performed using different data acquisition cards showed excellent linearity between voltage and force in the force range used. The linear interpolating line provided the proportionality factor used as calibration factor in the data acquisition front-end. The high linearity was expected in a system such as this because the

force transducer beam acted as a spring. The addition of mass to the force transducer increases the spring energy contained within the system. Removal of the mass resulted in the recovery of the energy with minimal loss to heat and friction. The loading applied to the force transducer was within the elastic limit of the Cu/Be beams and so there was no loss due to plastic deformation.

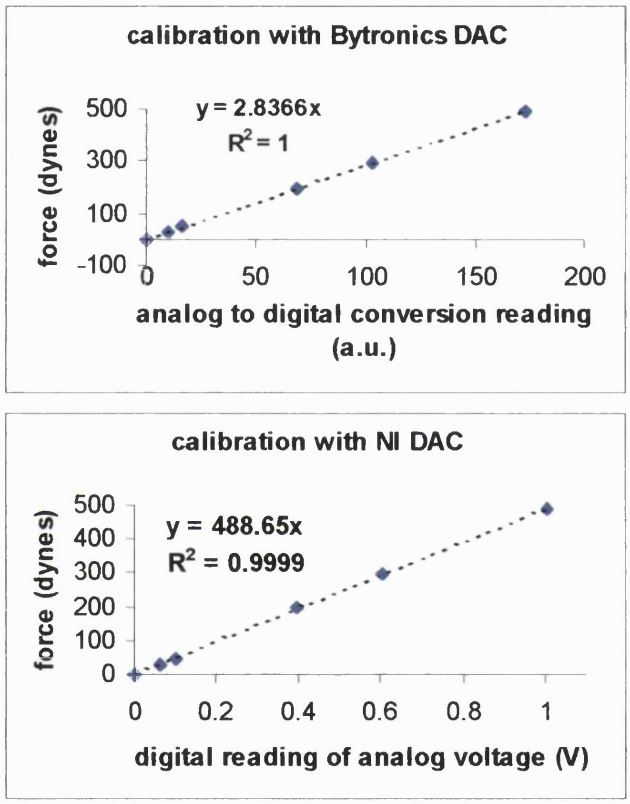

Figure 3-1 Calibration curves of 2 transducers. Data acquisition was done by two different analog to digital converter (ADC): Bytronics and National Instruments (NI). NI ADC provided a digital reading of the actual voltage while Bytronics ADC a directly proportional discrete reading (linear through a calibration factor). Conversion factors were obtained from the slopes of the interpolating lines (dashed). They resulted 2.83 and 488.65 in these graphs.

3.1.2 Baseline cell-free gel contraction

Cell collagen lattices were prepared as described in methods and attached to the CFM. Force was recorded for 24 hours.

Figure 3-2 shows the typical contraction profile of cell-free collagen lattice. Force rose in the initial 4 hours, after which a plateau was maintained till the end of the 24 hours.

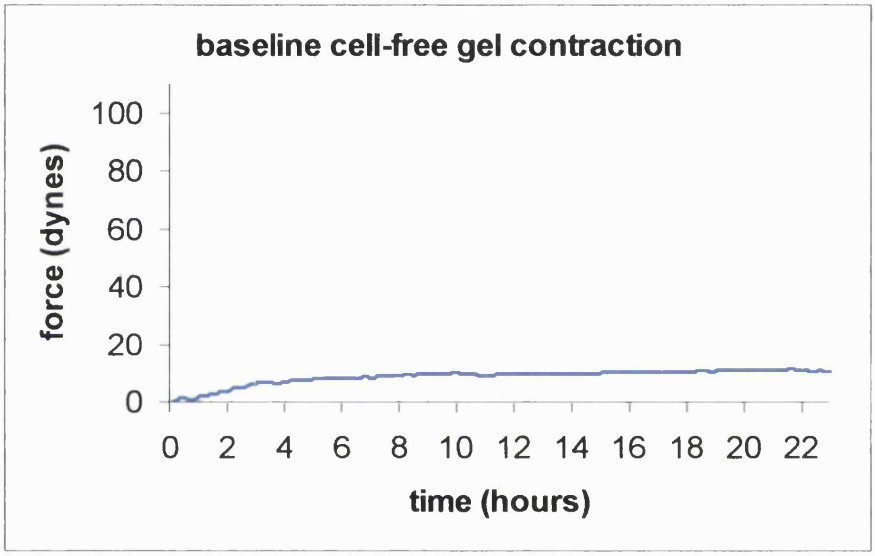

Figure 3-2 Representative contraction profile of a cell-free collagen gel. This was used as the matrix baseline contraction.

This basal contraction was always present and constituted a small percentage of the contraction forces generated by cells. Additionally, since the curve was constant over time, it was irrelevant when relative differences between forces in cell contracted lattices were considered. For these reasons, baseline force has not been subtracted from the contraction profiles which will be displayed in this work.

3.1.3 Calibration of the Tensioning Culture Force Monitor (tCFM) and Interface Adhesion Measuring Device (IAMD)

Force transducers were calibrated in the same way as described for the CFM. For the interface strength measurement (on the IAMD) a thicker beam was used and was calibrated over a larger range of dead weights (up to 10g, i.e. up to 9800 dynes).

The motion of the platform was calibrated against the force output of the force transducer; this was achieved by either a rigid link or cell-free collagen gel as a link between the two components. The programmed motion was activated and the data recorded. To make sure that there was sufficient space to apply the desired displacement to the gels, a spacer of 5 mm was inserted at one end of the rectangular cast and removed after the gel was set. In this way, the possibility that one bar of the gel could reach the edge of the cast well was prevented.

The cycle consisted of loading the collagen gel above the currently registered force by a force corresponding to the reaction to 0.614 mm displacement (i.e. 1.06 % of the total gel length).

The displacement was applied to the matrix by moving the motorised stage and first anchor point away from the force transducer (the other anchorage). Reaction force to 0.614 mm displacement was 40.71 ± 3.66 dynes in cell-free collagen gels. The rate of displacement was 40.92 μm/min (which, translated in rate of loading, was 2.71 ± 0.25 dynes/min for cell-free gels). The force reaction to the applied strain in cell-populated gels was dependent on the cellular remodelling of the matrix, hence on culture conditions. When the total displacement was reached the cycle continued with a 15 minute rest period. Unloading was at the same rate as the loading, again followed by a 15 min resting period.

3.1.3.1 Cyclical Over Loading (COL) in the tCFM

A representative full run of the cyclical overloading on a cell-free collagen lattice and a detail of 5 cycles are shown in Figure 3-3.

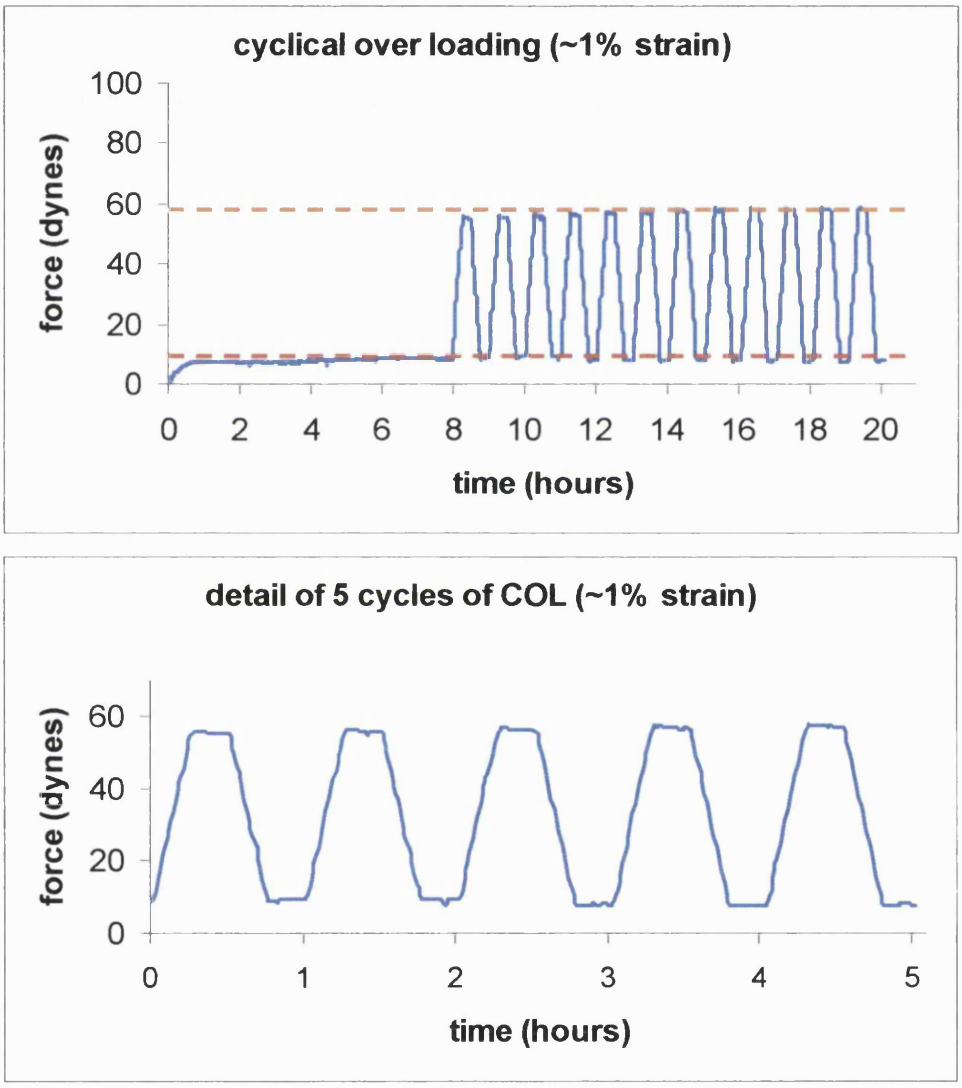

Figure 3-3 Representative full run of the cyclical overloading (COL) program on a cell-free collagen lattice in the tCFM and detail of 5 cycles. The full cycle lasted 1 hour. Each loading ramp consisted in a displacement of 0.614 mm (~1% strain) reached in 15 minutes. Unloading was done at the same speed (stage returned to its original position). Between each ramp of loading or unloading a 15 resting period was inserted.

Figure 3-4 shows that the same displacement and rate of load as in COL applied on stiff link (in place of a collagen lattice).

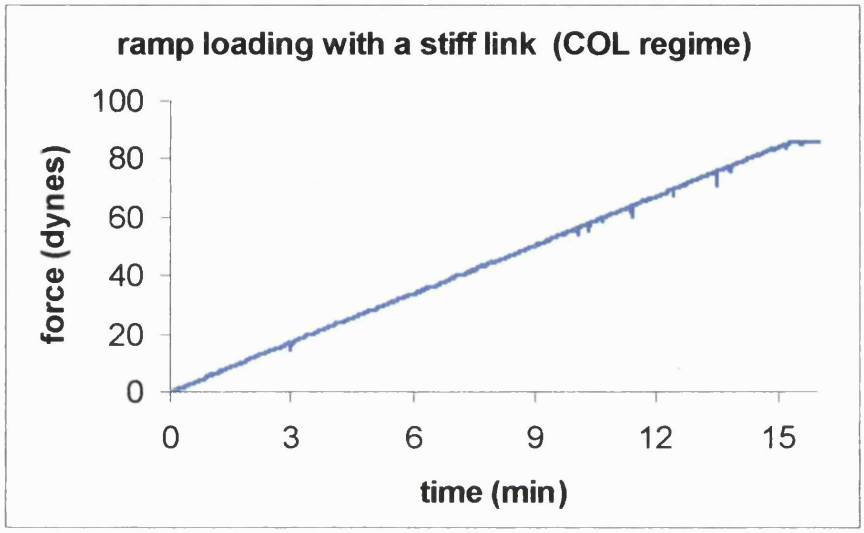

Figure 3-4 Initial ramp loading in a COL cycle. Same displacement and rate of loading were applied to a stiff link connecting force transducer to fix point.

The reaction force to the ramp in displacement was 82.60 ± 0.63 dynes, that is about twice the reaction force generated by the collagen lattice.

This showed, as expected, that the collagen lattice generated a lower reaction force than the stiff link for the same applied displacement. Since the stiff link was inextensible compared to the force sensor, the force measured can be considered to be determined solely by the displacement of the beam of the force transducer. The linearity of force ramps and the flat resting period with virtually no relaxation for collagen lattice - similar to the stiff link - indicates that, mechanically, the lattices behaved like a linear elastic material in the regime of loading (1% strain in 15 minutes) applied.

3.1.3.2 Ramp loading in the IAMD

Force transducers were calibrated similarly to the CFM, but at room temperature. Additionally thicker Cu/Be beams were employed for the force sensor and a greater range of weights (up to 10 g) was used for calibration.

The motor was programmed to move at a speed of 0.05 mm/sec (or 3 mm/min) along a total displacement of 25 mm (therefore the distance was covered in 8.33 minutes). When a stiff link was used to connect the force transducer to the stage, the reaction force was over 10000 dynes, hence over the calibration limit. However this was not relevant to the current application where that level of force was never reached as interface failure occurred always before (see chapter 6 for details). Whether higher forces were needed to break the interface constructs, thicker transducer beams with greater force range could have been fabricated.

3.2 Elastic versus viscoelastic behaviour of the collagen gel matrix

The known viscoelastic behaviour of the collagen lattices was tested in the tCFM in order to determine a loading regime in which linear elastic conditions could be maintained.

The strain amplitude was maintained constant and the strain rate was varied. Two rates were employed: slow, 40.92 μm/min (or 2.45 mm/h); and fast (i.e. 100 times faster) 4092.5 μm/min (or 245.5 mm/h).

Figure 3-5 shows the average response to ramp strain and resting period used in COL regime. Note the near horizontal force after at the constant strain showing that force was retained elastically by the lattice.

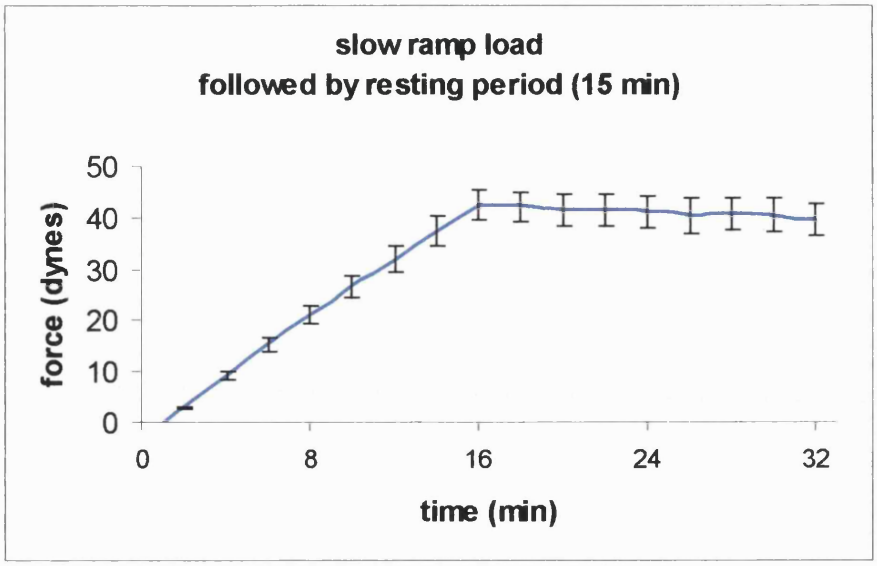

Figure 3-5 Strain ramp (~1%) at slow speed (2.45 mm/h). Vertical bars are SE (n>3).

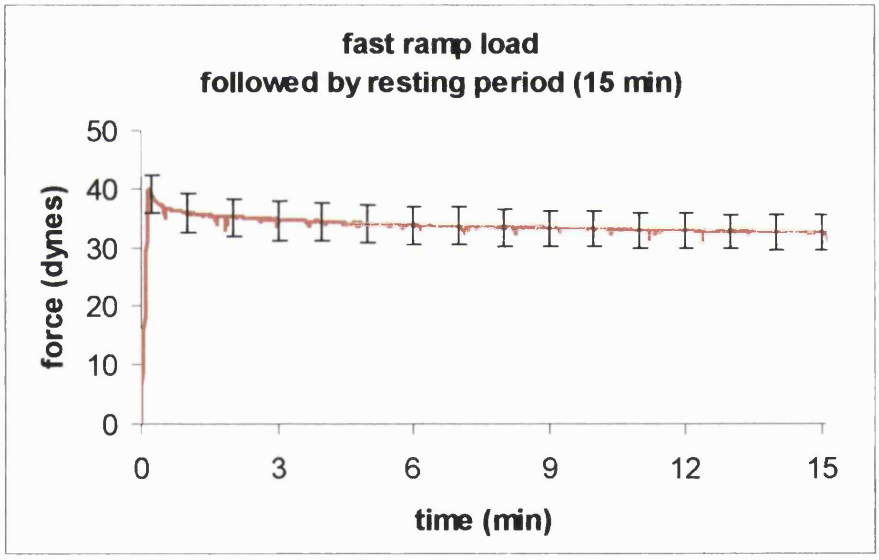

Figure 3-6 Strain ramp (~1%) at high speed (245.5 mm/h). Vertical bars are SE (n>3).

Figure 3-6 shows the average response to ramp strain and resting period used in 100 times more rapid loading speed compared to COL regime. Note the rapid force relaxation at constant strain showing that viscoelasticity behaviour was predominant. The total force drop over the

resting period was 2.86 ± 0.61 in the COL regime (and 7.88 ± 0.33).

The accuracy of the linear interpolation in the 7.5 minutes following was high for $R^2 = 0.98$ and low $R^2 = 0.77$ for slower and faster stretching respectively. Concerning the timescale, 80% of relaxation happens within 14.5 minutes in slow loading and within 4.5 minutes in fast loading.

In total the stress relaxation in the fast ramp loading is 2.75 fold greater than the slow ramp. However, it is not the absolute difference in force drop that matters here but dynamics of the relaxation. A fast ramp load causes a steep exponential decay curve (i.e. relaxation) that reaches its asymptotic value rapidly, (increases with stretching ramp speed). The asymptotic value is the relaxation at infinite time, which is normally well approximated with finite timeframes over which the force drop over time is less than a certain percentage. When the strain is brought back to zero the typical phenomenon of hysteresis will be evident, i.e. the force will not go back to its value before the loading but will be less, showing that the material has been permanently deformed (plastic deformation).

Hysteresis due to repeated cycles at relatively low frequency

It has been shown the stress relaxation response to strain applied at rates 100 times faster produces significant differences in the single ramp test. However even at lower loading rates such as 5 times greater than the COL, the effect of hysteresis can be seen (Figure 3-7). The trend lines located on the baseline force and on the upper level of the force response to load show that energy is accumulated (lattice increases apparent stiffness). Therefore not only the single cycle must be examined in term of speed of ramp loading versus relaxation but also considering the effect of the accumulation of cycles. In conclusion the chosen regime of cyclical load (COL) showed to maintain the material response in the elastic range that is highly desired if the cell force response to the loading is to be investigated.

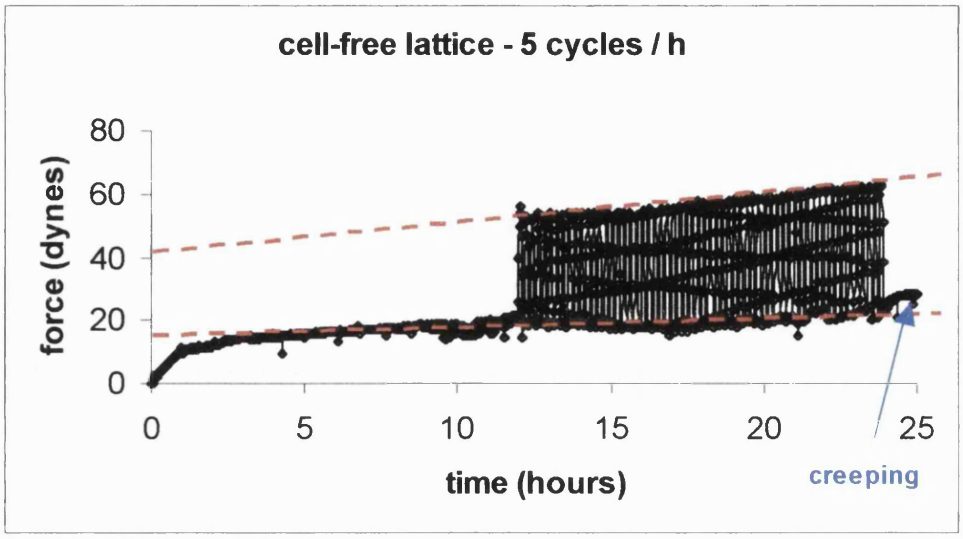

Figure 3-7 Representative full run of the cyclical loading program on a cell-free collagen lattice in the tCFM at a speed of 5 cycles / hour. Each loading ramp consisted in a displacement of 0.614 mm (~1% strain) reached in 3 minutes. Unloading was done at the same speed (stage returned to its original position). Between each ramp of loading or unloading a 3 resting period was inserted. Note the trend lines (red dashed lines) showing how the amplitude of the cycles increases indicating that an hysteresis effect is present and energy is accumulated (lattice increases apparent stiffness).

3.3 Theoretical calculation of the actual strain applied by the tCFM

As stated above, the total displacement applied to the collagen lattices during cyclical loading was 1.06 % of their total length, which is equivalent to a nominal 1.06 % strain. However, this is a rough estimate that does not take into account the displacement of the force transducer beam under load that reduces the actual gel displacement. Thanks to the linear response of the transducer we could easily calculate the total deflection of the transducer beam using the classic beam theory (Callister, 2003). This relates maximum displacement of a beam to the applied load and the

properties of the beam (including length, inertia and elastic modulus) as shown schematically in Figure 3-8.

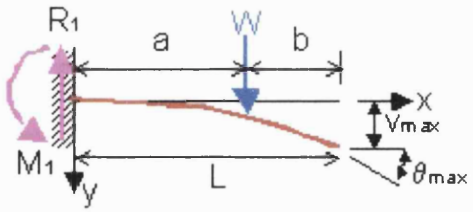

Figure 3-8. Schematic representation (under classic beam theory) of an ideal beam of length L, fixed at one end, under a load W.

$$\upsilon_{max} = \frac{WL^3}{3EI}$$

where:

u_{max} is the maximum displacement of the unconstrained extreme of the beam from the original point of resting (Figure 3-8).

W is the load applied to the beam

L is the total length of the beam

E is the elastic modulus of the beam material

And I is the inertia expressed as:

$$I = \frac{wh^3}{12}$$

where w and h are the width the thickness of the beam.

The known parameters in our system are:

u_{max}= 0.613 mm = 0.0613 cm

L=85mm = 8.5 cm

w=10mm = 1 cm

h: h1=0.15, h2=0.39 mm or h1=0.015, h2=0.039 cm

$E_{copper\text{-}berillium\text{-}CA172}$ = 131÷117 GPa = 1.24 10^{12} dynes/cm^2 (mean value)

Knowing u_{max} the load W can be easily derived from:

$$W = \frac{\upsilon_{max} 3EI}{L^3}$$

Figure 3-9 shows the force-displacement curves for 2 transducer beams having thickness h1=0.15 mm and h2= 0.25 mm. The blue and red lines represent the calculated curves. Circles and squares represent the measured average values for h2 and h1 respectively. Dashed lines are the linear interpolations of the measured points (R^2 =0.9998). The ratio between the measured elastic moduli of the 2 transducer beams was 4.53 ± 0.01 with an error of 2.18 % in respect to the ratio of the calculated elastic moduli (that was 4.63).

The measured curves were overall always lower than the calculated. This difference at the peak of applied strain was 19.92% ± 0.16 % for h1 beams and 21.67 ± 0.24 % for h2 beams.

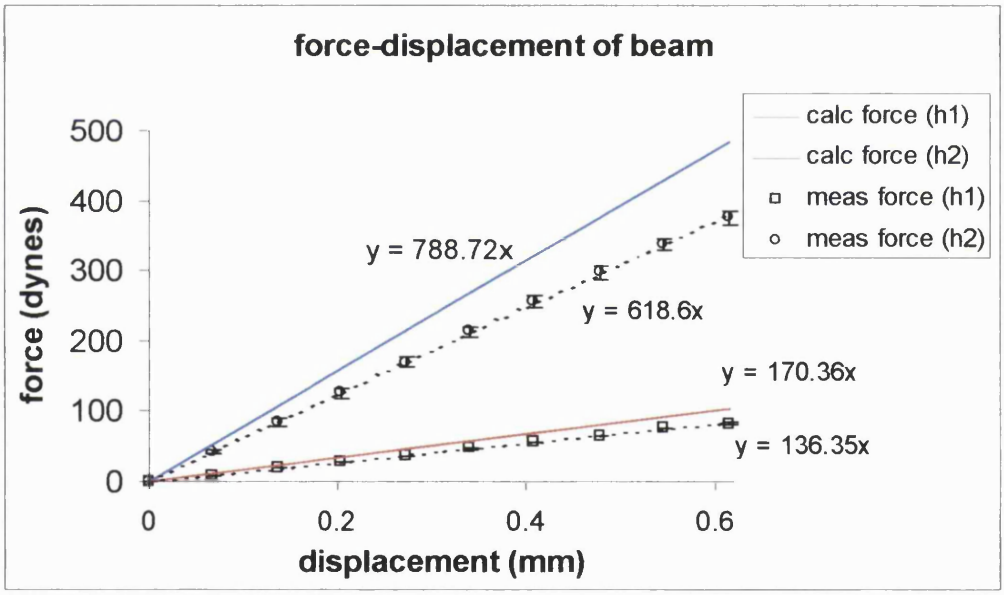

Figure 3-9 Force-displacement curves for 2 transducer beams having thickness h1 = 0.15 mm and h2 = 0.25 mm. The blue and red lines represent the calculated curves. Circle and square markers represent the measured values for h2 and h1 respectively (average of 3 repetitions). Dashed lines are the linear interpolations of the measured points (R^2 =0.99).

The theoretical curves could be used to calculate the exact strain applied to the collagen gels on the tCFM, providing a general overestimation

around 20% above the measured values. This is valid independently from the thickness of the force transducer beams used.

The reason for the difference between measured and calculated values might be due to some geometrical imperfection of the system causing losses in the reaction force. Nevertheless, this systematic error showed to be constant between different beams and machines used for this test. Hence, the calculated curves could be used to obtain the actual strain applied to the gels during measurement of engineering stiffness, due the knowledge of the systematic error and the near perfect linearity of the system.

Additionally, these calculations may be used to optimise the use of the different transducer beams depending on the application. For instance, where strain higher than 1% are to be applied to gels, a thicker beam is more appropriate to ensure that the nominal displacement of the tCFM stage is reflected in a similar actual displacement of the gel.

3.4 Stiffness measurement of cell-free collagen gels

Elastic modulus was measured by applying a 1.06% strain to the collagen lattice in situ at slow constant rate (2.45 mm/h or 4% strain/h).

Figure 3-10 shows that the reaction force to 1.06% strain rose from slow to fast strain and from compliant to stiff force transducer beams.

The elastic modulus calculated from the force response is shown in Figure 3-11. Again the same trend as in the force graph was seen, with modulus rising from slow to fast rate of loading and from compliant to stiff beams.

Increase in stiffness is known to depend on the rate of strain applied in viscoelastic material such as collagen lattice (Callister, 2003). The higher the rate, the higher the instantaneous elastic modulus. Instantaneous

means at the top of the strain ramp as soon as the strain reaches its peak. From this peak a relaxation is known to occur along which force reaches a steady level asymptotically (also called relaxation modulus).

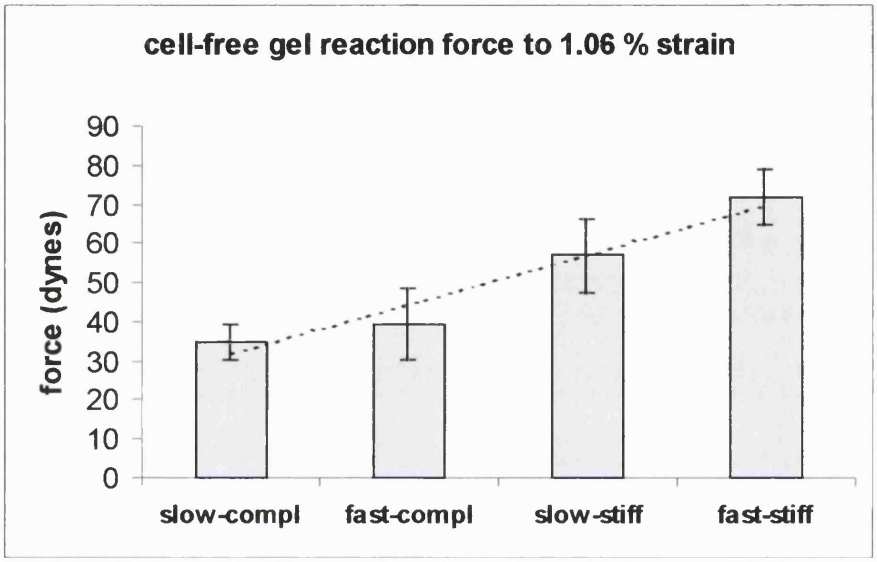

Figure 3-10 Force reaction to 1.06% strain (applied by a displacement of 0.613 mm of the linear table) applied at 2 speeds: slow (2.45 mm/h) and fast (24.52 mm/h). Force transducer Cu/Be beams were used with 2 different mechanical configurations: compliant (0.15 mm thick beam) and stiff (0.25 mm thick beam). Force response rose from slow to fast strain and from compliant to stiff beams (trend marked by the dashed line).

The differences in the elastic modulus due to the stiffness of the force transducer beams, however, were undesired since the measurement of mechanical properties must not change depending on the measuring system. This problem was solved by correcting the force reading using the calculations above (section 3.3). The correction showed that there was an increase in the actual displacement of 4.5 folds due the different beams.

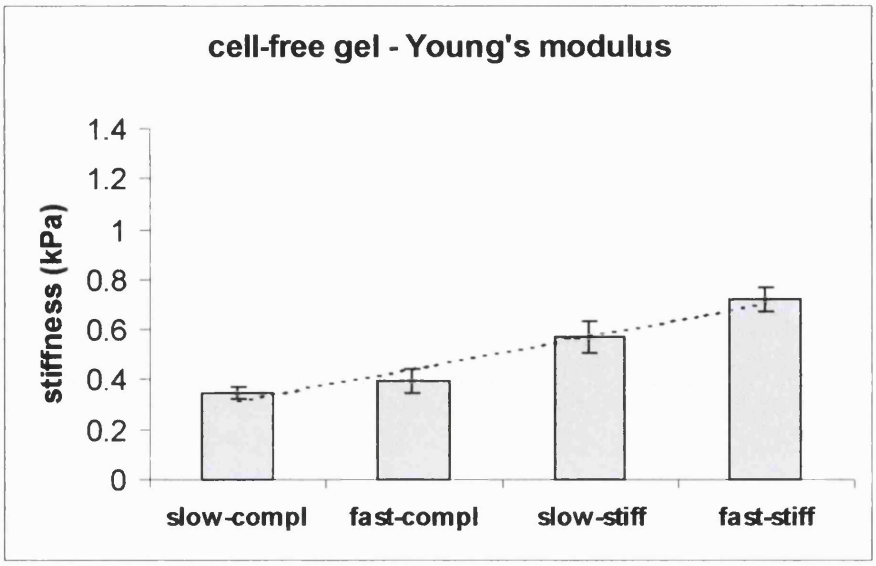

Figure 3-11 Elastic modulus calculated from Figure 3-10 by dividing the force values by the cross section of the lattices (considered invariant at this very low strains) and the strain value (i.e. 0.01). The same trend (marked by the dashed line) as in Figure 3-10 was seen in Young's modulus rising from slow to fast strain and from compliant to stiff beams.

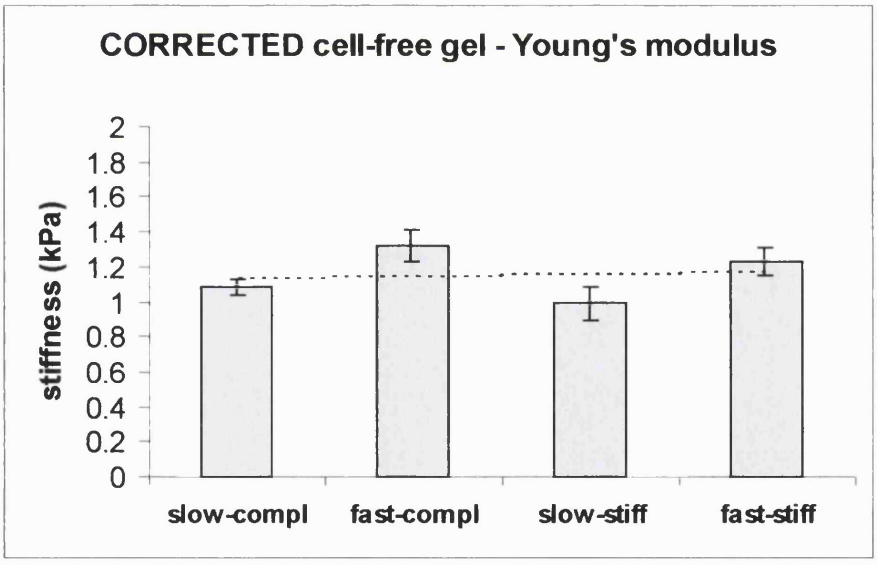

Figure 3-12 Young's modulus as in Figure 3-11 recalculated to account for the different deflection of the compliant and stiff force transducer beams. The trend (marked by the dashed line) changed from Figure 3-11. Mean values of Young's modulus were equalised (nearly flat trend) and appeared independent not only from the thickness of the beams but also from the rate at which strain was applied.

Figure 3-12 shows that Young's modulus were equalised by the normalisation of the force response to the actual displacement applied to the lattices.

The mean values of elastic modulus obtained with beams of different stiffness but at the same loading rate were not statistically different. This shows that measurements were independent from the stiffness of the beams used in the force sensor. An increasing trend was observed between the elastic modulus and the rate of loading, consistently with the theory of viscoelasticity; however at the rate used in this test the differences were not statistically significant.

3.5 Measurement of the local strain in the matrix at microscopic level

Collagen lattices (without cells) were prepared in H-shaped culture chambers. Confidential markers (made of segments of thin metal wire) were deposited in the lattices before gelation in order to test the relative displacement of these in respect to the macroscopic displacement of attachment bars at the extreme of the lattice. The culture chamber was positioned on the stage of an inverted light microscope (Zeiss, UK). One attachment bar was blocked within the culture chamber (in one recess of the H-shaped mould) and the other connected through A-frame to an external fix reference point. Strain was applied by displacing the stage of the microscope through a micrometer

Figure 3-13 shows the relation between macroscopic and microscopic strain (computed from the measured displacement). It is clear that in the initial phase there was an amplification of the microscopic strains compared to the applied macroscopic strains (3% macroscopic strain resulted in 10% microscopic strain). After this initial phase, macroscopic and microscopic

strains progressed linearly with a correspondence 1 to 1 for each step in increasing macroscopic step. This demonstrated a high uniformity in the collagen lattice. The non uniformity at low strains (0 to 3% macroscopic strain) could be due to local anisotropy of both fibrillar collagen matrix and markers. Markers consisted in short segments (<1 mm) of very thin metal wire (0.1 mm diameter). These segments might be subject to a large reorientation as soon as strain is applied which is stabilized as soon as these segments become aligned to the axis of load. This could be joined to a reorientation of local fibrils which would enhance the locally perceived strain. However the size of markers was two orders of magnitude greater than the local fibrils and hence the effect of fibril reorientation on the reorientation of markers can be neglected. Further tests should be performed with smaller round markers.

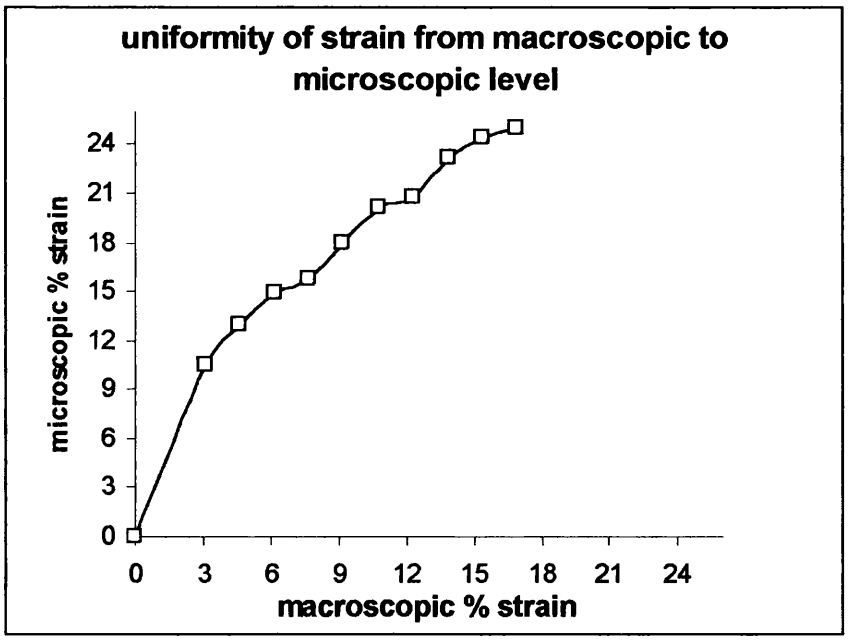

Figure 3-13 Uniformity of strain from macroscopic (applied to the lattice through the attachment bars) to microscopic level (strain measured by the displacement of markers embedded in the gel). After 3% at macroscopic level, strain increased in parallel at the same rate (gradient was 1.06) at both level (linear interpolation above 3% had a small error R^2=0.99). Below 3% strain, there was an amplification of microscopic strain by a factor 3.4.

In conclusion this test showed that collagen lattices have high mechanical uniformity. Additionally it demonstrated that strains applied at the ends of the lattices through the attachment bars are transferred linearly into the matrix at microscopic level and therefore to the cells.

Finally the anisotropy of the markers evidenced that, in anisotropic conditions, amplifications of microscopic strains at low macroscopic strains can be expected.

3.6 Automated image analysis for the measurement of gel compaction

In order to automate the measurement of gel area during contraction an image acquisition and analysis procedure was developed.

Image acquisition was achieved by the connection of a fibre optic camera (Scopeman 504, Moritex, UK) to a Power Mac 7600 by a standard frame grabber (resolution 1024 X 768). A procedure (or "macro") was developed under the NIH Image platform (a standard free software package for image analysis). The macro allowed to automatically acquire pictures sequentially in real time and produce a result text file storing the main measurements performed (also previously saved images may be used). The method developed was optimised for back illuminated samples with round shape (in circular Petri dishes or multiwell plates) and the principle could be extended to any shape.

The algorithm used a circular region as a reference area that included the area of the sample. This is set interactively for the first sample. Then for each image the program performs an automatic segmentation using an optimised threshold which can be further modified interactively from the user to correct for possible changes in background illumination and grey

levels. Once segmentation is approved by the user, the procedure generates automatically the value of the area, major and minor axis in pixel and writes this values to a text file. Then interactively the user is asked if another picture is to be analysed or the image processing is terminated. The full program code is reported in appendix B.

3.7 Image analysis procedure to quantify alignment in CLSM and SEM images

A custom-made computer procedure based on the spatial Fourier analysis was developed with the aim to estimate the degree of 3D anisotropy in CLSM and SEM projection images (2D projections of 3D scan).
The algorithm generated an orientation index (OI) ranging between 0, i.e. perfect parallel orientation, and 1, i.e. perfect random orientation. A similar method, applied to CLSM images only, has been shown to lead to a superior measurement of collagen orientation compared with histological evaluation by several experts (van Zuijlen et al., 2002). The automated procedure produces a power plot (result of Fast Fourier Transform, FFT) of random selected square areas taken from the original image. This new image contains an ellipse whose width/length ratio provides an estimate of the anisotropy (de Vries et al., 2000).

Figure 3-14 shows an example of the power plot images generated for from two representative SEM images for two conditions: well aligned fibres (upper triplet) and randomly orientated (lower triplet). The power plot changed shape from a very elongated ellipse to a near perfect circle. The images at the end of each row represent the result of the algorithm which, after a few filtrations to remove noise from the power plot, produces a binary image in which the object to be quantified is composed of pixels

having grey levels above an automatic threshold.

All the processing is done rapidly (~ 5 sec) by running two procedures loaded as macros in Scion Image (PC version). Results are automatically stored in a text file for further analysis. The procedure is attached in Appendix C.

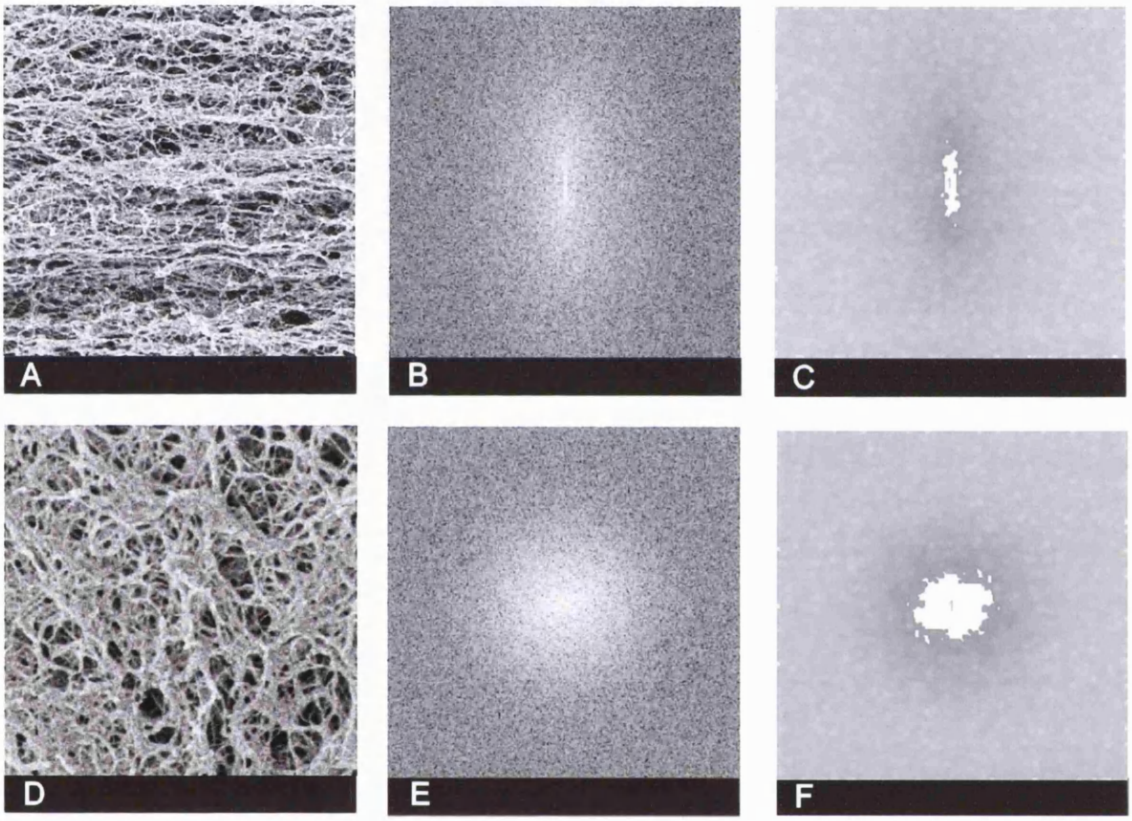

Figure 3-14 Automated quantification of anisotropy and orientation through image analysis. The pictures in each row represent the step of the algorithm for image analysis. Square selection 256 X 256 pixels from SEM images (A, B) were FFT transformed (B, E). The power plot was than processed (C, F) and the axis of the obtained ellipses were ratioed in order to obtain OI (OI was 0.13 for C and 0.81 for F). The axis of alignment in the starting image (A, D) was parallel to the black bars at the bottom of the images.

3.8 Acquisition of the baseline back-scattered spectrum to set the reference spectrum.

Prior to any spectral measurements of collagen lattices, the ESS system and probe were calibrated with a reflectance standard (Spectralon™, Labspere, Inc., North Sutton, NH) which had a spectrally flat, diffuse reflectance >98%, over the entire wavelength range of the system (i.e. 300 to 900 nm). The typical overall system response to the spectral standard is shown in Figure 3-15.

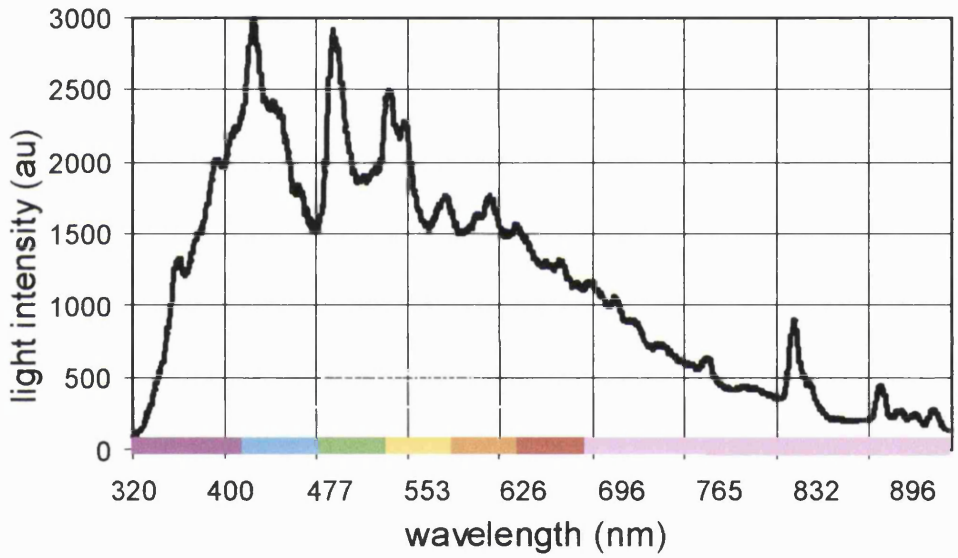

Figure 3-15 Typical overall system response to the reflectance standard (Spectralon™) between 320 and 900 nm. The features present in the spectrum are only function of the system transmission/measurement characteristics.

The purpose of referencing the system to a known standard is to normalise the spectral data against the overall system response. This technique effectively minimises any variations in the spectral transmission among different probes, thermal effects, coupling efficiency of the probe, drifts in detector/spectrometer response, etc. The reflectance standard and probes were sterilised by 70% ethanol soaking for 1 hour.

3.9 Development of collagen-bases interfaces: from fracture model to wrapping model

The development of collagen-based interfaces evolved through two models called *fracture* and *wrapping* model. The difference between them lies mainly in the way the gel-to-gel interface was generated.

Both models were based on 3D collagen gel substrata and relied entirely on the migration of cells from a cell-seeded side of the interface to a cell-free side. The hypothesis was that their migration would initiate and bring about mechanical integration of the two gel sections. In both models the key parameter was the mechanical integration, measured as the ultimate strength of the interface (i.e. the stress needed to completely break the interface).

3.9.1 Fracture model

3.9.1.1 Model concepts and assembly method

The fracture model was based on the generation of two fracture lines within a standard CFM gel. These lines contained a reduced amount of matrix (compared to the rest of the gel) and constituted the mechanically weakest point of the construct. Figure 3-16 represents schematically an assembled dual interface construct generated using the fracture model. The central cell-seeded compartment was separated from the two cell-free compartments at either side by two stainless steel barriers during casting and then by fracture-interfaces. The entire construct was attached at both ends to connectors (e.g. attachment bars) for further mechanical testing. Blocking connectors in the culture chamber, hence the total length of the interface construct, produced a tension across the construct as the central compartment was contracted by resident cells.

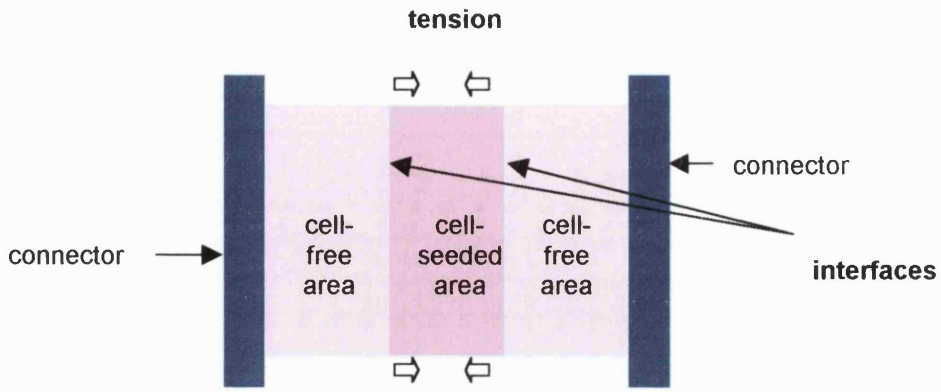

Figure 3-16 Sketch of the dual fracture interface construct. Note that tension developed in the construct due to cell-mediated contraction of the central compartment, if the connectors are blocked.

The fracture lines were generated by modulating the integration of opposing layers. This was achieved by increasing the time for which the new and existing gel compartment were separated during setting time for the new section of the gel. The longer the time the barriers were left in place, the less baseline integration was achieved. This technique, which depends on a constant gel setting time, required the development of rigorous protocol of collagen gel buffering to obtain good reproducibility. Parameters affecting gelation such as room temperature and quantity of gel neutralising agent, were kept constant (room temperature at 20 °C and neutralising agent determined as described in chapter 2). The setting time was determined empirically to 1 minute at 37 °C. The criteria for determining this time were that the components would not detach as the medium was added, but would not mix producing an integration which was too strong. Attachment bars and barriers were placed in the H-moulds and the liquid gel was poured in the 3 compartments generated by the barriers. The lateral compartments received a volume of 1.8 ml cell-free gel, the central one a volume of 1.5 ml cell-gel solution (concentration 1 millions cells / ml). Then culture chambers were promptly placed in incubators (at 37 °C, 5% CO_2). As 1 minute

incubation period elapsed, barriers were removed from the culture chamber directly inside the incubator (hence with the least movement of the construct which would cause gel mixing). The interface constructs were then left in the incubator until completely set. After full gelation 25 ml of complete culture medium were added and the culture chamber returned to the incubator.

Figure 3-17 shows assembled dual fracture interface constructs and the custom made chamber (left picture) employed for assembling them. Once the construct was assembled two mechanical configurations were possible. The first was to allow the cells to contract the central part freely by letting the entire construct floating untethered in the culture media (Figure 3-17, right picture). The second was to anchor the connector bars attached to each end of the construct so that its length would remain constant. This isometric contraction generated tension through the construct (Figure 3-17, left picture).

The tensioned construct appeared a very efficient way to obtain an engineered (ordered and orientated) structure, based only on endogenous cell contraction. Additionally it was hypothesised that the gradual orientation of collagen fibrils in the system would increase the cell migration efficiency.

Both tethered and untethered options showed inherent problems connected to the contraction of the central component. The large deformations of the central compartment, generated in the untethered configuration, caused difficulties in evaluating the cross-sectional area of the interface. Hence, this effect caused problems in the estimation of the interface ultimate strength compared to time zero baseline (non deformed). The tethered configuration produced less deformation (Figure 3-17, left picture) than the untethered. However this carried additional difficulties involving the need to achieve a basal break strength which was able to resist the tension between the opposing layers. This basal break strength had to be limited, though, since too strong basal integration caused significant mixing of the opposing parts in which the interface fractures

were "lost" in a continuum perfect integration. Methodologically the effect of tension in tethered constructs also caused additional complexity and other parameters needed to be controlled e.g. cell density and serum concentration.

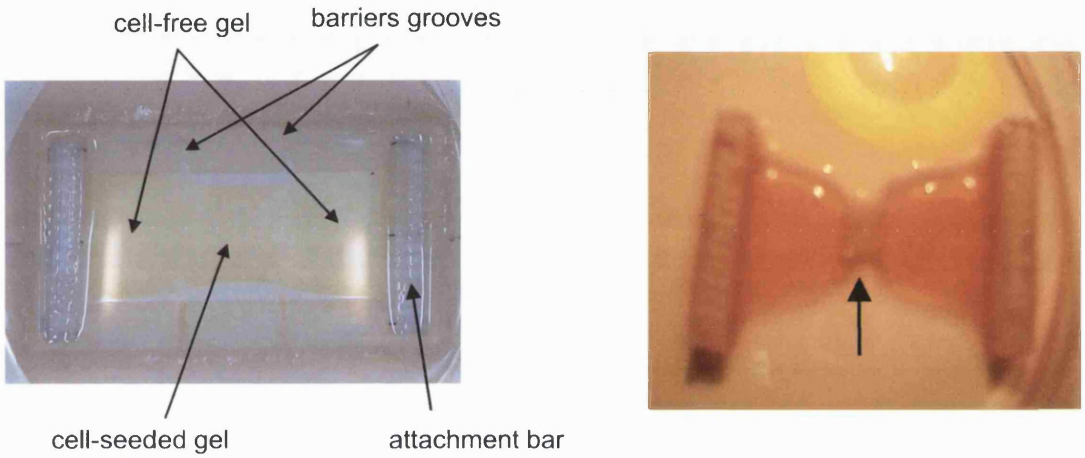

Figure 3-17 Photograph of formed dual fracture interface construct in tethered (left picture) and untethered (right picture) configuration. Shrinking of the central cell-seeded compartments was due to cell-mediated contraction. Note the heavily deformed central compartment arrowed in the untethered construct.

3.9.1.2 Mechanical test of the interface ultimate strength

The basal interface ultimate strength (i.e. at zero time culture) was tested by a stepped loading till the construct failed.

In order to test the interface break strength, the construct was placed in the large petri dish to permit the long displacement necessary to reach the failure point. The construct was anchored to a fix point at one end and to a force transducer at the other end. The fix point was then moved manually stepwise by a micrometer (with fixed steps of 0.1 mm on the x-y stage) at regular time points (1 step/min). Force was recorded in the CFM until failure. Failure was confirmed by visual inspection (Figure 3-18).

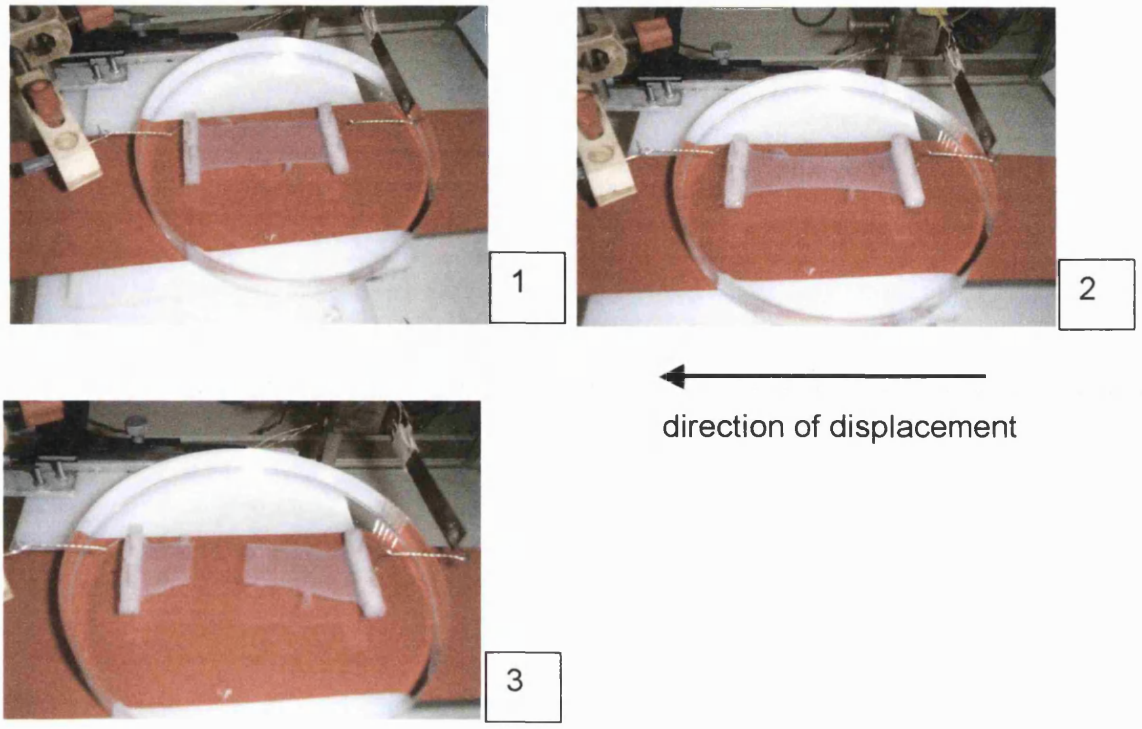

Figure 3-18 Sequence of the failure point measurement. The anchor point (left hand side) was moved stepwise (1 mm step/min)by a micrometer away from the force transducer (right hand side). This caused the internal stresses to increase until the weakest point failed. The time course of the test was between 25 and 30 minutes.

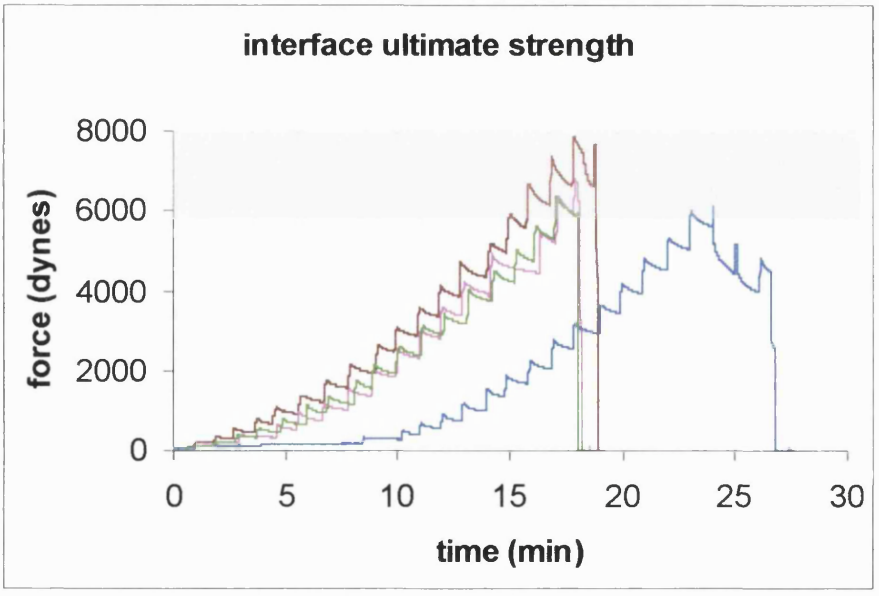

Figure 3-19 Ultimate strength measurement of baseline interface constructs (no cells in the central compartment). The grey band represents the variability among them.

Results of these fracture tests performed are shown in Figure 3-19. A remarkably high force (average force was 8153.13 ± 928.86 dynes, n=4) was required to break the collagen-collagen interface. This was much higher than typical cellular contraction force. Most importantly there was a considerable band of variation between replicate interface samples.

This showed that the fracture model produced reproducible fracture at the collagen-collagen interfaces (rather then the bulk or collagen-bar interface) but with the high forces compared with the range of cellular contraction forces.

This led us to discontinue the fracture model as unpromising for measurement of cell-mediated integration and remodelling. In fact this variability was expected to be increased by the tension (in the tethered model) or large deformation (in the untethered model) caused by cell-mediated contraction. However, basic protocols, gel casting and break strength measurement from this model were central to the development of the final model: the wrapping gel system.

3.9.1.3 Cell migration tracking by light and fluorescent microscopy

The fracture model was also useful to test if cell migration across the interface could be tracked without stopping the construct cultivation or disturbing it. Phase contrast microscopy provided very limited information about cells due to the non-uniform background formed by the fracture interface. However fixation and staining (toloudine blue) gave good cell definition providing basic information about cell movement and redistribution with time. Figure 3-20 shows a fracture interface (tethered model) down to microscopic level after 5 days in culture. Cells travelled from the very dense, compacted gel on the left hand side towards the less dense gel on the right hand side via the low density matrix of the interface zone.

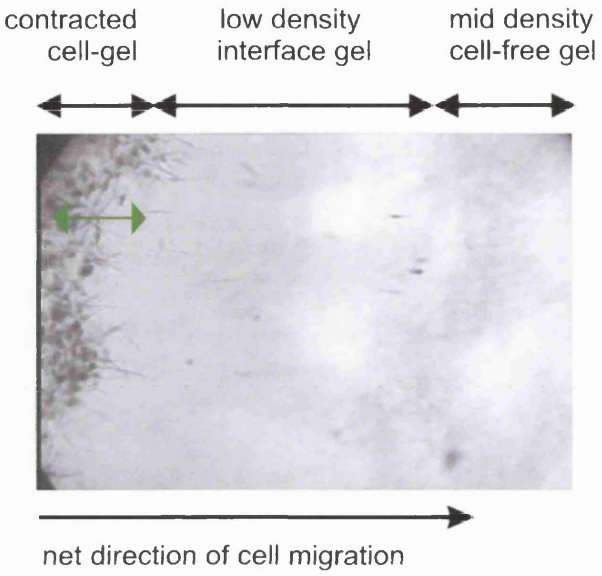

Figure 3-20 Low power micrographs showing cells (toloudine blue stained) stretching from the cell populated side towards the cell free side (3 areas are shown along the fracture line). The interface construct was cultured for 5 days. Then fixed, stained with toluidine blue and imgaged under phase constrast microscopy. Total magnification 100 times.

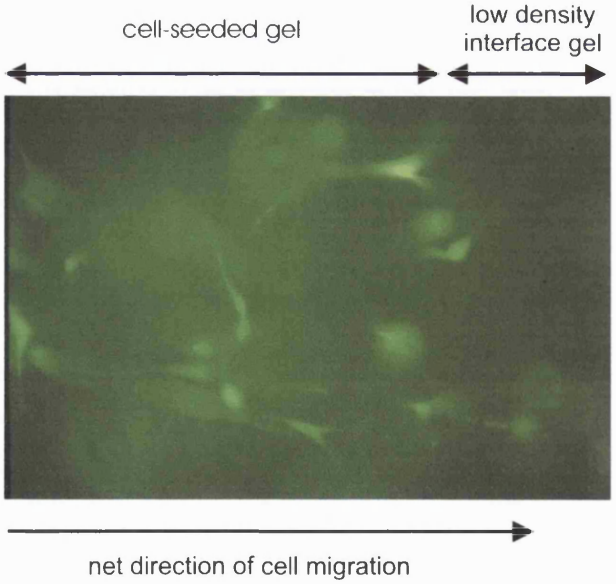

Figure 3-21 Fluorescence micrograph showing cells (tracker dye loaded cells) at the fracture interface boundary, comparable with that indicated by the green bar in figure 3-20. Living cells were imaged at day 5 at low power. Total magnification 250 times.

In order to image and follow cell migration without interrupting the experiment a vital fluorescent cell tracker dye (CellTracker™ green, Molecular Probes Europe, NL) was used (Figure 3-21).

Figure 3-21 shows cells loaded with cell tracker dye packing at the edge of the interface area. The main problem was to correlate the position of the labelled cells with the exact location of original interface between the gels which was completely invisible by this technique.

Additionally due to the 3D structure it was very difficult to obtain in focus images, indicating that confocal microscopy would have been more suitable for this work.

3.9.1.4 Conclusions on the fracture model

The fracture model generated reproducible fracture at the collagen-collagen interfaces (rather then the bulk or collagen-bar interface) and showed that gel-gel interface strength can be regulated even if with some variance. The model was discontinued mainly due to the unexpected problems caused by the contraction of the cell-seeded compartment which increased variability in interface ultimate strength. The fracture model also proved useful in showing that migration did occur across the interface, although it was difficult to track.

The built-in difficulty in this experimental setup suggested to discontinue the concept of controlling the integration of the interface by tuning the gel setting time. Generating interfaces based on complete gel setting, hence independently from the setting time, appeared a much simplified, hence more robust experimental setup. This concept led to the development of the wrapping model.

3.9.2 Wrapping Model

The "wrapping model" is a bi-functional interface between a cell-seeded element embedded into a cell-free collagen gel. The baseline adhesive strength between the two gel components was the bonding strength which formed at time zero.

Preparation of the cell-seeded pre-contracted lattices

Cell seeded collagen gels were prepared similarly as described for the Culture Force Monitor (CFM) experiments. Briefly a collagen gel mixture composed of 6 ml of acid soluble collagen type I (2.20 mg/ml, First Link, UK) and 0.750 ml of 10X DMEM (Gibco Life Technologies, UK) was neutralized by 235.5 µl of 5M NaOH. While still in liquid form, 5ml of the collagen gel were mixed with a 0.5ml suspension of 5×10^6 tendon fibroblasts. The rest of the gel was used to pre-coat two floatation bars fabricated with layers of polyethylene mesh sheets (10 holes per inch type, HeeBee Designs, UK). The collagen-cell suspension was poured into a H-shaped mould (H size:4 × 0.5 cm ; rectangular size: 6.5 × 2.5 cm) fabricated from Derlin™ blocks (Intertech Ltd, UK) and incubated in a 37 °C in a 5% CO_2 humidified incubator for 20 minutes. As the gel sets, the floatation bars – positioned along the H edges of the mould – integrate with it. Finally the set gel is topped with 20 ml of complete culture media supplemented with 50 µg/ml of ascorbic acid. These rectangular gels were cut in the middle with a surgical scalpel before being topped up with media and then released from the bottom of the mould. In this way the two identical pieces were allowed to contract freely in the absence of tension for 48 hours. This time point was chosen as the earliest point after which there is no significant further gel shrinkage and the gel could be considered to have stable shape and dimensions (data not shown).

Killed pre-contracted gels were prepared by (after 48 of cultivation) by substituting the media with distilled water for 2 hours and then replacing

the media to re-equilibrate pH.

Interface generation

A new culture chamber was designed and fabricated from Derlin™ blocks (Intertech Ltd, UK). This allowed vertical casting of the cell-free wrapping gel and the ability to use the device horizontally immediately after the interface was formed. The interior was T shaped with two communicating wells of different volumes (4 × 2.5 cm and 4 × 5 cm, both 1.5 cm deep). A cover was fitted and sealed perfectly into the narrower well, generating casting volume of 3.7 × 2.5 × 1cm. This allowed vertical insertion of the pre-contracted cell seeded gel into the cell-free wrapping gel from the upper uncovered larger well. 8 ml of cell-free collagen gel (prepared as above) were poured into the sealed-closed narrower chamber after an attachment bar was positioned at the bottom (figure 1). As the cell-free collagen gel set (after half hour of incubation at 37 °C in a 5% CO_2 humidified incubator), it formed a solid wrapping around the pre-contracted component and the culture chamber was positioned horizontally, the cover was removed and 25 ml of complete culture media supplemented with 50 μg/ml of ascorbic acid was added. From this point the interface constructs were incubated 37 °C in a 5% CO_2 humidified incubator for 7 days until final mechanical test of the adhesion strength. This test and the newly designed chamber are described in greater detail in chapter 6.

Chapter 4
Cell-mediated matrix remodelling

4.1 Methods

All materials and methods used were as described in chapter 2 and 3.

4.2 Results

The results presented in this chapter have been grouped into three sections.

In the first section are illustrated the morphological changes occurring in 3D collagen lattices after 24 hours of fibroblast-mediated contraction. Spatial remodelling was assessed at three magnification scales. This allowed us to correlate cell morphology and orientation with the ultrastructural appearance of the fibrillar collagen network. The spatial reorganisation was correlated to the mechanical constraints applied to the lattice.

In the second section different fibroblastic cell types seeded in collagen lattices were shown to generate different levels and patterns of contraction force on the tCFM. Two contraction profiles of dermal fibroblasts (Guzelsu et al., 2003) and transformed myoblasts (Cheema et al., 2003), whose phases were well characterised in previous studies, were compared to the new force profiles. The aim was to correlate distinct fibroblast modes of interaction with the matrix to the variations registered in the new profiles of force generation (e.g. adhesion, migration, cell-cell interaction, cytoskeletal

contraction, etc.). In this way, it is shown that dynamic information on cell-matrix interactions can be added and integrated to the static morphological information.

The two initial sections are introductory to the third section, in which the original hypothesis of this study has been tested. This suggests that 3D spatial remodelling by fibroblasts results in permanent shortening of the collagen network, which results in a macroscopic tension retained in the matrix (RMT) after cell tension component is removed (this hypothesis has been detailed in chapter 1). An actin cytoskeleton disrupting agent, i.e. cytochalasin D (CD) at high concentration was added to the culture to block cell force generation and remove the cell tension component.
Macroscopic tension retained in the matrix (RMT) was measured on the tCFM, in the same configuration as the levels and patterns of force generation measured prior to CD treatment. This direct correlation helped to explain the modulation of RMT in terms of the morphological spatial remodelling and force generation profiles seen in the previous sections.

RMT was identified in rat tendon fibroblast (RTF) populated lattices at early culture times (18 and 24 h). This contrasts with human dermal fibroblast (HDF) contracted lattices in which the tension was completely abolished when cell force generation was blocked (Eastwood et al., 1994; Kolodney & Wysolmerski, 1992). Development of significant RMT levels in HDF populated lattices has been thought to start at later stages in culture (Tomasek et al., 2002). Thus, RTF were further characterised with the two aims: (i) to explain the cellular mechanisms responsible for these differences and (ii) to test if RMT could be increased in a fixed culture time (24 h) by different treatments known to stimulate cell-mediated matrix remodelling. These included Transforming Growth Factor-β1 (TGF-β1), cyclical mechanical loading, and a combination of these two treatments. Morphology was assessed, again, after CD treatment for the various culture conditions in order to correlate spatial information concerning cell and fibrillar network to the tensional levels and profiles measured on the tCFM.

Mechanical stiffness of the lattices was also measured for all culture conditions to correlate it with RMT and to previous studies on permanent matrix remodelling (Wakatsuki et al., 2000).

4.2.1 Morphological changes in cell-mediated 3D spatial remodelling of unloaded and isometrically tensioned collagen lattices

Fibroblasts-populated 3D collagen lattices were cultured on the tCFM for 24 hours under two mechanical configurations:

1. stressed: both ends of the lattice were tethered so that cell-mediated contraction generated isometric tension, hence mechanical load on the cells.
2. relaxed: one end of the lattice was left untethered, so that cell-mediated contraction resulted in lattice compaction under no load

At the end of the experiments lattices were fixed and processed as described in the method section and the central area was examined by confocal laser scanning microscopy (CLSM), scanning and transmission electron microscopy (SEM, TEM).

Two cell types were analysed, i.e. human dermal fibroblasts (HDF) and rat tendon fibroblasts (RTF). Since these cells yielded very similar morphological appearances, only HDF populated lattices are displayed as representative. Cell morphology and the collagen fibrils ultrastructure were analysed in relation to the mechanical condition of the construct.

The degree of 3D anisotropy in CLSM and SEM projection images (2D projections of 3D scan) was estimated by custom-made computer procedure

based on the spatial Fourier analysis. The algorithm generated an orientation index (OI) ranging between 0, i.e. perfect parallel orientation, and 1, i.e. random orientation. A similar method, applied to CLSM images only, has been shown to lead to a superior measurement of collagen orientation compared with histological evaluation (van Zuijlen et al., 2002).

Under no load the matrix shrank to about 50% of its original length and cells assumed a star-like shape without any preferred orientation or organisation (Figure 4-1-B). In contrast, fibroblasts in uniaxially tethered gels assumed a spindle-like shape, orientated along the principal axis (Figure 4-1-A).

The computed OI for CLSM images was 2.4 times greater in uniaxially tethered as compared to untethered lattices (0.29 ± 0.04 tethered, 0.73 ± 0.03 untethered).

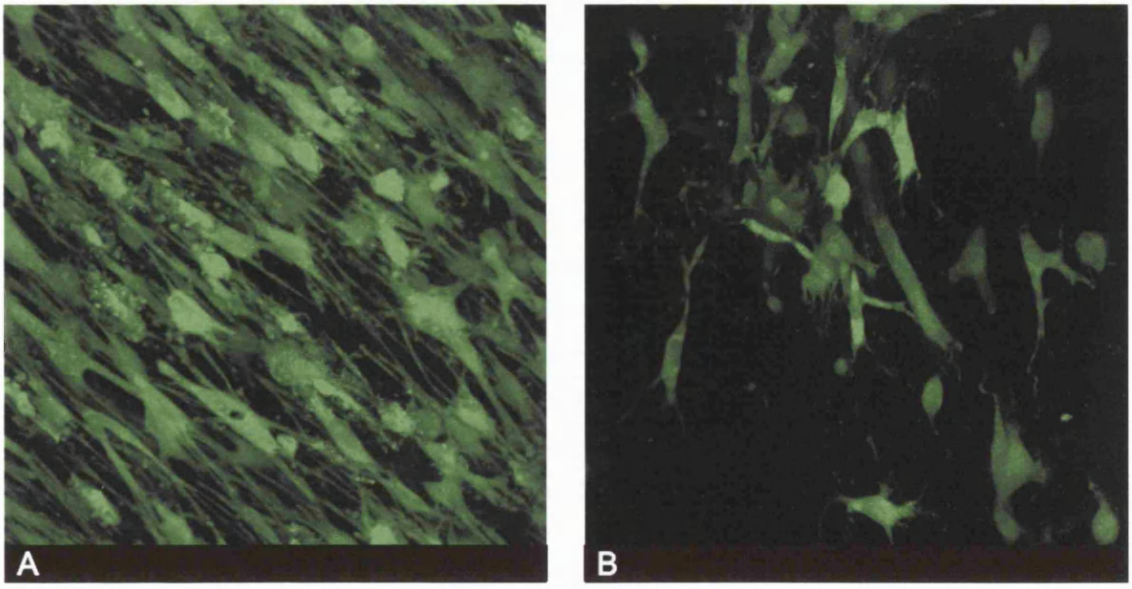

Figure 4-1 Micrographs (CLSM projections) of fibroblasts in 3D hydrated collagen lattices under uniaxial tethered configuration (A) or untethered (B). Cells were stained with green fluorescent tracker dye and imaged by CLSM (40X objective).

Analysis of the ultrastructure on SEM images showed a reorganisation of the collagenous fibrillar network to highly orientated bundles of fibrils along the axis of tension in tethered lattices (orientated parallel to the scale bars in Figure 4-2-A/B). Fibroblasts were visibly orientated and elongated along the load axis (Figure 4-2-A).

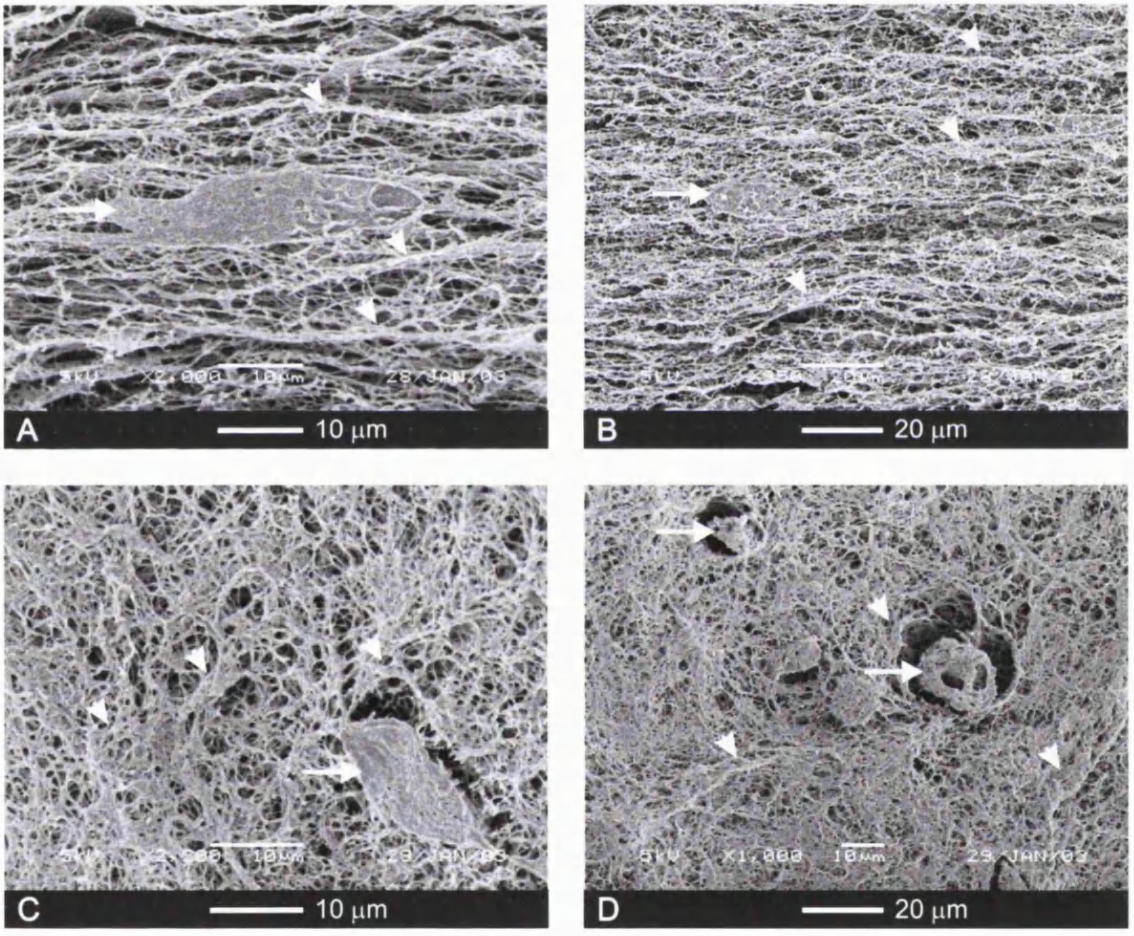

Figure 4-2 SEM micrographs of ultrastructure of 3D hydrated collagen lattices contracted by fibroblasts under uniaxial tethered configuration (A, B) or untethered (C, D). The orientation of the axis of uniaxial load is the same as the scale bars. Cells (arrows) and bundles of fibrils (arrow heads) appeared highly orientated in tethered lattices while randomly distributed in untethered lattices.

Conversely, in lattices contracted by fibroblasts under no load, the fibrillar collagen network appeared like an isotropic mesh of fibrils and was more densely packed (Figure 4-2-C/D). Cells assumed predominantly rounded with a few spindle shapes (Figure 4-2-D).
Lysis of small areas of gel around the cells, produced discrete channels and cavities in the fibrillar collagen network were evident in the unloaded lattices (Figure 4-2-D), but not in uniaxially tethered ones (Figure 4-2-B).

The computed OI for uniaxially tethered lattices was 2.2 fold lower than for untethered (0.36 ± 0.07 tethered, 0.80 ± 0.06 untethered), demonstrating much greater parallel orientation.

TEM ultrastructure showed that fibroblasts assumed a star-like or rounded shape with dendritic processes in unloaded conditions (Figure 4-3-C/D). Sparse collagen fibrils could be observed in random organisation, generally packed into thicker bundles in the proximity of cells (Figure 4-3-C/D). In contrast, in uniaxially tethered lattices on the tCFM fibroblasts assumed a spindle-like shape and were orientated both parallel to the principal axis (white dashed line in Figure 4-3-A/B) and parallel to each other (Figure 4-3-A). Sparse collagen fibrils could be observed generally following cell orientation (hence orientated parallel to the principal axis) and packed in thicker bundles in proximity of cell edges (Figure 4-3-B).

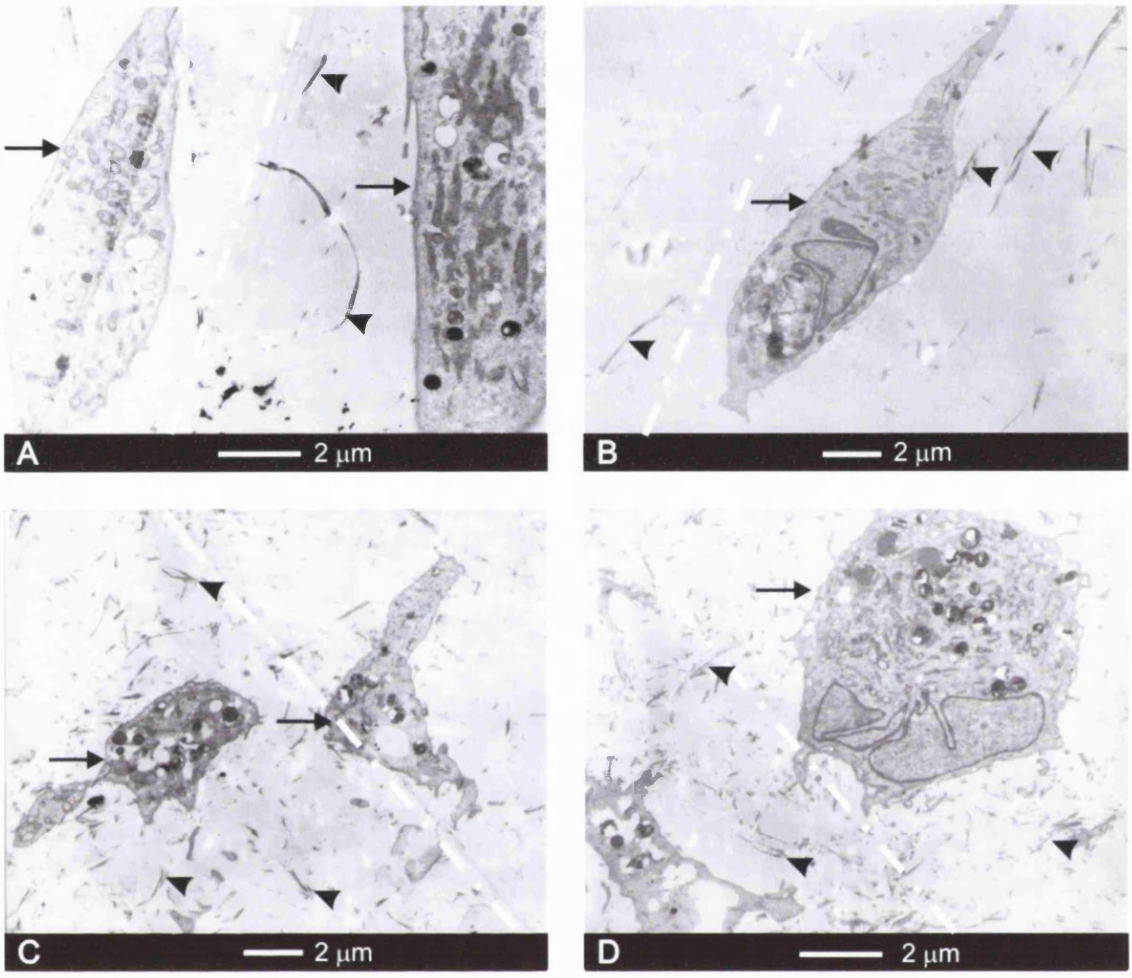

Figure 4-3 TEM micrographs showing the ultrastructure of 3D hydrated collagen lattices contracted by fibroblasts (arrows) under uniaxial tethered configuration (A/B) or unloaded (C/D). The longitudinal axis of lattices has been drawn on the images (white dashed line). Fibroblasts isolated (B/D) or grouped (A/C) appeared elongated and aligned to the longitudinal axis and between each other in tethered gels (A/B) or randomly shaped and orientated in untethered lattices. Sparse collagen fibrils packed in bundles (arrow heads) were visible in both mechanical configurations but appeared more elongated in the uniaxially tethered (A/B).

4.2.1.1 Summary of section 4.2.1

The key points that can be drawn from this section are:

- Mechanical conditions can affect dramatically the cellular and fibrillar network architecture after 24 hours in standard culture condition.

- Different magnification scales showed that cellular orientation and shape (seen on the lowest magnification scale, i.e. CLSM level) correspond to changes at the ultrastructural level.

- At SEM level, profound ultrastructural changes could be correlated to the cellular orientation observed at CLSM level. Highly ordered structures made of uniformly distributed and aligned arrays of fibrils were opposed to very irregular isotropic structures of randomly orientated fibrils packed in thick bundles around big lacunae in coincidence with cell bodies.

- At TEM level, not only showed that fibroblasts assumed different shapes, but also provided information on their local interactions. Orientated fibroblasts were aligned parallel to each other and to the axis of load. Sparse bundles of fibrils around cell's membranes appeared also aligned at this local level (consistently with the ultrastructural alignment seen at lower magnification scale, i.e. SEM). Non orientated fibroblasts showed no preferred direction of interaction between each other and with bundles of fibrils in proximity of their membranes.

4.2.2 Remodelling dynamics of different cell types

The spatial remodelling of 3D collagenous lattices is caused primarily by the forces exerted by resident fibroblasts on the surrounding fibrillar network. The mechanism of how cells exert force necessary for collagen matrix remodelling is unclear (Tamariz & Grinnell, 2002). These forces have been shown to be originated by different cell-matrix interactions, including translocation of fibrils due to traction through extension and retraction of cellular processes (Freyman et al., 2002; Grinnell, 1994; Guzelsu et al., 2003) during cell spreading and locomotion, and compaction of fibrils due to contraction of cell cytoskeleton during homeostatic tension equilibrium (Brown et al., 1998). All these cell-matrix interactions are modulated by many factors, generally grouped as mechanical and biochemical factors. Cell concentration has been shown also to increase force generation proportionally (Freyman et al., 2001; Kolodney & Wysolmerski, 1992) but this effect, in turn, might change the mechanical environment that becomes a feedback signal to the cells in a circular loop (Brown, 2002). In this study the effect of cell concentration was not tested (constant 1 million cell per ml, hence constant 5 million cells in tethered lattices on the tCFM).

Examples of 3D spatial remodelling by cell-matrix interactions and how this is influenced by mechanical environment have been shown above in the morphological study. Uniaxially tethering the lattice caused the fibroblasts to generate highly ordered structures in 24 hours with cells and collagen fibrils orientated along the axis of load. If the collagen lattice is tethered uniaxially, deformation is blocked along that axis causing an isometric tension to develop along it. This tension can be precisely quantified through the tCFM model. Force generation by human dermal fibroblasts (HDF) has been characterised on the same model in previous studies (Brown et al., 1998; van de Hulst, 1981). Different phases of the force profile, corresponding to different levels and gradients of force, have been correlated to specific cellular activities.

The aim of this section is to compare the well-characterised HDF contraction profile with other fibroblastic cell types. The hypothesis was that if different profiles of force generation were produced by different cell types, then the implication would be that different types of cell-matrix interactions occurred over time. That is, different profiles of force generation by cells would imply different microscopic and macroscopic remodelling dynamics, with effects on cell morphology, ultrastructure, stiffness and ultimate strength of the contracted lattice.

Fibroblastic cell types were extracted from different types of connective tissues (i.e. dermis, tendon, bone marrow). Fibroblasts were also collected from rat tendon injury sites (Zavahir et al., 2001) or from uninjured rat tendon tissue.

Finally force generation on the tCFM was tested for a non fibroblastic cell type, i.e. the C_2C_{12} immortalised myoblast cell line. In a recent study (Cheema et al., 2003) the different phases of C_2C_{12}-mediated contraction were correlated to specific cellular functions. Similarly to HDF profile, the well-characterised profile of C_2C_{12} was compared to other force generation profiles of fibroblastic cell types. This comparison would further test the hypothesis that force generation profiles can be used to discriminate between stages of cellular activity implying different remodelling dynamics.

4.2.2.1 Contraction profiles generated by different fibroblastic cell types

Force generation profiles were acquired on the tCFM from 3 fibroblastic cell types: human dermal fibroblasts (HDF), rat tendon fibroblast s (RTF) and human bone marrow fibroblasts (HBMF).

The contraction profile generated by HDF has been largely studied in previous researches (Brown et al., 1996; Delvoye et al., 1991; Eastwood et al., 1994; Freyman et al., 2001; Kolodney & Wysolmerski, 1992). Here it was reproduced and displayed in order to correlate the well characterised phases of force generation with force generation from other fibroblastic cell types. Different phases of force generation (displayed in Figure 4-4) have been shown to be correlated to different cellular states in the 3D collagen lattice (Eastwood et al., 1996).

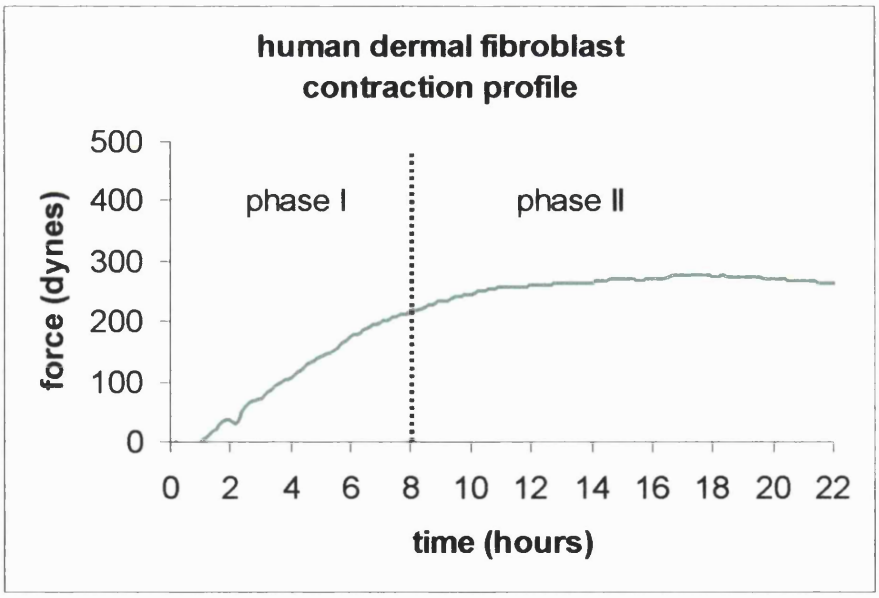

Figure 4-4. Representative contraction profile generated by human dermal fibroblasts (HDF). Note the two distinct phases: I) traction and II) homeostatic contraction.

Phase I, between 0 and 8-10 hours is characterised by traction. During this period, a near linear increase in force can be observed.
In phase II (from 8-10 hours onwards) fibroblasts exert contraction force maintaining the tension that they generated in the preceding phase. This force plateau has been considered the reaching of an equilibrium status, namely homeostasis, in which cell residual internal tension is exactly balanced from the external matrix tension (Brown et al., 1998).
A further third phase starting other 20 hours has been indicated as "contracture" phase. In this period it has been hypothesised that fibroblasts consolidate the deformations generated on the collagen network by depositing new matrix. However this third phase has been difficult to identify with certainty because it does not correspond to a clear change in the force profile.

The cellular action in phase I and phase II have been shown to correspond to changes in the collagen matrix that is initially heavily deformed during cell adhesion, spreading and migration until a degree of tension and stiffness is reached where cells can maintain a balance between their internal tension and the stiffness of their external support (Brown et al., 1998). In this phase, fully spread fibroblasts generate force through the cytoskeletal motor elements which bridge between collagenous fibrillar network (Brown et al., 1998).

Force generation profile by rat tendon fibroblasts (RTF) is shown in Figure 4-5. Initially, from 0 to 4 hours, force rose linearly, similarly to HDF, at rate of 14.1 dynes/h, i.e. half the force rate of HDF. Force reached a plateau earlier than for HDF and maintained a tensional homeostasis for 4 hours (4 to 8 hours).
The force generated up to 8 hours by RTF was on average 78.1% lower than the force generated by HDF.

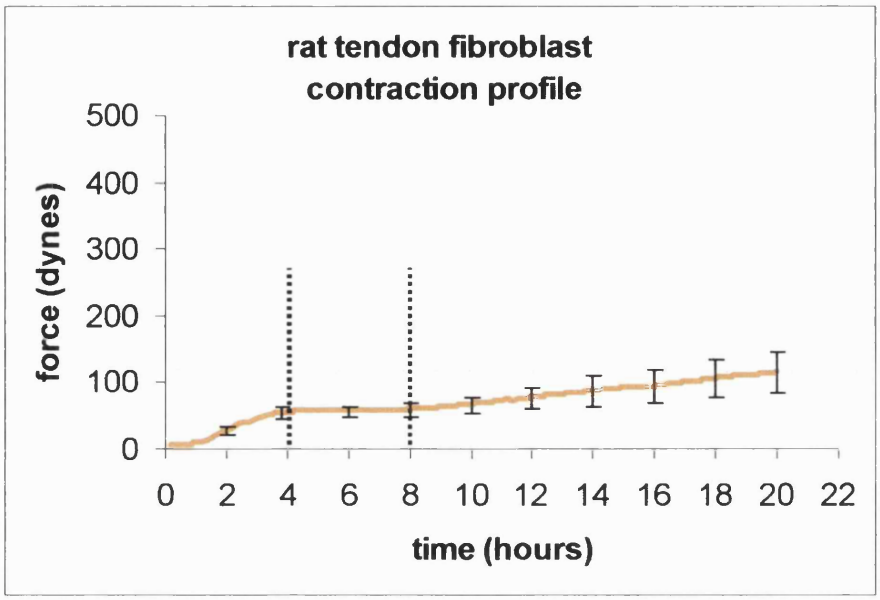

Figure 4-5. Contraction profile produced by rat tendon fibroblasts (RTF). Curve represents the mean force generation (n=5). Error bars represent SE. Dotted lines mark the distinct phases in force generation profile.

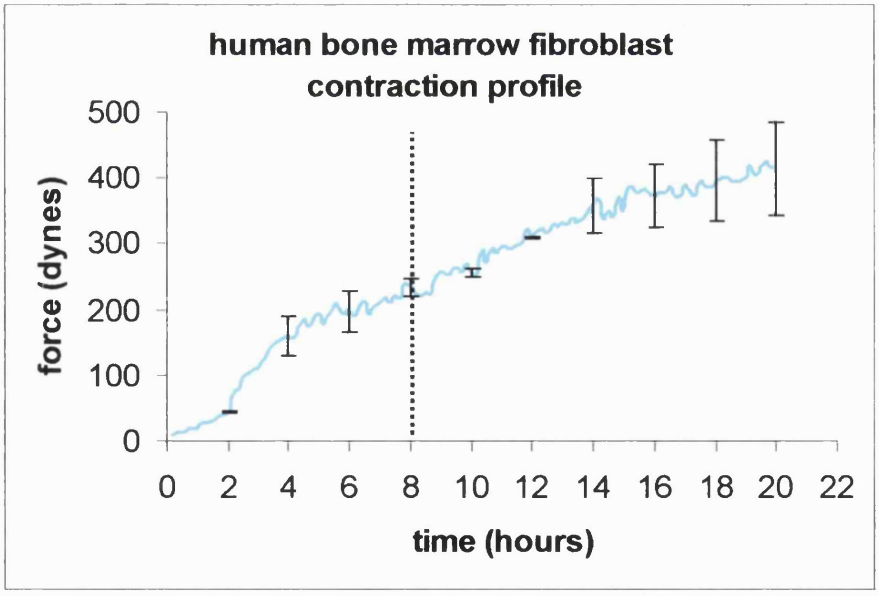

Figure 4-6. Contraction profile produced by human bone marrow fibroblasts (hBMF). Plotted curve represents the average of 3 experiments. Error bars represent SE. Dotted line represents the time point of phase change in HDF force generation which was not observed in hBMF.

A new feature in the RTF profile was that from 8 hours onwards the force generation again began to rise at a rate of 3.9 dynes/h. Unlike HDF a discrete peak force was not attained since force continued to increase for as long as the culture was maintained (22 hours). By 22 hours RTF had reached a level of force generation on average 60% lower than the force level for HDF.

The contraction profile generated by hBMF (Figure 4-6) was different from the two other cell types. The most prominent feature was that there was no plateau in force generation, rather a continuous near linear rise in force at 19.9 dynes/h between 0 and 22 hours. Again, as for RTF, a discrete peak was not reached in the experimental period since force continued to increase throughout to 22 hours. At 22 stage hBMF generated most force of the 3 cell types examined (1.5 and 3.8 fold higher than HDF and RTF respectively).

Cell types / Profile features	HDF	RTF	hBMF
Gradient 0-4 h (dynes/h)	33.9	14.1	44.8
Gradient 4-8 h (dynes/h)	26.9	-0.4	15.2
Gradient 0-8 h (dynes/h)	31.5	6.9	30.7
Gradient 8-22 h (dynes/h)	2.7 (0.6 in 12-22h)	3.9	16.1
Point force at 4 h (dynes)	106.8	53	158.5
Point force at 8 h (dynes)	218.5	55	233.5
Point force at 22 h (dynes)	262.8	110	426.1

Table 4-1 Comparison of the contraction profiles of 3 fibroblastic cell types (HDF, RTF and HBMF). Time is expressed in hours, force in dynes, force gradients in dynes/h.

In summary different fibroblastic cell types generated different contraction profiles in standard culture conditions. Some common features such as the initial steep rise of force (from 0 to 4 hours) could be correlated, with the initial part of phase I for the HDF. Therefore this initial phase could be attributed to cell adhesion and spreading for all fibroblasts types. Tensional homeostasis was found only for HDF and RTF, in which type it was maintained for only a limited time (4 hours). It was not possible to draw conclusions on the cellular activity (e.g. spreading, locomotion, cell-cell interactions) during this plateau phase. The linear rise in force generation after 8 hours for RTF was similar to the rise observed for hBMF although with a much reduced gradient. Again it was not possible to draw conclusive correlation between force profile and cellular activity in this phase.

4.2.2.2 Contraction profiles generated by tendon repair cells (TRC) collected from rat tendon wound sites and by RTF treated with ± TGF-β1

Force generation profiles were generated in the tCFM from collagen lattices seeded with tendon repair cells (TRC) collected from rat tendon wound sites or RTF treated with TGF-β1

Figure 4-7). Force generation for TRC and RTF ± TGF-β1 presented distinct profiles.

The curves for all treatments were similar in the first 4 hours after which force generation for TRC tended to be higher than for RTF treated with TGF-β1. This difference increased with time, i.e. 22.5 hours, where it was 25.0% higher. Both RTF and RTF treated with TGF-β1 generated significantly more force than RTF alone over the whole time period after 4 hours. TRC contraction profile was biphasic with a net rate of force increase of 27.7 dynes/h (from 0 to 12 hours) reducing to 7.1 dynes/h between 12 and

22.5 hours.

Force generation for RTF treated with TGF-β1 appeared to follow a similar general pattern to untreated RTF, but a much greater rate of force generation after 6 hours. A shorter plateau was observed between 3 to 6 hours (instead of 4 to 8 hours) at similar force level as for RTF. After 6 hours force generation restarted and kept rising till the end of 22.5 hours (gradient of force rise 12.3 dynes/h, i.e. 2.6 fold faster than for RTF). The force gradient for RTF treated with TGF-β1 between 12 and 22.5 hours was greater for TRC, implying that they may have converged to a similar maximum force level. Peaks of force generation were acquired from the last point of the recorded force profiles (22.5 hours) due to the near linear rise of all the three curves displayed. Both TRC and RTF treated with TGF-β1 showed significantly higher forces than RTF ($p<0.05$) with peak forces levels 3.1 and 2.4 folds higher than RTF force levels respectively.

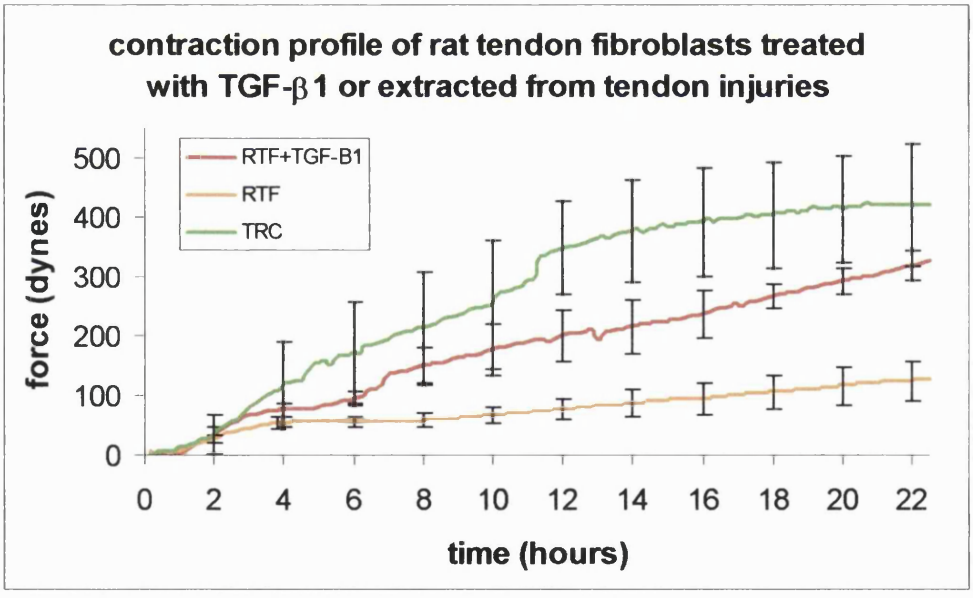

Figure 4-7. Contraction profile generated by tendon fibroblasts treated tendon fibroblasts with 12 ng/ml TGF-β1 (RTF+TGF-β1) and extracted from a tendon injury site (TRC). Non treated RTF contraction profile has been replotted for comparison. Plotted curves represents the average of 3 to 5 experiments. Error bars represent SE.

In summary, different contraction profile were produced from fibroblastic cell types coming from rat tendons. The fibroblasts population derived from a tendon injury site had resided for 3 days in the milieu of cytokines and growth factors during early stages repair. These are known to modulate fibroblast to myofibroblast differentiation (Clark, 1996; Gabbiani et al., 1971). RTF were treated with TGF-β1 (12 ng/ml) only from the beginning of the experiment on the tCFM, hence this was an acute rather than chronic response to the growth factor. RTF and TRC cell lines produced distinct contraction profiles, suggesting that different phases of cellular activity might be involved in force modulation. With the available data, cell-matrix interactions in these phases could not be defined with certainty. However, similarities between the initial phases (from 0 to 4 hours) of these curves and with the phase I of HDF contraction suggest that traction force generation due to adhesion and spreading were the most likely underlying cellular processes. A short tensional homeostasis (from 3 to 6 hours) was maintained in RTF with and without TGF-β1. It was not possible to draw distinct conclusions on the cellular activity during this plateau phase though it seems likely to be a result of the same process described previously (Brown et al., 1998). The near-linear rise in force generation after 8 hours observed for all tendon fibroblast types was the most common basic feature. This contrast markedly with the most common HDF behaviour, to maintain relatively constant force (Brown et al., 1998). Again it was not possible to draw direct conclusions on the cellular activity during this phase, but it would seem that RTFs operate a different longer-term force regulation mechanism.

Tendon injury fibroblasts are thought to be a mixed population of cells from surrounding tissues (tendon, sheath, fascia) activated by local growth factors with a minute proportion of progenitor cells, attracted by wound factors to the injury site, from the blood (Jones et al., 2000). Bone marrow stromal progenitor cells were shown in this study to generate strong contraction forces with similar rising force gradient in phase II. TRC

cultures were found to contain a proportion of cells positive for stem cell markers, such as CD34 and CD44 (Zavahir et al., 2001). Therefore a contribution to additional force might come from such a subpopulation.

Another important contribution to the force upregulation in TRC experiments was could be due to the appearance of a myofibroblast phenotype.

A muscle type actin, α-smooth muscle actin (α-SMA), has been identified as a marker for this phenotypic change (Darby et al., 1990; Gabbiani et al., 1971). Expression of this marker in fibroblasts has been correlated to increased force generation (Hinz et al., 2001). So TRC and RTF were stained to test a possible differential expression of α-SMA (Figure 4-8). Both fibroblastic types stained positively for α-SMA, although the expression involved only a subpopulation of cells.

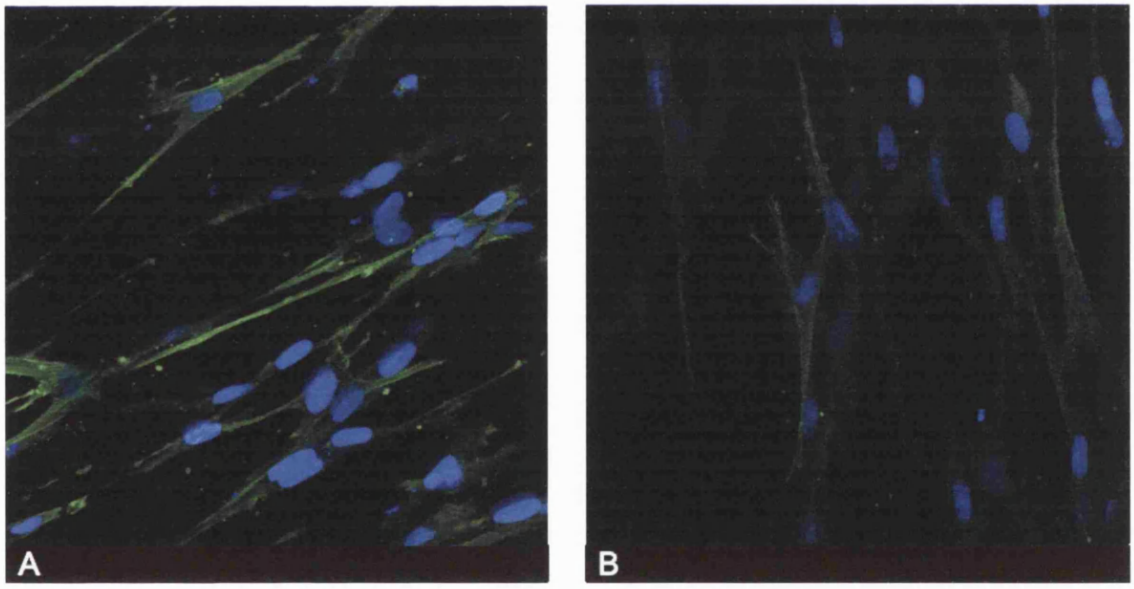

Figure 4-8. Micrographs showing expression of α–smooth muscle actin of (A) tendon injury cells (TRC) and (B) rat tendon fibroblasts (RTF) after 24hr in culture in 3D collagen lattices on the tCFM model. Cell nuclei (Hoescht stain, blue) and α–SMA fibres (FITC stain, green) were stained and imaged by CLSM (400 times magnification).

Therefore it appeared that expression of α-SMA could not alone explain the upregulation of contraction. This suggested that there is no simple relation between α-SMA and contraction, though more quantitative measure of α-SMA would be needed to draw firmer conclusions. A widely held hypothesis (assumption) is that myofibroblasts contribute disproportionally to force generation and so their number should be proportional to total force.

4.2.2.3 Contraction profiles generated by immortalised rat myoblasts (C_2C_{12})

Contraction profiles were generated on the tCFM using non fibroblastic cells, i.e. one immortalised rat myoblast cell line known as C_2C_{12}.

The resulting force profiles were very consistent with a recently published study on C_2C_{12} in the same mechanical configuration (Cheema et al., 2003). The contraction profile generated by C_2C_{12} was different from all fibroblastic cell types so far tested. A long initial lag phase was evident (from 0 to 8 hours) and is apparently due to a delayed cellular adhesion and spreading (Cheema et al., 2003). This is different from all forms of fibroblasts tested, which were characterised by a very early force onset corresponding to immediate extension of cellular processes.

Tensional homeostasis was not present over this time scale (but was reported by 66h by Cheema). The linear rise in force generation after 8 hours has been correlated with onset of cellular spreading and beginning of intercellular interactions (Cheema et al., 2003). Force generated by C_2C_{12}, in fact, seems to correlate with cell-cell interactions, similarly to endothelial cells where force generation began when a near continuous cell sheet had formed over the surface of the collagen gel (Kolodney & Wysolmerski, 1992). Cell-cell interactions (e.g. cell-cell attachment and fusion) are the base for further differentiation stage in which C_2C_{12} fuse and form multinucleated myotubes (Cheema et al., 2003). The peak force measured at the end of the culture time (i.e. 22.5 hours) was 137.2 dynes, hence similar to RTF peak

force level. The gradient of force generation by C_2C_{12} from 8 hours onwards was higher than that of RTF (35% faster force rise), but lower than all other fibroblastic cell types examined above.

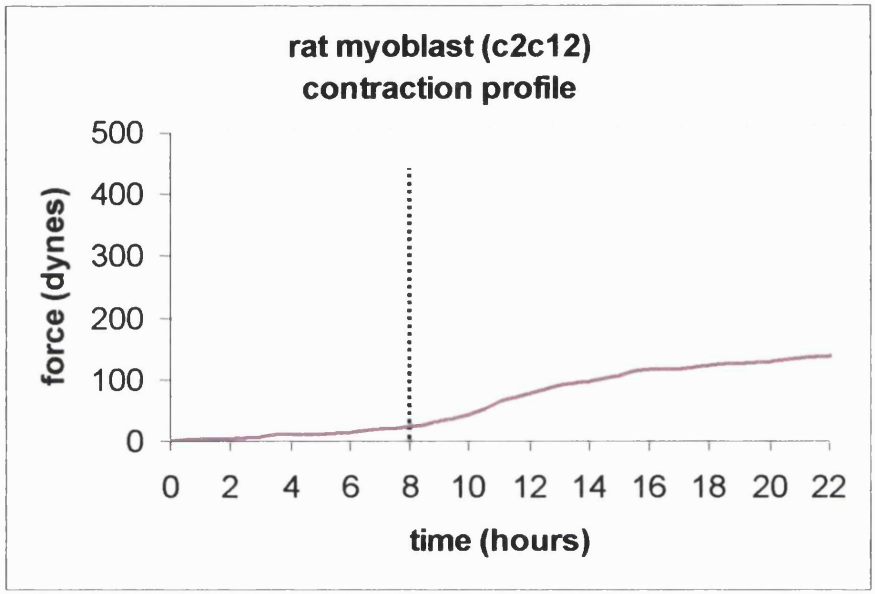

Figure 4-9. Representative contraction profile produced by immortalised rat myoblasts (c2c12).

The resulting cell remodelling, however, was completely different from fibroblasts. Long multinucleated myotubes were formed in the C_2C_{12} populated lattices (Cheema et al., 2003), while regular orientated arrays of interconnected cells were observed RTF populated lattices (Figure 4-1).

Other features in the acquired force profiles, generated by different fibroblastic cells, did not show similarities to C_2C_{12} force time course. This suggests that distinct features in force generation profiles might be due to different cellular functions.

4.2.2.4 Summary of section 4.2.2

The key points that can be drawn from this section are:

- Different fibroblastic cell types generated distinct contraction profiles in the tCFM, indicating specific dynamics of cell-matrix interactions might be specific for each cell type.

- Cell-matrix interactions were inferred by correlation with well-characterised cell types, i.e. HDF and C_2C_{12}.

- All fibroblastic cells types had an initial steep rise in force generation in common attributable to the initial deformation of the matrix caused by cell adhesion and spreading.

- The morphology of lattices contracted by HDF and RTF on the tCFM did not show quantifiable differences (in terms of OI). However, force generation profiles appeared different in force levels and temporal evolution.

- The long force rise after 8 hours in rat fibroblasts may indicate a different long-term force regulation mechanism to HDF. This may be due to specific cell-cell and cell-matrix interactions which are not identifiable through morphological appearance.

4.2.3 Modulation of matrix remodelling by tendon fibroblast: mechanical and biochemical cues.

The amount of matrix remodelling in the cell-contracted collagen lattices was quantified in the tCFM as the tension retained in the matrix (RMT) following removal of the cell force component by cytochalasin D (CD). This technique is outlined in details below in subsection 4.2.3.1.

As a background to this (1) normal contraction of rat tendon fibroblasts (RTF) was first characterised; (2) effective doses of CD were determined to completely abolish cell force with no recovery; (3) the effect of RTF confluence state (prior to use in CFM) on force generation was determined. Generation of RMT in RTF collagen gels was compared to human dermal fibroblasts (HDF). Differences were found between the two cell types in the ability to generate RMT suggesting a possible species-specific link (i.e. at cells plus rat collagen). This hypothesis was tested crossing species of origin for collagen type I (extracted from bovine skin instead of standard rat tail) and for fibroblasts (cells from bovine tendons instead of rat tendons).

Finally a detailed characterisation of RMT was made in RTF populated collagen lattices. RMT was shown to increase with culture time in standard culture conditions.

Thus, RTF were further characterised with the two aims: (i) to explain the cellular mechanisms responsible of these differences and (ii) to test if RMT could be increased in a fixed culture time (24 h) by different treatments known to stimulate cell-mediated matrix remodelling.
The treatment tested were:

- TGF-β1 treatment, i.e. 12 ng/ml added to the FPCL from time zero
- Cyclic mechanical loading over 16 hours (from 8 to 24 hours).
- Combined treatment (CT), i.e. the two treatments above used in combination (i.e. TGF-β1 + cyclic mechanical loading).

Additionally a treatment known to reduce the matrix synthesis, i.e. depletion of ascorbate from standard culture medium, was tested in order to

investigate the role of matrix production on the matrix remodelling.

Finally, the ability to quantify early matrix remodelling by the newly defined matrix retained tension (RMT) was compared with a traditional engineering material parameter, the elastic modulus.

Statistical analysis of the data was performed by Student's t-test and parametric one-way ANOVA test, with no substantial differences in results. The use of parametric data analysis, in place of non-parametric which is more suitable for small n numbers, was justified by the type of data which are completely independent from each other and therefore can be assumed to have a Gaussian distribution. The same statistical analysis was applied to all the data presented hereon in this chapter.

4.2.3.1 Quantitative measurement of remodelling measured as residual matrix tension (RMT)

Residual matrix tension (RMT) can be defined as the tensional force stored in the matrix after removal of the cell force component from the total contraction force (Figure 4-10). The cell component elimination is achieved by disrupting the tensile part of the cytoskeleton with cytochalasin D, which depolymerises the filamentous actin structures. An isometric tension measuring device such as the Culture Force Monitor (CFM) is needed to accurately separate the cell generated force from the tension stored in the matrix (i.e. physically shortened collagen network).

Figure 4-10 shows a representative contraction profile of a rat tendon fibroblast (RTF) populated collagen gel (see Figure 4-5 for a detailed description of the different phases in RTF contraction profile between 0 and 24 hours). Addition of 20 μg/ml of CD at 24 hours caused a sudden rapid force drop (rate of 90 dynes/h) in the first 30 minutes. The gradient of fall then changed (29.3 dynes/h between 0.5 h and 1 h) and continued to

decrease until the curve reached a plateau between 1.5 to 2 hours (with minimal gradient, 7.9 dynes/h).

As the force drop had been reduced to a near plateau by 2 hours after treatment, this time point was used as reference time point to measure the amount tension retained in the matrix (RMT). The 2 hours time point were RMT is measured is indicated by the lines drawn on the graph in Figure 4-11. Additionally, calculations showed that 85% of the total force drop (measured 12 hours after treatment) occurred within the first 2 hours.

RMT in this representative experiment was 46 dynes which is well above the cell-free gel contraction (steady tension of ~10 dynes).

Therefore the cells had modified permanently the dimensions of the matrix such that it could not return to its original size once the cell contribution had been removed.

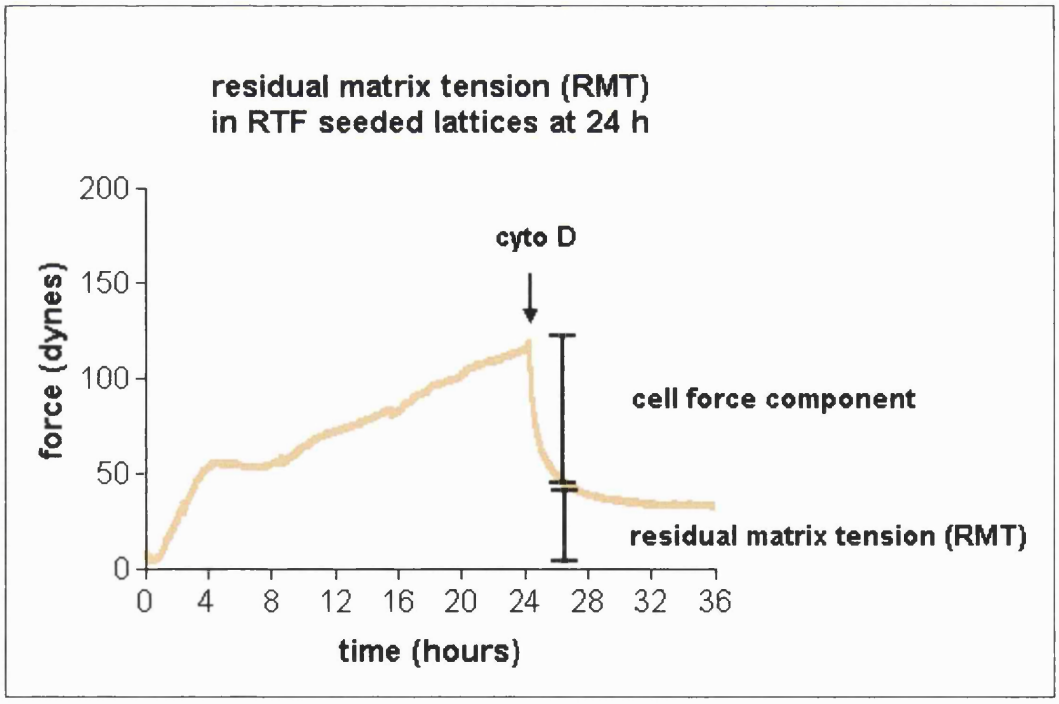

Figure 4-10 Representative graph of rat tendon fibroblast (RTF) populated collagen gel contraction on the CFM under standard culture condition treated with cytochalasin D (CYTO D) at 24 hours. Cytochalasin D removed the cell force component very rapidly and after 2 hours the residual matrix tension (RMT) was measured.

4.2.3.1.1 Total elimination of the cell component

The dose of cytochalasin D was calibrated to completely abolish any cell dependent force in a way that subsequent doses at later stages would not produce any further detectable change in the force profile. In order to test this, a second dose was added and the culture medium was replaced with distilled water (hypo-osmotic culture conditions) to cause complete cell lysis and death. The dose of CD was such that any cell recovery in force generation in the following 12 hours was abolished. The effective concentration for this was 20 μg/ml as shown in the dose test described below in section 4.2.3.3.1.

Figure 4-11 shows the effect of a repeated dose of CD and subsequent treatment with hypo-osmotic culture media.

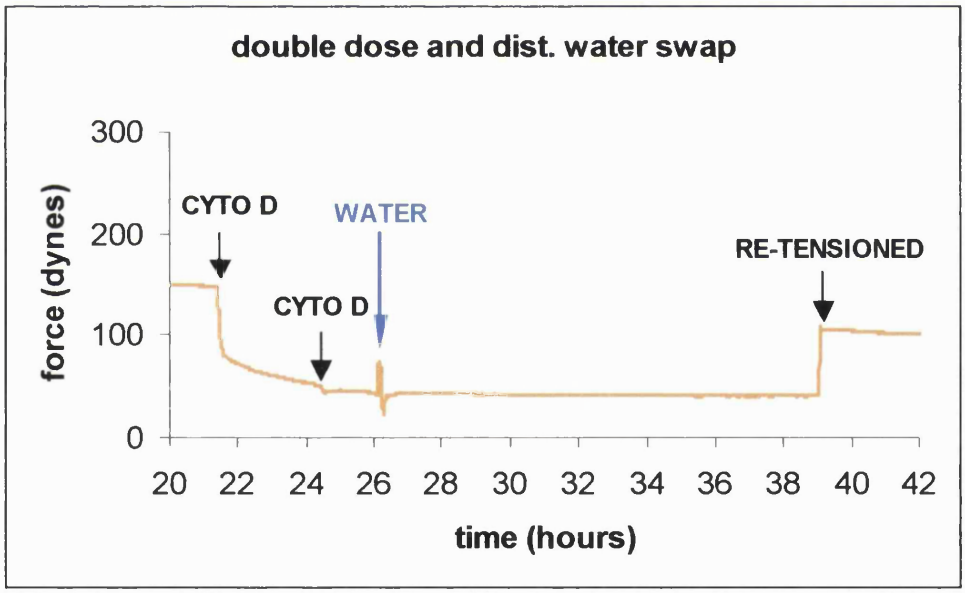

Figure 4-11 A repeated dose of 20μg/ml cytochalasin D at 21.5 h and 24.5 h and subsequent change to hypo-osmotic culture medium (water dilution) at 26.5 hour point did not alter the residual matrix tension reached 3 hours after the first treatment. The perturbation in the curve was due to the transient change in fluid level during the change in medium. Tension was put back after several hours and there was no sign of drop, i.e. the remodelled matrix is able to hold the previous level of tension (before CD treatment) with minimal relaxation.

The first dose of CD was given at 22 hours. A rapid drop was registered followed by plateau within 2 hours. The second dose was given 3 hours later resulting in no further change of matrix tension. After 2 hours from the second CD treatment, culture medium was replaced with distilled water (as shown from the short perturbation on the force curve).

Finally, tension was put back (external addition of 60 dynes) after the change of media with water with no sign of subsequent force drop. This demonstrated that the matrix itself was able to hold the new tension even following cell lysis. Therefore the force drop observed is indeed only the removal of the cell-based tensile component. It was concluded that the tension measured after cytochalasin treatment was due only to the new physical properties of the matrix.

4.2.3.2 Residual matrix tension is found in RTF but not in HDF populated lattices after 18 hours

This experiment investigated if there were differences between human dermal fibroblasts (HDF) and rat tendon fibroblast (RTF) in their ability to shorten the collagen network (rat type I) and so store a residual tension (RMT).

Figure 4-12 shows the contraction profile of HDF and RTF populated collagen gels treated with CD at 18 hours.

The differences between the contraction profiles of HDF and RTF populated gels have been outlined previously (section 4.2.2.1). It is worth noticing that the HDF contraction profile reached a force equilibrium at 12 hours that was maintained until 18 hours when CD was added. In contrast, RTF contraction force was still rising at 18 hours when CD was added.

Addition of CD to the RTF gel caused a rapid force drop, followed by a plateau (at ~30 dynes) within 2 hours similar to the 24 hr treatment (Figure 4-10). This steady state was not reached in the HDF populated gel in which

the force kept decreasing with a steep gradient and reached the baseline value for cell-free gels within 3 hours of treatment.

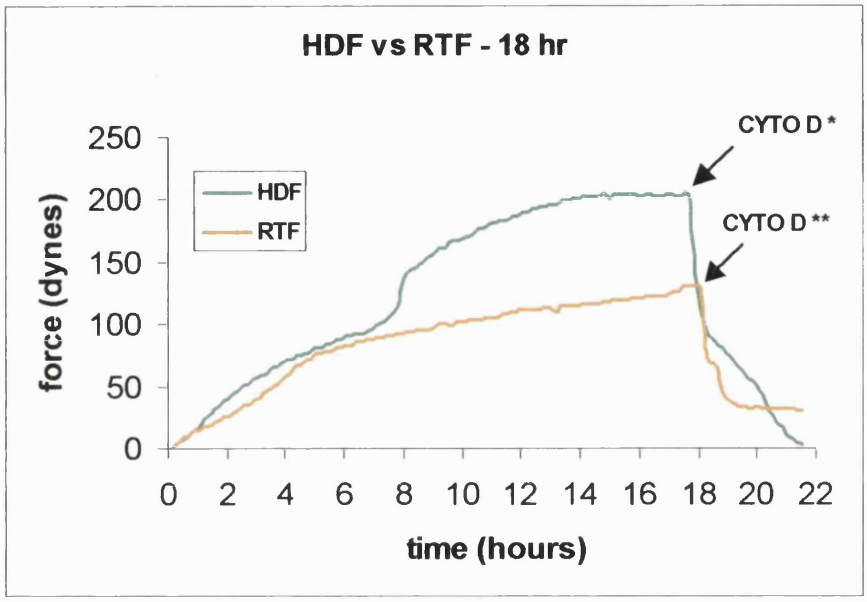

Figure 4-12 Representative contraction profile of human dermal fibroblasts (HDF) and rat tendon fibroblasts (RTF) populated collagen gels treated with cytochalasin D at 18 hours. Three hours after treatment force was completely abolished in the HDF populated gel while it reached a plateau (around 30 dynes) in RTF seeded gels. RTF required a 10 times higher dose of cytochalasin D (CYTO D **) compared to HDF (CYTO D *) to give significant loss of cell generated tension.

It should be noticed that RTF were given a dose of CD 10 times stronger than HDF. This higher dose was suggested from the results of the experiment presented previously (section 4.2.3.3.1).

4.2.3.3 Background characterization of rat tendon fibroblast culture

RTF and HDF showed a significant difference in their ability to permanently shorten the collagen lattice as shown in the previous section. Another difference between these two fibroblastic cell types was found in the profile of force generation. However, this difference was not reflected in the morphology of cells and fibrils (as described in the initial part of this chapter). RTF were further characterised in order to investigate cell responses that might be specific to this fibroblastic cell type (4 parameters). HDF were used as a reference cell type as they had been extensively studied in the past.

(1) It was noticed that the standard CD dose (2 μg/ml) used to abolish contraction in HDFs (Kolodney & Wysolmerski, 1992; Brown et al., 1996) had little effect on RTFs and so doses of 2 and 20 μg/ml were compared. The aim was to identify the concentration of CD that would completely abolish RTF force generation.

(2) Longer-term experiments (one week) using unloaded round lattices seeded with RTF or HDF showed that rat cells generated a remarkably higher matrix degradation activity compared to human cells.

(3) In order to test possible species matched/mismatch effects between cells and collagen, experiments with crossed species were performed. The following combinations were tested:

- unloaded collagen lattices, seeded with RTF, were prepared with type I soluble collagen extracted from bovine skin instead of standard rat tail.
- CFM lattices, prepared with standard rat tail collagen, were seeded with bovine tendon fibroblasts (BTF). Note, this also act to control the tissue origin (tendon as opposed to skin).

(4) Finally the contractile response of RTF in non confluent state or in fully confluent state was tested.

4.2.3.3.1 Blocking fibroblast-mediated force generation required higher concentration of cytochalasin D in RTF than in HDF

A concentration of 2 μg/ml of cytochalasin D has been used extensively to depolymerise actin and block contraction (Brown et al., 1996; Kolodney & Wysolmerski, 1992; Wakatsuki et al., 2000; Wakatsuki et al., 2001).

This experiment compared the effect of 2 μg/ml concentration of cytochalasin D (CD) with the 20 μg/ml used here to completely abolish the cell force generation (with no further recovery over 12 hours). Treatment of HDFs with 2 μg/ml completely abolished force (Figure 4-12).

Figure 4-13 shows the effects on RTF collagen gel contraction of CD at 4 hours. 2 μg/ml did not completely abolish force generation. Cells recovered within 10 hours and started generating more force. Conversely 20 μg/ml completely blocked cell force generation with no sign of recovery in the following 12 hours. The background level of tension retained was the level of natural contraction of the collagen gel itself (~10 dynes).

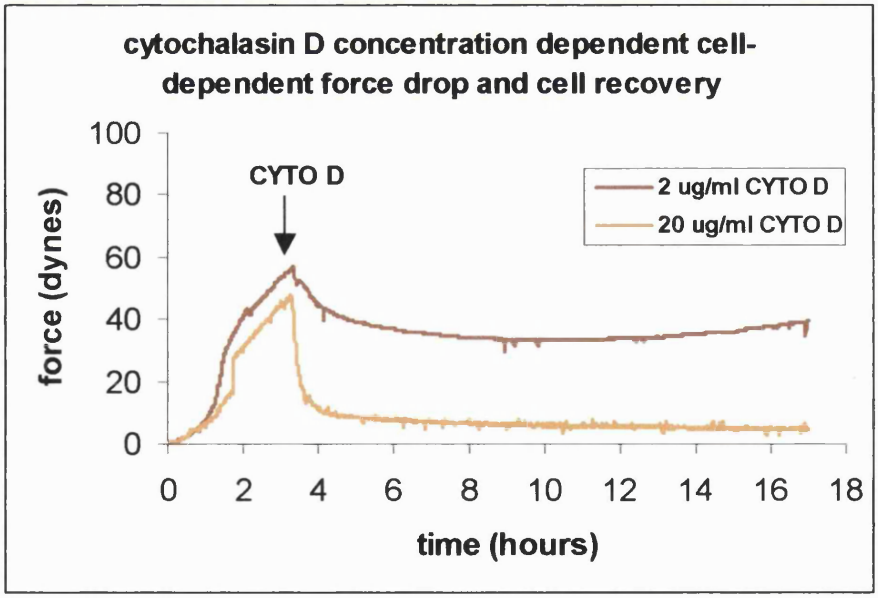

Figure 4-13 RTF populated gel contraction profile treated with cytochalasin D (CYTO D) at 4 hours. Two concentrations were used: 2 μg/ml (upper trace) did not abolish completely the cell force component. Cells recovered within 10 hours and restarted generating force. Conversely a concentration of 20 μg/ml completely abolished the cell force component with no sign of recovery.

4.2.3.3.2 Rat tendon fibroblasts but not human dermal fibroblasts perform an aggressive matrix degradation in load free conditions.

Cell machinery has the ability to lyse a collagen matrix by secretion of matrix metalloproteinases (Prajapati et al., 2000a; Tomasek et al., 1997) and by collagen fibrils phagocytosis.

In order to qualitatively test cell-mediated matrix degradation, longer-term (one week) contraction experiments with unloaded round lattices were performed. Matrix degradation was observed macroscopically as reduction or even complete dissolution of the matrix in the central area of the lattices, leaving an annular shape.

In this first series of experiments RTF or HDF were seeded into round collagen lattices and left to contract in absence of load (free floating) for one week (Figure 4-14). The collagen lattice contracted by RTF was very compacted and formed a ring of collagen (Figure 4-14-B), indicating that the matrix had been completely degraded in the central area. Conversely HDF contracted lattice was less compacted and did not show macroscopically visible degraded areas (Figure 4-14-A).

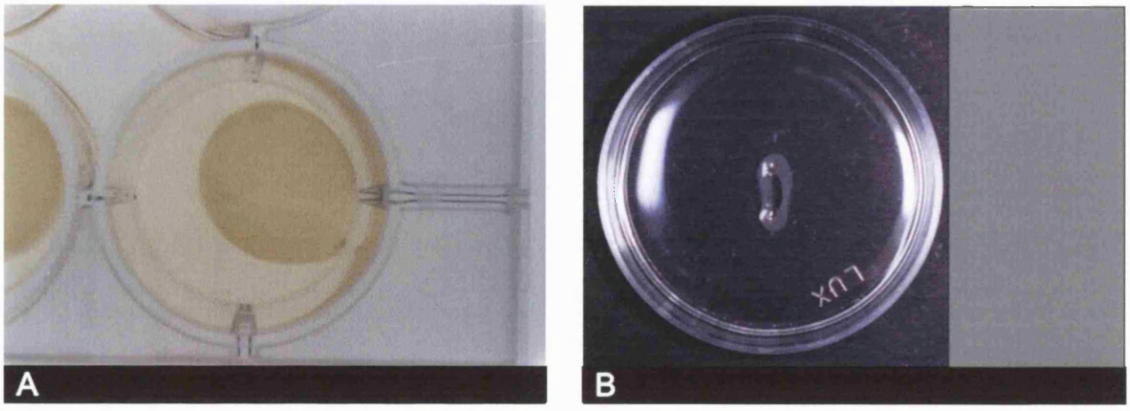

Figure 4-14 Photographs of collagen lattices contracted by HDF (A) or RTF (B) under no tension (free floating) for a week. The central area of the RTF contracted lattice was completely degraded, leaving an annular shape (B). No macroscopic lysing process was visible in the HDF contracted lattice (A).

To test the idea that these "remodelling" events require protein specificity (match) between the supplied collagen lattice (rat) and products (collagen, proteases etc.) from cells (rat or human), crossed experiments were performed. Collagen lattices, seeded with RTF, were prepared with bovine skin type I collagen instead of rat collagen. In addition, collagen lattices, made of standard rat tail collagen, were seeded with bovine tendon fibroblasts (BTF), hence controlling for tissue origin.

Changing collagen species (from rat to bovine) did not stop the strong matrix degradation performed by RTF (Figure 4-15-B). The lattice contracted by RTF formed a large visible lysed area in the centre (though perhaps less than for the rat collagen gel 4-14-B). Rat collagen lattices seeded with BTFs did not show visible lysis and resembled those with HDFs.

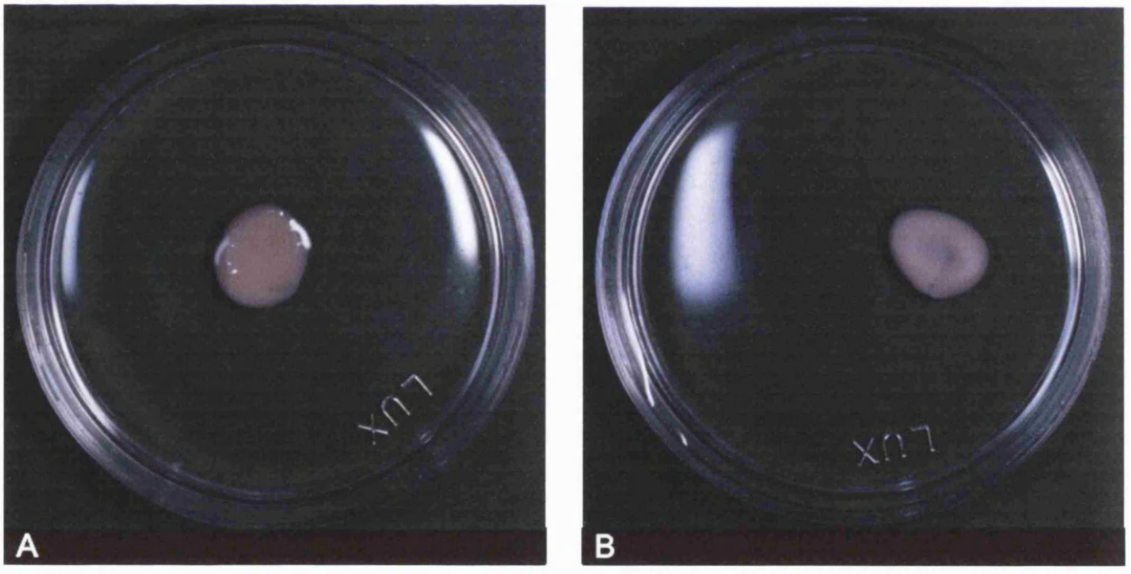

Figure 4-15 Photographs of a collagen lattices contracted under no tension for a week. (A) Lattices, prepared in the standard way (with rat tail collagen) and seeded with bovine tendon fibroblasts (BTF), showed no evidence of macroscopic lysis. (B) Lattices, prepared with bovine collagen and seeded with RTF assumed an annular shape with only a thin layer of matrix present in the central area.

In conclusion, the strong lytic action which resulted in macroscopic degradation of the central area of circular free-floating lattices was unique to rat tendon cells. Other types of fibroblastic cells did not behave in the same way. Possible affinity between cells and collagen of the same species did not appear to be the cause of the observed phenomenon.

4.2.3.3.3 Force generation and remodelling by tendon fibroblasts does not reqire a cell-collagen species match

This experiment tested possibility of a species-specific response between rat fibroblasts (RTF) and human fibroblasts (HDF) reported previously (section 4.2.3.2). For this, bovine tendon fibroblasts (BFT) were compared with RTF for force generation and response to and CD at 23 hours (Figure 4-16).

The contraction profile of BTF represented in Figure 4-16 shows an early peak reached within 4 hours (comparable to Figure 4-5 for RTF). Between 4 and 16 hours the force decreased slightly leading to an equilibrium phase (16-23 hours).

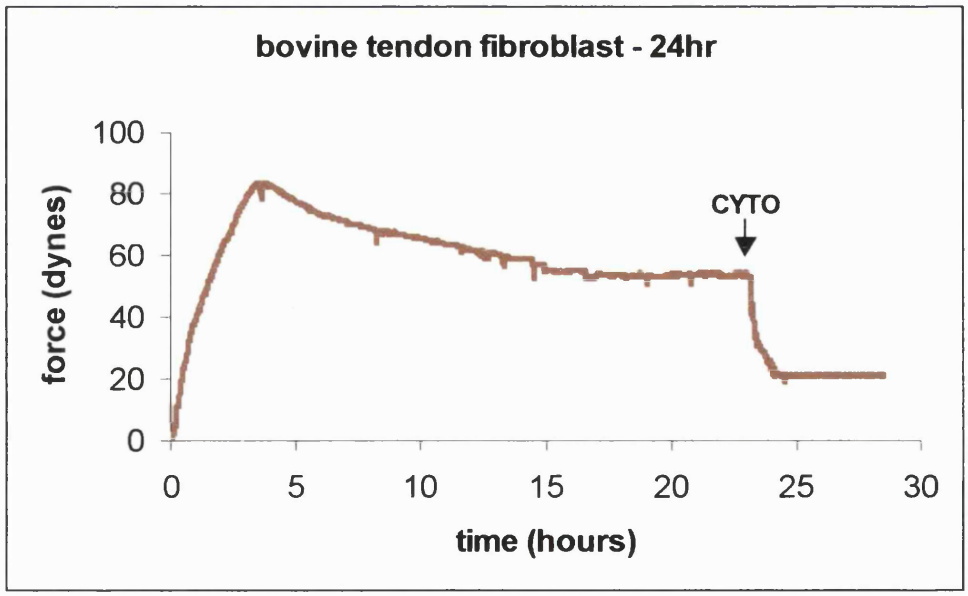

Figure 4-16 Representative contraction profile of bovine tendon fibroblasts treated with cytochalasin D at 24 hours.

Peak contraction force of bovine cells was lower than for rat cells (~50% lower) mainly as there was no increase over later time points. The total force drop 2 hours after treatment was 64% with an RMT of 30 dynes (force carried on dropping (after 2 h time point) till ~20 dynes level which was maintained stably).

BTF response to CD treatment had similarities with RTFs, with an initial force drop leading to a plateau within ~2 hours after treatment. The main difference was in the absolute values of force which were lower overall for BTF contracted gels.

The important conclusion from these experiments is that, in both species, tendon cells were able to effectively modify the matrix and store tension over the 24 hours time period, in contrast to dermal cells.

4.2.3.3.4 Rat tendon fibroblasts cultured on standard plastic flasks

RTF were highly proliferative in standard culture conditions on plastic flasks (doubling time was around 24 hours as measured by cell counting). They completely and uniformly covered the surface of the culture flask. RTF had a spindle like shape but this became rounded as the culture became confluent.

4.2.3.3.5 Effects of cell confluence on the generation of contraction force: inhibition of the response to TGF-β1

Cells plated in 225 cm^2 flasks were used either fully confluent (100% of the surface covered for 3-5 days) or sub-confluent (around 90% covered). Immediately after casting the collagen gel with these two cell populations, TGF-β1 (12 ng/ml) was added (time zero).

Figure 4-17 shows the contraction profile generated by RTF over 22 hours. Test cultures were supplemented with TGF-β1 in standard culture

conditions. The 100% confluent RTF produced slightly less contraction than sub-confluent cells and this was little altered by TGF-β1. However, addition of TGF-β1 to cells harvested sub-confluent produced a major increase in force generation. Gels seeded with sub-confluent cells + TGF-β1, produced an increase in peak contraction force 3 fold greater than the same cells without TGF-β1.

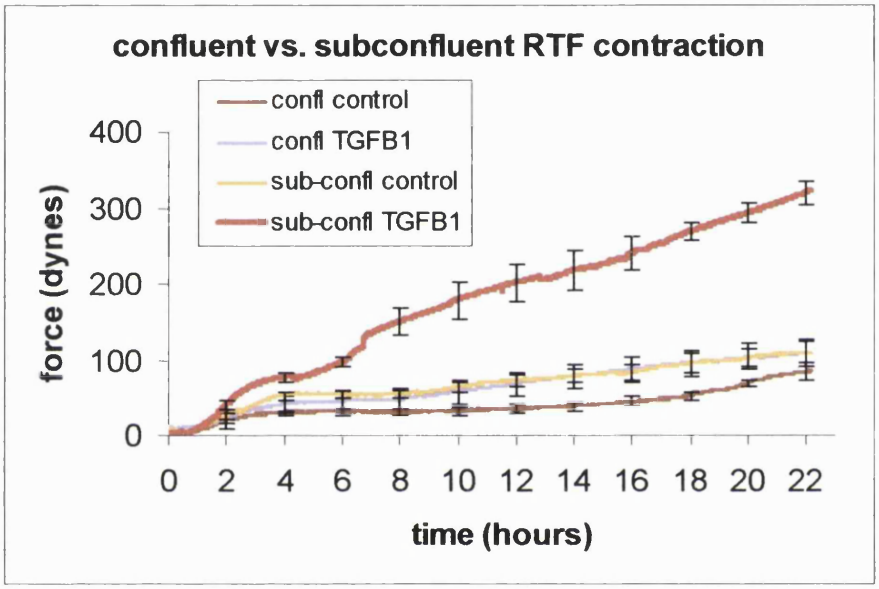

Figure 4-17 Force generation of 100% confluent and sub-confluent rat tendon fibroblasts, with or without TGF-β1 (given at time zero). Error bars represent the standard error on the mean (SEM) sampled at regular intervals. Each curve represent 3 or 4 replicates ($n \geq 3$). Note: TGF-β1 stimulation in this system was in the phase II contraction period in contrast to previous reported stimulation of 0-8h phase I traction reported (Brown et al., 2002) seen in serum depleted gels.

The initial phase of contraction (0 to 4 hours) corresponding to cell spreading and traction was similar for all profiles, but the subsequent contraction plateau phase was different between the treatments. Untreated confluent cells had the longest plateau tract (4-16 hours). Confluent TGF-β1 treated and untreated sub-confluent showed a similar equilibrium phase between 4 and 8 hours (i.e. gradient close to zero). However, sub-confluent

cells plus TGF-β1 produced only a transient plateau phase (nominally from 4 to 4.5 hours) after which force generation rose again (average gradient between 4.5 and 8 hours was 21.7 ± 7.3 dynes/h). The gradient of force rise between 8 and 22 hours was 12.1 ± 1.6 dynes/h for sub-confluent TGF-β1 treated but only 3.88 ± 0.82 dynes/h and 3.75 ± 0.85 dynes/h for non treated sub-confluent and confluent respectively.

Figure 4-18 summarises the results of this set of experiments. Grouping the two conditions into confluent and sub-confluent showed that the confluence was the only statistically significant factor ($P<0.05$ on non-parametric 2-way ANOVA, TGF-β1 was not significant in this set of data).

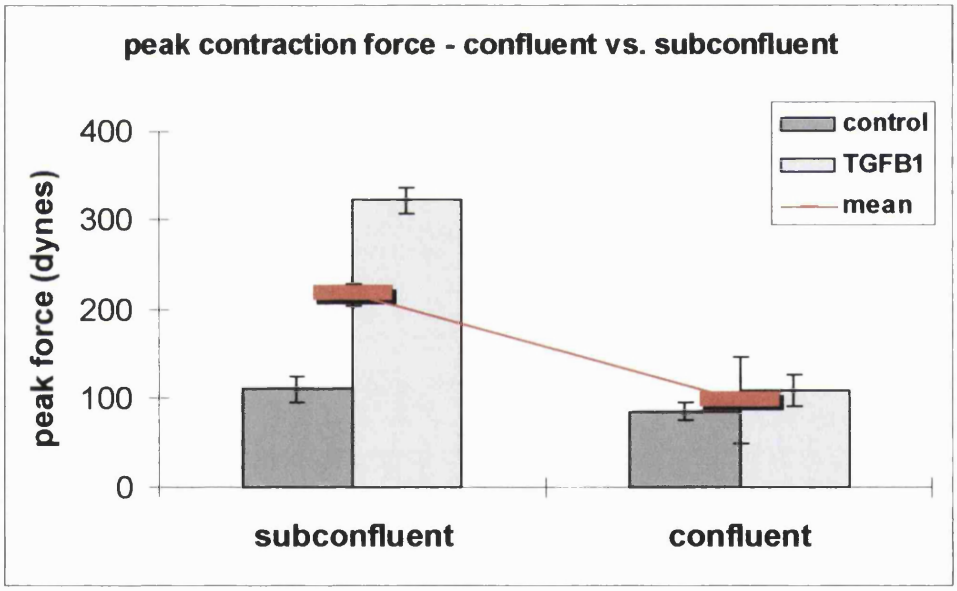

Figure 4-18 Representation of the peak contraction force for confluent/subconfluent RTFs seeded in collagen lattices, treated or untreated with TGF-β1. The two conditions have been grouped in confluent and sub-confluent to test the statistical significance ($p<0.05$) of the confluence factor. The red bars show the mean for the 2 groups, black vertical bars are the standard error (SE). Statistical difference between the two groups was entirely due to their response to TGF-β1, regulated by the degree of confluence.

It is concluded that maintaining cells in 100% confluent culture conditions has an inhibitory effect on RTF response to TGF-β1, measured as

inhibition of cell force generation. There were not significant differences in the cell force generation (100% or sub-confluent) in absence of TGF-β1.

This implies down regulation of TGF-β receptor expression at high levels of cell-cell contact or some other downstream signal in this pathology.

At a practical level, non-confluent RTF cultures were used for all further experiments.

4.2.3.4 Residual matrix tension (RMT) changes with culture time and culture conditions

The experiments reported in this section are divided into 2 groups: the first shows the effect of culture time on cell-mediated matrix remodelling in standard culture conditions. The second group tests the effects of targeted culture treatments on fibroblast-mediated matrix remodelling, over a constant 24 hours culture period.

For all experiments in both groups, residual matrix tension (RTM) was measured 2 hours after addition of 20 μg/ml of cytochalasin D (see sections 4.2.3.1 and 4.2.3.3.1). For all the graphs reported the error bars represent the standard error on the mean (SEM) sampled at regular intervals. Each contraction profile plotted represents 3 or 4 replicates.

4.2.3.4.1 Changing levels of RMT with increasing time in culture

Cytochalasin D (CD) was given at 4, 24, and 61 hours and RTM was measured (Figure 4-19 to 21). Addition of CD at 4 hours produced complete loss of tension, down to that of the endogenous collagen gel baseline (5 to 10 dynes). Over 80% of force fell off within 30 min of treatment. At 24 hours, CD did not completely abolish tension, rather leaving 47 ± 1.5 dynes at the 2 hours stage.

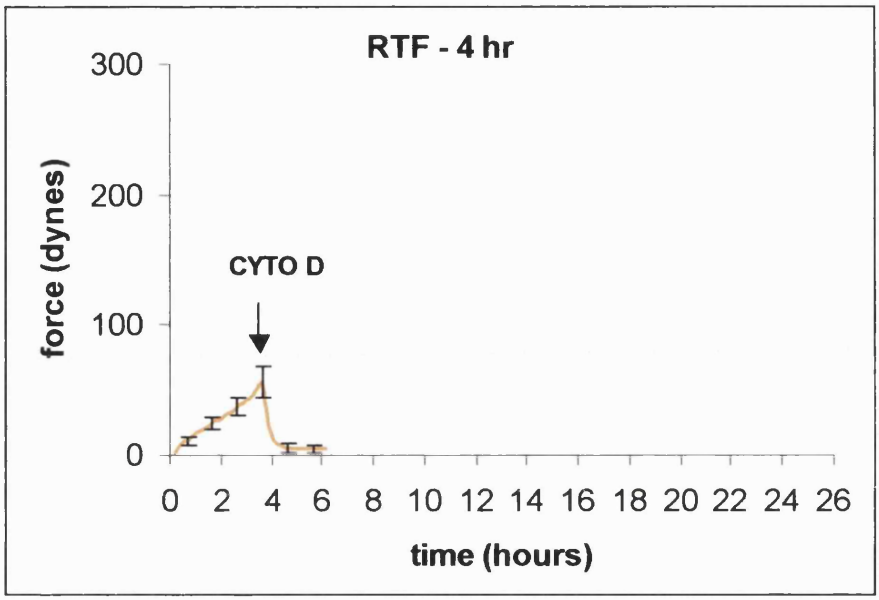

Figure 4-19 RTF were allowed to isometrically contract the matrix for 4 h in standard culture condition, at which point cytochalasin D (CYTO D) was added (indicated with the arrow).

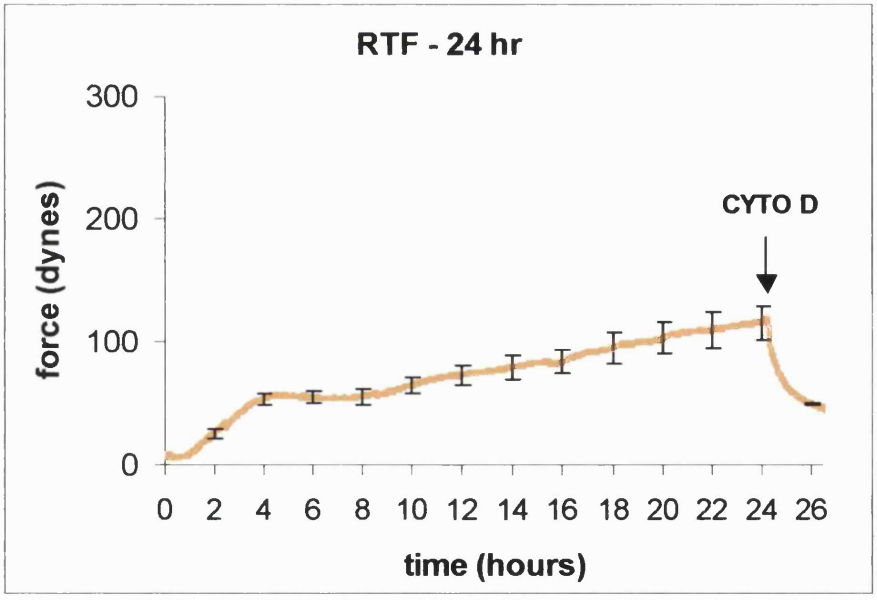

Figure 4-20 RTF were allowed to isometrically contract the matrix for 24 h in standard culture condition, at which point cytochalasin D (CYTO D) was added.

Figure 4-21 shows the equivalent profile with CD added at 61 hours with again a clear residual tension of 90 ± 21.2 dynes at 2 hours post treatment. It was important to note that in 24 hours and 61 hours traces there was again a slow rise in force generation (8 hours onwards) after the initial equilibrium phase (post traction) between 4 and 8 hours. This rise was approximately linear from 8 hours onwards up to 36 hours at which stage the gradient reduced.

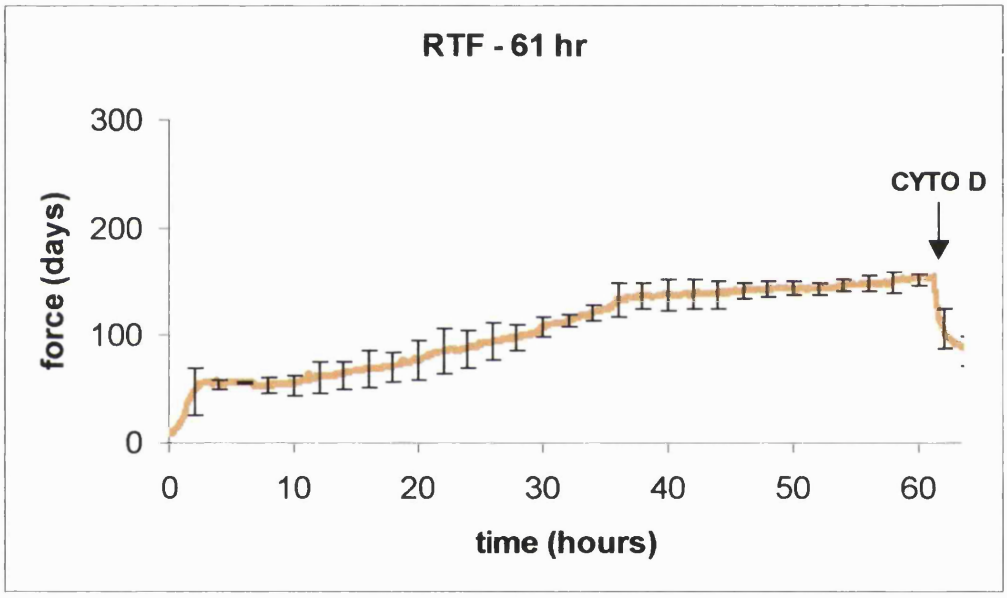

Figure 4-21 RTF were allowed to isometrically contract the matrix for 61 h in standard culture condition, at which point cytochalasin D (CYTO D) was added.

The RMT results of this set of experiments are summarised in Figure 4-22. RMT rose almost linearly (R^2=0.97) with culture time (rate 1.4 dynes/h), starting at baseline level at 4 hours time point to approximately 90 dynes total by 61 hours. RMT was 10.6 ± 3.0 fold greater than baseline at 24 hours and 18.1 ± 4.75 at 61 hours. The increase at 24 and 61 hours were highly significant.

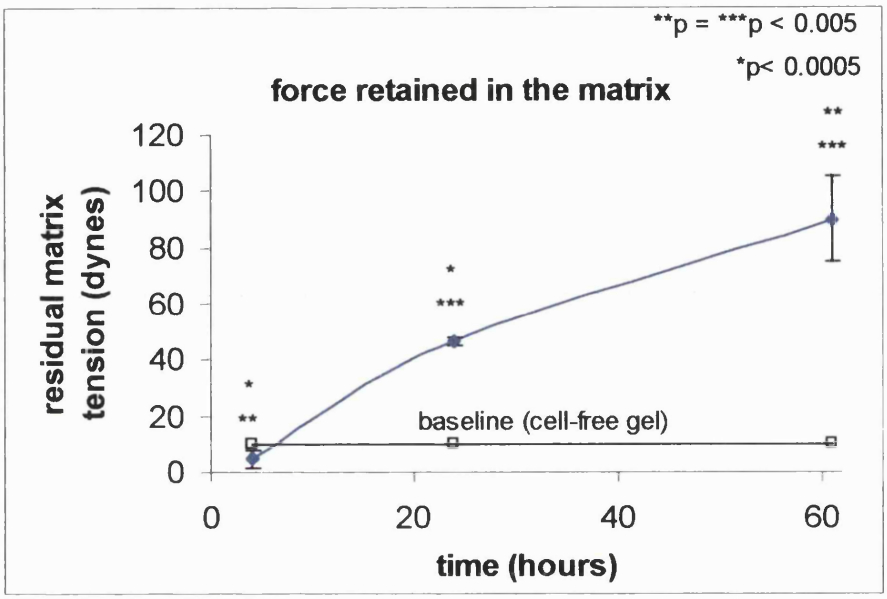

Figure 4-22 Force retained in the matrix when cytochalasin D was given at different time points: 4, 24 and 61 hours. RMT increased steadily over culture time. Error bars represent SE. 4 hours point was not significantly different from the baseline cell-free contraction. 24 and 61 hours points were significantly different from 4 hours point (*p<0.0005, **p<0.005 respectively) and between each other (*p<0.005).**

4.2.3.4.2 Analysis of 24 h RMT – Effect of different treatments

The objective here was to test if it is possible to predictically alter RMT using specific changes to culture and mechanical conditions. For this, a single time point was used (24 hours). In each case cytochalasin D (CD) was added to the culture and force response monitored.

A) TGF-β1 TREATMENT

TGF-β1 at a concentration of 12 ng/ml was added at time zero, immediately after the CFM collagen gel seeded with RTF had been set and topped up with medium. Figure 4-23 shows the contraction profile over 24

hours with and without TGF-β1. Both profiles have been described above (section 4.2.3.3.5). Briefly, the initial phase (0 to 4 hours) of cell traction was similar with and without TGF-β1. Between 4 and 8 hours without TGF-β1 the profile showed a long equilibrium phase (gradient was -0.36 ± 0.18 dynes/h). With TGF-β1 the plateau phase was very short and the force started to rise again from 4 hours onwards (the gradient between 4 and 8 hours was 21.7 ± 7.3 dynes/h). The force rose almost linearly between 8 and 24 hours in both contraction profiles with gradients of 12.1 ± 1.6 dynes/h for TGFB1 treated and 3.88 ± 0.82 dynes/h without addition. The peak contraction force induced by TGF-β1 was 3.01 ± 0.45 fold greater than without growth factor ($p<0.05$).

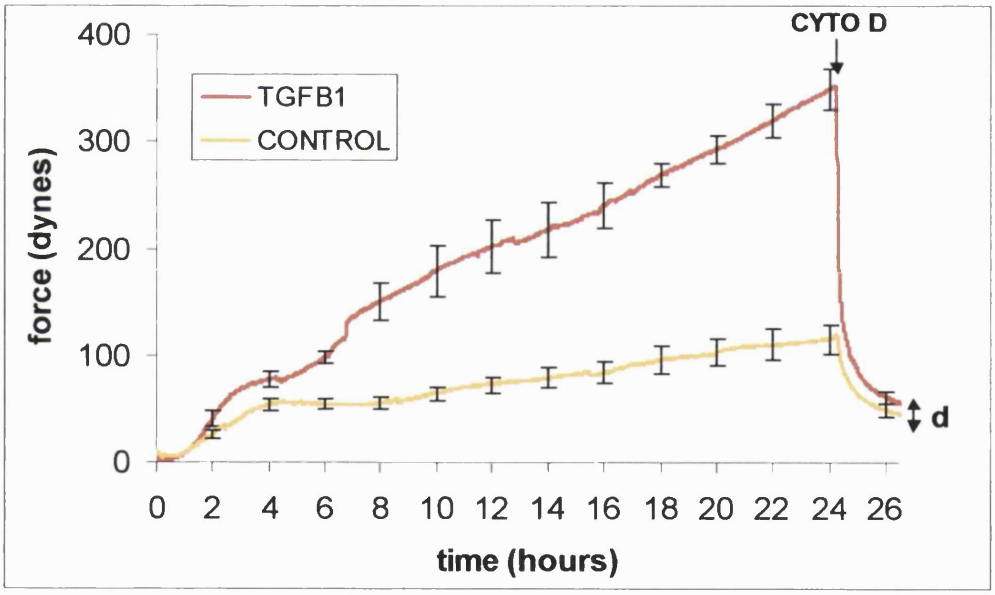

Figure 4-23 Effect of TGF-β1 on RTF contraction and remodelling. The arrowed line "d" (see zoom of this in Figure 4-24) represents the difference in force retained (RMT) with or without TGF-β1 at 2 hour.

Addition of CD at 24 hours caused a rapid force drop in all cases that reached a near plateau within 2 hours. The total force drop (2 hours post

CD) was 301.3 ± 16.6 dynes in the TGFB1 treated, a 4 fold greater drop than for non treated cultures.

Figure 4-24 is a zoomed detail of the last half hour before the RMT end point (26.25 hours, 2 hours post CD). The detail confirms that the residual force did indeed reach a plateau for both treated and untreated control curves. Both gradients were almost flat gradients over this last half hour.

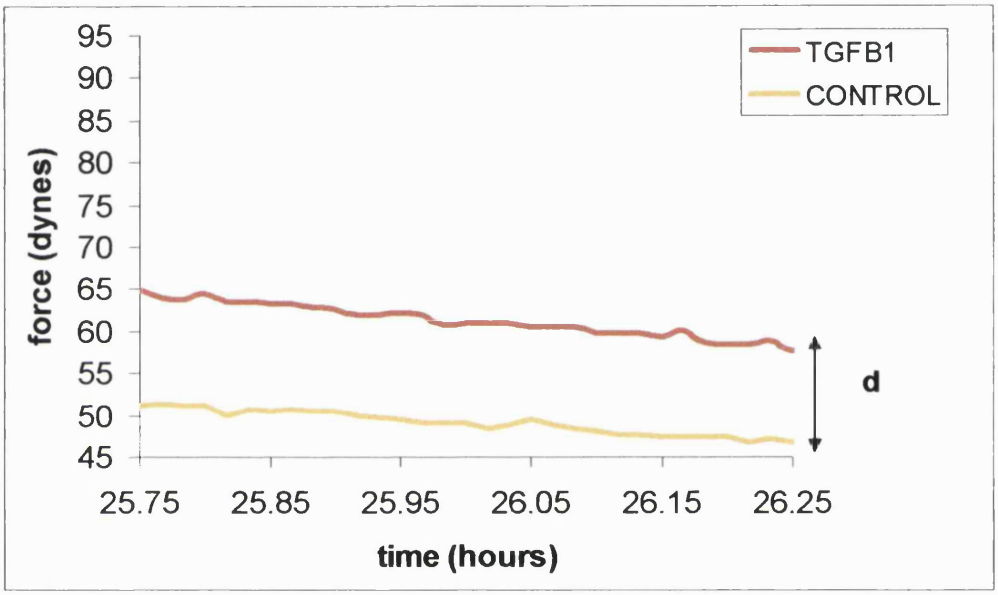

Figure 4-24 Detail of the last half hour before the RMT end point (26.25 hours, 2 hours post CD). The difference "d" (arrowed line) in force retained (RMT) with or without TGF-β1 is evidenced in this representation.

The average RMT in TGF-β1 treated (57.5 ± 10 dynes) was 17.1 ± 6.4% higher than untreated (47 ± 1.5 dynes) but this increase was not statistically significant.

This lack of statistical significance was due to unusual high variance to response to batch of TGF-β1 used in this experimental series. In a parallel, repeat series of tests (using TGF-β1 supplied by PeprotechEC, UK, instead of Sigma, UK, at slightly higher concentration, i.e. 15 ng/ml instead of 12 ng/ml) much lower variance was seen and the increase in RMT in this case

was significant (experiment carried out in collaboration with Dr. Nicholas Wilson-Jones). It should be noted the high level of agreement between the two series of experiments and similar shift in force due to TGF-β1. Again the RMT (2 hours post CD treatment) was higher with rather than without TGF-β1 (i.e. 46.6 ± 6.0% higher than non treated). However, in this case the greater RMT with TGF-β1 treatment was significant ($p < 0.05$).

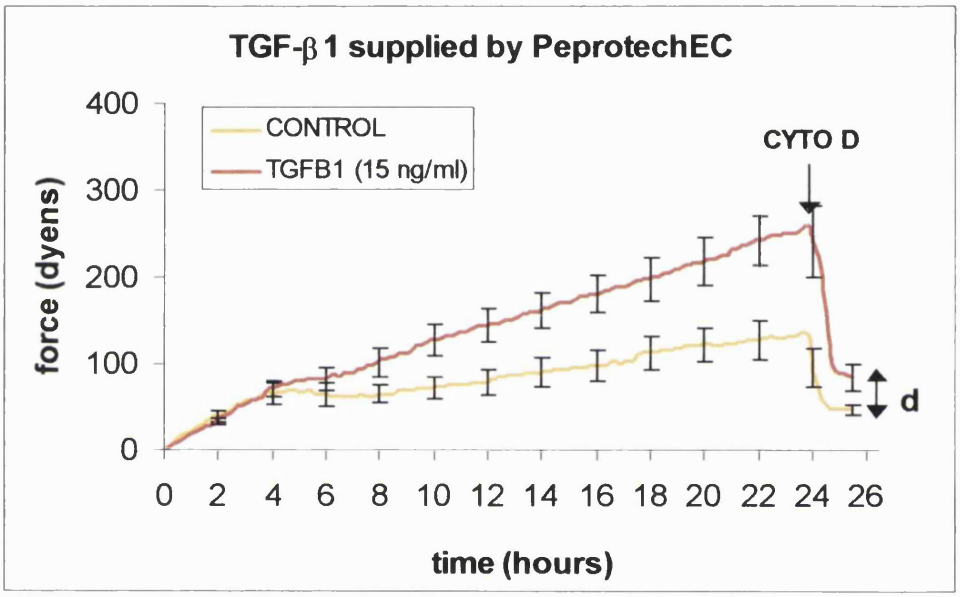

Figure 4-25 Repeat of the experiment shown in Figure 4-23 with TGF-β1 from a different supplier (PeprotechEC, UK in place of SIGMA, UK) and a higher concentration 15 ng/ml in place of 12 ng/ml. These data were produced in collaboration with Dr. Nicholas Wilson-Jones.

Comparison of Figure 4-23 and Figure 4-25 indicated differences in response between 2 batches of TGF-β1 from different manufacturers. Also the concentration used were slightly different. The highest concentration caused significant increase in RMT between TGF-β1 treated and untreated RTFs. Further studies are necessary to determine if small differences in TGF-β1 concentration from the same batch and supplier can affect the RMT.

B) CYCLIC MECHANICAL LOADING

A regime of slow cyclic mechanical loading (1 cycle/h) at small strain amplitudes (~1%) was superimposed on the standard contraction between 8 and 24 hours. Figure 4-26 shows the contraction profile over 24 hours of RTF populated gel under standard culture conditions (control) or stimulated with cyclic mechanical loading for 16 hours. The initial phase (0 to 8 hours) for cyclically loaded and control had exactly the same trend. Initial traction (0 to 4 hours) and subsequent equilibrium phase (4 to 8 hours). Contraction force was overall slightly higher than in the control condition in this initial phase but this difference was not significant. Between 8 and 24 hours the control force generation rose almost linearly as described previously. Superimposed mechanical loading did not alter this trend (dashed blue straight line in Figure 4-26). The average gradient between 8 and 24 hours was 5.2 dynes/h for the cyclically loaded trend line across the load pattern and 3.88 ± 0.82 dynes/h for control, consistent with a small increase in the rate of force generation. Differences in force levels were not significant over 24 hours (baseline levels along the cyclic loading pattern were considered).

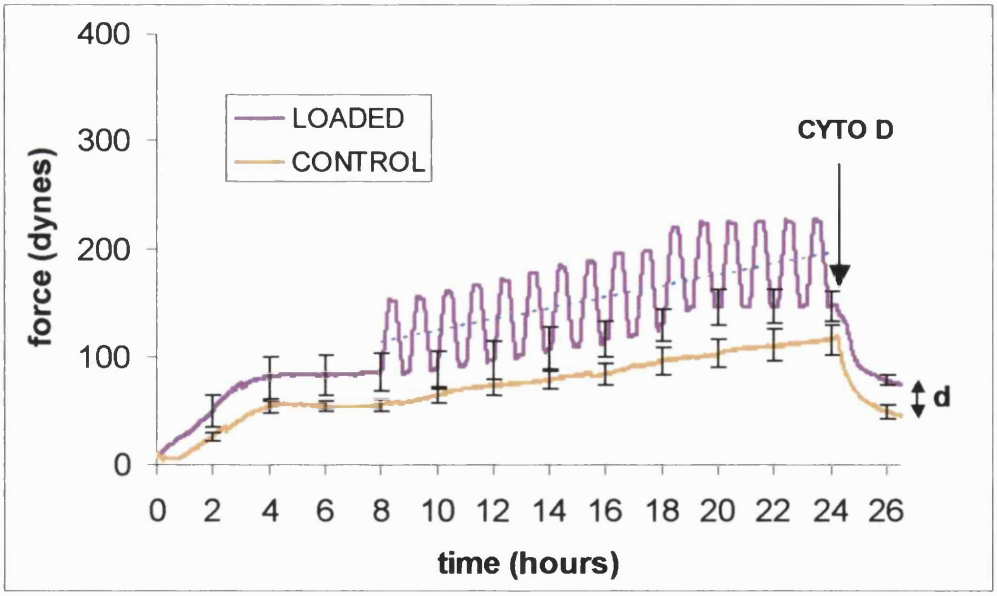

Figure 4-26 Cyclic mechanical loading superimposed on the standard contraction curve. The arrowed line "d" (see zoom of this in Figure 4-27) represents the difference between control and loaded in RMT at 2 hours.

Addition of CD at 24 hours caused a rapid force drop that reached a plateau within 2 hours for both traces. Figure 4-27 is a a zoomed detail of the last half hour before the time point (26.25 h) where RMT was measured (i.e. 2 hours after cytochalasin treatment). As before, the magnification allows us to verify that the force indeed reached a plateau with almost flat gradients for both curves.

The mean value of RMT was 1.58 ± 0.05 folds higher in mechanically loaded stimulated (64 ± 21.5 dynes) than control (47 ± 1.5 dynes). The increase was statistically significant.

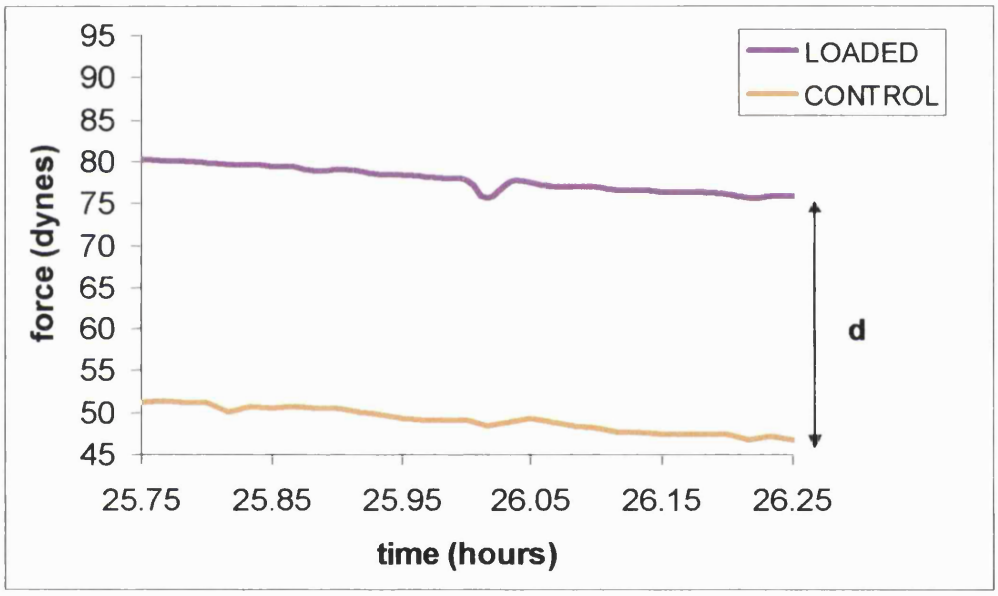

Figure 4-27 Detail of the last half hour before the RMT end point (26.25 hours, 2 hours post CD). The difference "d" (arrowed line) in force retained (RMT) with or without cyclic mechanical loading is evidenced in this representation.

C) COMBINED TREATMENT (TGF-β1 AND CYCLIC MECHANICAL LOADING)

The combined treatment (CT) was composed of TGF-β1 and cyclic mechanical loading. The two single treatments have been described earlier in this section.

Figure 4-28 shows the contraction profile over 24 hours of RTF populated gel under control culture conditions or treated with the combined TGF-β1 and cyclic loading. The initial phase (0 to 8 hours) for the CT profile was similar to that seen for TGF-β1 treatment above (Figure 4-23). There was a traction phase (0 to 4 hours) slightly higher than control. The subsequent equilibrium phase (4 to 8 hours) observed in the control was largely replaced by a steep ramp (gradient was 31.6 ± 20.6 dynes/h).

The average gradient between 8 and 24 was 9.9 ± 4.5 dynes/h for the trend line across the load pattern in the CT profile (dashed red line in Figure 4-28), compared with 21.7 ± 7.3 dynes/h for the profile of TGF-β1 alone and 3.88 ± 0.82 dynes/h for the control. Therefore the force rise along the load pattern in CT (8 to 24 hours) had a linear increase at a rate between TGF-β1 alone and the control. This indicates that mechanical loading had a slight flattening effect on the steep linear rise seen for TGF-β1 alone but did not abolish the effect (CT gradient remained more than 2 fold greater than the untreated control). Variation between replicate runs was substantial, particularly in the central part of the profile (8 to 18 hours), potentially due to interference or synergy between the two regimes. For comparison Figure 4-29 shows the contraction profiles of single and combined treatments. The graph clearly indicates how the combined treatment resulted in a superimposition of effects. The effect of cyclic loading could be roughly superimposed on the contraction profile with or without TGF-β1.

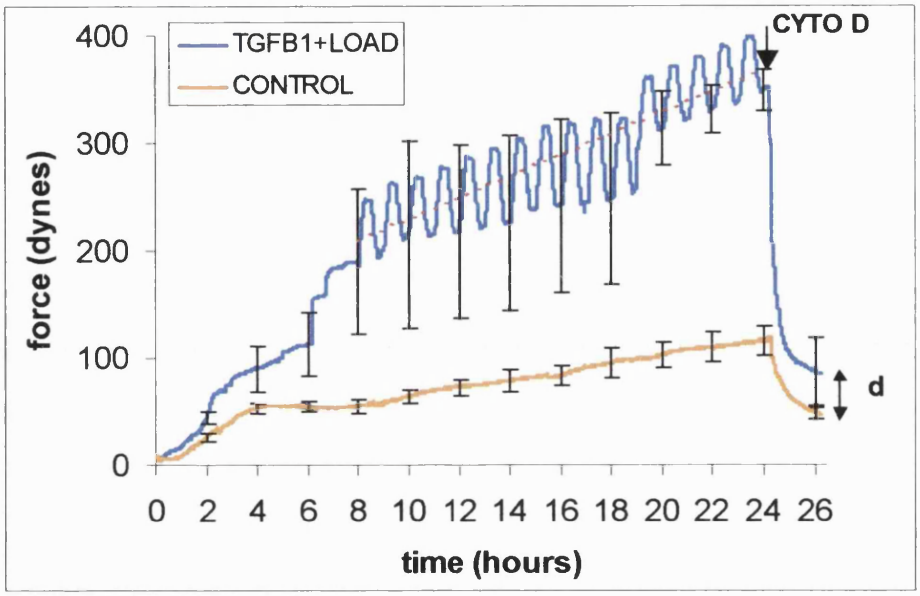

Figure 4-28 Effect of combined treatment (CT) made up of TGF-β1 treatment and cyclic superimposed mechanical loading. The arrowed line "d" (see zoom of this in the Figure 4-30) represents the difference between control and CT in the force retained in the matrix at 2 hour.

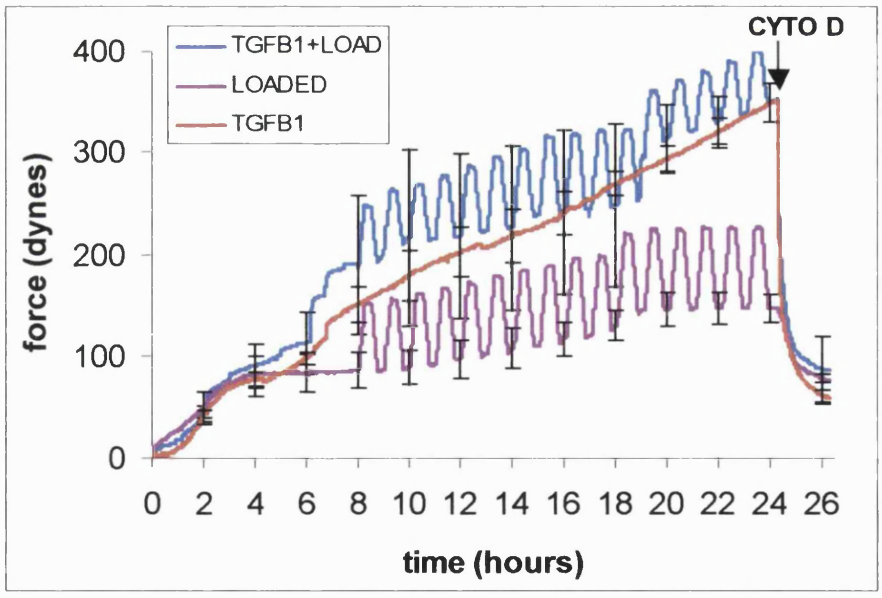

Figure 4-29 Contraction profile of the combined treatment (i.e. TGF-β1 and mechanical loading) plotted together with the single stimulations, mechanical loading only (LOADED) and TGF-β1 only.

Addition of CD at 24 hours caused a rapid force drop that reached a plateau within 2 hours for both traces. Figure 4-30 is a zoomed detail of the last half hour before the RMT end point (26.25 h) where RMT was measured (i.e. 2 hours after cytochalasin treatment). Again there was a clear plateau for both treated and control curves, with almost flat gradients.

The mean RMT was 1.7 ± 0.5 fold higher in CT treated (81.3 ± 29.5 dynes) than control (47 ± 1.5 dynes), though this increase did not reach statistical significance, due to high replicate variance in the treated group.

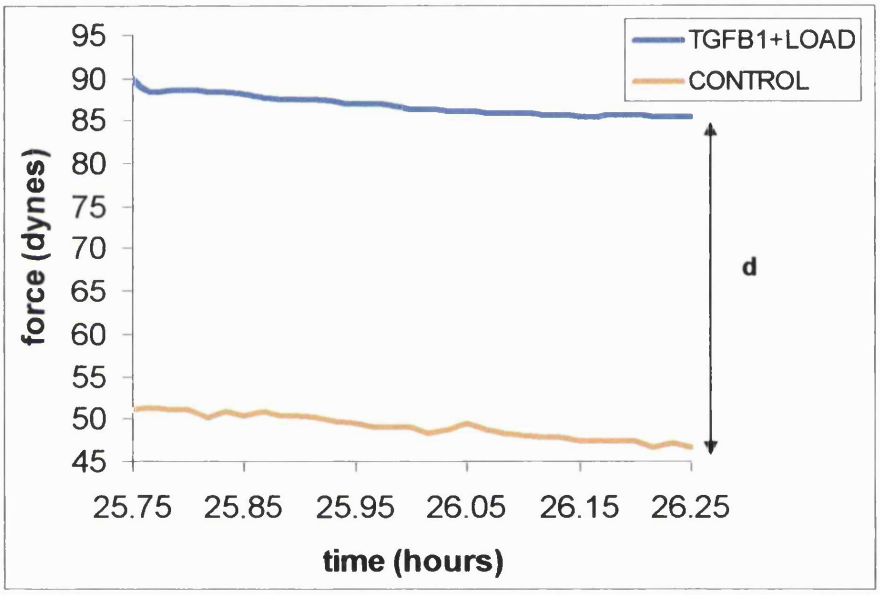

Figure 4-30 Detail of the last half hour before the RMT end point (26.25 hours, 2 hours post CD). The difference "d" (arrowed line) in force retained (RMT) with or without combined treatment (TGFB1 and cyclic loading) is evidenced in this representation.

In summary the mean RMT was higher in CT than when the single stimulations were applied (e.g. 1.4 fold higher than TGF-β1 alone). However this increase in RMT level was not statistically significant.

D) DEPLETION OF ASCORBATE

Since ascorbate is a key factor in collagen synthesis, the RMT test (addition of CD at 24 hours) was carried out on cultures in ascorbate-free medium. The aim of this experiment was to identify possible correlation between collagen production by cells and the degree of matrix remodelling, measured as RMT at 2 hours post CD treatment.

Figure 4-31 shows that both contraction profile and residual matrix tension were similar with and without ascorbate under these conditions.

RMT at 2 hours after CD treatment was the same at 47.2 ± 8 dynes and 47 ± 1.5 dynes for with and without ascorbate respectively.

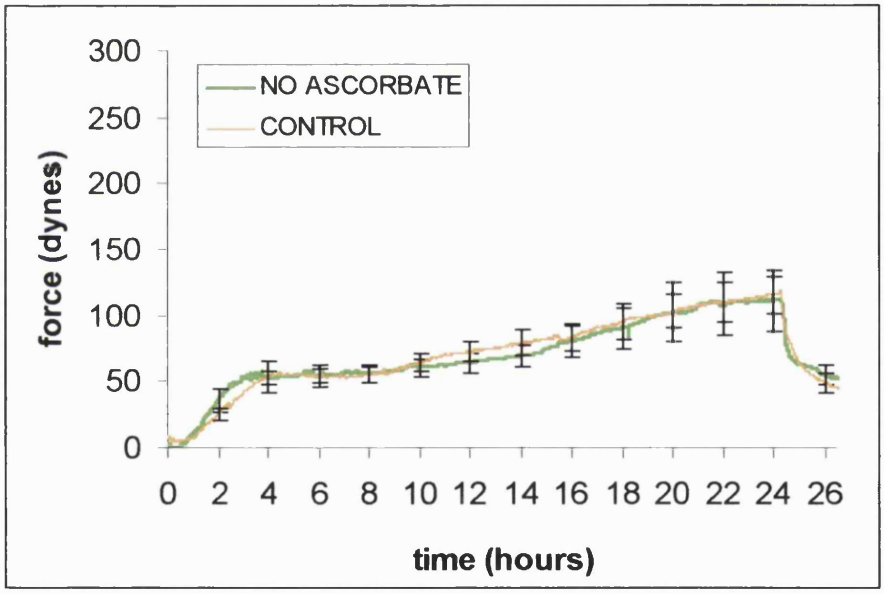

Figure 4-31 Effect of removal of ascorbate from the culture medium on RTF contraction and remodelling.

It is concluded that the short term absence of ascorbate has no effect on the early matrix remodelling (24 hours) compared to standard culture conditions. The effect of ascorbate depletion could be more evident for the treatments, such as cyclic loading and TGF-β1, which are known to enhance matrix production by cells. These combinations were not tested in the current study.

SUMMARY OF RMT ANALYSIS (2 HOURS POST CYTOCHALASIN TREATMENT

Figure 4-32 summarises the results obtained for the retained matrix tension (RMT) measured two hours after cytochalasin treatment.

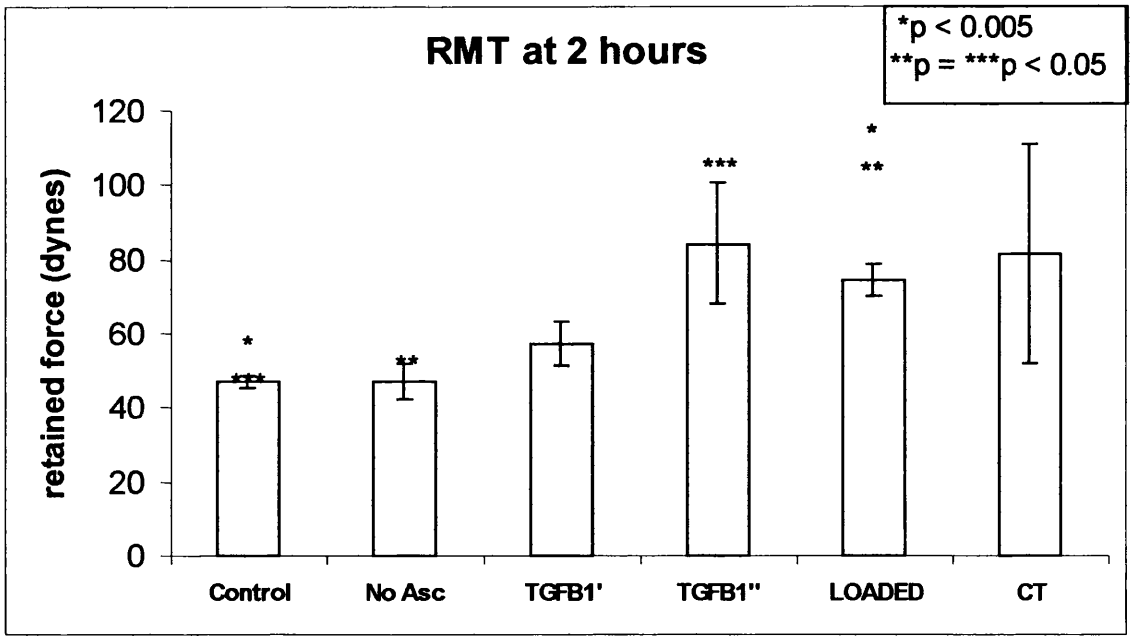

Figure 4-32 Tension retained in the matrix (RMT) 2 hours after addition of cytochalasin D depending on different culture conditions. Vertical bars represent SE. Statistical significance is represented by symbols above columns associating them in pairs. RMT value in cyclic loaded lattices (labelled LOADED) was significantly higher than in both control (*p<0.005) and depleted ascorbate (p<0.05) lattices. TGF-β1' and TGF-β1" represent the two different batches, i.e. SIGMA and PeprotechEC respectively. Only RMT value in TGF-β1" treated lattices was significantly higher than in control lattices (***p<0.05). Columns not paired by symbols were not significantly different between them.**

In Figure 4-32, the highest mean RMT value, excluding TGFB", was achieved for combined treatment (CT). This suggested that CT had at least an additive response (effect is sum of the two single stimulation effects)

although there was a large variance, which compromised its statistical significance.

RMT value in cyclically load lattices was significantly higher (1.6 fold greater) than control and depleted ascorbate cultures.

TGF-β1' and TGF-β1" represent the two different batches, i.e. SIGMA (Figure 4-23) and PeprotechEC (Figure 4-25) respectively which were used at slightly different concentrations (12 and 15 ng/ml respectively). Only RMT value in TGF-β1" treated was significantly higher than control. Mean RMT values in TGF-β1' treated and CT (in which TGF-β1' was used) resulted both higher than control but did not reach statistical significance due to high replicate variance of the treated groups.

Depletion of ascorbate from culture medium did not alter the average RMT value measured for control condition.

In conclusion cyclical loading and TGF-β1 (batch TGF-β1") treatments produced a significant increase in the collagen matrix remodelling after 24 hours of culture compared to control. Combined treatment (with batch TGF-β1') did not increase RMT significantly compared to either treatment, indicating that the effect of the combination was neither additive nor synergetic.

Additional information on the dynamics of the force curves in the timeframe preceding RMT measurement (i.e. 0 to 2 hours post CD treatments) are needed in order to understand the mechanisms of formation of RMT under the different treatments.

4.2.3.5 Analysis of the force drop during the first 2 hours after cytochalasin D treatment.

The force profiles in the initial 2 hours post cytochalasin D (CD) treatment were analysed in order to investigate the dynamics of the force in the lattices for the different treatments.

Figure 4-33 shows the percentage of force drop in the 2 hours post CD treatment. TGF-β1 treated lattices presented the highest percentage of force drop (84%), while cyclically loaded lattices the lowest (44%).

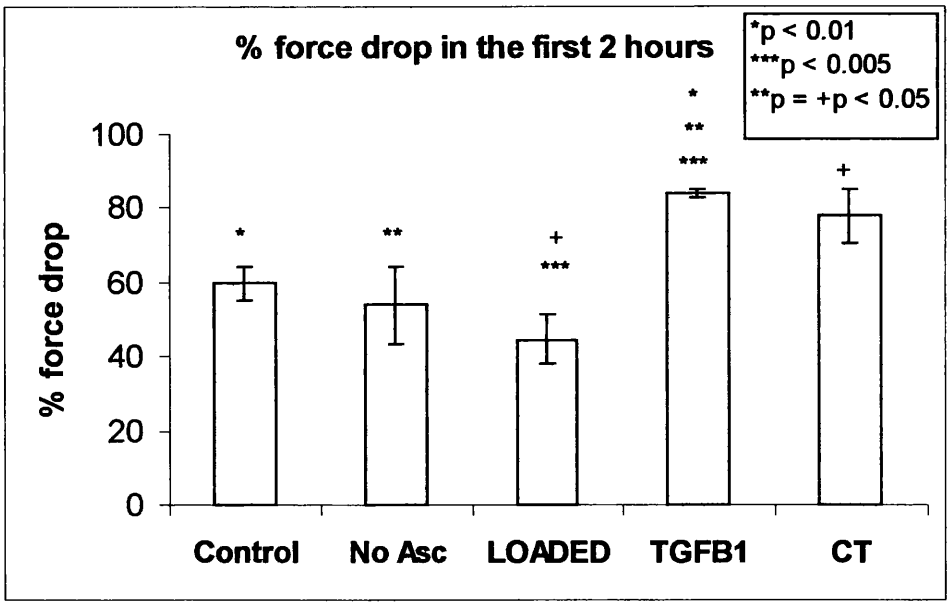

Figure 4-33 Percentage of mean force drop in the first 2 hours post CD addition for the different treatments. Force drop was calculated as the difference between the force at time 0 (immediately before CD treatment) and RMT at 2 hours. Vertical bars represent SE. Statistical significance is represented by symbols above columns associating them in pairs. Percentage of force drop in TGF-β1 treated lattices was significantly higher than control (*p<0.01), depleted ascorbate (p<0.05) and cyclically loaded (labelled LOADED, ***p<0.005). CT treatment produced a force drop percentage significantly higher than cyclically loaded (+p<0.05), and higher than control and depleted ascorbate but not statistically significant. Columns not paired by symbols were not significantly different between them.**

When TGF-β1 was added to the cultures with and without combined cyclic loading, the percentage of force drop (Figure 4-33) was significantly higher than control. This indicated that increased cell force generation corresponded also to increased force drop when the cell tensile cytoskeleton was disrupted.

Cyclic loading treatment had the effect of reducing force drop both when TGF-β1 was present (i.e. CT lower than TGF-β1) and in absence of the growth factor (i.e. cyclically loaded lower than control).

It is concluded that TGF-β1 and cyclic loading treatment produced different effects and that these are almost antagonistic on the percentage force drop after CD treatment.

The gradients of the force curves between the 10 and 20 minutes time points post CD addition were analysed. The aim was to assess the early dynamics of the force drop leading to the total percentage drop at 2 hours post CD treatment (Figure 4-33).

The gradients of dropping force over the first 10 and 20 minutes after CD addition for the different treatments are shown in Figure 4-34. TGF-β1 treatment produced the greatest gradient of force drop at 10 minutes, 9.1 fold greater than control at 10 minutes. The gradients of force drop at both 10 and 20 minutes in TGF-β1 and CT were significantly higher than all the other culture conditions in both.

Gradients for TGF-β1 and CT treatments were almost halved between 10 and 20 minutes (£$p<0.01$ and ^$p<0.05$ respectively). This indicated that most of the force drop in TGF-β1 treated happened very rapidly and started slowing down already after the first 10 minutes.

In absence of TGF-β1 the gradients were approximately constant over the first 20 minutes, with small (and non significant) differences between the 10 and 20 minutes gradients.

In conclusion the effect of the different treatments on of the force drop rate at early time points (10 and 20 minutes) was consistent with the effect seen (Figure 4-33) on the percentage of total force drop at later stage (2

hours post CD treatment). TGF-β1 treatment (± cyclic loading) increased both the percentage of force drop at 2 hours post CD treatment and the slopes of the force drop at early time points. The dynamics of this effect were evident in the analysis of the gradients at early time points, which showed how the high gradient of force drop, in TGF-β1 treated lattices, started to decrease between 10 and 20 minutes after CD treatment. This was also consistent with the plateau (very low gradient) in the force curves, that were reached within 2 hours post CD treatment.

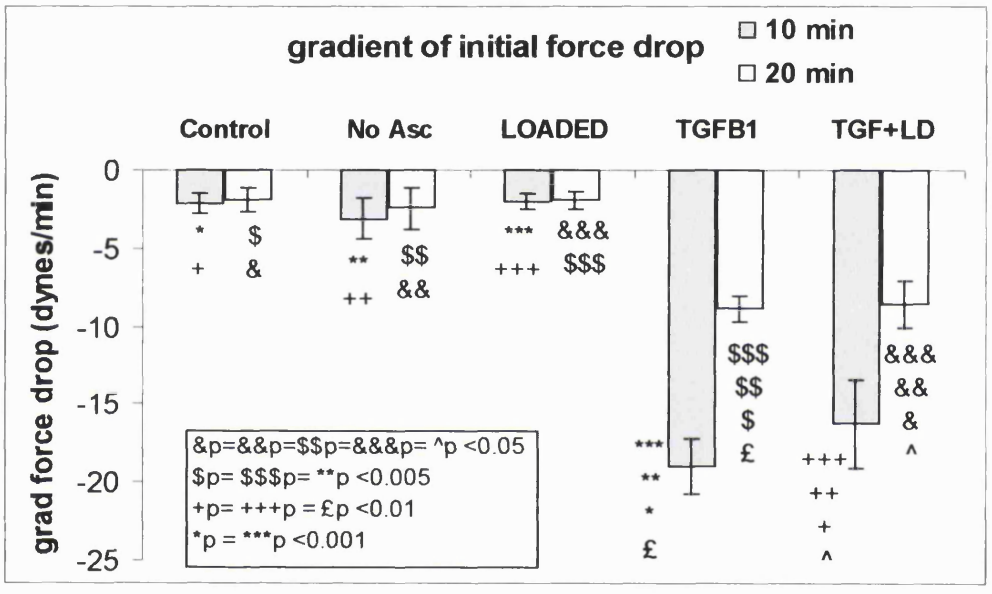

Figure 4-34 Gradient of force drop immediately after cytochalasin treatment (i.e. calculated in the intervals 0-10 min and 0-20 min). Gradients were computed from the best interpolating line (R^2 >0.90) on each force drop curve. Vertical bars represent SE. Statistical significance is represented by symbols above columns associating them in pairs. Gradients of force drop at 10 and 20 min in TGF-β1 and CT treated lattices were significantly greater than respective 10 and 20 min gradients in control, depleted ascorbate and cyclically loaded (labelled LOADED), with p-values as shown. Gradients of force drop at 20 min in TGF-β1 and CT treated lattices were still significantly greater than gradients at 10 min in control, depleted ascorbate and cyclically loaded (labelled LOADED), p-values not shown for graphic clarity reasons. The gradients of force drop at 10 in TGF-β1 and CT were significantly greater than TGF-β1 and CT gradients at 20 min (£p<0.01 and ^p<0.05 respectively). Columns not paired by symbols were not significantly different between them.

4.2.3.6 Measurement of RMT at 12 hours post cytochalasin D treatment and analysis of the force drop from 2 to 12 hours

After the initial rapid force drop and following stabilisation within 2 hours, a very slow decrease in force between 2 and 12 hours was noted. This slow force drop was analysed with the hypothesis that most of the changes measured were due to the remodelled matrix alone. Hence, this further analysis aimed to study the stability of the remodelled matrix in the longer term, assuming minimal cellular remodelling activity along the period under investigation. This assumption was supported by observation of cell ultrastructure under the TEM 12 hours after CD treatment (see section below in this chapter). In addition, many investigators reported complete abolition of cell contractile activity in presence of high concentration (> 2 μM) of CD for extended periods of time (Grinnell & Ho, 2002; Roy et al., 1997; Sawhney & Howard, 2002; Tamariz & Grinnell, 2002).

For convenience, the tension retained in the matrix measured at 12 hours after CD treatment will be labelled RMT_{12} while RMT alone will refer to the measurement at 2 hours.

Figure 4-35 shows the mean values of tension retained in the matrix measured at 12 hours (RMT_{12}). The RMT_{12} value for cyclically loaded lattices was the highest and significantly higher than for TGF-β1 (51%) treated, control (35%) and depleted ascorbate (42%) lattices. The mean value of RMT_{12} for TGF-β1 treated lattices was 25% lower than control, though this was not significant. Naturally this effect was much greater when expressed in relation to max force generated in TGF-β1 treated cultures.
The mean value of RMT_{12} in CT lattices was close to RMT_{12} in cyclically loaded alone, suggesting that superimposed mechanical loading altered TGF-β1 effect on relaxation. Therefore over the longer-term, CT had neither synergetic nor additive response but rather syncretic (effect is the mean of the 2 single stimulation effects). This observation cannot be affirmed

conclusively due to the large variation and the small sample size (n=2) that caused RMT_{12} value for CT to be not significantly different from control and TGF-β1 values.

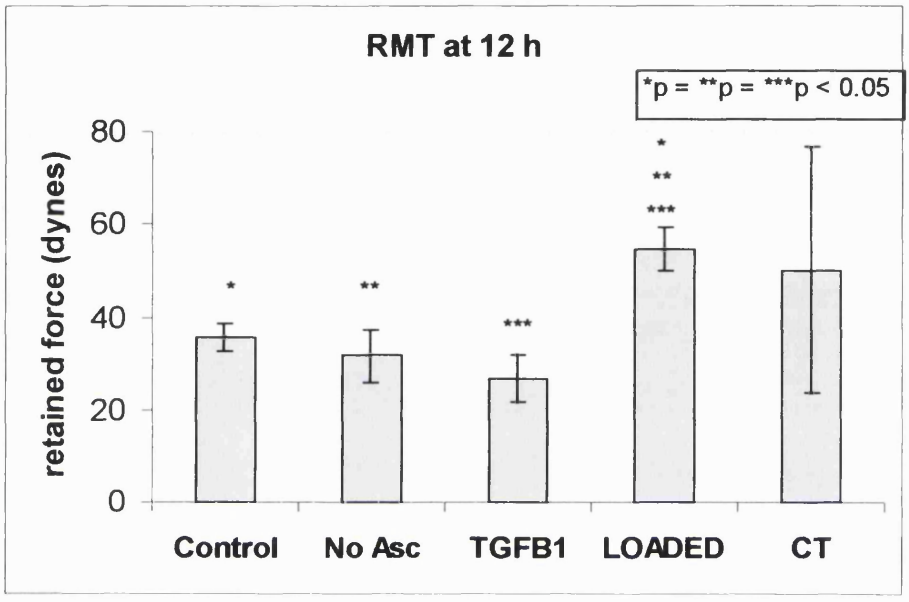

Figure 4-35 Tension retained in the matrix (RMT_{12}) 12 hours after addition of cytochalasin D depending on different culture conditions. Vertical bars represent SE. Statistical significance is represented by symbols above columns associating them in pairs. RMT_{12} value for cyclic loaded lattices (labelled LOADED) was significantly higher than for control (*p<0.005), depleted ascorbate (p<0.05) and TGF-β1 treated (***p<0.05) lattices. Columns not paired by symbols were not significantly different between them.**

It is concluded that, over the complete 12 hours period of RMT monitoring, cyclic loading and TGF-β1 appeared to have distinct (even antagonistic) effects on mechanical properties of the remodelled matrix.
By this parameter cyclic loading significantly increased matrix strength (in contrast to TGF-β1 which appeared to actually reduce it compared to control).

The dynamics of the force drop between 2 and 12 hours was analysed in the same way as the 0-2 h period. The percentage force drop displayed in Figure 4-36 shows a general reduction compared to 0 to 2 hours period (Figure 4-33) as expected from the reduced rate of force drop.
However, comparison between treatments (Figure 4-36) showed that again TGF-β1 treatment (± cyclic loading) produced the highest percentage fall (~53% with TGF-β1 (± cyclic loading) compared to ~30% without TGF-β1, $p<0.05$).

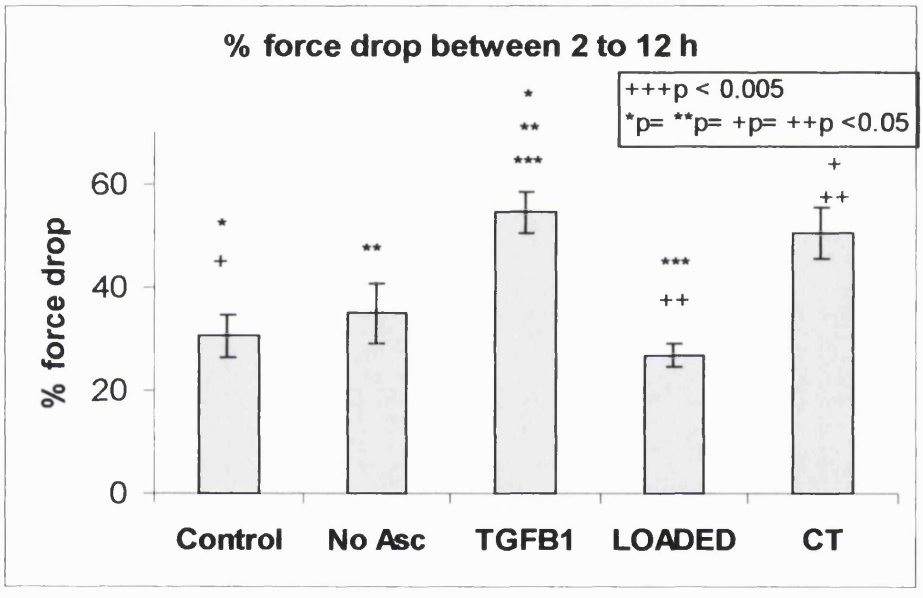

Figure 4-36 Percentage of force drop between 2 to 12 hours, post CD addition, for the different treatments. Force drop, here, was calculated as the difference between RMT and RMT_{12}. Vertical bars represent SE. Statistical significance is represented by symbols above columns associating them in pairs. Percentage of force drop for TGF-β1 treated lattices was significantly higher than control (*p<0.05), depleted ascorbate (p<0.05) and cyclically loaded lattices (labelled LOADED, ***p<0.005). CT produced a percentage of force drop significantly higher than for control (+p<0.05) and cyclically loaded (++p<0.05) lattices. Columns not paired by symbols were not significantly different between them.**

Cyclic loading treatment produced a small fall in percentage of force drop (24.8% compared to 30.5% in control) but this more stable matrix could

be relatively destabilised (greater force drop increased by 1.9 fold, $p<0.05$) by treatment with TGF-β1 (i.e. cyclic loading + TGF-β1).

Again this supports the idea that the higher level of RMT produced by TGF-β1 (even in presence of loading) produces less mechanically stable new matrix structure.

Figure 4-37 shows the average speed of dropping force between 2 and 12 hours post CD addition for the different treatments.

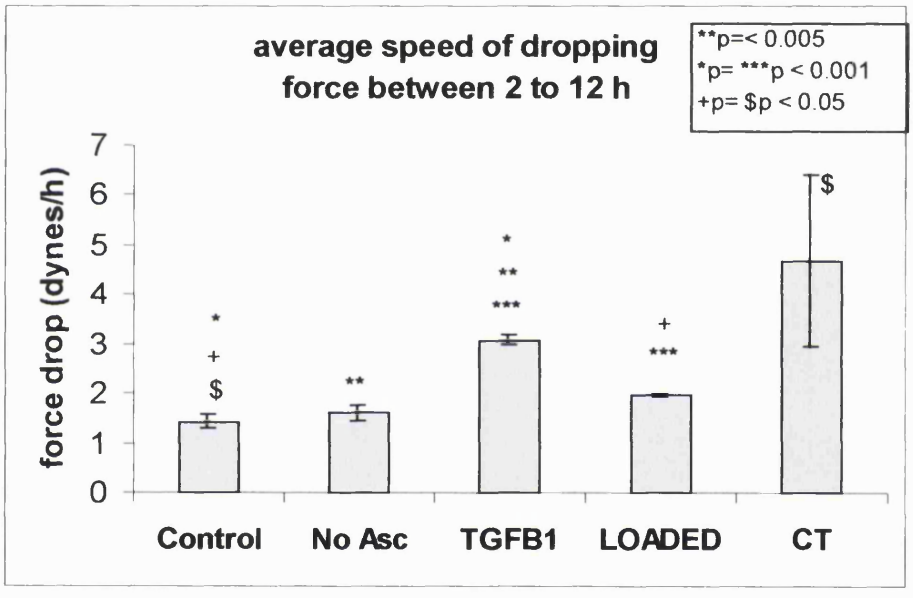

Figure 4-37 Average speed of dropping force between 2 and 12 hours, post CD addition, for the different treatments. Vertical bars represent SE. Statistical significance is represented by symbols above columns associating them in pairs. Average speed of dropping force for TGF-β1 treated lattices was significantly higher than control (*$p<0.001$), depleted ascorbate ($p<0.005$) and cyclically loaded lattices (labelled LOADED, ***$p<0.001$). CT produced the highest average speed of dropping force and was significantly higher than control ($p<0.05$). and Cyclically loaded lattices had a faster speed of dropping force than control (+$p<0.05$). Columns not paired by symbols were not significantly different between them.**

Differences between the low speeds (between 50 and 20 fold lower compared to the 0 to 2 hours period) showed that, again, TGF-β1 treatment

(± cyclic loading) produced the highest average speed of dropping force (3.0 and 4.6 dynes/h with TGF-β1 and CT respectively) compared to without TGF-β1, $p<0.05$). Average speed of dropping force in cyclically loaded lattices was significantly higher (27.4%) than in control. CT treatment seemed to achieve a near additive response (sum of the two responses) on this parameter. Hence CT appeared to produce an increased plasticity in the new material, which caused it to keep deforming over prolonged time. This was not consistent with the trend shown in the percentage of force drop between 2 and 12 hours in which CT treatment did not produce an additive response but an average of the effects.

In conclusion, all treatments have shown to significantly increase the average speed of dropping force between 2 and 12 hours compared to control. This indicates that there was a significantly higher relaxation in the new material between 2 an 12 hours due to the treatments, which was particularly increased when TGF-β1 was added to the cultures.

4.2.3.7 Detailed analysis of the mechanical properties of the newly remodelled collagen matrix represented by RMT. Definition of the pseudo-viscosity parameter ρ

Analysis of the tension relaxation over time after CD treatment, in respect to the total tension generated in the lattices before CD treatment, showed that there was a fall in proportion between the total tension before and the residual tension after cytochalasin treatment. This effect was particularly evident in the TGF-β1 treated lattices where increased cell-mediated contraction force was followed by an increased in force drop percentage.

In order to analyse if a correlation was present between the initial level of total tension before force drop and the average speed at which force dropped, these two parameters (paired for each treatment) were plotted on a scatter graph and linear regression was computed. The average speed of dropping force in the timeframes 0-2 hours and 2-12 hours post CD treatment was calculated as the ratio between total force drop and timeframe. This approximation was possible thanks to the relative linearity of the force curve in the 2 timeframes considered ($R^2 > 0.95$ and $R^2 > 0.90$ respectively).

Figure 4-38 shows a scatter graph displaying the starting level of tension (i.e. the peak force before CD treatment) and the average speed of dropping force, in the 2 hours after CD treatment,

Points in the graph (Figure 4-38) clustered together along the linear interpolation showing that there was a clear direct proportionality ($R^2 > 0.98$) between the two parameters displayed. Hence lattice relaxation after CD treatment was directly proportional to the initial level of force before CD treatment. This level of force corresponded to the degree of deflection of the force transducer beam which worked like a linear spring applying a load to the lattice. Since the time of cellular actin cytoskeleton depolymerisation is constant, the differences in force drop (and rate of force drop) can only be

attributed to the relaxation of the newly remodelled material caused by the load generated by the spring action of the force transducer beam.

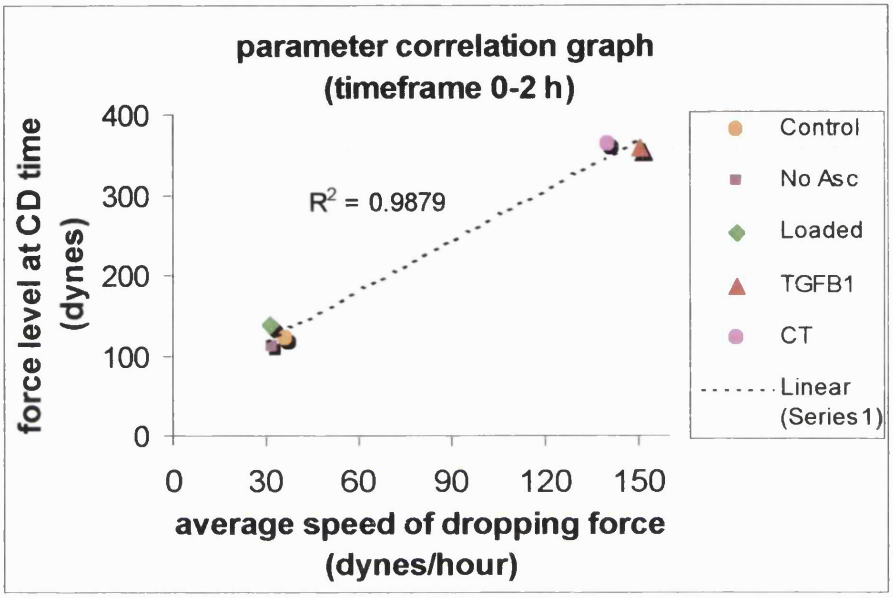

Figure 4-38 Scatter graph displaying the tension level just prior to CD addition versus the average speed of dropping force in the first 2 hours after CD addition for the different treatments. Each point represents a different treatment, is constituted by a pair of the average values of the two parameters (n≥3). The linear regression line (dashed) showed the high correlation of these data.

Correlation of the same parameters of Figure 4-38 but shifted to the timeframe 2 – 12 hours post CD treatments, was tested in Figure 4-39. In this, the starting level of tension was the force at 2 hours after CD treatment and the average speed of dropping force was calculated in the timeframe 2 – 12 hours.

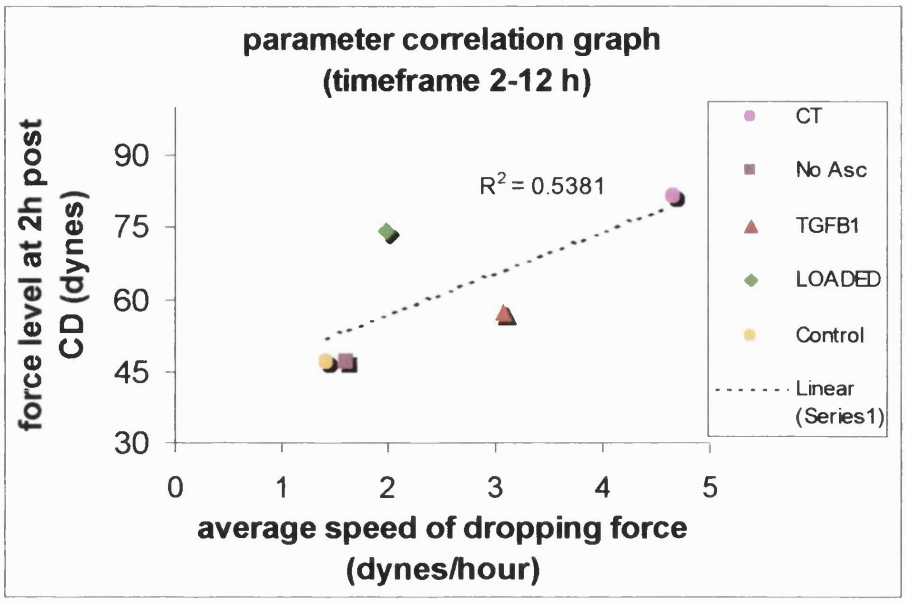

Figure 4-39 Scatter graph as in Figure 4-38, displaying the tension level at 2 hours post CD treatment (which is also the max force over the 2-12 h timeframe) versus the average speed of dropping force in the timeframe 2-12 hours for the different treatments. The linear regression line (dashed) showed that there was not a good correlation of these data.

Linear regression (Figure 4-39) showed that the values were not well correlated any longer. Hence, direct proportionality between the spring action of the force transducer beam and material relaxation was not as strong as in the previous timeframe (0-2 h).

This suggests the presence of weak bonds holding the architecture of the remodelled material. High loads were able to rapidly break these weak bonds until stronger bonds were reached and the relaxation diminished. The number of these stronger bonds, depending on the treatments, caused the differences in RMT levels measured. Therefore the subtle differences, among the remodelled matrices under the different treatments, appeared to play a role in the material relaxation in this later timeframe (2-12 h post CD). Lattice relaxation profiles, due to CD treatments, were analysed in comparison with standard material relaxation curves due to strain steps applied to the lattices. Relaxation of viscoelastic materials is characterised

by an exponential decay of stress with time to an asymptotic value that depends on the magnitude and rate of strain applied. This seemed to resemble the relaxation in tension measured after CD treatment in contracted lattice. By changing the time scale from linear to logarithmic, the decay curve of force drop can be transformed into an almost straight line (Figure 4-40).

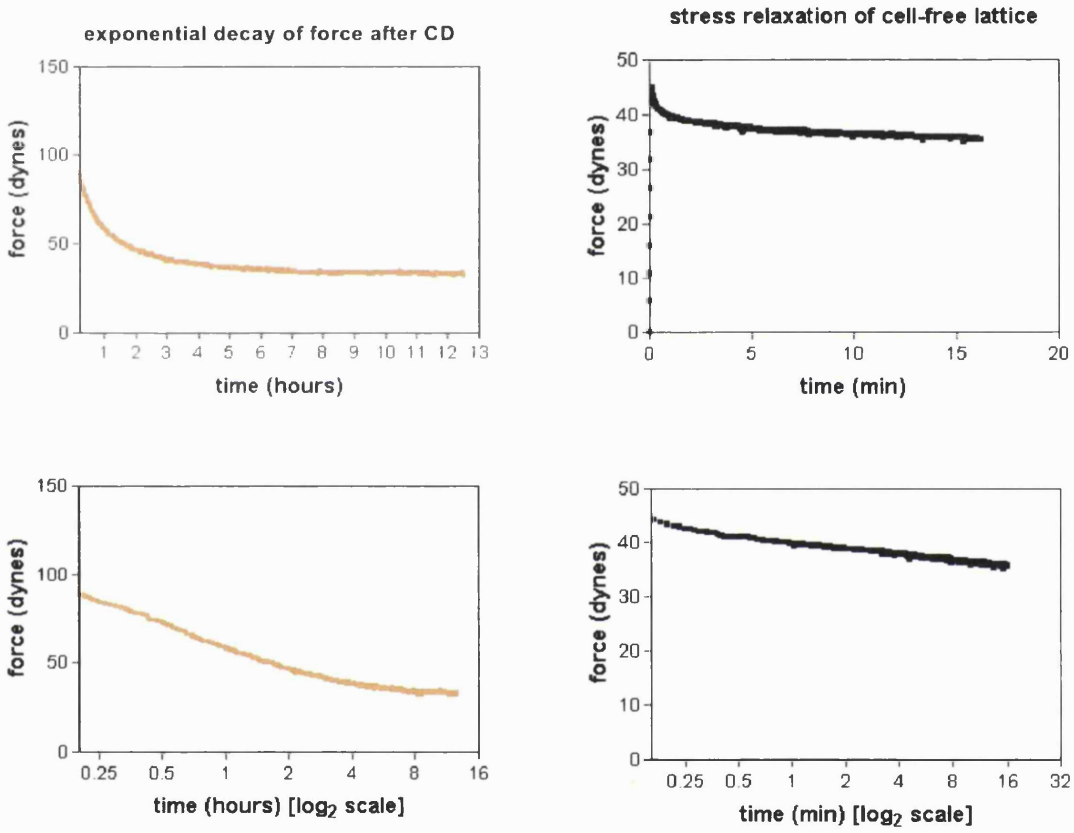

Figure 4-40 Exponential decay of force in the 12 hours following CD treatment (given at 24 hours) in FPCLs cultured for 24 hours in standard culture conditions (left panel). In the right panel, the exponential force decay in a cell-free lattice subjected to a step strain on the tCFM (1% strain, generating a load similar in magnitude to the force drop caused by CD treatment, i.e. ~50 dynes). Note the different scales and speed at which asymptotic equilibrium is reached.

From Figure 4-40 it is clear that the part of the force drop curve that was better approximated by the logarithm was the initial part between 0.2

and 2 hours (linear confidence: R^2=0.99). This confirms that the material behaviour was mainly a viscoelastic relaxation in the initial 2 hours.

So the gross material behaviour looked like a typical viscoelastic relaxation under the action of a constant strain. However, the theory of linear viscoelasticity has no simple mathematical description for this type of relaxation in which the strain is not externally applied but internally, from rapid removal of tensile structures located interstitially inside the material (i.e. the cells). This causes subsequent relaxation of the newly remodelled material. In this case there is neither external strain nor external load, but is the material itself that undergoes changes in its mechanical properties, a bit like a composite polymer under heat (thermal-relaxation).

The relaxation of the cell-free collagen lattice subject to external strain (Figure 4-40, right panel) was one order of magnitude faster than the relaxation due to CD treatment (Figure 4-40, left panel). The difference between the two types of relaxation suggests that, again, the structures involved in the relaxation of the CD treated lattices might be the new weak bonds holding the architecture of the newly remodelled structure. The cascade failure of these bonds, from weaker to increasingly stronger might involve different molecular mechanisms from the step-strain relaxation.

The decrease in correlation between the initial tension and the speed of dropping force, in the two timeframes examined (0-2 h and 2-12 h), suggested that there could be small differences in the material properties of the lattices that were initially hidden by the gross material relaxation behaviour.

To this aim, a *ratio parameter*, named ρ, was defined as the fraction between the initial tension level and the average speed of dropping force in the timeframes considered (i.e. 0-2 h and 2-12 h).

The similarity of the tension drop curve with a material relaxation curve suggested that the Newtonian law of viscosity could be used to physically describe this phenomenon. Newtonian law relates the variation of stresses σ with time to the derivative of the strain variation by a constant called

viscosity η as follows:

$$\sigma(t) = \eta \frac{d\varepsilon}{dt}$$

The viscosity η determines the degree of resistance of the material to the changes in the rate of deformation at a given stress. The law of viscosity applies to each point of the fluid and the rate of deformation represents the local velocity of the point. In the case of uniform stresses expressed as fluid pressure and other geometrical constraints the Hagen-Poiseuille equation can be used:

$$\frac{\Delta P}{\Delta l} = \left(\frac{32\pi^2}{d^2} \right) \eta v_f$$

where P is the pressure over the length l, v_f the average flow velocity, d the pipe diameter and, again, η the viscosity of the fluid.

The viscosity η is the constant of direct proportionality between pressure and flow velocity in laminar flow. Similarly the ratio parameter ρ, defined above, could be seen as a *pseudo-viscosity* that expresses the mechanical resistance of the material against the speed of lattice relaxation. Following the analogy, the initial level of tension can be seen as the difference of pressure between two points in a pipe where the fluid is flowing. The average speed of lattice relaxation can be seen as the average velocity of the laminar flow. Thanks to the linearity of the elastic spring action of the force transducer beam, material deformation is directly correlated to force changes (through a calibration factor). Hence the average speed of lattice relaxation is the same as the average speed of dropping force (just linearly rescaled). Analogous to the viscosity η in laminar flow, the ratio parameter ρ can be seen as the constant of direct proportionality between the initial tension and the average speed of dropping force in the timeframe considered. Hence, the following expression can be written for the ratio parameter ρ:

$$F_{peak} = \rho \cdot v_{fd}$$

where F_{peak} is the peak force reached before force drop started and v_{fd} is the

average speed of dropping force.

The prefix "pseudo" for the pseudo-viscosity parameter ρ must be used because it has no valid physical units (inverse of time) and it is time variant, differently from the constant viscosity η of Newtonian fluids.

Figure 4-41 shows a representation of the mean value of ρ in the timeframe 0 – 2 h (post CD treatment) for the different treatments.

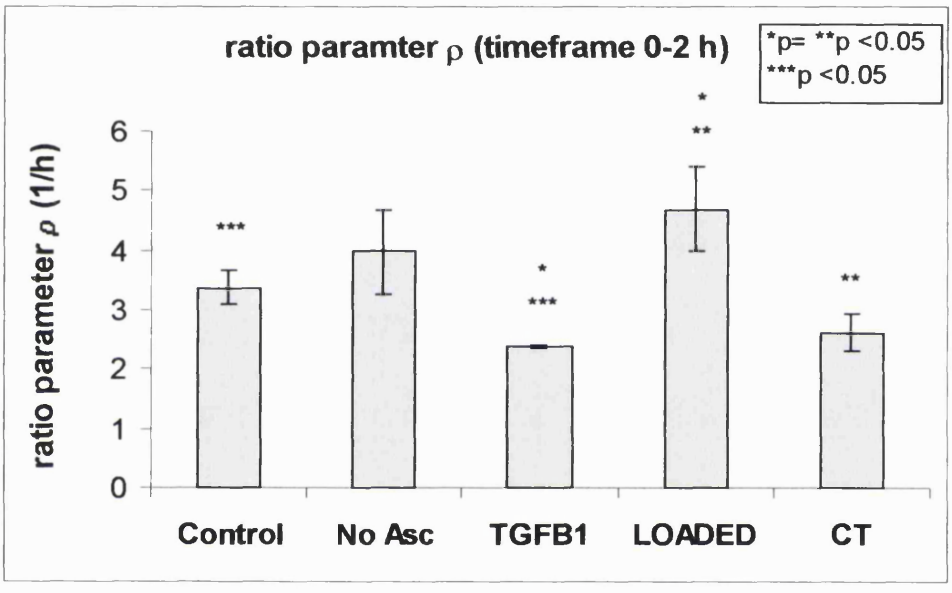

Figure 4-41 Graph of the mean values of the ratio ρ of the peak force before CD treatment over the average speed of dropping force in the following 2 hours. Vertical bars represent SE. Statistical significance is represented by symbols above columns associating them in pairs. Cyclic loading treatment produced the highest pseudo-viscosity ρ. Mean ρ value in TGF-β1 treated lattices was the lowest, significantly lower than in cyclically loaded lattices (*p<0.05) and in control lattices (*p<0.05), but not significantly lower than in CT treated lattices. Mean ρ value in CT treated lattices was significantly lower than in cyclically loaded lattices (**p<0.05) but not significantly lower than in control lattices.**

As expected the values of ρ did not differ greatly between each other, but enough to show important relative differences. Cyclic loading treatment

produced the highest pseudo-viscosity in FPCLs, while TGF-β1 treatment the lowest. TGF-β1 treatment appeared to be the predominant factor in that it significantly reduced the pseudo-viscosity ρ ± cyclical loading relative to control lattices.

The trend of the parameter ρ (0-2 h timeframe), which includes dynamic information, was in contrast with the trend of RMT at 2 hours, in which an increase in all treatments was observed in comparison to control. Hence we seem to be seeing a gross increase in matrix shortening across the board but with subtle, underlying differences in material properties.

In order to test if this opposed trend between ρ and RMT was maintained at later stage of relaxation, ρ was examined in the 2 – 12 hours timeframe post CD treatment (Figure 4-42). The differences in mean ρ values increased in this timeframe compared to the former timeframe (0 – 2 h), as expected from the correlation graphs (Figure 4-38 and Figure 4-39) which showed a reduced correlation between the two parameters composing ρ from the 0 – 2 h to the 2 – 12 h timeframe.

However, the percentage differences between the different treatments were similar to Figure 4-41. Mean value of ρ in cyclically loaded lattices was still about 2 fold greater than in TGF-β1 and CT treated lattices. This confirmed that the direct correlation of the 2 parameters composing the ratio ρ in the first 2 hours post CD treatment was caused by the high forces involved which masked the subtle differences in remodelled material properties evidenced by ρ. The main change in ρ trend between the 2 – 12 h timeframe and the 2 – 12 h timeframe was found in the control lattices whose ρ increased considerably relative to TGF-β1 (± cyclic loading) treated lattices.

This indicated that control lattices had a higher long term resistance to the spring action of the transducer. This was consistent with the measured absolute RMT_{12} (Figure 4-35) where the results of RMT at 2 hours were reversed and the control lattices retained a higher tension than TGF-β1 treated lattices. Therefore in the later stage after CD treatment (i.e. 2 – 12 h timeframe) the trend of RMT_{12} and ρ became more consistent. This

indicated that ρ was highly influenced by the force dynamics and became consistent with RMT (i.e. the static parameter) when the dynamics were reduced, such as in the later timeframe between 2 and 12 hours.

Less consistent were ρ (in 2-12 h timeframe) and RMT_{12} trends in relation to CT treated lattices. In CT treated lattices, ρ was lower than in cyclically loaded lattices while mean RMT_{12} value was almost the same as in cyclically loaded lattices. However, the reason for this discrepancy can be understood by looking at the significant highest force drop at 12 hours which reduced ρ and the high variation in RMT_{12} values for CT treatment (leading to non-significant difference from any of the other values).

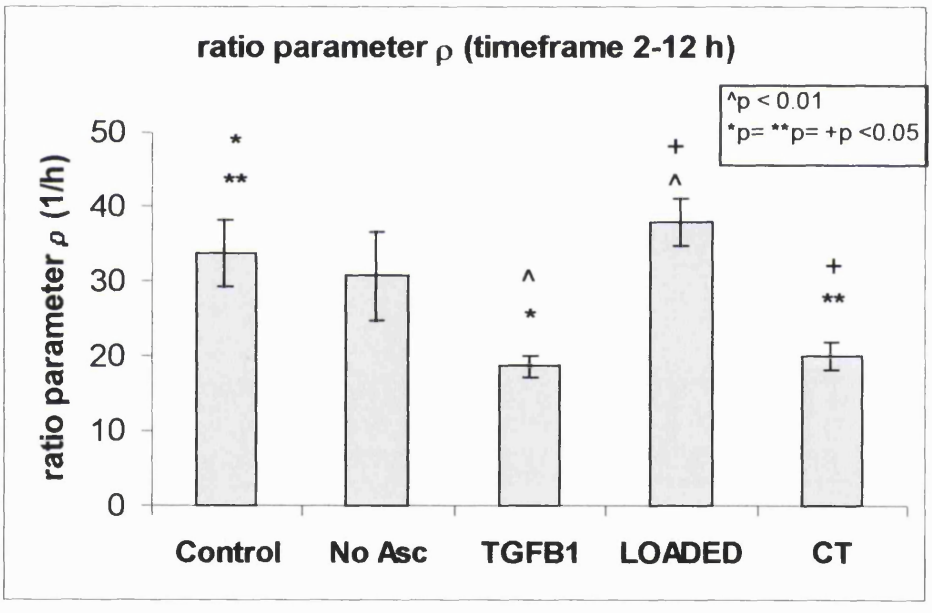

Figure 4-42 Graph of the mean values of the ratio ρ of the average force retained at 2 hours post CD treatment (i.e. the max initial force in the 0-12 h timeframe) over the average speed of dropping force between 2 and 12 hours post CD treatment. Vertical bars represent SE. Statistical significance is represented by symbols above columns associating them in pairs. Again (Figure 4-41) cyclic loading treatment produced the highest pseudo-viscosity ρ. Mean ρ value in TGF-β1 treated lattices was significantly lower than in control (*p<0.05) and in cyclically loaded lattices (^p<0.01) but not the same (reduced levels) in CT treated lattices. Mean ρ value in CT treated lattices was significantly lower than in cyclically loaded lattices (+p<0.05) and also than in control lattices (p<0.05)..**

In conclusion, a good correlation was found in the first 2 hours post CD treatment between the initial tension and average speed of dropping force, indicating that the relaxation of the remodelled matrix after CD was directly proportional to the degree of contraction force before CD treatment. Since the time of cell actin cytoskeleton disruption due to cytochalasin D can be assumed to be constant across the different treatments. This difference can be attributed to the properties of the remodelled material.

Correlation between the level of initial tension and relaxation speed decreased with time as forces and relaxation rates decreased (timeframe between 2 and 12 hours after CD treatment). This reduced correlation suggested that subtle, different properties of the remodelled materials were present due to the different treatments.

Comparison of CD induced relaxation with a standard material relaxation test evidenced that different mechanisms were involved in the two different relaxations. It is postulated that new, weak bonds (and their gradual rupture) were mainly responsible of the observed relaxation.

The cyclic loading treatment produced the highest pseudo-viscosity ρ consistently over both the timeframes used in the analysis, i.e. 0 – 2 h and 2 – 12 h post CD treatment. TGF-β1 treatment with and without combined cyclic loading significantly reduced this parameter ρ.

RMT and ρ trends for the different treatments were opposed in the initial timeframe (0 – 2 h post CD treatment) but became consistent in the later timeframe (2 – 12 h). This showed that the dynamic response to the different treatments contained in the pseudo-viscosity parameter ρ converged to static response contained in RMT when the changes in forces were reduced.

Therefore these two parameters can be used in combination to quantify the amount of matrix remodelling which had been produced but which was now cell independent:

- RMT measures the amount of shortening of the matrix and its ability to hold a given tension at a chosen time point;

- ρ measures a dynamic property of the material similar to viscosity which is independent from the chosen time point.

4.2.3.8 Ultrastructural morphology before and after cytochalasin treatment (SEM and TEM microscopy)

The ultrastructural morphology of lattices treated with cyclic mechanical loading was examined by SEM and TEM microscopy, before and after cytochalasin D treatment.

Figure 4-43-A shows that collagen fibrils were well aligned at the end of 24 hours (before CD treatment) and thicker bundles of fibrils were present and uniformly distributed.

In contrast (Figure 4-43-B), fibres alignment was completely lost 12 hours after CD treatment. Randomly orientated fibril bundles and big lacunae or channels in proximity of cells were observed indicating a cell shape change due to CD treatment. Lacunae might also indicate a possible matrix lysis activity of the cells that is well known to be triggered in response to cytochalasin (Lambert et al., 2001).

A cell-free lattice subject to cyclic mechanical loading for 24 hours is shown for comparison (Figure 4-43-C). It is immediately evident that there was no alignment in collagen fibrils, which were also more uniform and not as packed as in the cell-populated lattices.

Analysis of fibrillar composition of the FPCLs at TEM level (Figure 4-43-D) showed that thick and elongated in lattice treated with cyclical mechanical loading were still present at 12 hours after CD treatment. This was in agreement with the thick bundles observed in the SEM images for the same condition. However, the local alignment observed for some thick bundles of collagen fibrils at the TEM level was not apparent at the SEM level.

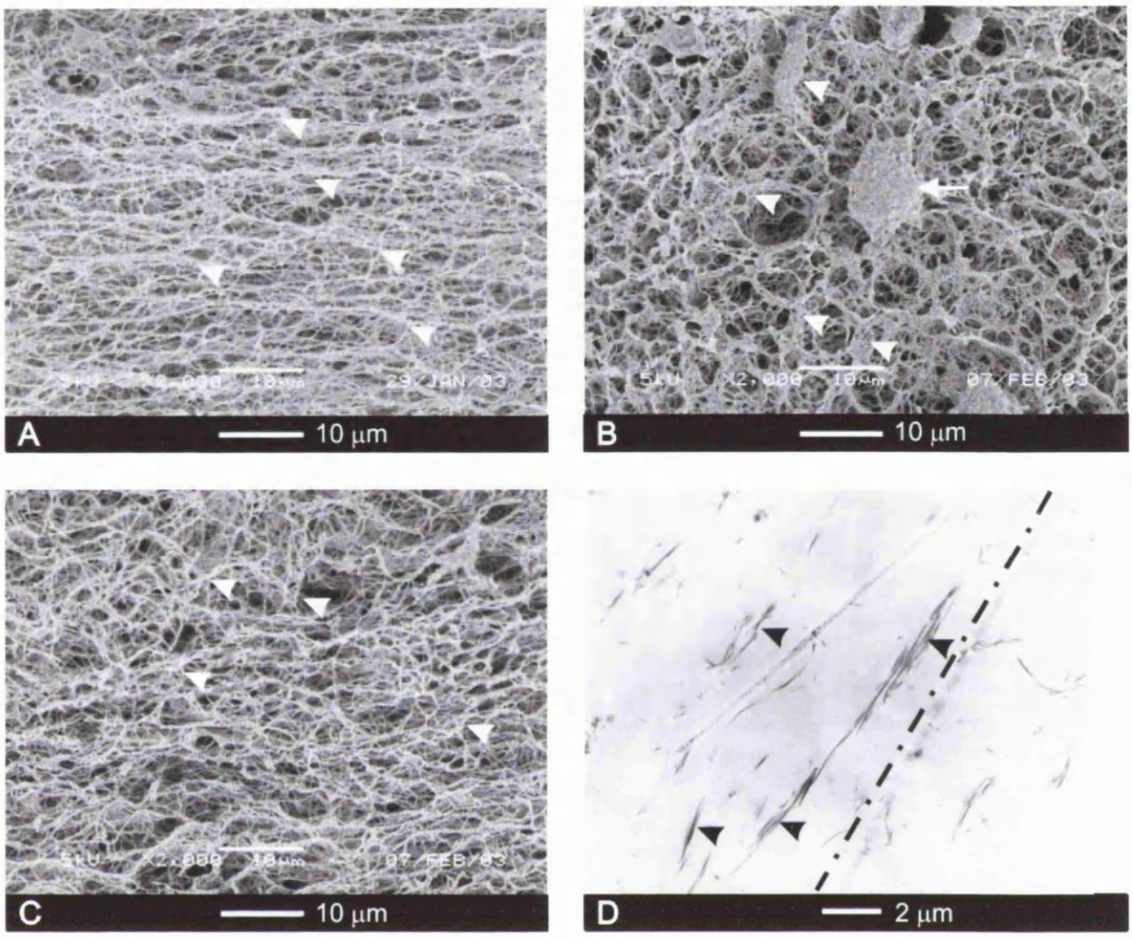

Figure 4-43 A – B: SEM micrographs of ultrastructure of cyclically loaded FPCLs, at (A) 24 hour, immediately before CD addition, and at (B) 36 hours, 12 hours after CD treatment. The orientation of the axis of uniaxial load is the same as the scale bars. Bundles of fibrils (arrow heads) appeared highly aligned before CD treatment while were randomly with large lacunae surrounding rounded cells (arrows). (C) A cyclically loaded cell-free lattice is shown for comparison. Bundles of fibrils (arrow heads) were randomly distributed but appeared less densely packed. Additionally more regular lacunar spaces were present compared to the CD treated lattice. (D) TEM micrograph showing the ultrastructure of cyclically loaded FPCL 12 hours after CD treatment. Sparse collagen fibrils packed in thick bundles (arrow heads) were visible. In some cases, these were appeared elongated and aligned along the axis of load (black dashed line).

The ultrastructural morphology of fibroblasts was examined by TEM microscopy in cyclically loaded FPCLs treated with cytochalsin at 24 hours and fixed at 30 minutes and 12 hours post CD treatment (Figure 4-44).

Figure 4-44-A shows that cells had a spindle-like shape and were still aligned to principal axis of the lattices in the 30 minutes post CD group. However cells had lost completely both their shape and orientation by 12 hours after CD treatment (Figure 4-44-B).

Cells exhibited the typical diffuse macrovacuolation induced by CD treatment, that has been reported to be completely reversible (Brett & Godman, 1984).

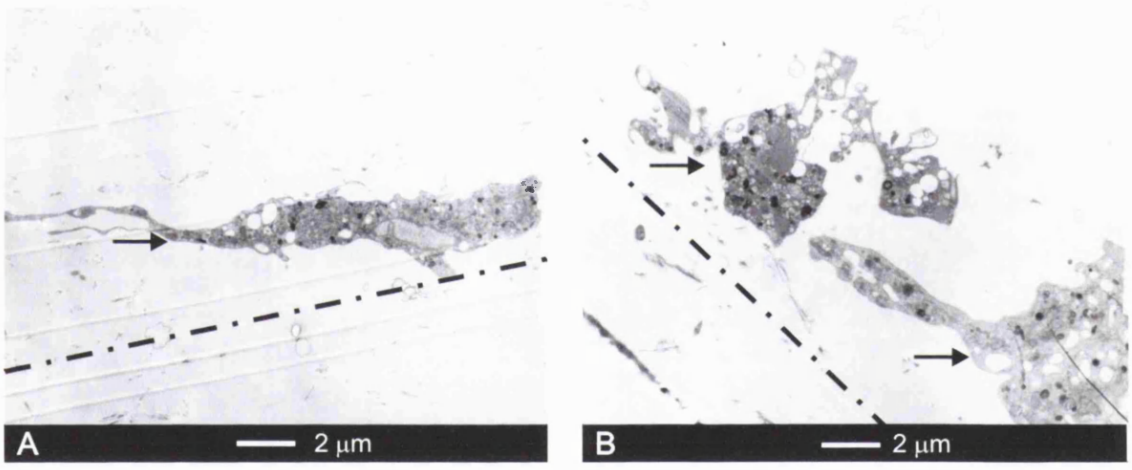

Figure 4-44 TEM micrographs showing the ultrastructure of cyclically loaded FPCLs after CD treatment at 30 minutes (A) and at 12 hours (B). Fibroblasts (arrows) at 30 min post CD treatments were still elongated and aligned along the axis of load (black dashed line). In contrast, after 12 hours post CD treatment fibroblasts assumed less elongated shapes (though not completely rounded) and lost any alignment to the axis of load. Diffuse macrovacuolation (clear circular spots inside cytoplasm) induced by CD treatment was present at both time points.

4.2.3.9 Engineering material stiffness before and after cytochalasin D

Stiffness of FPCLs was measured by applying a 1% strain to the collagen lattice in situ at slow constant rate (2.45 mm/h or 4% strain/h).

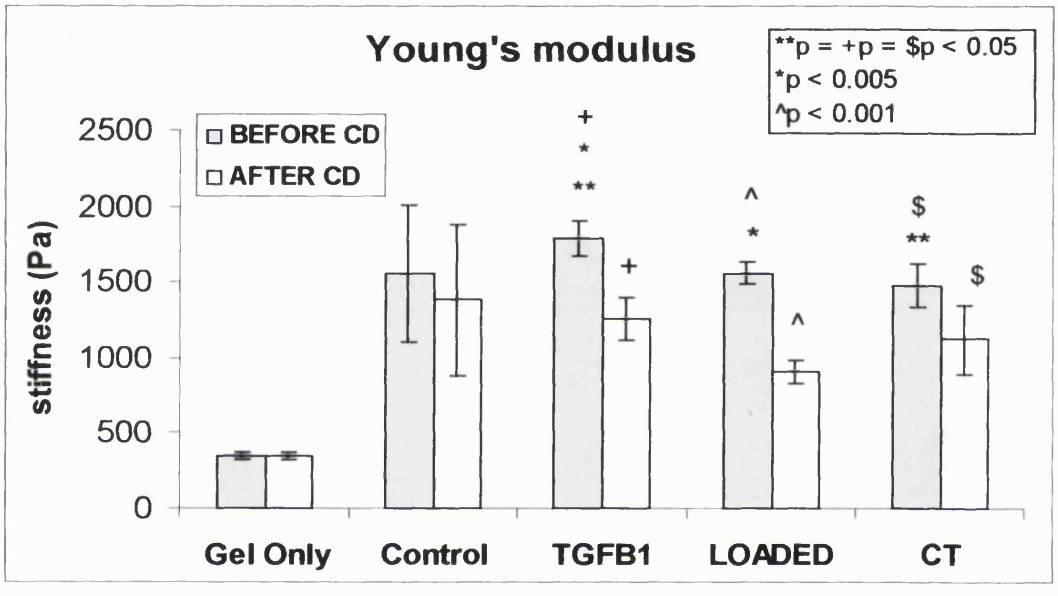

Figure 4-45 Mean elastic modulus (also called Young's modulus) of FPCLs for the different treatments before and 12 hours after cytochalasin treatment. The mean stiffness of cell-free collagen lattices is also displayed for comparison. This was significantly lower than all treatments (due to cell contraction over 24 h) even after CD treatment (p-values not shown for graphic clarity). Vertical bars represent SE. Statistical significance is represented by symbols above columns associating them in pairs (excluding gel only). The stiffness of TGF-β1 treated lattices was significantly higher than cyclically loaded (*p<0.005) and CT (p<0.05). Significantly different were also the values of stiffness before and after CD addition for all treatments (i.e. TGF-β1, cyclic loading and CT). However, there were no statistical differences in the stiffness of the lattices measured at 12 h after CD.**

Figure 4-45 shows the mean elastic modulus of FPCLs measured before (at 24 hours time point) or 12 hours after CD addition for the different

treatments. Elastic modulus of cell-free collagen lattices are displayed for comparison.

As expected, FPCLs elastic modulus was reduced after removal of the contribution due to cell stiffness (i.e. disruption of actin cytoskeleton by CD treatment). For simplicity, the analysis of the elastic modulus results has been divided in two groups, namely before CD and after CD.

STIFFNESS BEFORE CD

All cell-contracted lattices were stiffer (elastic modulus between 4.3 and 5.1 fold greater) than cell-free lattices consistently with previous results (Wakatsuki & Elson, 2003; Wakatsuki et al., 2003)

TGF-β1 treatment produced the highest stiffness modulus at 24 hours time point, significantly greater than cyclic loading treatment. This is consistent with enhancing effect of TGF-β1 on cell force generation and its profibrotic stimulation.

Cyclic loading treatment appeared to reduce the elastic modulus even in presence of TGF-β1, where the lowest stiffness was registered.

STIFFNESS AFTER CD (12 H TIME POINT)

All cell-seeded lattices were significantly stiffer (elastic modulus between 2.6 and 4.0 fold greater) than cell-free lattices even after removal of the cell stiffness component by CD.

Notably, cyclically loaded FPCLs had a lowest elastic modulus, though this was not statistically significant due to large variance.

The effect of cyclic loading treatment on the elastic modulus parameter after CD treatment was in stark contrast with the effect produced on RMT_{12} and ρ (2-12 h timeframe) parameters. While RMT_{12} and ρ were significantly increased, the elastic modulus was reduced compared to all the other treatments. A similar inversion of effects was seen for TGF-β1 treatment. The values of these parameters produced by CT treatment fell in between the values produced by TGF-β1 and cyclic loading treatments.

In general, since differences in elastic modulus among the differently treated FPCLs (at 12 h post CD addition) were not statistically significant, it is correct to consider this parameter as unable to identify the differences in matrix remodelling caused by the different treatments. These were instead identified by the parameters RMT and ρ.

Nevertheless, it is clear that cell activity in the matrix (remodelling), under all conditions, had produced substrates 4-5 fold stiffer than they were presented with in 24 hours.

In conclusion, the measurement of elastic modulus of FPCLs showed that fibroblasts were able to significantly remodel the collagen matrix. Elastic modulus in FPCLs where cell stiffness had been removed by CD treatment was still significantly higher than cell-free lattices.
TGF-β1 treatment significantly increase elastic modulus in FPCLs compared to the cyclic loading treatment which appeared to reduce the effect of the growth factor when treatments were combined.

The elastic modulus measured in FPCL at 12 hours after CD addition was unable to identify significant differences in the effect of the different treatments on matrix remodelling.

4.2.3.10 Summary of section 4.2.3

- Residual matrix tension (RMT) has been defined as the measure of matrix shortening after removal of the cellular contractile component in FPCLs by cytoskeleton disruption.

- RMT was present at 18 h in RTF but not in HDF. The reason does not lie in species-based substrate specific matching but in differences in the behaviour of different fibroblastic types.

- RMT increased with culture time in a near linear fashion over 61 hours of culture time (rate 1.4 dynes/h).

- RMT at 24 h time point increased by both cyclic and TGF-β1 treatment by different mechanisms. TGF-β1 may act by upregulating total contraction force, hence increasing fibril compaction. Cyclic loading by enhancing fibril alignment to the axis of load. Differences in material properties suggest that these effects lead to different patterns of covalent and non covalent interfibrillar bonding. Combination of the two treatments did not elicit an additive RMT response.

- RMT measurement at 12 hours (RMT_{12}) indicated that cyclic loading treatment produced a more stable shortened matrix compared to TGF-β1 treatment (± cyclic loading).

- Pseudo-viscosity ρ was defined to account for the dynamics of FPCL relaxation post CD treatment. Cyclically loaded lattices had the highest pseudo-viscosity (best resistance to relaxation) while TGF-β1 treated were the least stable lattices. CT treated lattices had an intermediate pseudo-viscosity between cyclically loaded and TGF-β1

treated lattices.

- Morphology after CD treatment showed that fibroblasts gradually lost alignment and orientation from 30 minutes (still aligned) to 12 hours (randomly orientated) time points.

- Engineering elastic modulus was measured in FPCLs before and after cytochalasin treatment. Before CD addition, treatment with TGF-β1 resulted in significantly stiffer substrates. After CD addition elastic modulus was reduced for all treatments, though there were no significant differences between treatments. For all treatments, before and after CD addition, elastic modulus in FPCLs was always significantly greater than the starting gel alone.

4.3 Discussion

Spatial remodelling of 3D collagenous network by resident fibroblasts has been recognised to lead many important physiological events such as morphogenesis, growth, adaptation, repair (Grinnell, 2000; Harris et al., 1981; Sawer, 1911; Tomasek et al., 2002). Its regulation appears to be led by a complex combination of mechanical and biochemical factors united to a genetic imprint (Cowin, 2000; Ingber, 2002; Silver et al., 2003; Tomasek et al., 2002).

Fibroblast-populated collagen lattices (FPCLs) have been used for many years as the simplest, yet closest, model of the complex interplay of factors that drive the remodelling process in vivo (Brown, 2002; Tomasek et al., 2002).

For the first time in this study, the dramatic 3D spatial remodelling of FPCLs over 24 hours in standard culture conditions was shown morphologically at three levels of detail. Organisation of cells and fibrils observed in CLSM and SEM images was shown to be consistent with cell morphology and presence of fibril strands in TEM images. Importantly, these dramatic structural changes were observed after only 24 hours in the tCFM model.

Previous studies reporting the development of cells and collagen fibrils alignment in FPCLs show some temporal discrepancies. Some investigators reported that alignment could be obtained by 24 hours (as in this study) simply by uniaxially tethering FPCLs (Bellows et al., 1982). Other researchers reported an increase or acceleration in the alignment process with the use of external uniaxial mechanical loading (Eastwood et al., 1998b; Mudera et al., 2000; Seliktar et al., 2000; Theodorou et al., 2003) or aligned fibrils pre-orientated by powerful magnetic fields (Guido & Tranquillo, 1993). Finally other research groups reported much longer culture time to obtain similar aligned conformations (Awad et al., 2000; Huang et al., 1993).

We now know that these temporal discrepancies between different uniaxial models, in the achievement of highly aligned structures, were principally due to the use of (i) lattices with different stiffness, due to different initial collagen concentration or crosslinking (Torres et al., 2000), (ii) different geometries in the uniaxial setups, and (iii) different cell types. The effect of different geometries within 3D constructs has been studied in detail by finite element analysis (Eastwood et al., 1998b). Changing aspect ratio of the lattice (i.e. uniaxially tethering the longitudinal sides of FPCLs) caused a change in the reorientation of the principal isostrain lines and, consequently, the orientation of the cells away from the principal axis of loading. Concerning the effect of cell types, however, no apparent morphological differences in the alignment of cells and fibrils were observed in this study for the two fibroblastic cell types analysed (HDF and RTF). The degree of alignment of cells and fibrils was also dependent on contraction force: at very low forces (below 50 dynes) no reorientation could be observed (data not shown).

Therefore, the morphological study indicated that there were two fundamental factors driving spatial remodelling in FPCLs:

1) the force that cells apply to the collagenous fibrillar network (this can be observed only on the tCFM model) during lattice contraction;

2) the mechanical constraints applied to the matrix.

It is important to note that force generation is one of the key players in the cell-mediated spatial remodelling of collagen matrices. Hence the use of a mechanically defined model such as the tCFM seemed the most appropriate to investigate remodelling mechanisms and their temporal dynamics.

Different contraction dynamics, between human dermal fibroblasts (HDF) and rat tendon fibroblasts (RTF) were measured in the tCFM. These differences in force measurement did not correspond to differences in morphology and ultrastructure. From a morphological perspective, it might appear unimportant how contraction force is generated over time if the final morphology is the same. This was the case for two fibroblastic cell types

(HDF and RTF) tested here, in which alignment of structures appeared to be triggered by threshold levels of force generation. Over these thresholds alignment was obtained irrespective of the force evolution over time. However this cannot be generalised as other cell types have lead to the identification of specific contraction profile for specific remodelling processes. For example, for non-fibroblastic cell types, such as C_2C_{12} (immortalised myoblasts cell line), the different phases in the profile of force generation have been shown to correspond to changes in cellular phenotype involving fusion and generation of myotubes (Cheema et al., 2003). Also, not all cell types necessarily use the same means of locomotion (traction) or have the same response to local strain.

4.3.1 Definition of RMT to quantify cell-mediated permanent 3D spatial remodelling of collagen lattices

Studies on FPCL remodelling, caused by cell-mediated contraction, have been focussed on the cell, i.e. its interaction with the matrix modulated by expression of adhesion proteins and cytoskeletal fibres contraction through intracellular signal transduction pathways (Grinnell, 1999; Knapp et al., 1999; Mudera et al., 2002; Parizi et al., 2000; Tranquillo, 1999; Woodhead-Galloway, 1980).

In this work, the investigation of spatial remodelling was conducted from a new viewpoint. The attention was addressed to one of the effects of the remodelling which consists in the stable, enduring shortening of the matrix through permanent reorganisation of the collagenous fibrillar network. The expression "permanent reorganisation" means that the remodelling of the architecture and the mechanical properties of the matrix are independent from the mechanical and structural contribution of the cells at the time of measurement. Hence, "permanent" does not mean that matrix

remodelling could not progress, but that the cell mechanical contribution had been removed. Indeed it is inevitable that these matrix structure and material properties are highly dynamic – though progressive.

This study first investigated connective tissue remodelling through quantitative measurement (on the tCFM) of the permanent shortening of FPCLs. The method is based on the residual tension that the matrix (i.e. the passive tensile element) retains after removal of cell mechanical contribution through disruption of actin cytoskeleton.

The validity of the method is limited to contractile cell types, or "collagen remodeller" cells.

Wakatsuki and colleagues (2000) first demonstrated the additivity of active and passive components in the mechanical stiffness of collagen lattices pre-contracted for two days by resident fibroblasts. These components of stiffness were separated eliminating the active one (i.e. cells stiffness) by a high dose of cytochalasin D, leaving the passive one (i.e. matrix stiffness). Their work provided useful information on the material properties of the cell-contracted collagen matrices before and after cell removal, showing that fibroblast contraction caused an increase in matrix stiffness even when cells were removed. In that experimental model great care was taken to "freeze" the cell action by serum starvation in the 16 hours before the measurements. In that way a good level of reproducibility on the material measurements was achieved but the dynamics of matrix stiffening was not investigated.

Previous publications (Eastwood et al., 1994; Kolodney & Wysolmerski, 1992) reported a total abolition of the measured contraction force upon cytochalasin addition at 24 hours time point. In this study, it has been shown that different cell types can generate different levels of permanent remodelling (at early time points, i.e. 18 hours).

Grinnell and Ho measured the permanent remodelling (which they called "actin independent contraction") as the potential elastic energy stored in the stressed FPCLs after disruption of cellular actin cytoskeleton by CD. Potential elastic energy was measured releasing the stressed FPCL from the

substrate and measuring the reduction in volume. Actin independent contraction was reported to be up to 50% of the total contraction of FPCLs not treated with CD (Grinnell & Ho, 2002).

Other models, developed to assess permanent matrix remodelling, employed microscopic observation of anisotropy built in the matrix (Roy et al., 1997; Sawhney & Howard, 2002) which persisted after cell cytoskeletal disruption by CD (no force or contraction was measured).

The novelty of the approach used in this work consists in the measurement of the spatial remodelling as residual matrix tension (RMT). This tension is generated by cell-mediated isometric contraction (calculated as total contraction force minus active contraction component) and therefore it is itself a measure of the spatial reorganisation (as shown above by the correlation with morphological changes).

The difference between material stiffness and residual matrix tension is that, while stiffness is a mechanical parameter of the material, not directly correlated to the final permanent shortening, RMT is a direct measure of the capacity of the shortened matrix to sustain part of the total tension developed during cell-mediated contraction. This fundamental conceptual difference may be exemplified in vivo by the condition of Dupuytren's contracture where the effect of spatial remodelling is primarily the shortening of the collagen matrix of the palmar aponeurosis (with permanent finger flexing). This process may result in an increase of the mechanical stiffness of the tissue, but it is not a necessary consequence.

Another important aspect to be considered, in the assessment of mechanical parameters in a given system, is the amount of alteration produced in its initial configuration by the measurement process itself. This was achieved with the least disturbance in the measurement of RMT. The effect of removing the cell tensile component was measured directly on the same mechanical setup as a fall in tension. Even this measurement (RMT) involved the application of reactive loads which will undoubtedly break weak interfibrillar bonding and so lead to underestimations. Other groups quantified matrix remodelling by measuring the elastic modulus of FPCLs

(Huang et al., 1993; Wakatsuki et al., 2000). This involved the application of a relatively high strain (20%) to the lattices. Wakatsuki and Elson (2003) estimated that this stretching might have disrupted some of the collagen fibrils interactions responsible for the early stiffening prior to the formation of covalent cross-links. This caused the difference in the material resistance which they observed between the first (higher) and the subsequent stretching cycles (Wakatsuki & Elson, 2003). Measurement of the potential elastic energy tension permanently stored in the matrix causes again a complete change of the mechanical conditions from highly stressed to completely unconstrained (Grinnell & Ho, 2002; Tamariz & Grinnell, 2002). Therefore the methods employed so far failed to measure mechanical changes in the passive component (matrix upon active cell component removal) without altering substantially the mechanical configuration in which the material had been remodelled (sudden release of tension or application of high strains).

The mechanical configuration existing at the time of cell depletion is a unique product of the cellular action at that time point. The current model enables to directly correlate the tension developed during contraction and the cells ability to generate permanent shortening of the collagen network. In engineering terms, the example (mentioned above in chapter 1) of the problem of the mechanical resonance which developed unexpectedly onto the Millenium Bridge, showed how dynamical behaviours of the complex material-structure could not be predicted simply from material properties and calculations that apply to static structures.

In Table 4-2 the properties of the main methods used by different investigators to study 3D spatial remodelling are compared with the method used in this work, namely residual matrix tension (RMT).

Notably, the current method was the only one to be able to quantify permanent shortening in isometrically contracted FPCLs.

In addition, the tCFM model allowed us to perform traditional measurements of the elastic modulus of FPCLs that could be compared to

previous study.

Methods / Parameters	RMT	STIFFNESS**	POTENTIAL ELASTIC ENERGY***	FIDUCIAL BEADS DISPLACEMENT*
Property measured	Permanent shortening as retained tension	Permanent stiffness	Contraction due to cell-actin-independent pot. energy	Fibril permanent displacement
Physical unit	Tension (N)	Stiffness (Pa)	Size (m^2)	Displacement (m)
Correlation to spatial remodelling	Direct	Alteration	Indirect	Direct
Correlation to tension development over contraction	Direct	Indirect	Not measured	Not measured
Alteration of the mechanical structure or configuration during property measurement	No, simply cell component removed under the current tension developed	Yes, 20% stretch after cell component removal	Yes, The tension developed is released after cell component removal	No, No alteration, but mechanical information is completely missed (only spatial deformation)

Table 4-2 Summary of the main parameters currently used to measure the remodelling of the matrix after removal of the cell contraction component. Reference to methods can be found as: (*) (Roy et al., 1997; Sawhney & Howard, 2002)(**) (Wakatsuki & Elson, 2003); (***) (Grinnell & Ho, 2002).

The reference time point for measuring the residual matrix tension was 2 hours. This allowed plenty of time for the diffusion of the chemical through the medium (factor 100 dilution of the volume added) and through the gel and for the stabilisation of the level of tension after the sudden rapid drop. In effect, observations of the force profile confirmed that at the chosen time point the curve virtually reached a plateau (Figure 4-10). This finding and the measurement of very steep gradients of force drop in only the first

10 to 20 minutes (Figure 4-34) demonstrated that the cell force component had been completely removed by 2 hours. This also ensured that the measured decrease in tension was solely the stress-relaxation behaviour of the collagen gel matrix after the remodelling time. Other studies on permanent matrix remodelling measured the effect of CD treatment at earlier time points, i.e 15 min (Grinnell & Ho, 2002) and 30 min (Wakatsuki et al., 2000), missing possible dynamics in the matrix response.

One assumption which was made in the measurement of permanent matrix remodelling by RMT is that active and passive components in the matrix are additive and can be completely separated. In this study this was tested by adding multiple doses of cytochalasin and changing the standard culture medium into a hypotonic solution. Both treatments had no effect on RMT, showing that the first dose had been sufficient to eliminate the mechanical contribution of the cells. Previous studies by Wakatsuki et al. (2000) showed that additional disruption of the intermediate filament and microtubule cytoskeletal system (adding calyculin A to the cytochalsin treatment) did not produce any change in the mechanical properties of the remodelled collagen matrix, beyond that caused by CD (Wakatsuki et al., 2001).

The initial effective dose of CD was tested at 4 hours time point. Force generation was completely abolished at this early time point, with tension reduced to the basal level of cell-free collagen lattice contraction. There was no sign of recovery of force generation in the next 12 hours after CD treatment. RTF appeared to have a greater resistance to CD compared to HDF. A 10 times higher dose was needed to obtain complete force abolition with no recovery. The reason for this can be only speculated and might be associated to a competitive binding mechanism between CD and barbed end capping proteins anchoring actin filaments to the plasma membrane (Wakatsuki et al., 2001). By this mechanism, a greater content of actin capping proteins in the cytoskeleton may require a greater amount of CD to disrupt compete for biding with actin filaments. The recovery of force observed seems also consistent with this hypothesis. Faster metabolism of

rat fibroblasts compared to human might be responsible for increased synthesis of barbed end capping proteins. With time this leads to a saturation of the available CD binding sites and therefore reconstitution of actin cytoskeleton.

Cytochalasin treatment is known to produce additional effects besides the disruption of actin cytoskeleton, such as stimulation of matrix metalloproteinases (MMPs) synthesis (Tomasek et al., 1997). However, MMPs might start producing effective matrix degradation only in a later phase, after the last time point (i.e. 12 hours). This assumption is consistent with the very low changes in tension level observed between 2 and 12 hours. These changes remained similarly reduced also when cells were lysed in the presence of hypotonic solution (Figure 4-11), hence eliminating any further synthetic activity.

Nevertheless, it might be useful to measure MMPs synthesis and test their role in the remodelling process and their correlation with the different treatments used in relation to the measured RMT. For example it has been shown that a similar regime of mechanical loading to the one used in this study produced a downregulation in the enzymatic activity of some important MMPs (Prajapati et al., 2000a).

4.3.2 Effect of culture time, TGF-β1 and external mechanical loading on RMT

4.3.2.1 Differences in RMT between HDF and RTF over the same culture time

The exact cause of the difference observed between RTFs and HDFs could not be determined in this study. Explaining the mechanisms that regulate the different abilities to consolidate the matrix of these cell types might provide useful information for the understanding of the entire process by which cells permanently remodel the matrix. The difference in RMT generation between RTFs and HDFs provided evidence that RMT was not

simply caused by the level of cell generated forces. Cell-mediated lattice contraction causes adjacent fibrils to be moved in closer proximity. This was postulated to be the key mechanism by which collagen fibril self assembly and crosslinking is triggered (Guidry & Grinnell, 1986). However this mechanism alone cannot explain RMT generation, since similar or greater levels of force were generated by HDFs but did not result in similar levels of RMT. Packing, alignment and proximity are a major requirement but cell-mediated interfibrillar bonding is clearly also essential (see loaded cell free gel).

Basic tests allowed to further characterise rat tendon fibroblasts and exclude some hypotheses. The hypothesis that rat fibroblasts could be more efficient in generating permanent matrix remodelling than other fibroblasts from different species was eliminated by using tendon fibroblasts from bovine origin (BTF). These cells generated a measurable level of RTM after 24 hours of culture in standard conditions, suggesting that species match is not an issue (though tissue sources might be). However, since human tendon fibroblasts have not been tested it is not yet possible to generalise to humans. In addition, human fibroblasts, obtained from the palmar fascia of patients affected by Dupuytren's disease, produced high levels of RMT with over 50% of tension retained after 24 in standard culture condition (personal communication from Dr. Kate Beckett). A possible clue to explain these discrepancies in the behaviour of human fibroblastic cell types might come from the expression of αSMA. In fact Dupuytren's fibroblasts are known to express high levels of αSMA and are implicated in the permanent shortening of palmar fascia tissue in vivo (Tomasek et al., 1999).

The hypothesis of matrix specificity (collagen and cell from rat species) was discarded by using collagen of bovine origin. Changing the species of origin of native collagen from rat to bovine did not stop the acute lysis observed in the central area of round floating FPCLs. In addition, the crossed test with bovine tendon cells in rat collagen lattice - this time uniaxially tethered - showed that the ability to produce RMT, within 24

hours in culture, was independent from the combination of species of origin of cells and collagen. On the other hand BTF did not produce evident lyses in round floating lattices made with bovine (not shown) and rat collagen. Further experimentation involving additional crossed experiments is needed before conclusive interpretation of this phenomenon of lysis can be made.

4.3.2.2 Increase of RMT with culture time

RMT increased with culture time in RTF populated lattices at an almost linear rate over 61 hours (rate 1.45 dynes/h). The tension retained was up to 58 ± 11% of the total tension generated at 61 hours (or ~2.5 days). This trend was uncoupled from cell force generation as shown in Figure 4-46. RMT was abolished by CD treatment at 4 hours time point but increased with time at faster rate than contraction force from 24 hours to 61 hours.

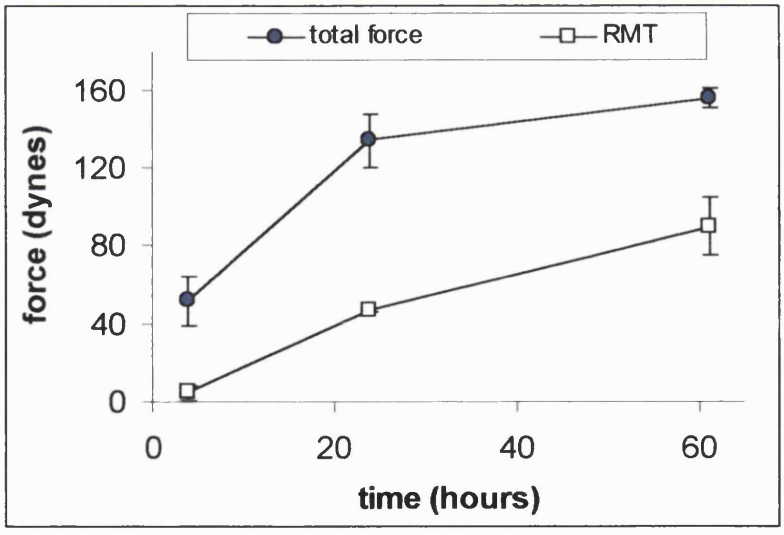

Figure 4-46 Time course of peak contraction force before CD treatments and RMT development from 4 hours to 61 hours. Error bars represent SE (where they cannot be seen the data point overlapped).

Eventually the two time courses might overlap with RMT increasingly closer to peak contraction force before CD treatment. Longer-term studies need to be carried out to demonstrate this convergence.
This finding is consistent with a recently published study (Grinnell & Ho, 2002) in which permanent matrix remodelling (which was called "actin independent contraction") was reported to increase with time reaching a maximum - at day 6 - between 42% and 64% (for LPA and TGF-β + LPA treatments respectively) of the total contraction obtained in CD untreated FPCLs.

Stiffness in FPCLs (including here matrix and cells contributions) was reported to increase significantly with culture time from as early as 2 hours (Wakatsuki et al., 2003). This should not appear in contrast with the finding that RMT was not significantly different from basal cell free contraction at similar early time points (4 hours). In fact, the two studies measured mechanical properties of different structures, i.e. cells and matrix together (stiffness measurement) and matrix only (RMT measurement). It is conceivable that cell stiffness was entirely responsible for the significant changes in FPCLs stiffness at early time points.

4.3.2.3 Increase in RMT response due to selected treatments

Two treatments were chosen in this study for their potential for increasing cell mediated remodelling and, potentially, RMT. Results in this work demonstrated that both treatments were able to increase RMT but through different mechanisms.

1) TGF-β1 TREATMENT

TGF-β1 is a well-known growth factor involved in tissue repair and cell differentiation processes. It has been shown that TGF-β1 increases the deposition extracellular matrix by cells (Sarkissian & Lafyatis, 1998), decreases matrix breakdown (Chegini, 1997; Desmouliere & Gabbiani, 1994; Reed et al., 1994). Additionally previous studies demonstrated that TGF-β1

promotes the rate of untethered lattice contraction (Montesano & Orci, 1988); (Riikonen et al., 1995; Tung & Fritz, 1991), tethered/released contraction (Grinnell & Ho, 2002) and uniaxially tethered contraction (Brown et al., 2002). In this study TGF-β1 response was tested with the hypothesis that it would increase/accelerate RMT generation through increased force generation by cells and, possibly, matrix deposition by cells which would work like an interstitial glue on the remodelled existing fibrillar collagen network (Tomasek et al., 2002).

The mechanism of TGF-β1 stimulation of cell force generation is not well understood. It has been suggested that it is correlated to cell differentiation from fibroblasts into myofibroblasts which showed an increased capacity to generate forces on their substrate (Desmouliere et al., 1993), possibly involving the expression of α–SMA (Hinz et al., 2001). However, the strong upregulation in RTF force generation at very early stages (from 4 hours onwards), consistent with a recent publication reporting a similar response of HDFs to TGF-β1 (Brown et al., 2002), is not compatible with the differentiation theory (known to occur between 3 and 5 days).

Fibroblasts collected from rat tendon wounds (TRC) produced a significant increase in force generation compared to RTF. This was consistent with previous reports of increased contraction generated by granulation tissue cells (Germain et al., 1994; Moulin et al., 1996; Petri et al., 1997; Tsai et al., 1995). TRC and RTF treated with TGF-β1 showed a similar upregulation in contraction force. Limited numbers of subpopulations of myofibroblasts (identified as α-SMA expressing cells) were found in both TRC and untreated RTF after 24 hours in culture in CFM collagen lattices. This observation reinforces the hypothesis that TGF-β1 treatment enhanced RTF force generation by primarily regulating their mechanical behaviour, though this might trigger further downstream cell differentiation pathways. Therefore it can be concluded that two different mechanism of stimulation might be responsible for similar upregulation in force generation TRC gels and TGF-β1 treated RTF gels. In TRC mediated

contraction there were essentially two factors which can be identified as responsible for increased force generation: the long duration of residence of cells (5 days) in the biochemical environment of the wound site and the presence of a heterogeneous cell population. In RTF mediated contraction the main factor increasing force generation was a rapid agonist stimulation by TGF-β1 treatment.

In this study TGF-β1 treatment had an agonist effect to force generation from early stages of contractions (around 4 hours). Brown et al. recently showed that contraction was increased at even earlier early stages (within the first 30 minutes of contraction) in low serum culture medium supplemented with increasing concentrations of TGF-β1 (Brown et al., 2002). In the current study TGF-β1 was added to standard 10% serum culture medium and the most likely reason for the temporal difference.

RMT was increased in lattices treated with 12 ng/ml TGF-β1 compared to control lattices, but the increase was not statistically significant possibly due to batch variations (supplier was Sigma, UK). In a parallel study with a similar dose of TGF-β1 (15ng/ml), but from a different supplier (PeprotechEC, UK) the increase in RMT was significant. Similar concentrations of TGF-β1 (as in this study) have been reported to achieve a maximal stimulation in force generation, while higher concentrations produced lower contraction (Brown et al., 2002). It was assumed that the difference between concentrations (i.e. from 12 to 15 ng/ml) was irrelevant and the most important factor causing different RMT responses was the batch/supplier factor. However further tests on possible TGF-β1 dose/response on RMT should be carried out. In particular, it has not been proved that optimal doses stimulating contraction would be optimal in increasing RMT generation. In fact, the trend of force generation and RMT production has been shown above to be uncoupled in their time course.

Grinnell and Ho (2002) reported no agonist effect of TGF-β1 treatment on contraction at early time points in TGF-β1 treated FPCLs (stressed). However, this effect was evident in longer-term experiment (up to 6 days).

Additionally agonist increase in contraction was seen in free-floating FPCLs. These discrepancies might be explained by the different mechanical conditions and the different measuring systems. Grinnell and Ho (2002) measured isotonic contraction (i.e. reduction of stressed FPCL volume upon release of tension). This measuring technique is intrinsically less sensitive than force measurement during isometric contraction. In fact the first model tests accumulation of cell forces in the matrix, while the second provides a direct real time measure of the forces of a population of cells through the collagen matrix (therefore forces do not need to be stored in the matrix in order to be measured). Since RMT and actin independent component of contraction are both measures of forces which are stored in the matrix (the cell component removed), these two parameters might be more comparable. The reduction of actin independent contraction compared to RMT at 24 hours (25% and 41% of total contraction/force respectively) in standard culture condition (+LPA or 10% serum respectively) might be attributed to the cell types used in the two studies. In Grinnell and Ho (2002) used human dermal fibroblasts (HDFs) in their experiments, a fibroblastic cell type which, in this study, was shown to be unable to generate any detectable RMT at least at 18 hours.

Nevertheless, the result of their study remain consistent with the current study, if different temporal dynamics in matrix remodelling are hypothesised between HDF and RTFs. Hence, increase in permanent matrix remodelling reported for HDF, over 6 days in culture suggests that also in the current model (i.e. uniaxially tethered lattices) HDFs might be able to produce a significant RMT response over prolonged period in culture. Hence this response might be similar to RTF with a shifted time frame.

2) CYCLIC MECHANICAL LOADING

It is well known that mechanical loading has the effect to increase cell matrix production (Kessler et al., 2001; Parsons, 2000; Parsons et al., 1999), decrease MMPs synthesis (Kessler et al., 2001; Prajapati et al., 2000a; Prajapati et al., 2000b) and increase matrix remodelling and turnover

(Goulet et al., 2000; Seliktar et al., 2000). The slow frequency, low amplitude cyclic loading regime, used in this study, has been previously shown to increase collagen production by fibroblasts (Parsons, 2000). The hypothesis was that stimulation of collagen production would increase RMT through a mechanism of interstitial fixation of the existing remodelled fibrillar collagen matrix. An hypothesis for the mechanism by which cell collagen production is implicated in increased RMT is outlined in the following section.

The advantage to using slow frequency and low amplitude strains (~1%) was that viscoelastic responses in the collagen lattice were avoided. These would have caused changes in tension unrelated to the cellular response.

Cyclical loading was the most effective treatment in increasing RMT at both time points (2 and 12 hours after CD treatment) in which it was assessed.

3) COMBINED TREATMENT

Although the combined treatments appeared superimposed on the force generation profiles, their effect on RMT response was not additive but an average between the responses to the single treatments. Large variations along the profile of force generation might be caused by cell responses to the concomitants treatments being triggered at different time points. However by 24 hours variations in force generation levels reduced, as if cultures entered a regime in which responses to both treatments were fully activated. The effect of TGF-β1 prevailed over cyclic loading in terms of dynamic response: the matrix relaxation was in fact similar to the TGF-β1 treated lattices without combined cyclic loading.

4.3.3 Analysis of the results

4.3.3.1 Analysis of relaxation after cytochalasin D treatment and hypothesis of new weak bonds

Analysis of stress relaxation showed that there was a good correlation between initial tension and speed of dropping force in the first 2 hours after CD treatment. This revealed an inherent difficulty in measuring the real level of residual tension, since there was a marked relaxation effect, seen as a gradual loss of tension, directly after the CD induced fall. Such an effect is usual and expected in terms of material mechanical properties but would lead to underestimate the total residual tension, particularly when pre CD forces were high.

Stress relaxation of a material is a normal mechanical function where pattern of stress are applied to complex or heterogeneous structure. Weaker bonds in the material are broken under these conditions, such that stronger elements become loaded. At this point deformation or relaxation ceases. In the instance of the CD treated FPCLs, lattice relaxation is not caused by externally applied strains but by the collapsing of interstitial tensile structures (i.e. cellular cytoskeleton). These tensile structures are disrupted very rapidly by the cytochalasin treatment as it could be observed from the steep gradients of the initial force drop in the relaxation curves (Figure 4-34). The rapid cellular response to CD was consistent with other previous studies (Brown et al., 1996; Grinnell & Ho, 2002; Kolodney & Wysolmerski, 1992; Roy et al., 1997; Sawhney & Howard, 2002).

Rapid disruption of the cellular cytoskeleton caused a steep force drop in the first 30 minutes followed by a slower relaxation between 30 minutes and 2 hours. This relaxation was completely different from the one of cell-free lattices, generated by a step load applied by a step strain. The relaxation of cell-free lattices in fact was much faster, showing plateau by 2 minutes (opposed to 2 hours), consistently with other previous report (Ozerdem & Tozeren, 1995).

Slow reagent permeability can be excluded as a cause of the slow relaxation because of the fast cell response observed which implies a high permeability of the gel. Furthermore repeated doses of CD (Figure 4-11) or higher concentrations (data not shown) did not alter the cellular response.

This rapid cell cytoskeleton depletion is important because it implies that the relatively slow relaxation observed (from 30 minutes to 2 hours) may be due to *new mechanical characteristics* of the internal structure of the lattice. The new structures in the fibrillar collagen network, generated by the cell-mediated remodelling process, are very likely to be held by *new weak bonds*. The degree of crosslinking of these new bonds may determine the degree of permanent consolidation of the remodelled matrix and so the extent of post CD relaxation.

4.3.3.2 Pseudo-viscosity ρ shows subtle differences in material properties

In order to account for dynamic force changes during relaxation of the remodelled matrix, a ratio parameter ρ, was defined. Physically ρ could be seen as a time variant pseudo-viscosity, i.e. the resistance of the material, expressed as reduced speed of deformation (or fluid velocity in the case of fluids), given a starting uniform stress (or pressure for fluids).

In this study ρ was useful to show that increased contraction and early RMT at 2 hours time point in TGF-β1 treated FPCLs did not correspond to an increase in resistance of the permanently remodelled lattice to relaxation (i.e. increase in ρ). It appeared that stimulation of high contraction forces caused an increase in matrix remodelling based essentially on reorganisation of the fibrillar network due to the strong stresses applied on it by the cells. Hence, as soon as the contractile cytoskeletal motor in the cells was removed, a great part of the tension was lost very rapidly. It may be speculated that this represents an enhancement of non-covalent collagen

bonding.

Control or cyclical loaded FPCLs better resisted to the sudden stress originated by cell cytoskeleton disruption, and relaxed less rapidly. It is speculated that this might be due to a different regulation of cell-matrix interactions which caused less force generation on the collagen fibrillar network but increased fixation, possibly through production of new matrix and more covalent bonding.

On the other hand it was not possible to test this hypothesis with this system because it was not possible to apply the same sudden amount of stress to lattices in which cells themselves do not produce the contraction force. External application of strains would alter completely this test whose aim was to quantify how the interstitial remodelling by the cells is able to permanently shorten the lattice structure. It could be argued that strong forces and time variant effects in the relaxation process invalidate the parameter ρ which has been defined for linear invariant correlations. From this viewpoint, threshold levels of tension at the point of cell cytoskeleton disruption would cause failure of the majority of the new weak bonds in the very initial phase of relaxation, compromising the subsequent resistance to relaxation (which is expressed by ρ). In this respect, the second part of the curve (from 2 to 12 hours) would be irrelevant as most of the differences in the new material properties would have been compromised long before.

This hypothesis, however, has been partially demonstrated as erroneous by the similar levels of initial tension, caused by different treatments (such as mechanical loading or standard static culture), which yielded significantly different levels of RMT and ρ. Therefore it is conceivable that RMT is underestimated due to the collapsing of new weak bonds at high stress levels, but that these non linear effects are limited and do not invalidate the pseudo-viscosity ρ.

ρ has been shown to be able to measure a dynamic mechanical property of the material similar to viscosity which is independent of the chosen time point of analysis (same trend in ρ was observed in the two relaxation

timeframes analysed). When dynamic force changes were reduced, the trend of ρ for the different treatments converged to that of RMT_{12}, demonstrating the analytical solidity of this parameter.

Pseudo-viscosity ρ in FPCLs subject to combined treatment (CT) remained difficult to interpret. Two possibilities appeared to be the most likely: 1) the response to TGF-β1 enhanced the cell contraction motor rather than in cell differentiation into a more "matrix consolidating type"; 2) the mechanical loading enhanced the consolidation of new bonds compared to TGF-β1 treatment alone but the very high load (due to TGF-β1), at the beginning of relaxation, broke many of the new weak bonds. This second explanation seems to be consistent with the trend observed for RMT: at 2 hours time point CT lattices had a higher level of RMT than TGF-β1 treated, showing that, although a lot of tension had been lost very rapidly (same low ρ level as TGF-β1), a few structures still able to hold a considerable tension were still present. These structures, though, carried on collapsing between 2 and 12 hours as it is demonstrated by the highest rate in force drop percentage.

The complexity of the relaxation process observed has evidenced that both RMT and ρ are important parameter in the characterisation of the mechanisms of cellular permanent remodelling and should be used in combination.

4.3.3.3 Comparison between elastic modulus and RMT parameters in the measurement of permanent matrix remodelling

The values obtained for the elastic modulus of FPCLs and cell-free lattices are in agreement with the values found in the literature, i.e. in the order of 1 kPa (Ozerdem & Tozeren, 1995; Wakatsuki et al., 2000).

The values of elastic modulus were not corrected to take into account the reduction in effective strain due to the deflection of the force transducer as shown in chapter 3. This is because relative differences were of interest in the current study. Corrected values of the elastic modulus are expected to be increased by 3.1 fold (hence remaining in the order of magnitude of 1 kPa).

Notably, consistently with previous studies (Wakatsuki et al., 2000), stiffness was significantly lower in cell-free lattices than in FPCLs treated with cytochalasin (therefore with cell stiffness component removed). This confirms that the elastic modulus of the original of the cell-free collagen lattice is permanently modified by the cellular remodelling.

Wakatsuki et al. (2000) applied 20% strain ramps to measure stiffness and reported significant differences in FPCLs stiffness between before and after CD treatment from ~10% strain onwards. This was consistent with the small differences in elastic modulus measured by 1% strain ramps in the current study. Hence, it is likely that increasing the amplitude of the strain ramp would amplify the relative differences in elastic modulus between before and after CD addition and among the different treatments.

TGF-β1 treatment generated the highest elastic modulus in FPCLs. However, after CD treatment, the modulus for TGF-β1 treated lattices was not significantly different from the modulus of the FPCLs subject to the other treatments. This suggests that cell stiffness caused the significant increase in the total stiffness of FPCL treated with TGF-β1, consistent with a direct effect of TGF-β1 on cytoskeletal assembly (Brown, 2002). The fact the elastic modulus after CD addition did not differ significantly for the

different treatments appears to be in contrast with the results obtained for RMT. This contrast was evident for cyclically loaded FPCLs in which RMT was significantly higher than control but elastic modulus (after CD treatment) was lower. However it is important to note that these parameters tested different properties of the permanently remodelled matrix. RMT tests the degree of matrix shortening under tension while the elastic modulus is a material parameter which is not necessarily dependent from the amount of shortening. This concept is explained for uniaxially tethered FPCLs (with or without cyclical loading) in the following ultrastructural mechanical models:

1) Model of the applied displacement (stiffness measurement):

When a strain is applied to a collagen lattice containing highly orientated collagen fibril bundles, these can slide along the load axis (slide along each other) much more than less-orientated fibrils (which must also rotate towards the load axis before sliding). Therefore elastic modulus is reduced when highly aligned fibrils, distributed in discrete discontinuous bundles, are present.

2) Model for isometric tension(RMT measurement):

When a sudden isometric load is applied (as after CD treatment) there is little displacement of fibres (isometric) while a stress field directed along the axial load is generated. Lattices containing aligned fibril bundles along the axis of the stress field are more resistant to internal axial stresses as each fibril bundle can withstand this stress along its stiffer axis with minimal deformation. On the other hand, less aligned, or shorter or less crosslinked fibril bundles are easily deformed by these uniaxial stresses.

This mechanical model was deduced from morphological studies that showed the formation of aligned bundles of fibre formation in cyclically loaded FPCLs (Figure 4-43-A). However this alignment appeared to be lost by 12 hours after CD treatment (Figure 4-43-A, 4-44-B). This observation was difficult to interpret and will require further longer term studies of the relaxation curve to determine if this induces changes in RMT at later stages (>12 h post CD treatment).

4.3.3.4 Method limitations

The main limitation in the current technique (i.e. RMT measurement) is that it is threshold based, i.e. a contraction force level above the level of cell-free collagen must be generated by the fibroblasts in FPCLs.

It is possible that high contraction forces can lead to an underestimate of RMT due to the deflection of the force transducer beam, acting as a spring, which might break some of the new weaker bonds generated during cell-mediated remodelling.

4.3.4 Mechanisms involved in cell-mediated spatial remodelling

4.3.4.1 An hypothesis to explain the difference in RMT generation between HDF and RTF. Possible role of α-smooth muscle actin?

The differences in the contraction profiles of HDF and RTF seeded lattices, but not in the morphological appearance of cellular and fibrillar network, might be correlated to the different levels of RMT measured for the two cell types after 18 hours of contraction. In HDF collagen lattices, addition of CD caused complete abolition of tension, while a significant tension above the cell-free-gel baseline could be measured in RTF lattices. Direct correlation between the measured RMT and the temporal evolution of the contraction profiles cannot be deduced. However it can be speculated that different phases of force generation are responsible for different phases of remodelling. The initial phase of force generation has been shown to be correlated to cell spreading and consequent traction in HDF populated lattices (Guzelsu et al., 2003; Tranquillo, 1999). The length of this phase appeared to be different for the two cell types: about 4 hours for RTF and

about 8 to 10 hours for HDF (also reported previously in (Brown et al., 1998; van de Hulst, 1981)). The subsequent phase, where the force profile flattens to a plateau, has been considered a contraction phase. HDF maintained the level of tension (from 10 to 18 hours) developed during the previous phase and appeared to have reached a tensional homeostasis (Brown et al., 1998). In contrast RTFs maintained the force only for a limited period (4 to 8 hours) after which they kept increasing the force almost linearly (8 to 18 hours).

Tomasek et al. (2002) have hypothesised that with time the contraction phase changes into contracture phase. During contracture phase HDF have been thought to undergo phenotypic transformation into proto-myofibroblasts. This causes the cell to be able to generate more force through development of special contractile machinery consisting of αSMA and focal adhesions. Proto-myofibroblasts then undergo phenotypic modulations which increase their synthetic activity of new matrix molecules and their remodelling activity of existing structures by lysing them through secreted matrix metalloproteinases (MMPs). This combined action of matrix deformation, lysis and interstitial fixation through newly synthesised collagen has been thought to be the basis of matrix consolidation (Tomasek et al., 2002).

The results of this study showed that RTFs were able to consolidate the matrix much earlier than the time needed for myofibroblasts differentiation would require. This does not exclude that the postulated mechanism could be still valid and simply applied by different fibroblastic types with different temporal dynamics, without need of changing phenotype.

On the one hand, the presence of α–SMA positive RTFs, in collagen lattices in standard culture conditions on tCFM, would suggest that cell differentiation might be implicated in the permanent remodelling. α–SMA has been considered a marker for myofibroblasts differentiation for many years (Darby et al., 1990; Grinnell, 1994; Serini & Gabbiani, 1999).

On the other hand it is increasingly evident from recent studies that

α–SMA is normally expressed (i.e. not through activation in wound site) by many connective tissue cells, including tendon and ligament fibroblasts (Spector, 2001), chondrocytes (Kim & Spector, 2000), osteoblasts (Kinner & Spector, 2002), and bone marrow progenitor cells (Kinner et al., 2002). Increased expression of α–SMA has been correlated to increased contraction of collagen lattices (Hinz et al., 2001) and collagen-GAG sponges (Spector, 2001). The mechanism of α–SMA expression by RTF, whether they naturally express it or they differentiate early in culture, cannot be inferred from the current study. However, it can be hypothesised that α–SMA might be implicated in the increased level of RMT generated in RTFs lattices compared to HDFs lattices for two observations since HDFs have been shown to express minimal level of αSMA in standard culture condition without stimulation over a short culture time (up to 24 hours) (Eastwood et al., 1998a; Hinz et al., 2001).

4.3.4.2 Model of the mechanisms of stimulation of matrix remodelling caused by TGF-β1 or cyclic mechanical loading treatments

Figure 4-47 represents a working hypothesis for the effect of TGF-β1 and cyclic loading treatments on the matrix remodelling process.

The effect of the two treatments on the remodelling capacity of cells has been hypothesised above: TGF-β1 stimulates the cellular contractile motor. This causes increased contraction forces which induce large deformation of the collagen network. Cyclic mechanical loading enhances matrix production and, through this, consolidation of the remodelled collagen network.

By putting the principal ultrastructural remodelling events in cascade additional factors and circular feedback mechanisms can be modelled.

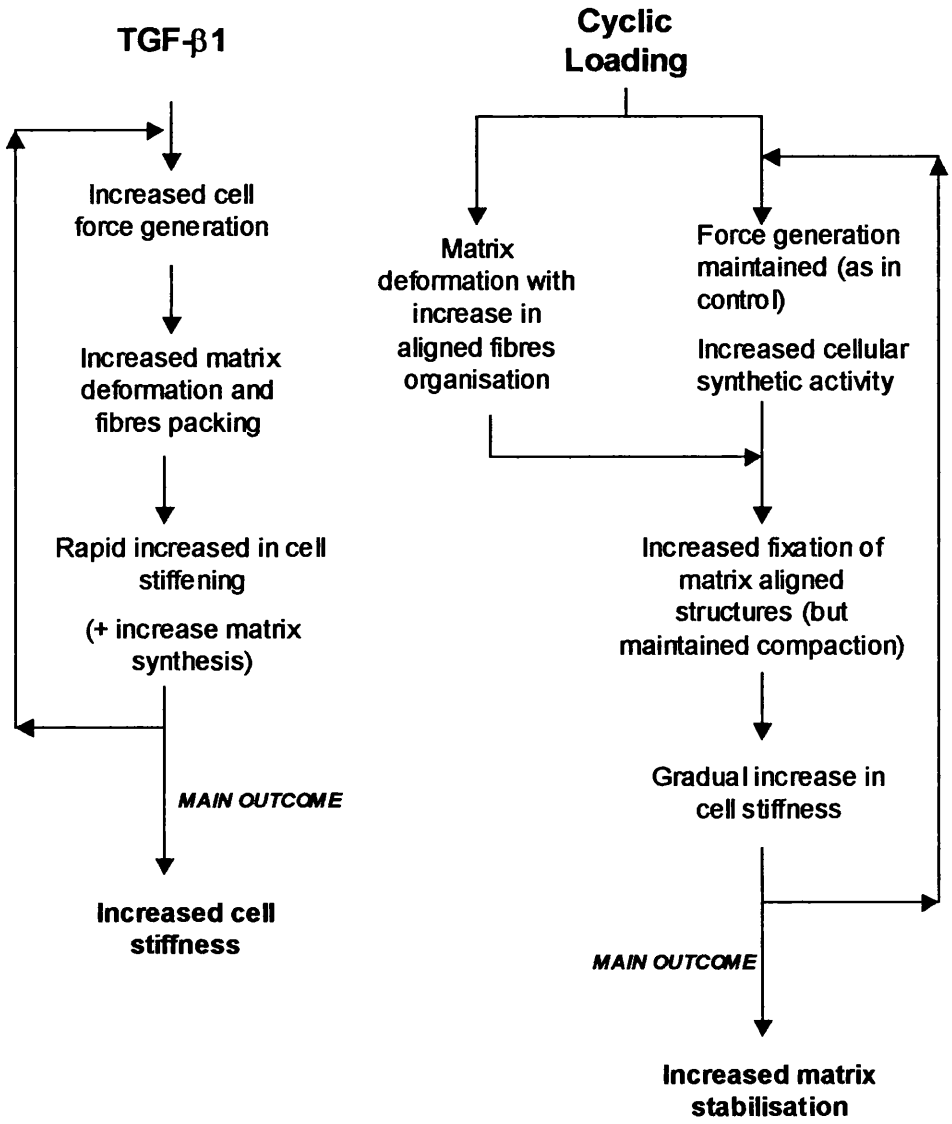

Figure 4-47 Diagrammatic representation of the events cascade in the matrix remodelling process generated by the different treatments. The main outcome for the different treatments are evidenced outside the feedback loop of events cascade. The principal outcome for the TGF-β1 treatment is the increased cell stiffness, while for cyclic loading is matrix consolidation (or permanent matrix remodelling).

TGF-β1 TREATMENT

The stimulation of force generation will have the effect of producing large deformation in the collagen fibrillar network and increased fibril compression and packing. In tethered FPCLs these cellular stresses are counter balanced by the reaction of the matrix which becomes stiffer. Stiffer substrates are known to enhance the generation of intracellular stress fibres, which are thought to balance the external rigidity of the substrate (Wang & Ingber, 1994). Intracellular stress fibres increase cell stiffness so that its internal stiffness reaches a balance with extracellular matrix stiffness (Pelham & Wang, 1998; Wang et al., 2002). Development of extensive cytoskeletal stress fibres provides cells with additional contractile machinery which increases their ability to generate contraction forces. In this case the event cascade is a closed feedback loop. The known effect of TGF-β1 stimulation of collagen production (Klein et al., 2002; Kubota et al., 2003; Lijnen & Petrov, 2002; Martelli-Junior et al., 2003; Nakatani et al., 2002) has never been quantified for the current experimental model. Hence the dynamics of this stimulation are not known. However the force measurement over the first 24 h showed that the upregulation in force is indeed the most significant response to TGF-β1 treatment (RMT showed small increase compared to the large contraction force increase). From the current study it is not possible to predict how long this circular loop can keep increasing contraction force level and stiffness. The main output of this mechanism is that cell stiffness increases as the feedback loop is iterated. This mechanism is consistent with the increase in cytoskeletal activity from early time points due to TGF-β1 treatment (Brown et al., 2002). This event cascade model for TGF-β1, stimulating remodelling is also consistent with the finding that increased force generation did not correspond to parallel increase in RMT, implying that most of the tension was held in the cellular tensile component, rather than in the matrix.

CYCLIC MECHANICAL LOADING

Cyclic mechanical loading had a double parallel effect on the matrix and the cells. In the matrix uniaxial disposition and packing of fibrils is increased by uniaxial strain of the fibrillar network (Dr. V. Mudera, unpublished data). In parallel, cyclical loading stimulates fibroblasts to increase new collagen synthesis and deposition (Parsons, 2000). Enhanced alignment of fibrillar structures by loading would then be increasingly consolidated (to a new matrix structure) by the new matrix synthesised by cells aligned to the fibrils. This gradual consolidation implies a gradual increase of the length and thickness of aligned bundles of fibrils. These fibril bundles would gradually increase in stiffness, due to the thickening and crosslinking rather than to lateral compression forces as in the case of the TGF-β1 treatment. Increased matrix stiffness has been suggested to increase cell cytoskeletal stiffness in reaction (Wang et al., 2001; Wang et al., 2002). Cell stiffness has been shown to increase in response to mechanical loading (Wang et al., 2001). However, the expected increase in cellular stiffness did not result in increased contraction forces compared to untreated lattices. Therefore the increase in cell force and stiffness was much more gradual than in TGF-β1 treated cells, similarly to untreated cells. This might be due to the gradual increase in matrix stiffness due to consolidation of the aligned collagen fibrils in the matrix which is different from strongly compressed structures generated by the strong cell forces.

Therefore, in this event-cascade model of remodelling for cyclical loading treatment, the main output is an increase in stabilisation of aligned fibrillar structures as the feedback loop is iterated.

This stabilisation is consistent with the finding that similar levels of force generation in control and cyclically loaded FPCLs corresponded to increased RMT in the latter.

The model of highly aligned structures is also consistent with the hypothesis that the measured reduced stiffness in cyclically loaded FPCLs is due to parallel sliding of aligned structures

4.3.4.3 RMT from a cytomechanics viewpoint

From a cytomechanics point of view, simply the presence of measurable RMT implies that the cells have remodelled the lattice to actively sustain part of the total tension to which tethered FPCLs are subject. Therefore it can be hypothesised that an active mechanism of cell stress shielding is present. This causes the cells to remodel and stabilise the matrix so that it can bear increasingly higher tension levels leaving only a small percentage of the total tension to be sustained by the cell component. This mechanical model of tissue formation is consistent with the actual conformation of connective tissues in their mature state (Brown, 2000). This mechanism, implying cells actively reducing the strain which they can sense, is also consistent with the concept of cell "hiding" from the externally applied strains (in this case by reorienting themselves), which was identified in previous studies (Eastwood et al., 1998b).

4.3.5 Implications of current results

4.3.5.1 Implications in wound healing

RMT provides another argument in the long debated mechanism of wound contraction. It is increasingly evident that it is not a muscular contraction of the cells pulling together the distal ends of the wound but indeed an interstitial iterated remodelling process that permanently shortens the wound area (Eddy et al., 1988; Tomasek et al., 2002).

An increased knowledge of the mechanism of matrix consolidation might be useful in the therapeutic prevention of scarring and contracture pathologies. From this study it appears that not only reducing force generation (hence contraction) but also reducing mechanical loading is important in the reduction of permanent remodelling.

4.3.5.2 Implications in tissue engineering

RMT is a fundamental parameter for tissue engineering as it provides a way to measure the degree of permanent matrix remodelling which is the principal load bearing system in connective tissue. Increased RMT implies increase in matrix stabilisation and resistance to tensile loading.

Human bone marrow fibroblasts (hBMF, also called bone marrow stem cells, hBMSC) have been used extensively in tissue engineering studies for their plasticity (i.e. the capacity of the cells to differentiate into different cell types). Additionally they are a good source of cells in terms of easy retrieval (from bone marrow aspirate) and rapid in vitro expansion. Previous studies showed that these cells were able to accelerate repair of Achille's tendons in vivo when delivered in a collagen gel medium (Young et al., 1998). Preliminary studies have characterised hBMF in tethered collagen lattices in terms of cell density versus contraction kinetics (Awad et al., 2000). In this study force generation by hBMF was measured for the first time in uniaxially tethered collagen lattices. Notably, their profile of force generation was similar to tendon repair cells and to TGF-β1 treated tendon fibroblasts, i.e. a ramp in force generation between 0 and 22 hours. hBMF generated much stronger forces than fully differentiated cells similarly to treated cells and repair cells. This might implicate an increased ability of these cells in remodelling the collagen network, resulting in high level of RMT. External mechanical loading might increase differentiation towards tendon fibroblast precursors as it has been recently shown in hBMSC seeded silk matrices (Altman et al., 2002).

TGF-β1 has been used in tissue engineering studies to enhance formation of engineered connective tissue (such as bone and cartilage, but not tendon and ligament tissue), mainly with the function of inducing cell differentiation. Here, TGF-β1 was used principally to stimulate cell force generation which increases collagen gel contraction and remodelling.

TGF-β1 was able to significantly increase the elastic modulus of lattice at 24 hours time point. However, elastic modulus was reduced after CD

treatment becoming not significantly different from the modulus generated by other treatments (after CD treatment).

In general, though, the modulus was still very low compared to the modulus of rat tendons. It is conceivable that extending culture time would increase stiffness modulus, consistently with previous studies (Huang et al., 1993) and with the increase in RMT with culture time observed in this study. Cyclic mechanical loading has been used extensively in tissue engineering studies to enhance cell matrix production (Huang et al., 1993) and increase material properties in tendon equivalents (Goulet et al., 2000; Seliktar et al., 2000). The slow frequency of loading and low strain used in this study cannot be found in other tissue engineering studies in which higher frequencies and strains were usually employed. The differences in the choice of different loading regimes depends on many factors, including matrix compliance, system geometry, cell types, and ultimately the hypotheses of effective loading regimes, such as similarities to physiological loading patterns. In this study, the chosen regime showed to increase collagen production by fibroblasts (Parsons, 2000). The chosen loading regime might not be optimal for promoting tissue formation (engineered tendons in this case). However, working in the elastic linear range of the material allowed to monitor cell force responses and remodelling avoiding matrix viscoelastic effects. Cyclical loading showed to increase RMT significantly above control. This finding might be useful in the modulation of matrix properties in engineered collagen based tissue templates although the internal mechanism of remodelling can only be speculated in this study.

Combined treatment did not produce significant increase in RMT and stiffness compared to cyclic loading, though it was higher than controls. It is hypothesised that the added effect of TGF-β1 would elicit a response in terms of RMT at later stages than 24 hours. This would be consistent with previous studies concerning fibroblast differentiation under TGF-β1 stimulation (Grinnell & Ho, 2002)and would make CT a very relevant treatment for tissue engineering purposes.

Chapter 5

Finite Element Modelling of cell-mediated lattice contraction

5.1 Introduction

The remodelling of collagen matrices by resident fibroblasts has been extensively studied and several models have been proposed (Barocas et al., 1995; Barocas & Tranquillo, 1997a; Barocas & Tranquillo, 1997b; Moon & Tranquillo, 1993; Murray & Oster, 1984; Murray et al., 1983; Sawhney & Howard, 2002; Sherratt & Dallon, 2002; Zahalak et al., 2000). The reason behind the extensive modelling of this process lies in the inherent difficulty in correlating the macroscopic scale to the microscopic scale. At macroscopic level the contraction process in FPCL results in substantial volume shrinking or force generation in uniaxially tethered models. At microscopic level contraction initiates with cell spreading and locomotion through cyclical extension. Retraction of cellular processes has been shown to deform the collagen fibrillar network, compacting fibrils at cell edges (Guido & Tranquillo, 1993; Mudera et al., 2002; Roy et al., 1997; Stopak & Harris, 1982; Tamariz & Grinnell, 2002). Multiplying by all the cells and iterating the process leads to global matrix shrinking (Eastwood et al., 1994; Grinnell, 2003; Roy et al., 1997; Tranquillo, 1999). An additional contribution to the compaction of fibrils has been identified in the cytoskeletal contraction. This causes fibroblasts to contract similarly to muscle cells pulling the fibrils centripetally to the cell body via the

attachment points (Tomasek et al., 2002).

The extensive work by Tranquillo and colleagues has lead to a sophisticated model describing the remodelling dynamics as a two-phase fluid solid system (Barocas et al., 1995; Barocas & Tranquillo, 1997a; Barocas & Tranquillo, 1997b; Moon & Tranquillo, 1993). This model stems from the earliest constitutive relations for tissue containing mesenchymal (Murray et al., 1983) and epithelial (Odell et al., 1981) cells. The objective of that work was to analyse pattern formation in continuum mechanical theories of morphogenesis. However, little detail on the mechanics of individual cells was included. In Tranquillo's model, to account for the progressive volume reduction and the inherent anisotropy of the fibrillar network constituting the collagen matrices, many parameters were added. This model has been validated for both untethered and uniaxially tethered lattices (i.e. from isotropic to increasingly anisotropic conditions). However, since it is a continuum model, cell distribution, forces, mechanical reaction of the matrix and local anisotropy distribution are represented as tensors and conservation equations. This implies that the local interactions between cells and fibrils are averaged in the global parameters or probability functions. However, in order to understand the mechanisms which induces cells to remodel matrix under certain preferred patterns, it is important to start from the single cell model and sum up the discrete contributions of the cell population within the matrix.

More recently an analytical model has provided a detail mathematical description of cell-matrix interaction, starting from the definition of single cell forces. This model focussed on time independent mechanical properties of pre-contracted (and relatively stable in macroscopic shape) lattices (Zahalak et al., 2000). Cell force generation was modelled as a muscle-like cell force generation, i.e. purely by cytoskeletal contraction. Therefore this theory cannot be applied to the tissue formation analysis in which tractional forces are believed to play a prominent role.

A hybrid mathematical model has been recently elaborated for the contraction of wound cells (Dallon et al., 1999). Discrete cells interact with a

continuum matrix filled with virtual fibres. The interaction is regulated by an regulatory factor which determines the degree of fibre spatial remodelling due to cell proximity and direction of migration. Through this mechanism a randomly aligned fibre network, representing an early wound site, becomes aligned to the patterns of cell migration across the wound space (Dallon et al., 1999). Although discrete and continuum levels are very efficiently joined through a rigorous mathematical formulation, the cellular forces and consequent matrix reaction stresses were not included.

The purpose of the current study was to generate a model based on the interactions between discrete cells and the gel as a continuum in which all contributions from boundary conditions and local stresses are taken into account.

The CFM model was used as paradigm, for the process of cell-matrix remodelling in collagen lattices for two principal reasons:

1) The tCFM allowed direct measurement of important mechanical parameters which were used for the design and validation of the model, including total cell force generation and elastic modulus.
2) The known uniaxial spatial reorganisation of cells (and matrix) was a simple parameter to be tested in order to validate the output spatial organisation obtained by the computer simulation.

The computer models were based on the Finite Element (FE) analysis which is a widely used method to model complex mechanical systems.

Due to the extremely heavy computation power required by this hybrid discrete-continuum model (see methods for details), it was not possible to implement this model for the whole 3D lattice. Hence, the analysis was subdivided into two levels: macroscopic and microscopic.

At macroscopic level, the contraction of the whole 3D lattice, uniaxially clamped, was modelled as thermal shrinkage. Values for matrix stiffness and degree of contraction were based on the experiment described in this thesis. The total reaction force and the distribution of principal strains and stresses were displayed. A similar analysis has been previously reported by Eastwood et al. (1998). The aim of their FE model was to analyse the

distribution of stresses and strains due to application of external strains to the lattices. Results of the current analysis were similar, showing, for the central area of the lattices, a large uniformity of stresses and strains aligned to the axis of load (see result section below for more details).

The FE analysis at macroscopic level provided the basis for the design of the microscopic model. This consisted of a small portion of the macroscopic model in which mechanical conditions had been previously determined. The idea was to recompose, at a subsequent stage, the macroscopic model by filling it as a patchwork with many microscopic models. The stresses calculated at the macroscopic level generated the boundary conditions for the microscopic model. This microscopic model simulation would then return reaction forces at the boundary that would be matched with the stresses determined at macroscopic level, iteratively. Due the large uniformity of the strains calculated along the central area of the macroscopic model, the microscopic matrix was assumed to be simply clamped uniaxially.

The microscopic matrix was modelled as 2-dimensional matrix because its thickness was substantially smaller than its other two dimensions. Cells were distributed on the matrix with a random position. The simulation involved the generation of tractional forces from the front of the cells and friction forces from the rear according to recent reports mapping cell locomotion forces on polyacrylamide sheets (Dembo & Wang, 1999).

The aim of this simplified microscopic model was to test the hypothesis that small directional differences in "perceived matrix stiffness" by initially randomly located and oriented migrating cells could explain the rapid cell alignment to the axis of load. The perceived matrix stiffness is the force needed by the cell to deform the matrix over a unit distance. This hypothesis was inspired by the work of Lo et al. (2000) and Thomas and Dimilla (2000), who showed that fibroblasts cultured on polyacrylamide sheets with a stiffness gradient migrate towards the direction of increasing stiffness. The computer model was originally formulated to simulate the migratory process as a series of discrete time steps. In each of these steps, cell and matrix

orientation would be altered as a function of current orientation and distribution of perceived matrix stiffness. However, the current microscopic model can only perform the first iteration due to the complexity of implementing the code. Nevertheless, this first step should allow the identification of the basic principles behind cell-matrix interactions, which was considered a priority for further development of the microscopic model.

In order to test the hypothesis that uniaxially tethered gels would generate small directional differences in perceived matrix stiffness, we compared the 'stiffness field' around cells in such a gel with that in a biaxially tethered gel. Experimental evidence suggests that in the latter gel, cell movement does but cell alignment does not occur. The hypothesis to be tested is therefore that uniaxial tethering increases alignment of the perceived gel stiffness vectors in the direction of tethering, which could explain cell alignment in that direction.

5.2 Methods

For the determination of parameters such as matrix stiffness, reaction forces in uniaxially tethered lattices, dimensions of cells and fibrils at the fine ultrastructural level etc., results presented in previous chapters (chapter 3 and 4) were complemented with data taken from the literature.

The Finite Element (FE) model was implemented on MSC.Marc (MSC.Software Corp., USA) software, running on Microsoft NT 4.0 operative system.

5.2.1 Implementation of the macroscopic model

Gel geometry and material

The total dimension of the macroscopic model were the same as the experimental CFM lattices (65 x 25 x 3 mm), but only one eighth of it was

modelled due to symmetry. The 3D mesh comprised 1000 8-noded hexahedral elements, with 1394 nodes (each element having a size of (3.25 x 0.625 x 0.3 mm). Constraints were applied as follows: nodes on symmetry planes constrained perpendicular to those planes and nodes on the attachment bars are rigidly linked to each other.

The gel was modelled as a linear elastic material with the following parameters: Young's modulus was 1kPa (as measured in chapter 3), and Poisson's ratio was 0.25.

The material was assigned a coefficient of expansion of 0.01. Temperature change was set to –30 ° C which yields a 30% material contraction. This value for the material shrinking was obtained by the average lateral shrinking of uniaxially tethered lattices cultured for 24 hours. The FE computation employed linear analysis.

5.2.2 Implementation of the microscopic model

Fibroblast-gel interaction

The interaction between fibroblasts and collagen gel was modelled using a discrete and continuum hybrid model similar one recently described (Dallon, 2000). In this model, gel deformation was described using continuum variables, while cell positions are described using discrete variables. Each cell i was given a gel position (x_i,y_i) and orientation (a_i).The continuum variables were solved on a mesh using the FE method, whereas the discrete variables were moved through the domain following assigned rules based on the geometry of model and other parameters.

A specific problem in this model was to formulate the relation between discrete and continuum variables. Cells exerts traction on the gel causing deformation, and the deforming gel alters the location of the cells and orientation of traction. The description of this interaction requires a problem-dependent interpolation function (Dallon, 2000). For the current case, a method similar to the "immersed fibre method" was used (Peskin

&McQueen, 1995). Similarly to the fibres, each cell was represented by a set of discrete points. These formed the geometry of the cell surface, set as two semicircles connected by straight lines. Cell length and width were 21 and 7 micron, respectively. The points representing the geometries were spaced at roughly 2 microns.

The traction force was assumed to be generated at the front of the cell, directed towards the centre of the front semicircle and distributed evenly. The total forward traction force per cell was 500 nN. This value was determined according to the average of a range of single cell forces reported in literature (Dembo & Wang, 1999; Eastwood et al., 1996; Zahalak et al., 2000).

Assuming a steadily moving cell, the cell must be in static equilibrium. The reaction force, equal and opposite to the total traction force, was distributed evenly over the rest of the cell surface as a sort of friction. Again similarly to the embedded fibre model, each point of the cell boundary was attributed a force equivalent to the local proportion of the total traction or friction forces per cell. These forces were then interpolated to the FE mesh using the interpolation function mentioned above.

A cell concentration of 10^6 cells/ml is commonly used in experiments. Such a concentration implies that each cell roughly occupies a square of 0.1×0.1×0.1 mm. To allow a reasonable number of cells, a 0.5×0.5 mm slab of gel was modelled, with a thickness of 0.1 mm. The slab contained 25 cells, distributed randomly.

Gel geometry and material

The finite element model comprised 10,000 linear 4-node plain stress elements measuring 5x5 microns each. The gel was assumed constrained at either all four sides or only two opposite sides (i.e. uniaxially). The gel was modelled as a linear elastic solid, with a stiffness of 1 kPa and a Poisson's ratio of 0.25.

Parameters investigated

The parameter "apparent gel stiffness" was calculated for each cell as the ratio between the matrix reaction to cell traction force and the local gel

displacement relative to the centre of the cell. Gel deformation was calculated relative to the cell centre to compensate for gross movements of the cell with the gel, which were particularly notable in the uniaxially constrained gel.

The gel slab was constrained either uniaxially or bi-axially (Figure 5-1). The uniaxial constraint was realized by constraining two opposite ends of the gel slab, while leaving the other two sides free. The biaxial constraint was realized by clamping all four sides of the gel slab. Figure 5-1 shows the result of one cycle of iteration in which the calculated cell traction was applied. Cell tractional forces caused deformation of the free sides of the gel in the uniaxially tethered (Figure 5-1-left picture). None of the boundaries were allowed to deform in the bi-axially tethered model (Figure 5-1-right panel).

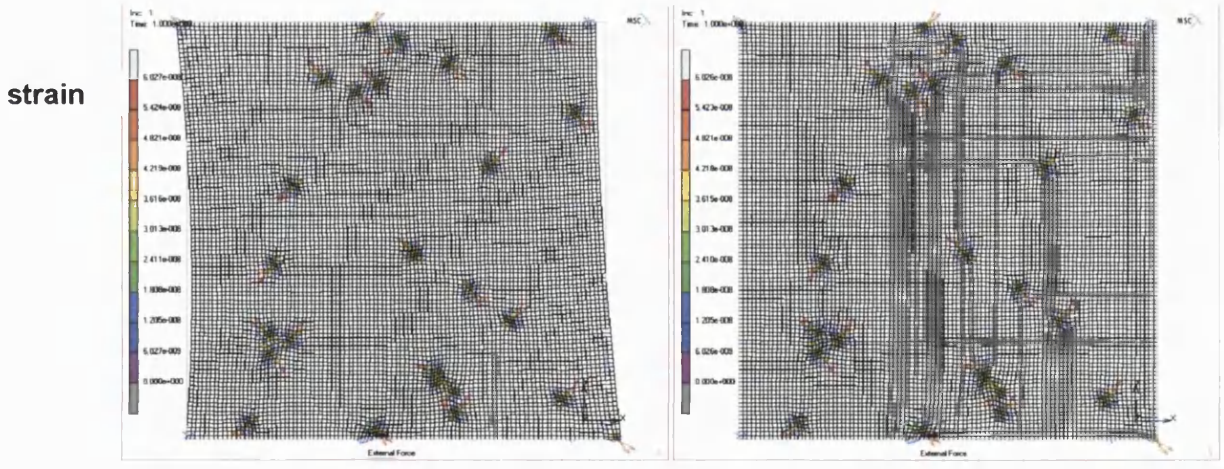

Figure 5-1. Result of the first iteration of the simulation of cell-matrix interaction in uniaxially (left picture) or bi-axially tethered (right picture) gels. Deformation occurred only in the non-tethered sides of the uniaxially tethered model. No deformation was allowed in the bi-axially constrained matrix.

5.3 Results

5.3.1 Model of macroscopic contraction

Figure 5-2 shows the distribution of the principal strain vectors in a quarter of a CFM collagen lattice, which was cut due to symmetry. The top represents the clamped side of the lattice, the bottom is the centre of the lattice.

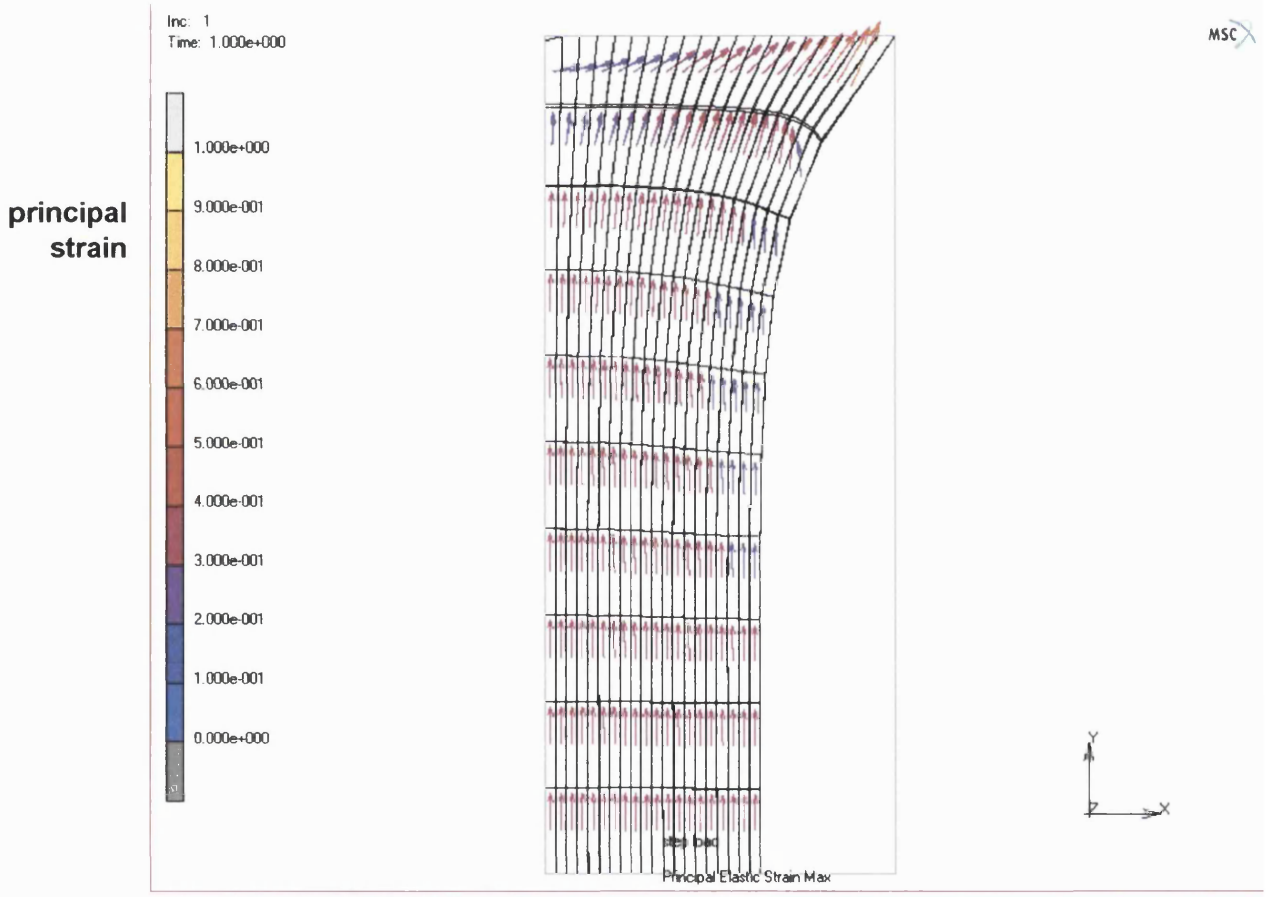

Figure 5-2 Graphical representation of the principal strain vectors in 3D collagen gels (viewed from the top). The principal strains were generated by 30% contraction, applied to the material by thermal shrinkage. The top represent the clamped side of the lattice, the bottom is the centre of the lattice which was cut due to symmetry.

The imposed value of 30% deformation (shrink) was derived from measurements of average lateral compaction (i.e. perpendicular to the load axis) in uniaxially tethered FPCLs after 24 hours in culture. The reaction force at the attachment bar had a value (i.e. 0.65 x 4 by symmetry = 2.60 mN) within the range of the actual contraction forces on the CFM. This result suggests that the cellular contraction at macroscopic scale can be approximated by contraction at molecular level in a linearly elastic material thermally cooled; not considering contraction time courses but only the end result.

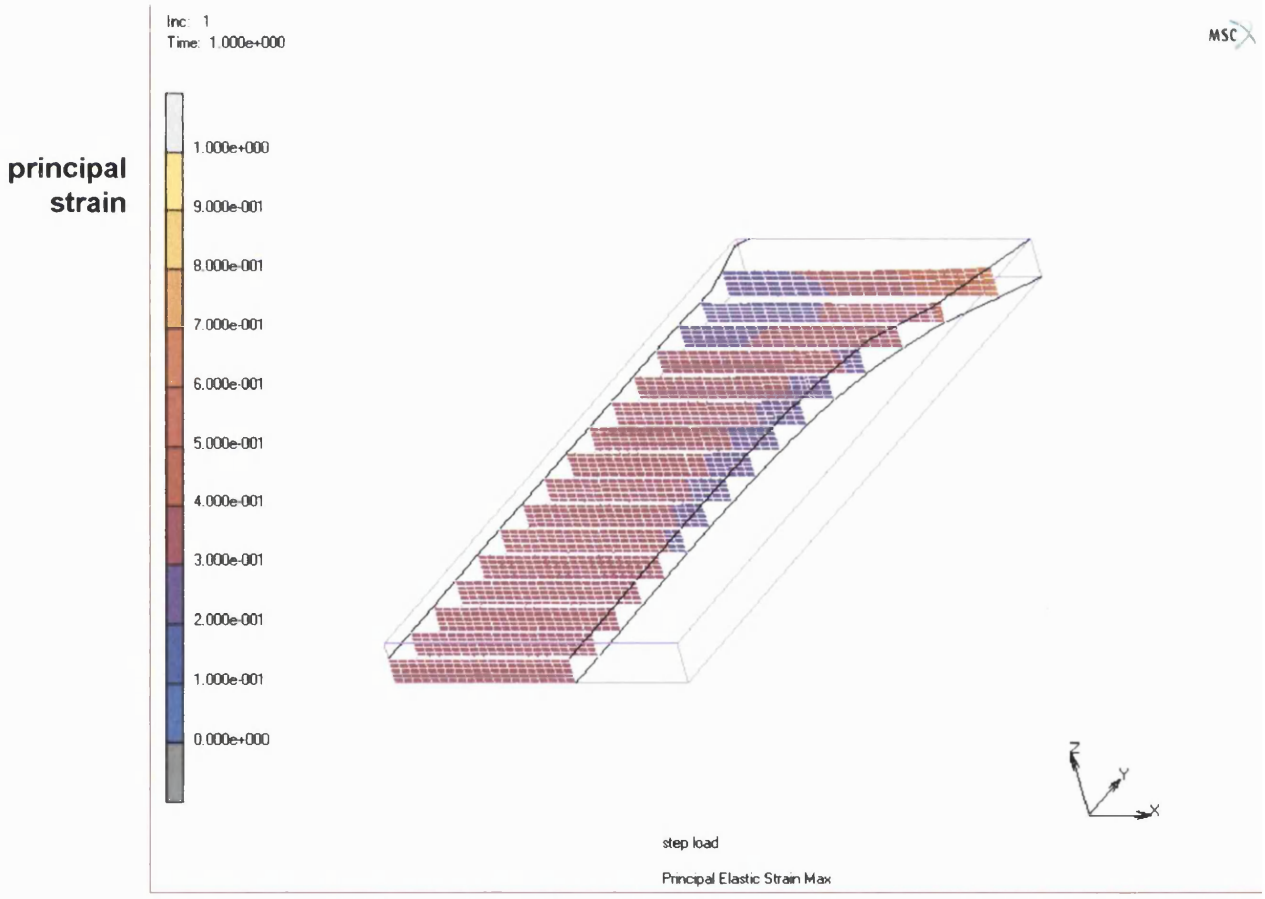

Figure 5-3 Uniformity of principal strains along cross sectional planes of 3D contracted collagen lattices. As in the Figure 5-2 the top represent the clamped side and the bottom is the centre of the lattice.

Figure 5-2 shows that the alignment of principal strain vectors along the axis of isometric tension. Due to the linear elasticity of the material the distribution of principal stresses was identical.

In order to estimate the degree of uniformity of the principal strain along the cross sectional area of the lattice, a representation of the strain levels along parallel planes was generated (Figure 5-3). A high degree of uniformity was clear in the planes towards the central area of the lattice, while disuniformities were present in the gel towards the attachment bar and along the external longitudinal edge (half way between the centre and the clamp).

In conclusion a high degree of uniformity of stresses and strain was found in the central area of of 3D lattices, uniaxially tethered. The vectors of the principal strains and stresses were highly aligned to the axis of load with distortion towards the attachment bar.

5.3.2 Microscopic scale model of cell-matrix interactions in collagen lattices

The result of the first iteration in the cell-matrix interaction simulation is shown in Figure 5-4. The positions of the cells in this graph are the random initial positions, hence some cells are isolated and some cells are in small groups. This distribution is similar to what could be observed ultrastructurally in cultured FPCLs (see chapter 4, Figure 4-3). The tractional forces exerted by the cells along the direction of their initial orientation caused the matrix to deform locally, but also on a larger scale. The local deformation was influenced by a combination of factors, i.e. the imposed uniaxial isometry, the cell-generated local stresses and the stresses propagated from neighbour cells.

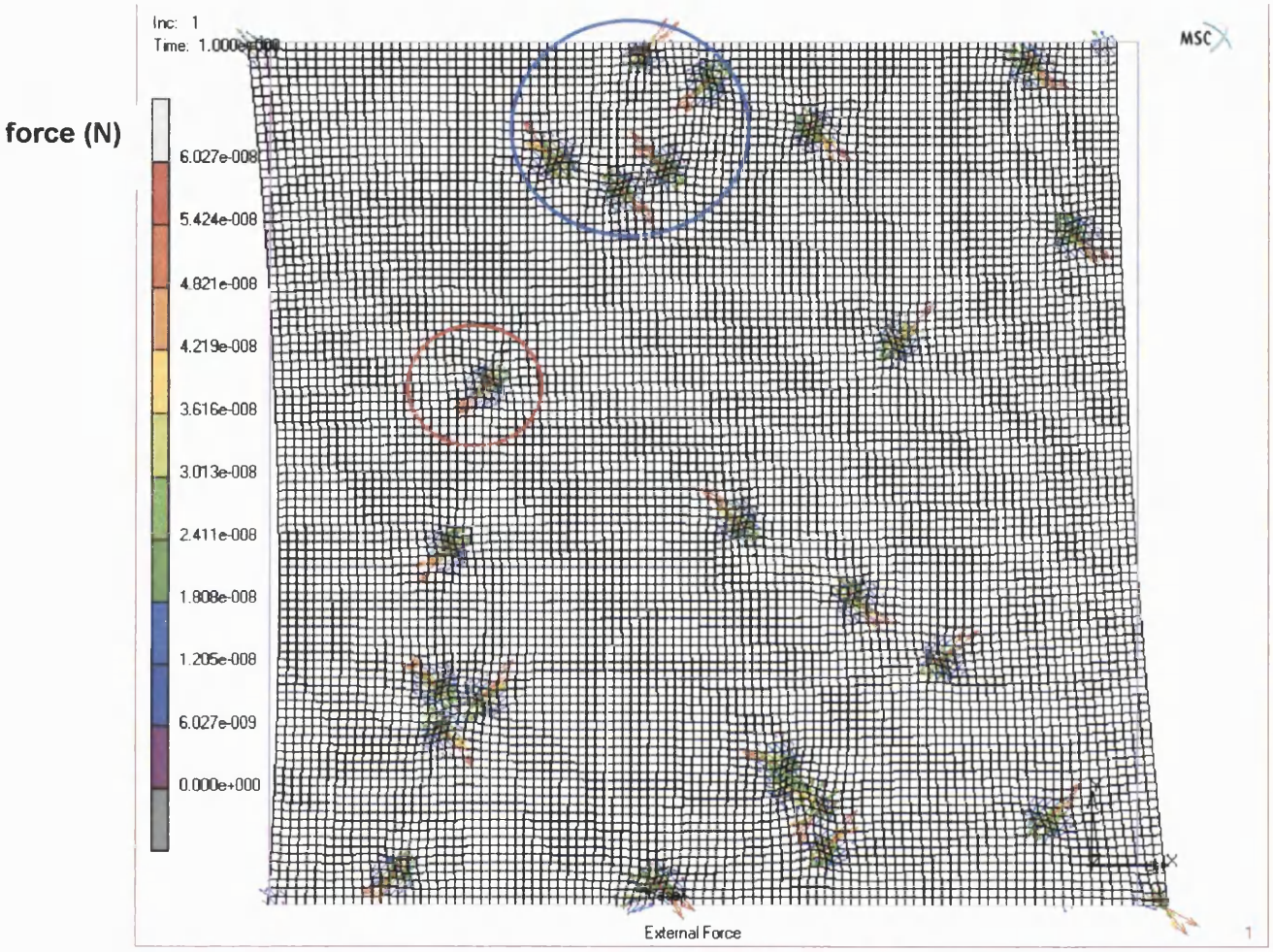

Figure 5-4 Representation of the cell traction pattern, distributed over the mesh domain (microscopic scale, i.e. 0.5 x 0.5 mm). Force scale ranges 6 –60 nN. Cells were randomly distributed and orientated. The cells started to exert traction from in their front part towards their body centre. The rear of the cell exerted distributed frictional forces onto the matrix. At the first iteration the matrix presented local deformations and the cells (visualised by the presence of their tractional forces) assumed different distributions. Some became close (blue circle) and other were found isolated (red circle). The arrows on each cell indicate direction and intensity (by colour range) of the reaction force to cellular traction in the matrix. The top and bottom edges of the gel are constrained, therefore the axis of load runs vertically to the picture.

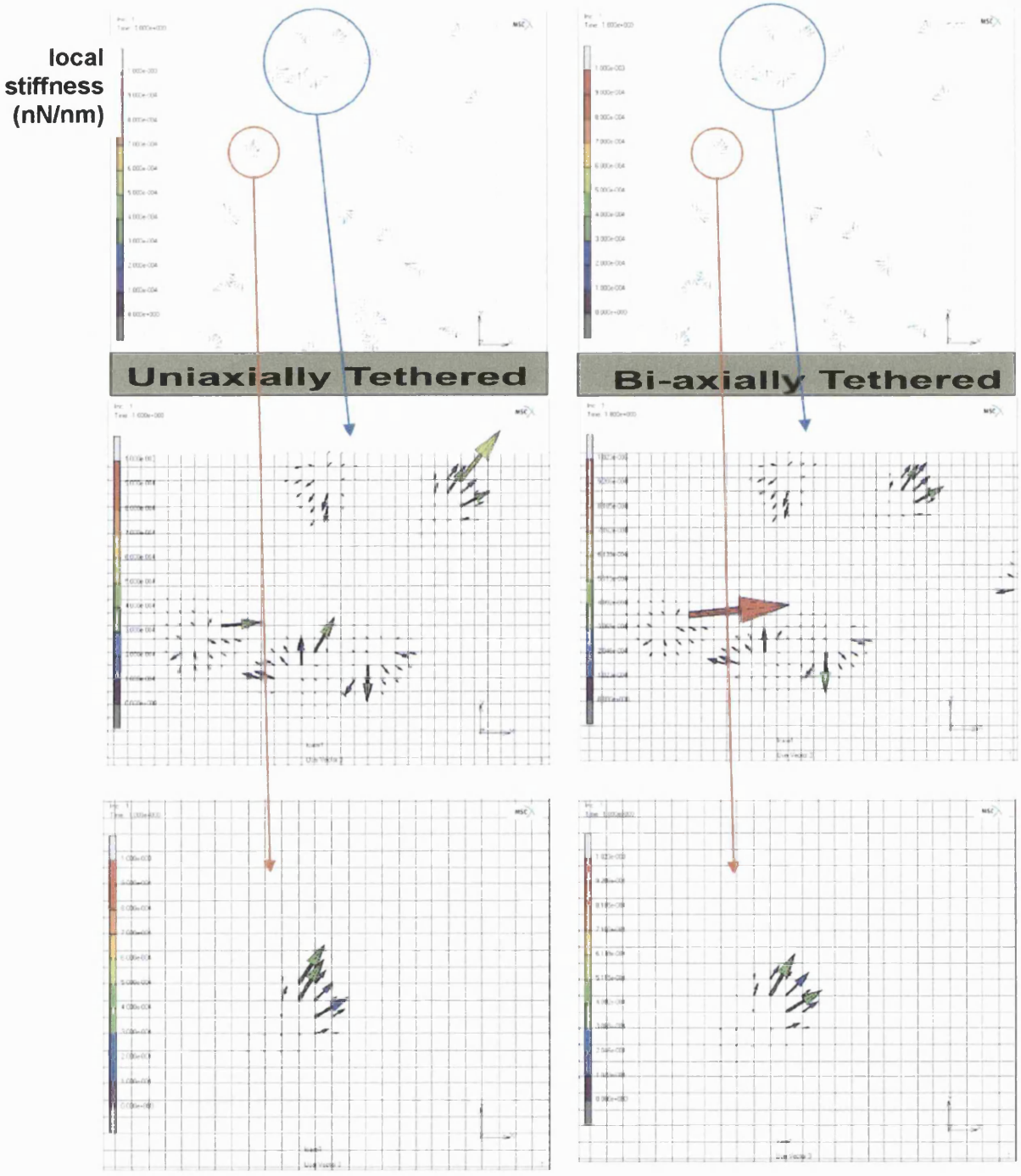

Figure 5-5 Apparent gel stiffness, calculated from Figure 5-4, displayed for uniaxially (left triplet, axis vertical to pictures) and bi-axially (right triplet) tethered gels. Scale bar range is 10^{-4} – 10^{-3} nN/nm. Exploded views of the stiffness vectors (displaying the direction and modulus of vector) for an isolated cell (red circle) and a group of cells (blue circle) are displayed below respective axial/bi-axial configurations.

The apparent gel stiffness experienced by each cell was calculated at the end of the first iteration of the simulated cell matrix interaction. Another computer simulation was run with all axis constrained (i.e bi-axially tethered gel) for comparison.

Figure 5-5 shows the perceived gel stiffness local to the cells in either uniaxial or bi-axial configuration. Orientation and modulus of the perceived stiffness are represented by vectors (arrows) in the exploded views of the representative gel areas selected (circles). Areas of the gel containing isolated cells (red circle) or grouped cells (blue circle) were analysed.

The analysis of areas containing isolated cells showed that in uniaxially tethered gel the stiffness vectors with greatest module (green colour) were orientated towards the load axis, while in biaxially tethered gels the stiffness orientation coincided with the cell orientation.

The analysis of areas containing grouped cells was less straightforward due to a greater weight of local contributions relative to the boundary conditions. Nevertheless, in uniaxially tethered gel the stiffness vectors withgreatest module (green colour) were prevalently orientated either towards the load axis or towards other cells. The perceived stiffness distribution for groups of cells in bi-axially tethered gells did not bias towards the vertical axis. The highest stiffness vector (red colour) was calculated in an area of the bi-axially tethered gel occupied by grouped cells. Importantly, this vector, representing a summation of many local contributions, was orientated almost perpendicularly to the vertical axis (i.e. the load axis in uniaxially tethered gels).

In conclusion, when a uniaxial constraint was applied to the gel, the apparent matrix stiffness perceived by the cells was found to be biased towards the load axis. In contrast, apparent stiffness did not show preferred orientations in bi-axially tethered gels. This result suggest that the boundary conditions have a direct affect on the apparent stiffness perceived by the cells.

5.4 Discussion

The cell-mediated contraction of a uniaxially tethered gel was modelled by a 3D shrinking linear elastic material uniaxially tethered, having the same elastic modulus as the cell-free gels. The result of 30% material shrink (similar to the experimental contraction) showed that stresses and strain were highly uniform in the central area of 3D gels. The direction of the vectors of the principal strains and stresses was highly aligned to the axis of load with distortions towards the attachment bar.

Notably, similar uniformity in the alignment of cells and matrix were observed experimentally in the central area of uniaxially tethered FPCLs after 24 hours in culture in the CFM (chapter 4). In contrast, poor cell alignment has been reported for the lattice areas in proximity of the attachment bars, in the area called "delta zone" (Eastwood et al., 1998).

The intuition of a cell "hiding from load" mechanism identified by Eastwood et al. (1998) can be reinterpreted in light of the results of the current model. In effect, principal strains were shown to be aligned to the load axis in the current FE model and cells were found to align to the same axis experimentally. However, at the microscopic level the orientation of principal strain vectors did not correlate to the boundary condition (i.e. vectors showed orientations independent of the uniaxial direction, data not shown). In light of recent experimental findings showing that cells tend to migrate towards the stiffest areas on 2D substrates the apparent gel stiffness parameter was tested. Local stiffness vectors showed to be highly affected by the boundary conditions of the matrix, already form the first iteration of the cell-matrix interaction simulation. Supposing the cells are attracted by increasing stiffness gradients (i.e. the move towards the stiffest local areas), this model can explain the alignment of cells from a purely mechanical viewpoint. Cells therefore align not to principal strains but to local stiffness gradients generated by local stresses ratioed to local deformations. At regime, after several iterations, it can be predicted that the

principal strains will be aligned, duo to the general alignment of cells and this could explain why this mechanical parameter has been previously (Eastwood et al., 1998) correlated to cell alignment. Additionally, the current results suggest that the cells "hide themselves from load" not by aligning and therefore reducing their exposure to strains (cell modelled with a spindle-like shape) but by actively moving towards the local stiffest areas of the gel which they perceive to be least deformable (and therefore where the least strains occur).

An intuitive example might help to explain the concept of the local stiffness as opposed to true stiffness of the whole gel. Suppose someone is pulling a rope which is hanging down. If a high resistance is felt to this pulling action, than one might decide that it is safe and dare to climb. In contrast, if the rope feels very flexible the decision might be opposite. Now, who is testing the rope by pulling does not know why it is stiff: maybe somebody at the top is pulling at the same time. Or maybe it is tied onto something which is stiff. But the important result is that it feels stiff to who is testing the rope. So, as the perceived rope stiffness is not necessarily the same as the true rope stiffness, the gel stiffness that the cells feel is not necessarily the same as the true gel stiffness.

Limitations

While interpreting the results, it should be kept in mind that a model necessarily makes assumptions. These assumptions obviously limit the validity of the model.

First, the collagen gel was assumed linearly elastic whereas collagen gel is known to behave as a viscoelastic solid (Barocas et al., 1995; Ozerdem & Tozeren, 1995; Zahalak et al., 2000). However, given the short relaxation times measured by these workers, an elastic approach seems justified for slow processes such as modelled here. Additional the linear elastic material was assumed as completely isotropic, while increasing degrees of ultrastructural anisotropy in the collagenous fibrillar network have been observed in cultured collagen lattices. The very presence of fibrils confers a

degree of internal anisotropy to the material. Methods to calculate the elastic modulus of materials made of entangled fibre networks have been proposed (Cox, 1952; Fu & Lauke, 1998). However these models would involve the use of complicated interpolation algorithm to account for the contribution of fibres entanglements at various locations and an additional discrete domain to track fibre positions and parameters. Additionally it is possible that the effect of fibre-induced anisotropy increases the alignment of the gradient of apparent local stiffness perceived by the cells. This might be caused by the high stiffness of collagen fibrils along the longitudinal axis and high compliance perpendicular to the axis. Hence, as soon as a fibril becomes orientated along the tethered axis, it becomes a line of maximum local stiffness. In fact, it cannot be longitudinally deformed due to intrinsic stiffness and at the same time it is tensioned longitudinally (due global isometric tension) which confers additional transversal stiffness (under a tension-stiffening mechanism). Additionally once matrix fibres have been suggested to generate contact guidance to which cell align (Tranquillo, 1999).

Secondly, fibroblasts cultured in 3D uniaxially tethered lattices have been demonstrated to generate a stable structural remodelling in the collagen matrix that increases with culture time (chapter 4). However, because this effect at early stages of contraction is considerably smaller than the active contraction by the fibroblasts, it was omitted in this first version of the model.

Finally, the model forms a two-dimensional representation of a three-dimensional phenomenon. Two-dimensional models are widely used in engineering to study patterns of stress and strain in three-dimensional structures. These models are particularly useful to study structures in which the essential mechanical dynamics can be gathered by two dimensions due to symmetry. Nevertheless, a particular problem in this study was to calculate representative values for the forces applied by the cells. The current model represented a piece of gel with a thickness of 100 micron. This caused cell to be actually unable to exert significant traction in

the third dimension. Interactions between neighbouring cells might be therefore privileged in the current model in respect to the 3D gels.

Relevance of computer models of cell-mediated remodelling

The relevance of computer models of cell-mediated contraction lies in the possibility to determine important principles based on factors/hypotheses that are very difficult to test/monitor/correlate experimentally. Additionally, once central principles are identified, computer models could be able to generate predictions of the result of the cell-matrix remodelling process, narrowing the range of variables to be tested experimentally. For instance, it could be predicted how the geometry of the 3D gel affects cell spatial remodelling. This might be important for tissue engineering purposes, in which control of architecture and mechanical properties of the engineered tissue is essential.

Chapter 6

Construction of templates for 3D connective tissue interfaces

The importance of tissue interfaces in surgical repairs and implantations has been highlighted previously (general introduction). A 3D culture model to support the engineered formation of bi-functional constructs would be an excellent tool to generate pre-engineered interfaces and, in general, study the mechanisms of connective tissue integration. In this area the mechanical strength of the interface is the key parameter to evaluate the goodness of the integration. Little work has been done in this area (Gosiewska et al., 2001b; Greiling & Clark, 1997b; Isogai et al., 1999; Schaefer et al., 2000; Sherwood et al., 2002), especially in controlled in vitro systems where the adhesive strength of the interface can be measured (Cacou et al., 1996b; DiMicco & Sah, 2001b; Obradovic et al., 2001b; Peretti et al., 1998; Silverman et al., 2000).

This chapter presents the development of a tissue interface model based on 3D collagen gel construct for use in mechanically loading bioreactors. The objective was to generate a 3D tissue interface in vitro that would allow prolonged culture time and final assessment of the tissue integration by quantifying the ultimate strength. The interface was created between a cell-free and cell-seeded gel. The latter can be regarded as an immature tissue equivalent.

6.1 Methods

All materials and methods used were as described in chapters 2 and 3.

Further details about the interface generation methods are outlined below.

6.2 Results

The results presented below describe the construction of collagen-gel-based 3D models of tissue interfaces. Interfaces were generated between a cell-seeded contracting gel and a cell-free gel. The interface templates evolved following both technical problems encountered and changes of concepts and understanding of the interface generation process. The templates design evolved from the *fracture* model described in chapter 3 to the *wrapping* model. The fracture model was useful to the development of the wrapping model since it provided the basic guidelines for the generation of the collagen gel based interfaces. These can be summarised as:

1. Interfaces between collagen lattices can be reproducibly generated and their basal strength (i.e. strength before cellular remodelling-strengthening) can be controlled.
2. The cell-mediated contraction must be reduced to a minimum in order to control the dimension of the interfacing area and/or the mechanical tension applied to the interface zone.
3. Cell migration across the interfaces was observed at day 5. This time point can be considered, under the current model, the time from which cell-interface remodelling commences.

The wrapping model, was generated by casting a pre-contracted cell-seeded gel to a wrapping cell-free gel. The cells of the cell-seeded gel had already contracted (untethered) their collagen to a stable matrix (i.e. minimal additional size change). Therefore cell-mediated contraction did not play a significant role in the interface formation process.

This model has been further characterized biomechanically by finite

element (FE) analysis.

The key parameter was the mechanical integration, measured as the ultimate strength of the interface (i.e. the stress needed to completely break the interface). The wrapping model was based on 3D collagen gel substratum and relied entirely on the migration of cells from a cell-seeded side of the interface to a cell-free side. The hypothesis was that their migration would initiate and bring about mechanical integration of the two gel sections.

6.2.1 Wrapping model

6.2.1.1 Model concept and assembly

The "wrapping model" is a bi-functional interface between a cell-seeded element embedded into a cell-free collagen gel. The baseline adhesive strength between the two gel components is that bonding which is formed at time zero when cell-free gel is set. The idea here is that under constant and controlled preparation conditions for the formation of cell-free wrapping gel the interface adhesion strength (over time) should depend only on the activity of the cells resident in the cell-seeded component.

A pre-contracted collagen gel seeded with rat tendon fibroblasts formed a the first (cell-seeded) component. 48 hours pre-contraction produced a dense matrix with a trapeze-like shape with their longer base firmly attached to the terminal bars. At this stage, the pre-contracted gels were inserted into the cell free wrapping gel whilst it was still in liquid phase but rapidly setting and allowed to set into position.

Figure 6-1 shows this assembly in the vertical plane.

The result of this procedure was a well-bonded interface between a cellularised pre-contracted gel and the cellular wrapping element with known dimensions Figure 6-3-A. When set, the cover was removed (Figure

6-2) and the casting apparatus turned into the horizontal plane for either culture or testing of the interface strength. For mechanical testing the two attachment bars (Figure 6-3-A) were connected to the IAMD for controlled loading (Figure 6-3-B).

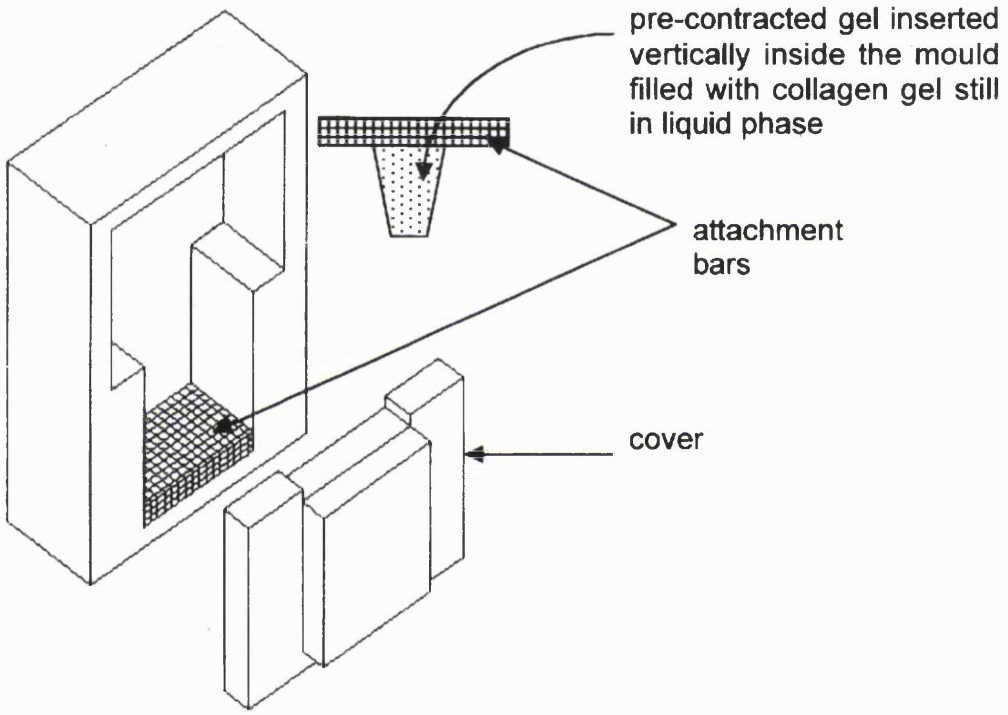

Figure 6-1 CAD diagram showing the assembly at the interface in the casting assembly. With the cover plate sealed in place on the lower tank and the well in the vertical position, a fixing bar is placed at the bottom of the lower chamber (hatched bar). The lower chamber was filled just below its top edge with cell free collagen gel solution. The pre-contracted implant was inserted into the upper chamber such that the attachment bar (hatched) rested on the shoulders of the lower chamber (i.e. out of contact with the second gel element) and the pre-contracted gel dipped into the collagen gel solution below.

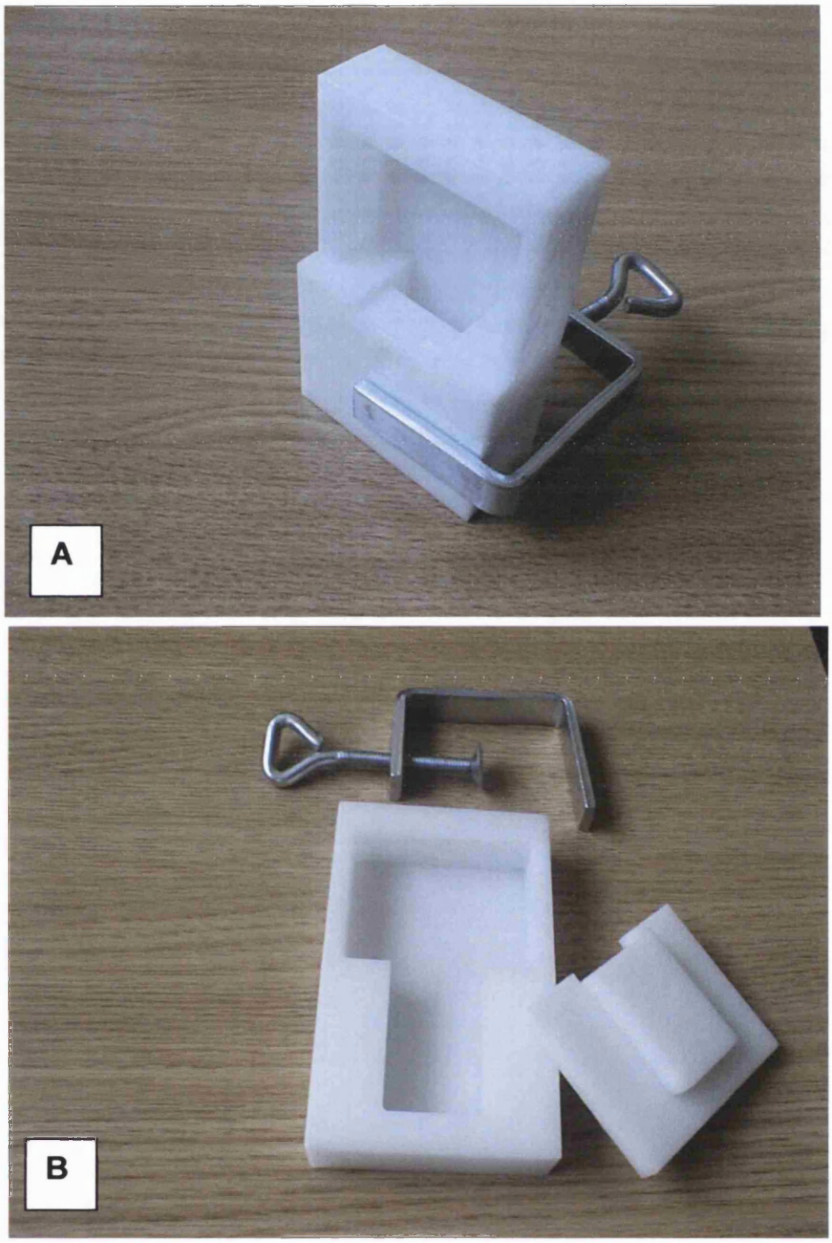

Figure 6-2 Photograph of the disassembled (A) and assembled (B) casting chamber. Once the gel was set the clamp was removed and the chamber returned to the horizontal plane and covered by a plastic lid.

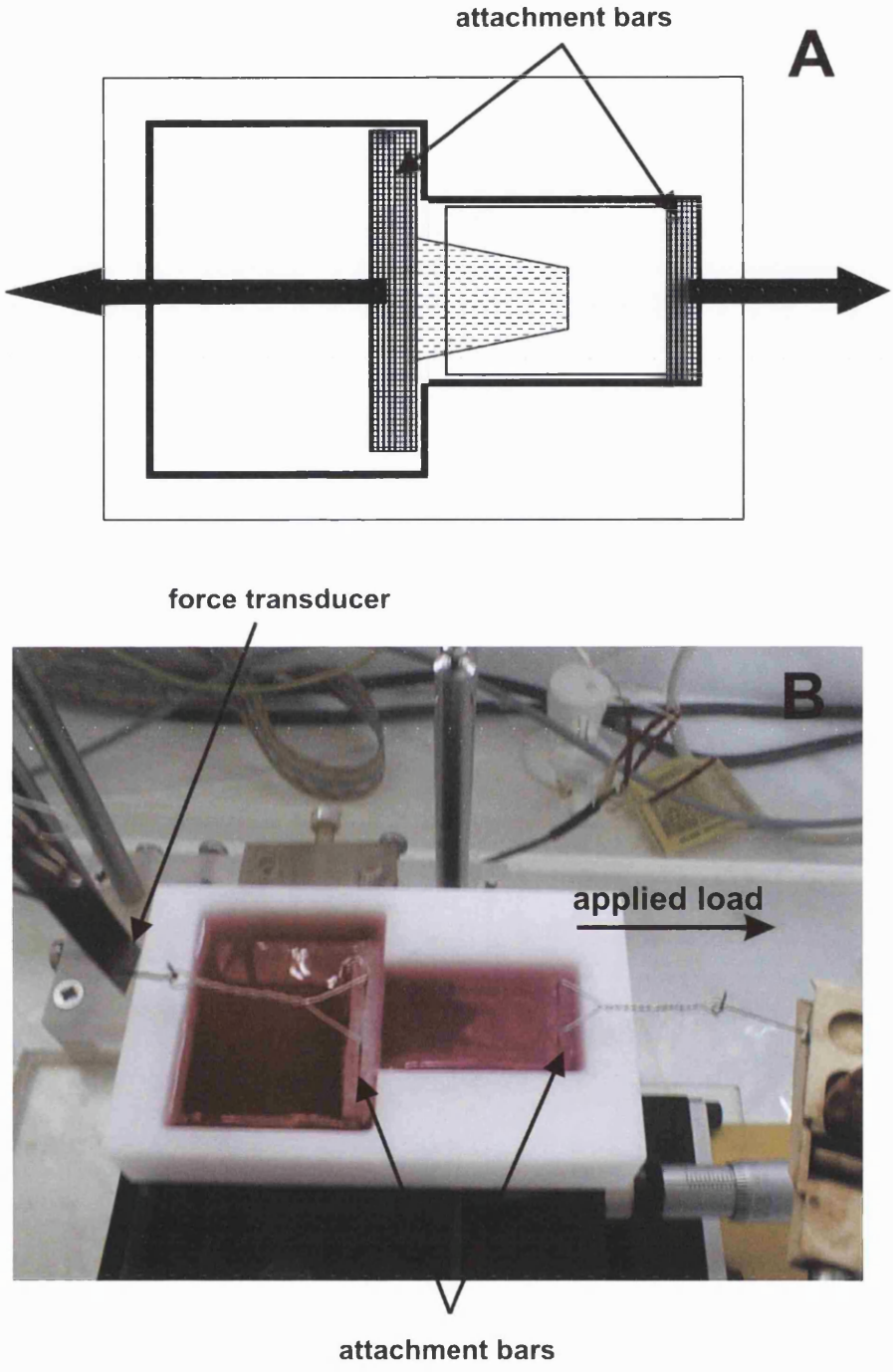

Figure 6-3 (A) Diagram showing the horizontal assembly of the model interface chamber Arrows show the direction of the uniaxial strain applied to the connector bars for the measurement of the interface adhesive strength.

(B) Photograph of the full assembly (on the IAMD) including culture medium (pink fluid) showing the pre-contracted collagen gel (left hand side, arrowed) being pulled out from the cell free wrapping collagen gel (right hand side).

The two chambers of the interface casting are shown in Figure 6-3-B. The larger left hand well contains medium for incubation and also houses the attachment bar which is attached to the contracted collagen gel. The contracted collagen gel reaches towards the smaller right hand well into which the cell free gel is anchored by its attachment bar (far right). This model was effective in forming reliable reproducible cell seeded interfaces with the possibility of introducing cells into one or both components. Under these conditions, the interface pull out force was proportional to the contact surface area which was measurable for each assembly. It was important to maintain constant hydration of the pre-contracted gel element before incorporation into the cell free gel as even slight dehydration at this stage was found to cause increased baseline adhesion. Also, the baseline adhesion level and sensitivity of the model could be modified by increasing or decreasing the depth to which the pre-contracted gel was inserted into the cell free wrapping gel (i.e. the contact surface area). At all times it was important to maintain clear separation between the pre-contracted gel attachment bar and the cell free wrapping gel.

6.2.1.2 Measurement of adhesive strength

Once this model was routine for gel fabrication, the baseline pull out strength of the interface was assessed using zero time of incubation. In this case the interface construct was placed on the IAMD and pulled at constant rate (50 μm/s) to load and, eventually, to fracture the gel interface. The baseline force levels are illustrated in Figure 6-4 by three specimen traces. As predicted, the interface remained the weakest element of this mechanical system and in all cases fracture occurred at this interface. The time zero, basal interface was characterised by a clear maximum force required for fracture (between 519 and 552 dynes).

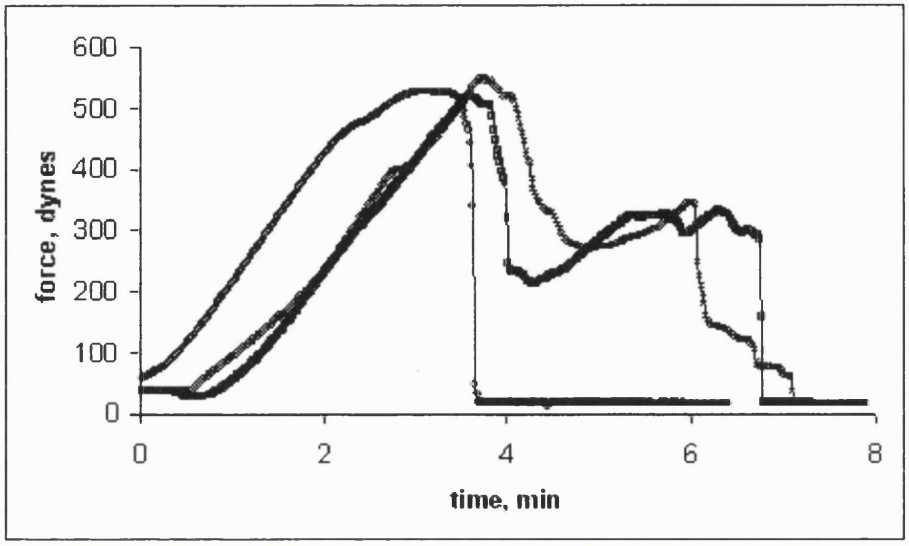

Figure 6-4 Graph of 3 specimens pull out responses showing force versus time using the IAMD for zero time interfaces.

At this stage some interfaces broke cleanly with no residual attachment but in some cases traces of long attachments remained and were broken subsequently with further extension. In all three cases shown here, time to rupture was also similar at around 4 minutes.

A second baseline measure involved 24 hours incubation period but with a killed pre-contracted gel component. A one-week test experiment carried out with this model was used to assess the contribution of cell-based integration across the interface and formation of new integrated connections over that time period.

Figure 6-5 compares the adhesive strength of this interface after one week of cell based integration with those formed with killed cells and at zero time with live cells. Shear stresses have been estimated as the ratio of the reaction force measured on the force transducer over the total contact surface of the cell-seeded element estimated sample by sample by image analysis.

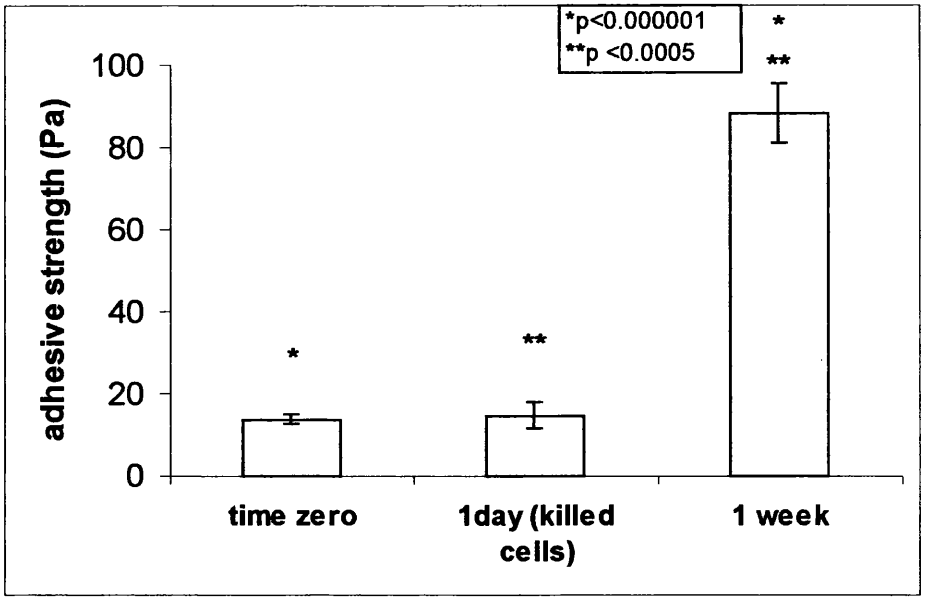

Figure 6-5 Histogram showing the adhesive strength of the interface at time zero, one day using kill cells, and after one week with living cells. Error bars represent SD (n=4). P-values were computed by standard Student's t-test.

The adhesive strength for the zero time live cell and one day kill cell experiments were not significantly different at around 14 Pa average. However, after one week of incubation in this model system, cellular contribution had caused a 6-fold increase in the interface strength, to over 88 Pa.

6.2.1.3 Circular (multiaxial) version of the wrapping model for the analysis of cell migration

A circular model was generated in a 12 multiwell plate to allow microscopy observation and assessment of cell migration. The interface was assembled in such a way that it replicated the vertical configuration in a multiaxial configuration, hence not suitable for mechanical testing (see methods). Briefly, a 48 h cell-seeded collagen gel was prepared and cast into a fresh cell-free wrapping gel (Figure 6-6).

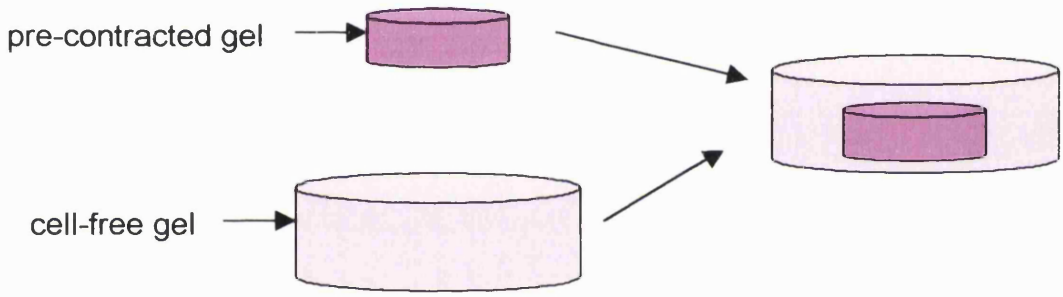

Figure 6-6 Sketch of the round gel assembly procedure.

A photograph of a circular construct is shown in Figure 6-8. The denser ring of the pre-contracted gel can be clearly identified surrounded by the cell-free wrapping gel. In prolonged culture this construct produced extensive lysis of the central cell seeded element. This was consistent with the findings reported in chapter 4 in the absence of a wrapping gel. Therefore overlaying the pre-contracted gel had no effect on the lysis process (rather this seems to be a special feature of RTFs).

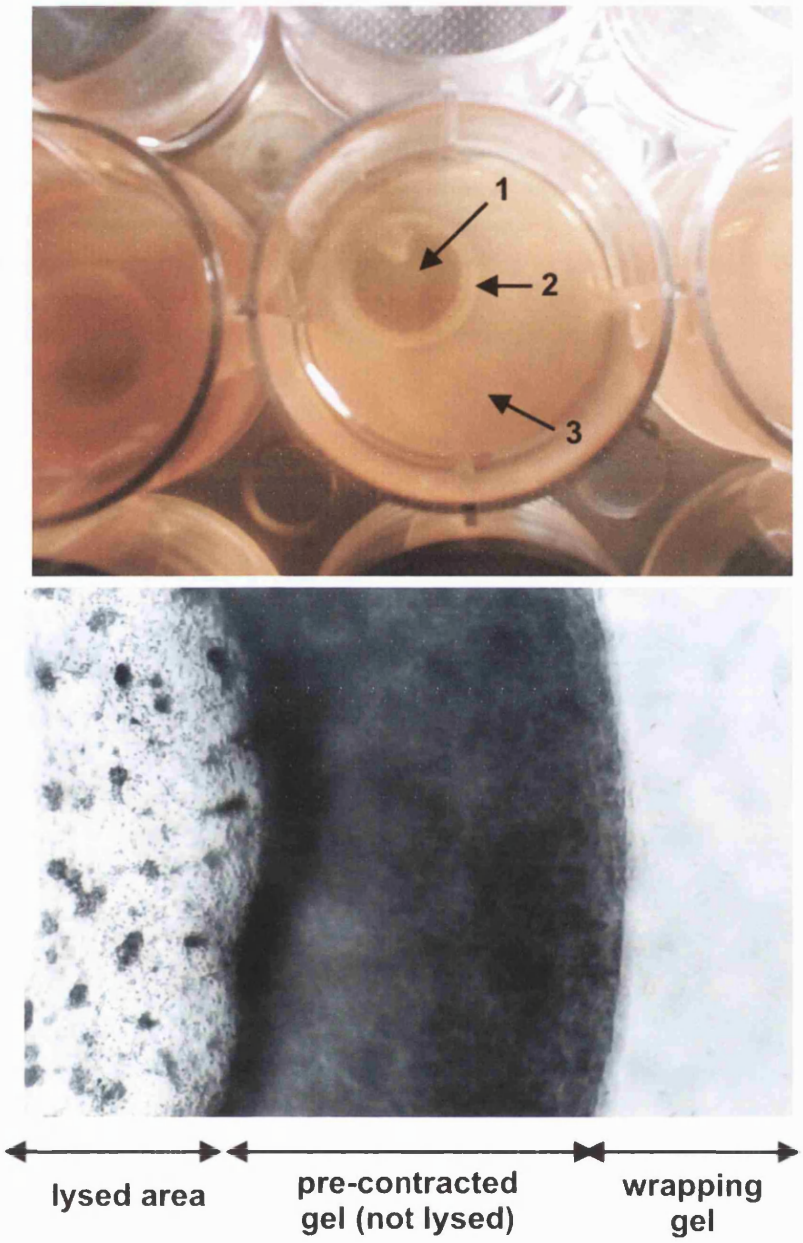

Figure 6-7 Photograph and micrograph of the circular version of the wrapping model. In the top picture, the denser ring of the pre-contracted gel (arrow 2) can be clearly seen surrounded by the wrapping cell-free gel (arrows 3). The bottom picture shows a phase contrast micrograph at low magnification of the pre-contracted gel reduced to a ring enclosing a lysed area (indicated by arrow 1 in the upper picture) and surrounded by the wrapping gel.

This model variant allowed clear, sequential imaging of living cels and their migration over time (phase contrast microscopy) and wasused to test the predicted involvement of trans-interfacial migration in the increase in interface strength (Figure 6-7 and Figure 6-8).

Cells were seen to migrate from the external edges of the inner gel into the outer wrapping gel. Figure 6-8 shows the appearance of cells as they grew out of a cell seeded collagen gel. Panel A shows the absence of cells on the wrapping gel closely opposed to the denser cell-seeded gel (left hand side) at time zero. Panel B and C show increasing accumulation of cells due to migration out of the pre-contracted element (left hand structure) at 4 and 8 days.

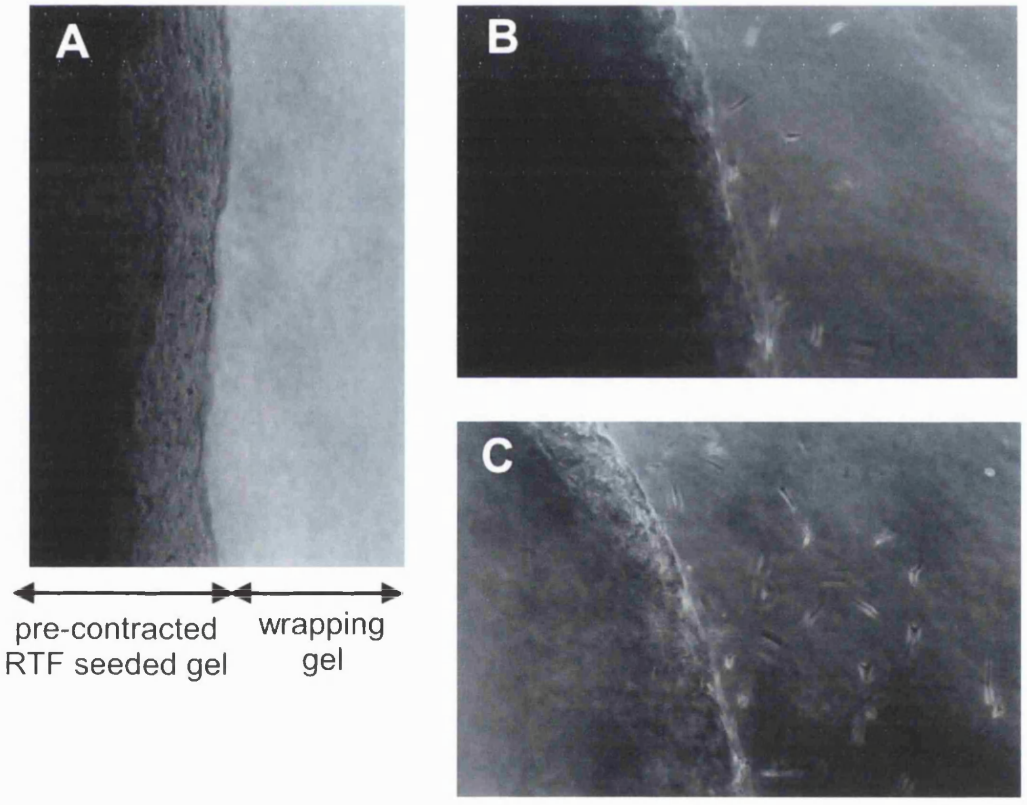

Figure 6-8 Photomicrographs of interfaces between pre-contracted collagen gel and cell free collagen gel at (a) zero time, (b) 4 days, (c) 8 days. Phase contrast microscopy, 10X objective.

6.2.2 Finite element analysis of the wrapping model

It was possible to construct a finite element model of the interface system (Figure 6-9).

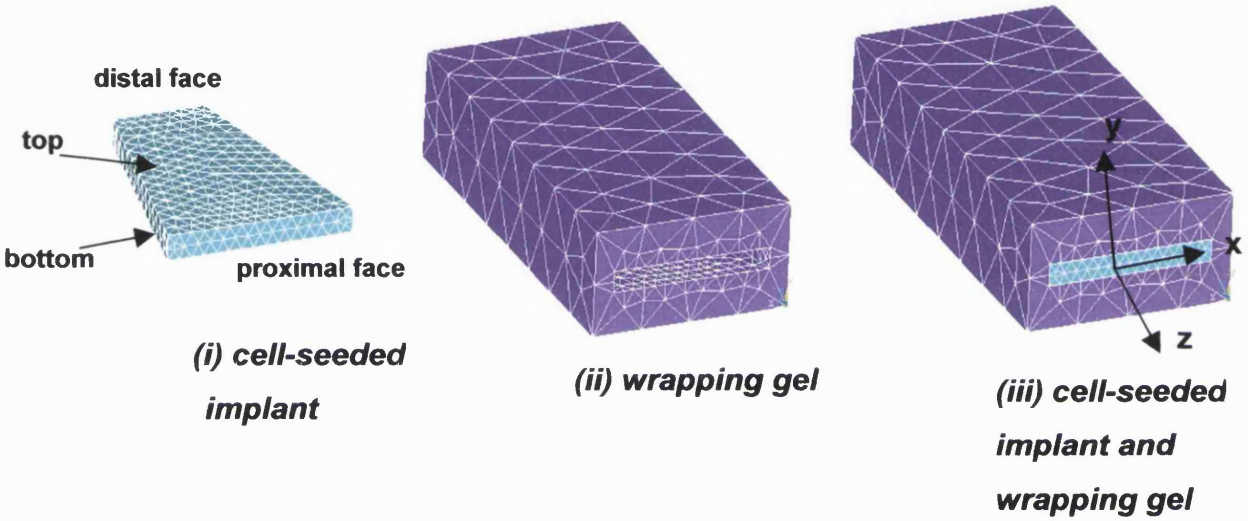

Figure 6-9 Finite element mesh of the interface construct: (i) Cell-seeded pre-contracted gel; (b) Wrapping cell-free gel; (c) Cell-seeded implant and wrapping gel. For clarity, the central gel is regarded as having a proximal face adherent to the attachment bar and a distal face within the wrapping gel.

Normal and shear stresses along the interface surfaces of the cell-seeded implant and the wrapping collagen gel were calculated using the finite element model. This predicted large shear stresses (τ_{YZ}) in the direction parallel to the applied load at the distal end of the top and bottom faces of the interface, (Figure 6-11). Highest shear stresses (τ_{XZ}) are predicted on the left and right hand edges of the interface, parallel to the applied loading (Figure 6-10).

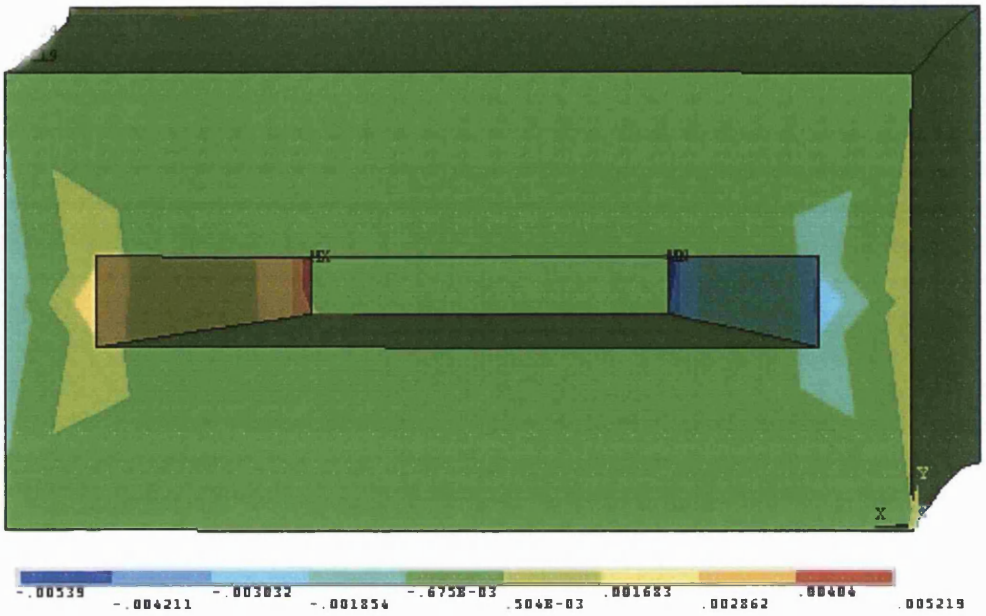

Figure 6-10 Shear stresses (τ_{XZ}) in the YZ plane (see Figure 6-9(iii) for coordinate directions) parallel to the direction of loading. All stresses are in MPa. The proximal face of the insert gel is facing outwards.

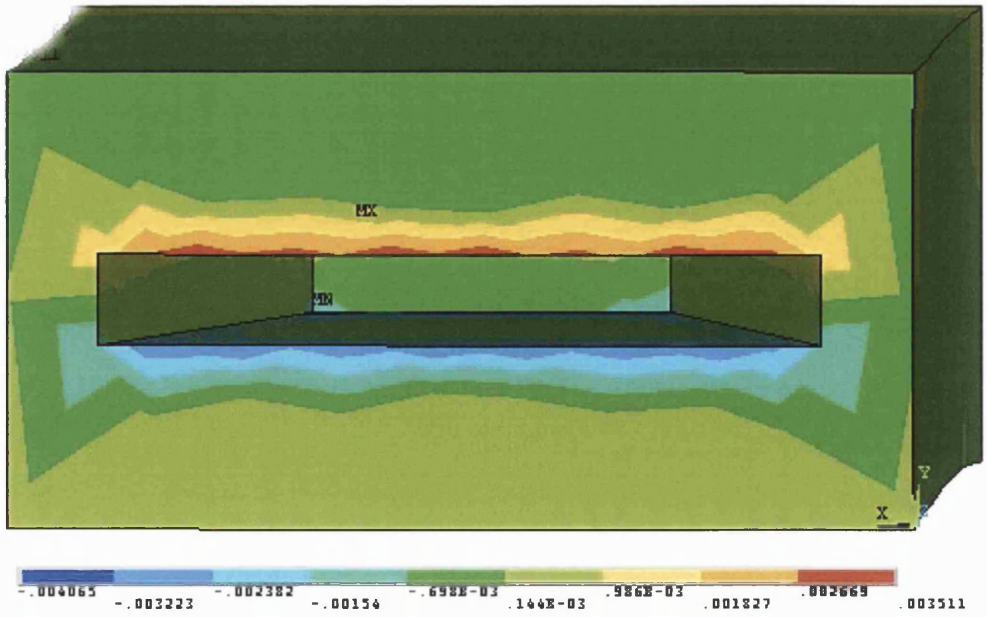

Figure 6-11 Shear stresses (τ_{YZ}) in the XZ plane (see Figure 6-9(iii) for coordinate directions) parallel to the direction of loading. All stresses are in MPa.

Due to the trapezoid shape of the cellular implant, the interface is at an angle to the applied load, and hence it is necessary to calculate the shear stress in the direction of the interface.

Figure 6-12 shows the predicted normal and shear stresses acting along the interface from the proximal face of the construct, illustrating the relatively constant sheer stress applied along most of the interface with elevation at the distal end of the trapezoid gel. This calculated trend is particularly emphasised for normal stresses (acting in the direction of loading, i.e. in the z dimension) where a sharp rise in stress is obtained at the distal end (20mm into the wrapping gel) of the implanted pre-contracted collagen gel.

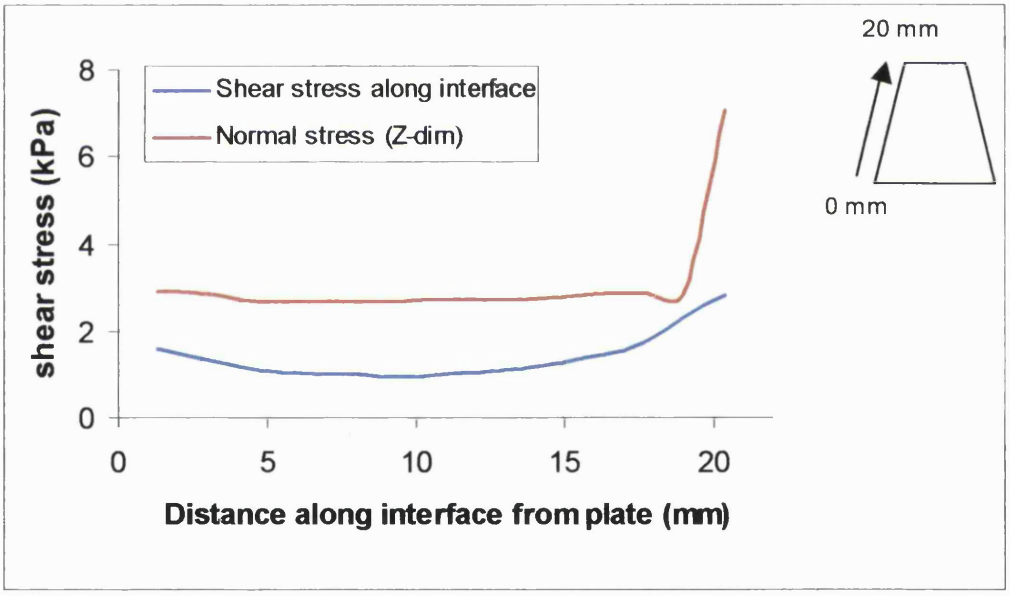

Figure 6-12 Graph showing the shear stress distribution along the length of the interface (in the z plane) from its proximal attachment bar to its distal end.

The finite element model predicted that failure of the interface would be initiated in the region of highest shear stress between the two components. Debonding at any one region of the interface would lead to an increase in the stress thrown onto the remaining intact interface resulting

in rapid failure. This is in agreement with the experimental data in which the force raised to a maximum value that coincided with a sudden failure, showing that after the bonding failed in one region, the remaining interface failed in a rapid cascade.

6.2.3 Problems encountered with the gel-to-gel assembly and preliminary tests of heterogeneous constructs

The weak point of the gel-to-gel interface construct was the adhesive strength between the pre-contracted gel and its attachment bar. This had to be more robust than the newly formed interface, especially at time zero (starting baseline). Therefore, each time the adhesive strength of the interface was greater than the one between pre-contracted gel and its connector, it was impossible to do the measurement and the entire experiment was discarded. As shown in the finite element section, the interface strength, before any cellular action, depends on the total surface area of the cell-seeded component. Additionally this was also affected by the degree of hydration of the sample to be interfaced, in that even differences in the use of clothing to remove surface water or short periods of air drying would enhance basal adhesion. Taken together these details frequently caused unexpected failure of experiments right from time zero.

Use of a modified cast to produce smaller cell-seeded constructs (details in the methods did not solve this problem indicating that the surface area reduction (20%) was not enough. Changing the shape (hence the casting and anchorage) of the pre-contracted gel could help as it could increase the contact surface to the connector. This parameter – for a fixed reaction force – affects the total stress generated at the connector-gel interface. But no attempts have been made in this direction.

Another important problem of the gel-to-gel interface construct was to

control the variation (up to 50%) in size of the pre-contracted gel. Image analysis was used to estimate the size of each gel sample. Insertion of a rigid frame in the pre-contracted cast did not solve the problem but as integration between the frame and the gel was poor and interfered with the interface measurement.

This led us to move to other substrates for the cell-seeded component. Studies to determine the baseline interface strength using rigid polylactic acid (PLA) constructs showed that the problem of connector debonding was completely solved as well as the problem of the varying size of the pre-contracted gel. PLA constructs were pre-soaked in standard culture medium for 24 hours (Figure 6-13), after which the wrapping gel model was cast. Basal adhesion strength for the PLA sheets was much greater (9546.3 ± 459 dynes) than the basal adhesion strength between gels, probably due to the high porosity (90%) of the PLA constructs. This suggests that the current dimension of the PLA sheets (2 X 1 X 0.3 cm) has to be reduced in order to reduce the basal adhesion strength before carrying on with the cellular experimentation.

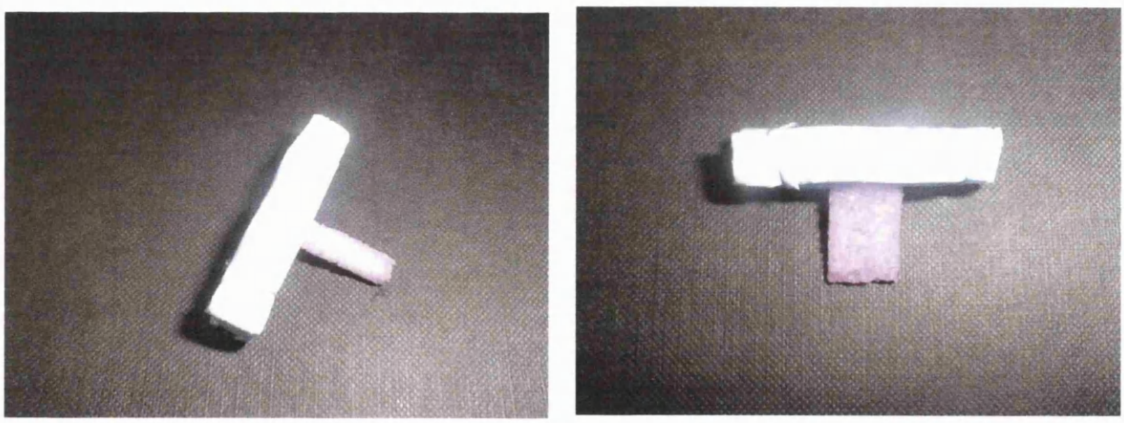

Figure 6-13 Porous PLA constructs (in shape of rod and flat sheet) soaked in standard culture medium for 24h (pink colour) and used to test the baseline adhesive strength to the wrapping gel.

6.2.3.1 Summary of the results obtained in the tissue interface study

The main results achieved throughout the study of interfaces are summarised in the following points:

- Mechanically connected bi-functional interfaces have been generated in vitro using either homologous or heterologous components.

- Interfaces were generated by a simple assembly procedure, based on the change of state of neutralised collagen gels from liquid to solid.

- Formed interfaces could be cultured for prolonged periods of time.

- Interface strength depends on the cell remodelling activity and progresses with culture time. After 1 week of culture interface strength was significantly increase compared to the basal strength at time zero or the strength measured at day 1 in experiments were cells were lysed by hypotonic treatment.

- Cellular-interface remodelling / strengthening has been correlated to cellular migration, whose onset was observed at day 4 in culture with progressive increase till the last time point observed, i.e. day 8.

- The setup developed for interface generation and culture, namely the "wrapping model" allowed to measure the mechanical properties of the interface constructs. Additionally it allows applying precise mechanical loading to the interface (effect not tested in the current study).

6.3 Discussion

The new models developed here were able to effectively generate solid 3D interface constructs in a controlled manner. The assembly procedure was based entirely on the property of collagen gel to rapidly change phase from liquid to solid. Therefore there was no need for additional compression to hold together the interface component during culture (Reindel et al., 1995) or special precision tissue biopsy to match the two parts of the interface (Gosiewska et al., 2001a; Obradovic et al., 2001a) in order achieve cell-mediated integration.

Some baseline adhesive strength was inevitable in both models. Unexpectedly, however it caused variability in the fracture model which did not allow further mechanical characterisation of the cell-mediated integration. In the wrapping model, however, the baseline adhesive strength could be modified by changing the total contact surface area and the superficial properties (like hydration and porosity) of the cell-seeded component.

Such templates, for in vitro engineering of tissue interfaces, are completely new in literature. As a result the stresses generated in the measurement of the ultimate adhesive strength were completely unknown. Consequently, finite element modelling was very important for interpretation of the mechanical characterisation studies on the wrapping interface model. This demonstrated that, although shear stresses played the principal role in the interface failure, there was also a non-negligible normal stress component especially at the distal end of the cell-seeded element (where it was predicted that failure would commence).

It has been shown that the tendon fibroblasts were able to emigrate from the pre-contracted compartment into the cell-free lattice and this supports the idea that cell-mediated integration is dependent on migration across adjacent surfaces. A number of groups have shown that fibroblasts

are able to migrate and cross three dimensional collagenous interfaces in vitro(Burgess et al., 2000; Gosiewska et al., 2001a; Greiling & Clark, 1997a; Sawhney & Howard, 2002), but the matrix and mechanical consequences of this are uncertain (Cacou et al., 1996a).

DiMicco and Sah (2001) were able to positively correlate the adhesive strength to the collagen deposition for cartilage explants, cultured for 14 days (DiMicco & Sah, 2001a). Interestingly for the model presented here, they showed that even when one of the two cartilage blocks was killed, the remaining cells were still able to build a strong integration. This suggests that cells deposit additional collagen, as bridging or connecting fibres across the interface, in our system during migration from the pre-contracted compartment to the cell-free gel. In vivo, collagen bridges have been observed ultrastructurally during their development in bone-tendon junction as early as two weeks postoperatively (Oguma et al., 2001).

A significant question could not be clarified: does the original position of the interface move or remain static? Some degree of movement would support what has been recently observed (Sawhney & Howard, 2002) in an experiment to visualise cell traction in 3D collagen gels. In this work Swahney and colleagues reported that net cell locomotion (and therefore migration) from explants would start only after a long matrix accumulation process due to the traction exerted by the cells on their nearby fibres as they start locomotion. We tried to visualize possible movements in the interface front by seeding the gel with small blue-dyed agarose beads. However the thickness of our construct (nearly 10 times that in Swahney's model) led to focal problems which prevented accurate localisation. It is possible that confocal microscopy of the culture under observation over some days (Knapp et al., 1999) may have solved this but this facility was not available.

Cell proliferation could not be excluded in the interface construct. However in an interface construct made by an intact tendon and collagen gel (Cacou et al., 1996a), it was shown that integration was not affected by inhibition of proliferation. Rather the commitment of a few cells to migrating across the interface was more important, presumably remodelling

and depositing new matrix. We can assume that something very similar happens in the present wrapping interface construct.

Mechanical loading in vitro and bioreactor cultivation have been shown to increase cell matrix production (Parsons et al., 1999) and cell metabolic activity in engineered tissue interface constructs(Obradovic et al., 2001a). The interface construct presented here can be potentially mechanically stimulated during cultivation using the IAMD as loading bioreactor.

In addition to gel-gel constructs, the casting system described here permits many combinations of tissue substrates, making it possible to build numerous complex interfaces, to model in vivo structures. For example it could be used to generate a bone-tendon interface where the cell-free compartment is seeded with tendon fibroblasts, joined to a tissue-engineered bone element seeded with osteoblasts. Similarly an osteochondral construct could be generated simply by substituting the tendon fibroblasts with articular chondrocytes in the example above.

In conclusion the experimental model designed and characterised here permits solid interface formation in a controlled manner with a well-defined geometry. It has the possibility to measure mechanical linkage and/or apply various regimes of mechanical loading. This has utility both as an in vitro functional model for the study of normal/pathological processes, and as a precursor to engineered tissue interfaces. The long-term findings of this research will be beneficial to the development of a new generation of tissue bioreactors.

Chapter 7

Monitoring cell-mediated collagen lattice remodelling by Elastic Scattering Spectroscopy.

This chapter describes an investigation into a novel use of elastic scattering spectroscopy (ESS) as a tool for minimally invasive monitoring of tissue engineered constructs as they develop.

It is well known that the elastically scattered light from tissue contains information about the biochemical composition and/or structure of the tissue (Nerem, 2000; Seliktar et al., 2000). Spectral signatures obtained from (living) tissue, by elastic scattering and diffusive reflectance spectroscopy, have been employed to analyse skin architecture (de Vries et al., 2000; Sady et al., 1995; Seliktar et al., 2000) and to discriminate malignant from normal tissue (Glassman et al., 1995; Seliktar et al., 2000) (Mourant et al., 1998; Wallace et al., 2000).

In the present study the potential for ESS in monitoring contraction/remodelling of cell populated collagen gels was tested. The approach was also used to assess the structural changes in different areas of the interface constructs described in chapter 5.

7.1 Methods

All materials and methods used were as described in chapter 2 and 3.

7.2 Results

The results presented in this chapter can be divided in 3 sections.

The first section tested the hypothesis that changes in particular ESS spectral signatures would correlate with known structural changes in fibroblast populated 3D collagen lattices (FPCLs). In the first instance, ESS was used to monitor cell-mediated gel contraction over well-known time sequences. This is known to involve reshaping of the collagen network from initial randomly oriented thin collagen fibrils to wider diameter compacted fibrils with varying degrees of orientation as seen in chapter 4 and in previous reports (Eastwood et al., 1996; Porter et al., 1998). Depending on the mechanical configuration of the lattices, 2 macroscopic parameters were used to monitor the known stages of matrix remodelling. These were the reduction in surface area of lattices (for the free floating model) and the contraction force generation (for the uniaxially tethered model in the CFM). ESS signatures were correlated to these macroscopic parameters as appropriate.

In the second section the potential for ESS to discriminate between different zones of the interface model was tested, this time by comparing ESS signatures from spatially distinct areas at the same time point. The interface model consisted of a FPCL, pre-contracted in culture for 2 days, and a wrapping cell-free lattice as described in chapter 6. The interface model was characterised by 3 distinct areas, including a cell-free gel zone, a pre-contracted gel zone and the interface zone which was an overlap between these two. After assembly, the interface constructs were cultured for 7 days, during which the interface zone has been shown to change due to cell migration and remodelling (chapter 6 and Marenzana & Brown, 2002). At the end of the culture time (7 days) the 3 mentioned areas were assessed by ESS.

Successful discrimination of these 3 areas by ESS at a fixed time point is thought to be the starting point for a possible eventual spectral

monitoring of the maturation of the interface zone in culture.

The third section tested how single physical variables in FPCLs would affect the ESS spectral signatures. In particular contribution of cell density and lattice thickness on ESS spectra were investigated. To test the effect of cell density in FPCLs on ESS spectra, floating lattices seeded with increasing cell concentrations were spectrally measured immediately after gelation to avoid contraction. The probing depth of the ESS signal was reported to be around 1 mm (Bigio et al., 1993; Mourant et al., 1996a). However this estimate was for a model of tissue in vivo were many more scatterers and absorbers are present compared to the FPCL model. To test if the thickness of the lattice had an effect on the spectral signature, cell-free lattices of increasing thickness were floated and spectrally tested immediately after gelation. This analysis of single variables in FPCLs might lead to identify specific spectral features contributing to the understanding of more complex ESS spectra. The acquired composite spectra are normally a combination of these specific variables with other ultrastructural changes of the collagen network due to cell-mediated spatial remodelling.

In all experiments spectral signatures of backscattered light was acquired in the range from 320 to 900 nm. The spectral intensity was normalised by the number of pulses from the xenon lamp and ratioed to the raw spectrum from the Spectralon (reference spectrum).

7.2.2 Optical measurement of contracting fibroblast-populated collagen lattices

Early stage known structural changes in FPCLs (starting thickness 3 mm) were analysed using elastic scattering spectroscopy in order to identify potentially characteristic spectral signatures. FPCLs were prepared and floated after gelation to allow free contraction. Spectra were acquired at two

time points (1 hour and 24 hours), at which large structural and compositional differences are known to occur (Grinnell & Lamke, 1984; Porter et al., 1998). These changes were monitored at the macroscopic level by measuring the amount of contraction as reduction of the surface area. The first set of spectra was acquired after 1 hour of culture (Figure 7-1, upper couplet). At this time point cell-mediated contraction of FPCLs had just started and the area reduction was minimal (lattice area was still 90% of its original area).

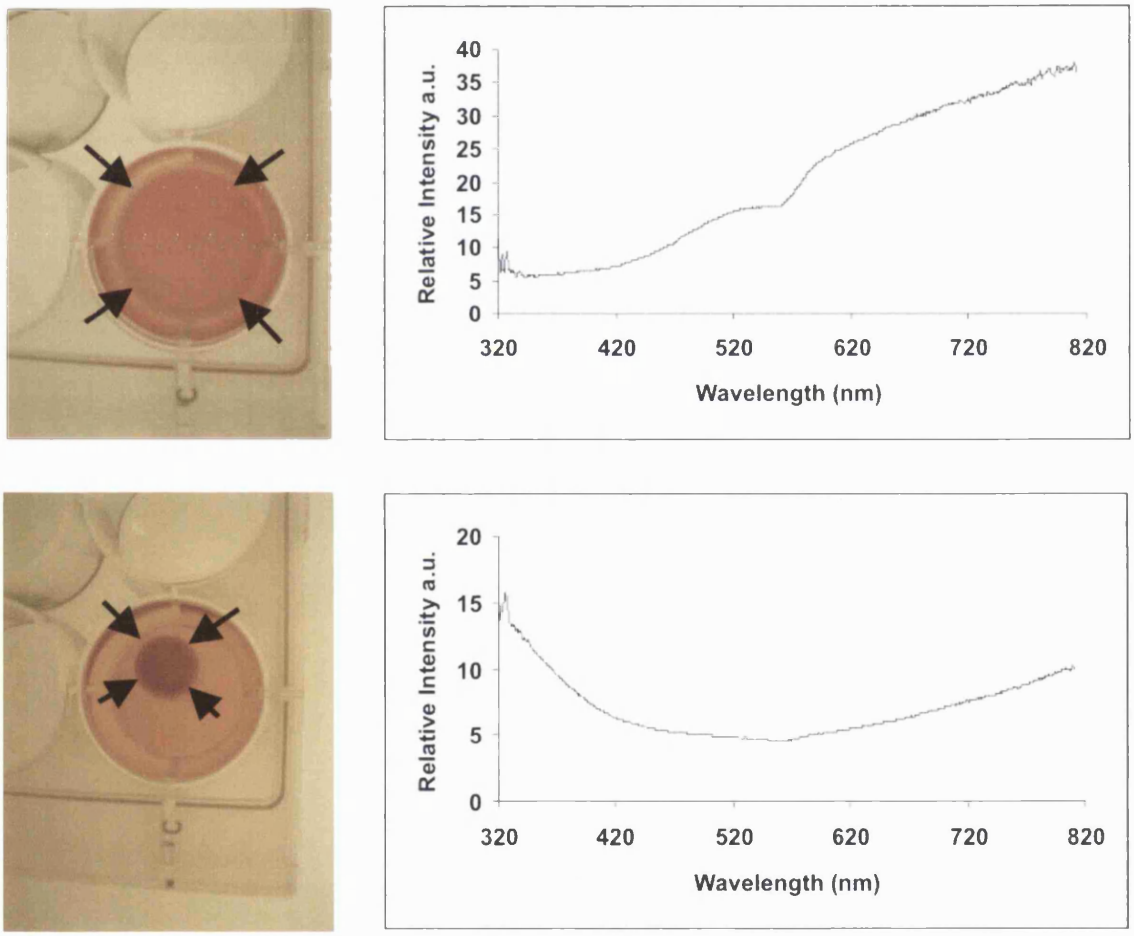

Figure 7-1 Picture of untethered gels in their well plates, coupled with their corresponding spectral signatures at 1hour after setting, gel area contracted to 90% of its initial size (upper couplet); and at 24 hours, gel area contracted to 20% of its initial size (lower couplet).

The spectral signature at 1 hour appeared a near linear line (R^2=0.97), with relative intensity rising with the wavelengths (gradient: $75.96*10^{-3}$). An evident local minimum at 560 nm corresponded to a peak absorption due to a known chromophore present in standard culture media, i.e. phenol red.

The second set of spectra was acquired after 24 hours of culture (Figure 7-1, lower couplet). At this time point FPCLs had contracted to 20% of their initial dimension. The spectral signatures at 24 hours time point appeared radically different from the spectra acquired at 1 hour. The near linear rising profile changed into a concave curve. The central part of this curve (420 to 620nm) was characterised by a plateau (gradient: $4.10*10^{-3}$). The initial tract of the spectra (320 to 420nm) had a steep decreasing gradient ($87.03*10^{-3}$), opposed to the increasing gradient observed in the spectra of the 1 hour time point. The local minimum at 560 nm was almost disappeared from the spectra, leaving a small deflection along the plateau segment.

Taken together these observations, indicate that ESS spectra changed significantly in response to the known structural changes which occurred in the collagen lattices due to cell-mediated collagen gel contraction and remodelling. However, two substantially different structures were tested at the two selected time points. One (at 1 hour time point) composed of very thin collagen fibrils and sparse cells beginning to spread. The other (at 24 hours time point) was made of thick bundles of compacted fibrils and fully spread cells and a much higher (around 5 folds) solid/liquid volume fraction.

Consequently, further experiments were designed in order to test if changes in ESS would correlate to finer degrees of structural changes in collagen lattices as they evolve over time. FPCLs were setup in 3 different mechanical configurations (Figure 7-2) in which cells are known to produce different changes in gel dimension, density and collagen remodelling (details of the setups can be found in methods).

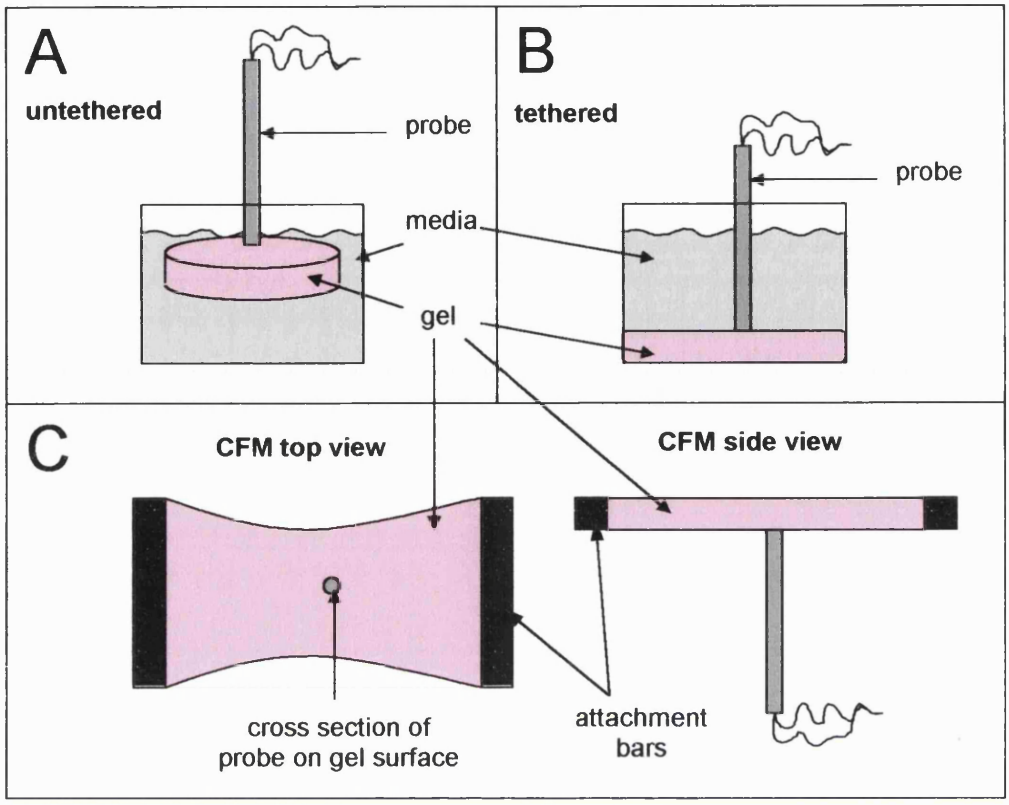

Figure 7-2 Collagen Gel Models. Schematic representation of the three different models employed. The untethered gel model, in which the gel is free floating and freely contracted (A); the tethered model, in which the gel is kept attached under tension (B). Upon release the gel goes into the untethered configuration (A). And the CFM model (C), in which gel is uniaxially tethered and the isometric tension, generated during contraction, is measured by a strain gauge transducer.

1) The first configuration (Figure 7-2-A) was a circular free-floating untethered contraction (as in Figure 7-1) with spectra collection at different time points.
2) The second was a circular tethered FPCL (Figure 7-2-B), released at 24 hours to allow untethered contraction based on tension by that time in the gel.
3) The third was a rectangular FPCL uniaxially tethered in the CFM, with collection of spectra at different time points (Figure 7-2-C). The development of a principally uniaxial tension in the CFM generated

alignment of cells and collagen fibrils, which was distinct from the other two circular configurations where orientation was far more complex and less ordered.

ESS signatures were correlated with size changes or force output measures, as appropriate.

7.2.2.1 Model A: ESS of untethered gel contraction

The spectral intensity was recorded, at different time points, from the same gel as it underwent unrestrained contraction by the resident fibroblasts for a total of 60 hours (Figure 7-3). The collagen gel geometric contraction by dermal fibroblast was essentially typical (Grinnell & Lamke, 1984; Tomasek et al., 1992), with a high rate of reduction of diameter and compaction in the first 8 to 10 hours (to ~20% of the initial area) which subsequently slowed such that there was little further change over the rest of the experimental time (24 hours onwards).

From temporal analysis of the acquired spectra, the changes of the normalised intensity at 500nm were found to strongly correlate to changes in the gel area with time (Figure 7-3). The normalisation of this identified spectral wavelength involved a ratio of the intensity and slope of the spectrum in the infrared (IR) region (615-810 nm) in order to take other temporal spectral features. This parameter was phenomenologically derived as well correlated with the changes in lattice area over time. The information from other wavelengths of the spectrum (besides 500 nm) was less straightforward to interpret (Marenzana et al., 2002).

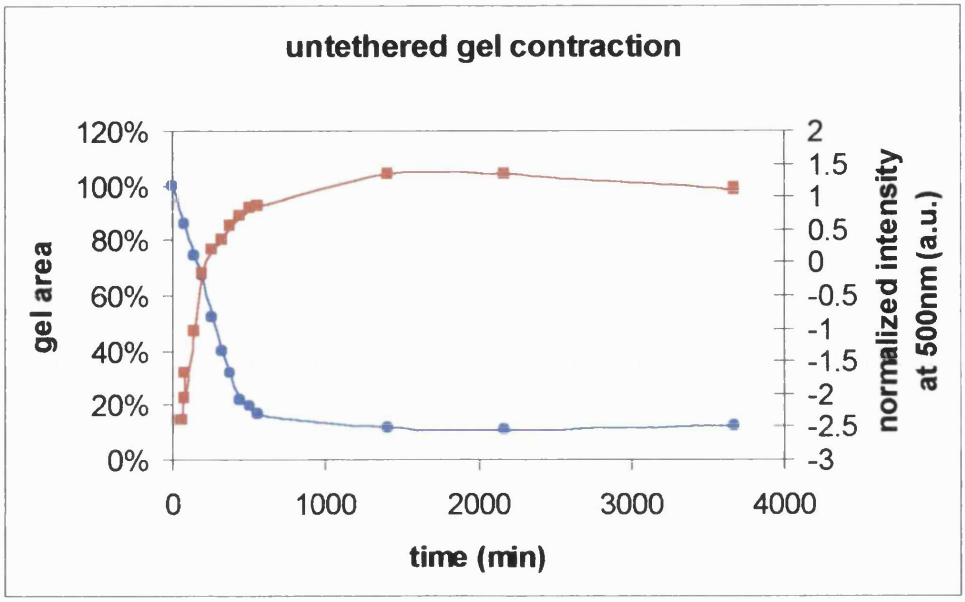

Figure 7-3 Untethered gel contraction followed by ESS spectra. The blue line represents gel area changes (displayed on the left hand axis), expressed as a percentage of the starting size, with time during untethered gel contraction. The red line represents spectral changes in the normalised intensity (displayed on the right hand axis) measured at 500nm, expressed in arbitrary relative units, recorded from the same gel at the different time points. The normalisation involved a ratio to the intensity and slope of the spectrum in the infrared (IR) region (615-810 nm) in order to take other temporal spectral features into account. The spectrum changes showed a strong correlation with changing gel dimension.

7.2.2.2 Model B: ESS of restrained-released gel contraction

The spectral intensity was recorded, at different time points, from the same gel during the contraction generated by the resident fibroblasts, which was biphasic: initially restrained and then released (Figure 7-4).

The gel was monitored for a total of 26 hours, including both the restrained contraction for 24 hours and subsequent free contraction. Collagen lattice contraction by these human dermal fibroblasts was typical

for the restrained-released model (Grinnell & Lamke, 1984; Porter et al., 1998; Tomasek et al., 1992). There was an initial contraction until internal gel contraction force reached equilibrium against the plastic culture dish (0 to 6.5 hours), after which there was no further contraction.

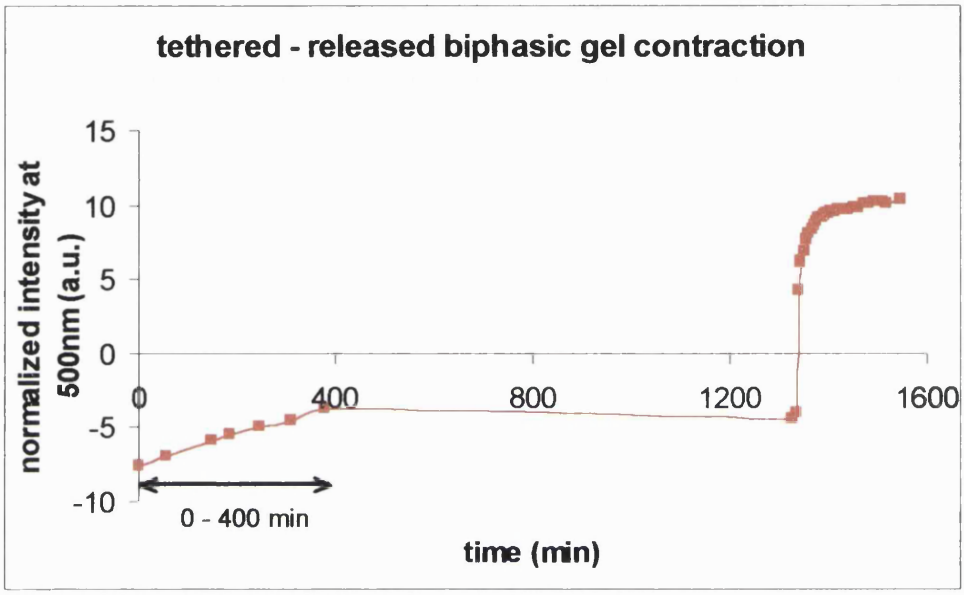

Figure 7-4 ESS spectra of the tethered - released gel contraction. The gel was kept under tension for 24 hours and then released to obtain a rapid contraction. The plotted line represents spectral changes in the normalised intensity at 500nm, expressed in arbitrary relative units, recorded from the same position on the gel at different time points. The spectral changes showed a strong correlation with gel feature changes. The relative intensity rises initially mirroring the increase in stress in the gel (0-400 min) until the internal gel contraction force reached equilibrium with the tension of the substrate to which it was attached (bar). Next the intensity of the spectrum plateaued while no further contraction was possible until lastly upon release of the gel from the substrate, the intensity rose again rapidly, following the rapid contraction of the gel.

Upon release of the gel from the substrate a very rapid fall of surface area was seen in the first 15 minutes, with a subsequent plateau for the rest of the experimental time (from ~1400 min onwards). The same

extrapolation on the full spectra as above (i.e. normalised intensity at 500 nm) showed a strong correlation with changes in collagen gel diameter during both the tension and release phases. Interestingly, fibroblast-mediated collagen remodelling produced almost the same end point for both the untethered and the tethered/release models, i.e. approx 20% of its original volume, although by different pathways.

7.2.2.3 Model C: ESS of CFM model (uniaxially tethered gel contraction)

The spectral intensity was recorded, at different time points, from the same gel whilst mounted on the CFM as fibroblast force generation proceeded (Figure 7-5).

The gel was monitored for around 200 minutes. Fibroblast-mediated isometric gel contraction resulted in a typical force-time plot of force generation (Delvoye et al., 1991; Eastwood et al., 1994; Kolodney & Wysolmerski, 1992) with a constant steep rising of force generation over this initial period, to 200 min. This showed that neither force measurement nor force generation by the cells were disturbed from the optical probe. Again, the same full spectra extrapolation showed a strong correlation between spectral intensity changes and force generation. In this model dimension changes were minimal (Eastwood et al., 1998).

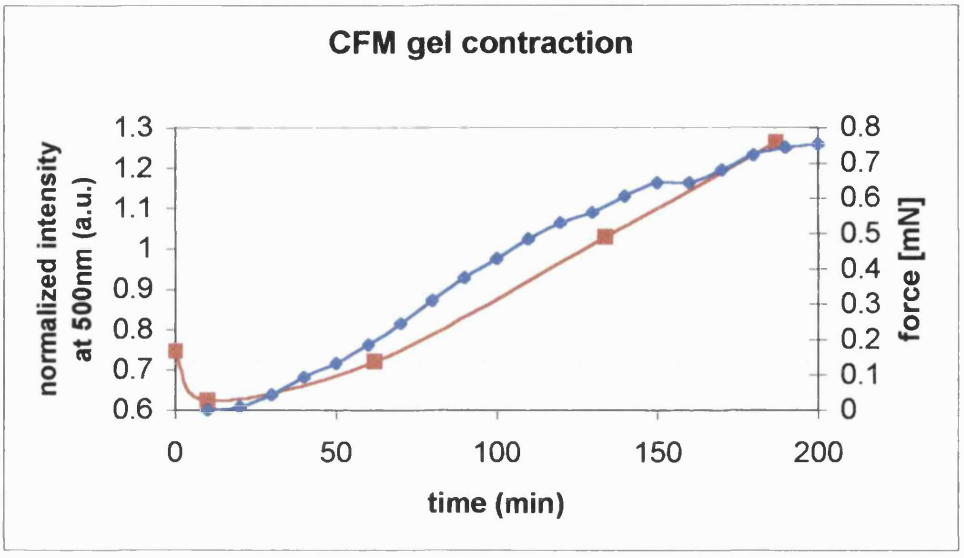

Figure 7-5 CFM force generation plot, overlaid with the ESS normalised 500 nm intensity plot with time. The blue line represents the force developed during the isometric contraction (displayed on the right hand axis). The red line represents spectral changes in the normalised intensity (displayed on the left hand axis) measured at 500nm, expressed in arbitrary relative units, recorded from the same gel at the different time points. The spectral changes showed a strong correlation with increasing tension across the gel related to changes in collagen structure in the gel during the near isometric contraction. This time course (0-200 min) represents a detailed analysis of the initial traction force generation period seen in Figure 7-4 (0-400 min).

7.2.3 Optical measurement of 3D collagen-gel-based tissue interfaces

In this set of experiments, spectra were taken from different areas across the collagen-collagen interface construct (chapter 6) to test the idea that ESS signatures will discriminate between the elements composing the construct. The interface model termed "wrapping model" consisted of a FPCL, cultured for 2 days, and a wrapping cell-free lattice (chapter 6). These constructs were characterised by well distinct areas, including cell-free zone, the cell-populated contracted zone and the interface zone between these two. After assembly, the interface constructs were cultured for 7 days, prior to the ESS test. Both the assembly modes of the wrapping model - model I, i.e. the uniaxial assembly for mechanical testing and model II, i.e. the circular assembly for microscopy imaging - were probed by ESS. The choice to test both the assembly modes of the same wrapping model was made because of unexpected differences found between them in terms of cellular remodelling. In fact, model II produced a remarkable gel lysis in the central area of the construct (chapter 6). So this new effect was subject to analysis by ESS.

As a preliminary test, the complete uniformity and isotropy of different zones of a cell-free lattice were probed by ESS. The hypothesis was that there would not be significant changes in the spectral signatures acquired from different points on a cell-free lattice.

7.2.3.1 Optical measurement of the spatial uniformity of cell-free collagen lattices

This experiment tested if the complete isotropy of a cell-free collagen gel was reflected in the ESS spectra. 2ml cell-free collagen lattices were cast in a 12 multiwell plate, and ESS spectra were acquired immediately after solidified lattices were floated in culture media. The spectral intensity was recorded at six different points on the surface of the same gel (from the centre towards the edge of the well, spaced ~ 1 mm). The acquired spectra from 1 to 4 (Figure 7-6) were superimposable, in stark contrast to the two taken at the points of the gel edge next to the dish wall (spectra 5 and 6).

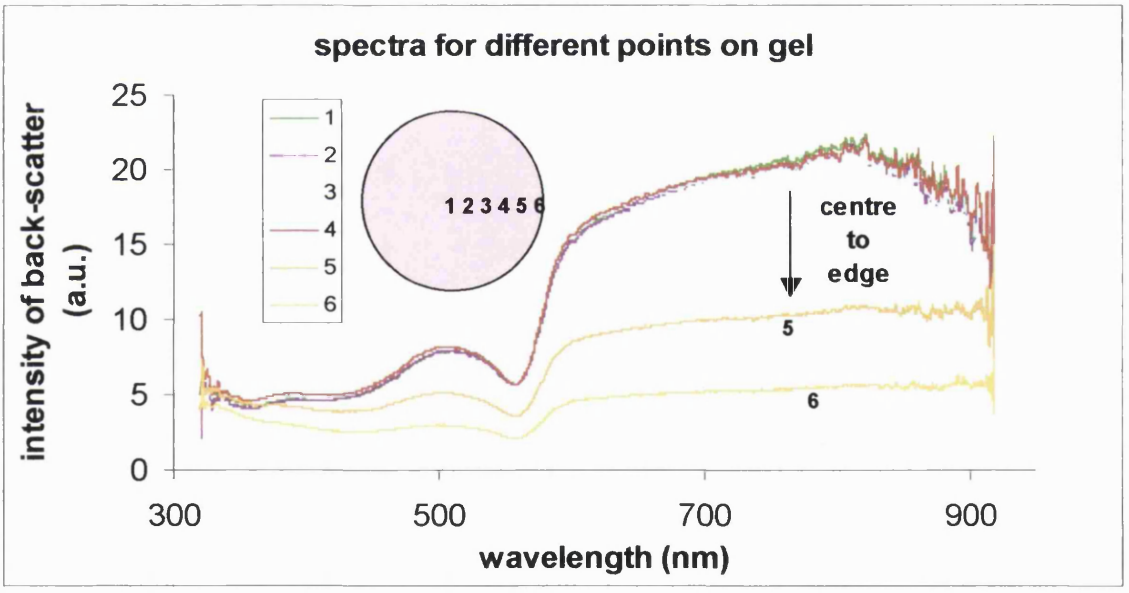

Figure 7-6 ESS spectra taken from different points on the surface of a cell-free lattice floating in culture media. Points were numbered from the centre towards the edge progressively (spaced ~1 mm).

Figure 7-7 displays a histogram of the normalised intensity at 500 nm for the different points (normalisation as described above). The four points

closer to the centre (away from edges) were not significantly different. In contrast the 2 points at the edge (5/6) were significantly different from the former four and between each other.

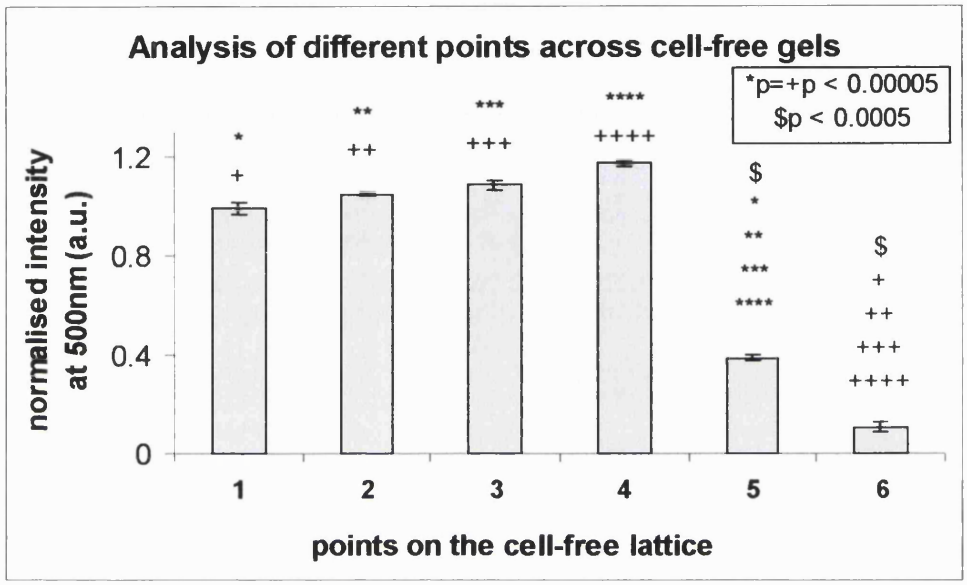

Figure 7-7 Mean normalised spectral intensity at 500 nm collected from different areas of the gel. Vertical bars represent SE. Statistical significance is represented by symbols above columns associating them in pairs. The two edge points (5 and 6) were significantly different between them ($p<0.0005) and from all the other 4 points (for all paired columns with 5 or 6 p<0.0005). Columns not paired by symbols were not significantly different between them. The four points away from the edge (1-4) were not significantly different among each other.

This experiment suggests that the bulk of the collagen lattice is relatively uniform. The changes occurred to ESS spectra were due to discontinuity of the optical media in proximity of the interface between gel margin and dish wall.

An important implication of these ESS measurements is that the small volumes of the lattice, which were sampled by the optical system, could be used as representative of the entire gel.

7.2.3.2 ESS of model I interface construct (assembly for mechanical testing)

Interface constructs (chapter 6) were assessed by ESS after 7 days in culture, before undergoing the adhesive strength measurement (therefore at the maximum of their maturation in culture that has been tested in this study).

Figure 7-8 shows that the composite spectral signatures were modified depending on the different areas of the interface construct. All spectra presented a marked absorption peak at 560 nm attributed to the presence of phenol red in the culture media. The spectrum from the wrapping cell-free gel and pre-contracted gel are represented in the left right panel respectively. In the central panel are displayed two spectral signatures, which were acquired from the interface region, one on the centre of the area of overlap of the lattices (labelled "inside") and one on the edge of the same area (labelled "edge").

Gradients and local oscillations of the tracts of the spectra before and after the peak absorption were analysed. The final segment of spectra (615 to 810 nm) had similar shapes and similar levels of intensity but differed in the gradients. The steepest gradient was registered for the pre-contracted gel area ($-56*10^{-4}$), followed by the interface edge area ($-34*10^{-4}$) and similar values for the wrapping gel and inside interface areas ($-23*10^{-4}$ and $-20 * 10^{-4}$).

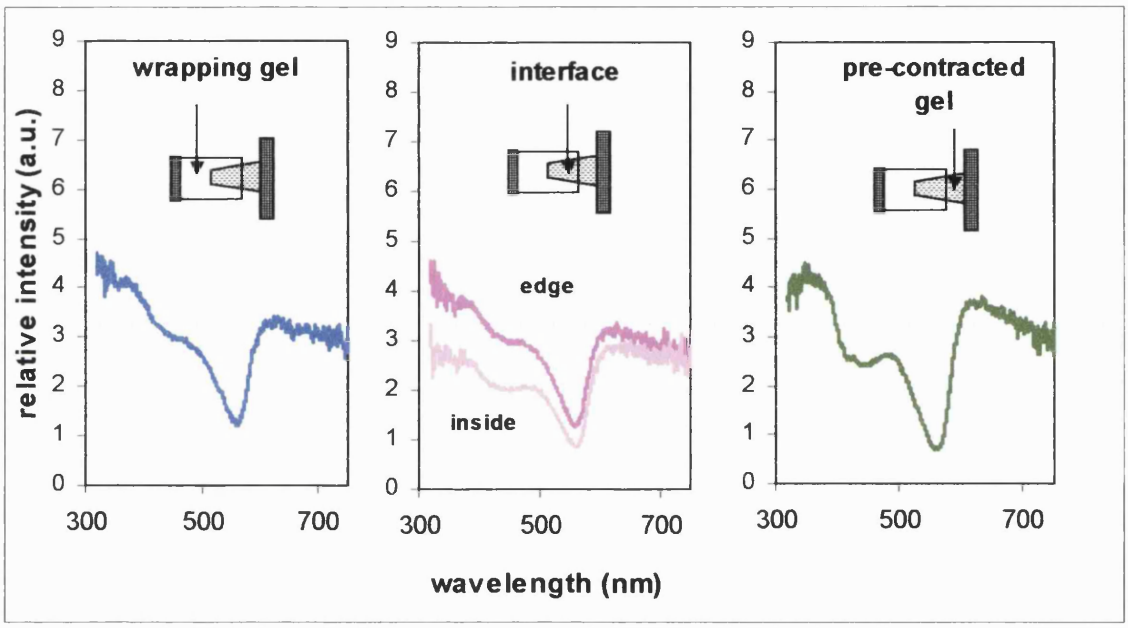

Figure 7-8 Spectral signatures of different areas of the wrapping model interface construct in the assembly for mechanical test. 3 regions of the construct were assessed: the wrapping gel alone (left panel), the interface area (central panel), which included the central zone ("inside") and the edge zone ("edge") and the pre-contracted gel alone (right panel).

The initial tracts of the spectra (320 to 500nm) were characterised by more marked features in terms of local maxima, oscillations and gradients. The steepest gradients were measured for spectra acquired from the pre-contracted gel area ($-125*10^{-4}$) followed by the gradients for two areas on the edge and inside the interface ($-83*10^{-4}$ and $-52*10^{-4}$) and on the wrapping gel area ($-11*10^{-4}$). Analysis of these slopes suggested that there might be an increasing trend in correlation with increasing density of collagen packing and presence of cells. That is gradients in the initial tract of spectra (320-500) increased from the wrapping gel area to the "inside" area of the interface and to the pre-contracted gel. The area on the "edge" of the interface was difficult to interpret due to possible optical edge effects altering the matrix structural information contained in the spectral

signatures. So for the interface area, edges were excluded from the analysis and only the central part (i.e. the overlap zone between cell-free gel and pre-contracted gel) was considered. Edge effects are normal and expected in optical measurements and are known to be able to deflect the light path and alter scattering (Bohren & Huffman, 1983).

The general correlation obtained between spectral slopes (in the tracts 320-500nm) and 3 distinct areas of the interface construct was promising for further analysis. In order to interpret the measured signals and identify key features of the spectral signatures that could be representative of specific changes in the examined tissues, 3 stages of analysis were applied:

a) normalisation of the signal to invariants,
b) identification of characteristic local peaks
c) identification of specific wavelengths that correlate to matrix structural changes

a) Normalisation of the signal to invariants

ESS spectra acquired for the different areas were normalised by the spectral signature of the culture medium alone that represented an invariant baseline for all the acquisition.

Figure 7-9 shows the same spectral signature displayed in Figure 7-8 ratioed by the spectral signature of the culture medium. The spectrum taken from the wrapping gel (left panel) was transformed into an almost flat line around the unity. This indicated that the culture media and a cell-free gel which floated in it generated the same spectral signature and therefore had similar optical properties. In absolute terms, this result might be used as an indication of the sensitivity of the ESS technique, since cell free-gel comprises only of random meshwork of fine collagen fibrils in approximately 98% culture medium. However, in relative terms, this transformation (i.e. ratioing by the culture medium spectra) highlighted the differences in spectral signatures that did exist between the interface area (central panel)

and the pre-contracted gel alone (right panel). An increase in features, such as oscillations and intensity shifts can be noticed going from the left to the right panel. This was correlated to the increase in the density of the matrix, the presence of the cells and the layers through which the light travelled.

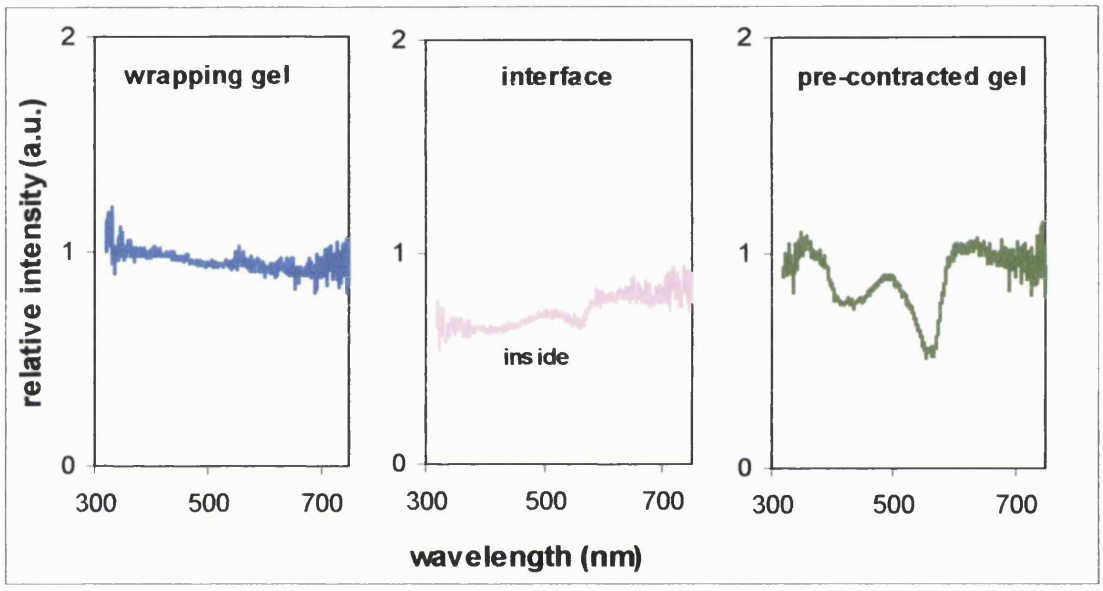

Figure 7-9 Spectral signatures, acquired as described in Figure 7-8, ratioed by the spectral signature of the culture medium. To avoid edge effects, which could affect the optical measurements, only spectra acquired from the central area of the interface zone (labelled "inside") were analysed.

The ratioed spectrum of the interface region (excluding edges) appeared a mean of the ratioed spectra of the two single elements. It appeared that spectral features of the pre-contracted gel were smoothed by the overlaid layer of wrapping gel, which the light had to cross before reaching the surface. Gradients were significantly different in the first segment of the spectra (320 to 500 nm) but not in the second segment (615 to 810nm). Computed slope values were positive ($2*10^{-4}$) for the interface zone and increasingly negative for the wrapping gel zone and the pre-contracted gel zone ($-5*10^{-4}$ and $-11*10^{-4}$ respectively). These results differed from the previous ones in which the slope (320 to 500 nm) of the

non-ratioed spectrum of the interface area was middle range between the pre-contracted gel and the wrapping gel.

Hence it appeared that the relative spectral differences between the slopes in the region 320 and 500 nm were not dependent only on matrix structural changes but were also affected by the spectral features of the culture medium.

b) Identification of characteristic local peaks

ESS spectra acquired for the different areas of the interface construct (Figure 7-8) were analysed in the region 320-420 nm where characteristic local peaks could be identified. Again, to avoid optical edge effects, which could affect the measurement of structural features, only spectra acquired from the central area of the interface zone were analysed. Figure 7-10 shows the interpolation of selected tracts of the spectral signatures with polynomial curves (second order) in the region of interest. Shifts in average peak wavelength and intensity could be found for the different areas probed in the interface construct.

These parameters were analysed in the scatter graph displayed in Figure 7-11. Pairs of values derived from the pre-contracted gel area clustered in a completely separated and unique domain (i.e. a range of variables defining one condition). This domain spanned in the area delimited by wavelengths below 370 nm and peak intensity values above 0.4 arbitrary units. However the other 2 groups (i.e. wrapping gel and interface area) did not form separate clusters and fell in essentially the same domain.

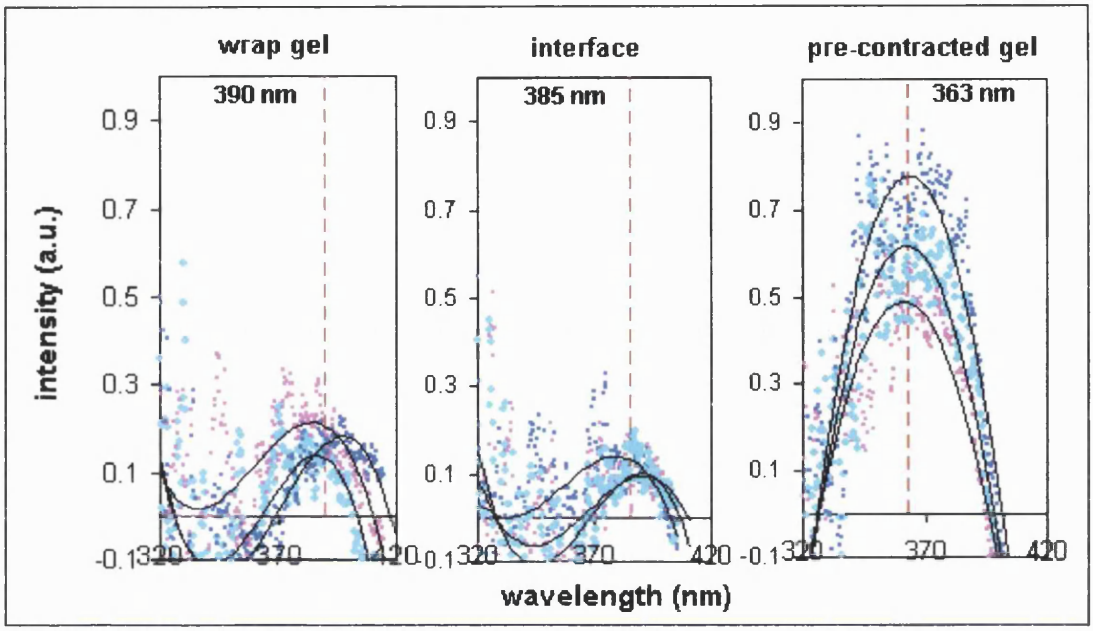

Figure 7-10 Characteristic peaks in the region 320-420 nm of the spectral signatures taken from different areas of the interface construct (representative signatures over the full spectrum 320-900 have been shown above in Figure 7-8). To avoid optical edge effects, which could affect the measurement of structural features, only spectra acquired from the central area of the interface zone (previously labelled "inside") were analysed. Three separate measurements (three colours) were plotted. Shifts in average peak wavelength and intensity could be found for the different areas probed in the interface construct.

It is worth noting that the region of characteristic peaks (320-420nm) identified here, has been reported previously as the spectral region for the collagen autofluorescence (Glassman et al., 1995; Sady et al., 1995). This is important for the interpretation of these data, since the highest relative intensity was obtained from the pre-contracted gel area which also contained the highest density of collagen fibres and therefore would be expected to have the greatest autofluorescence and scattering. Concerning the wrapping gel area and interface area, the maximal intensity was not significantly different, showing that local peaks in the region 320-420 nm

were not able to discriminate these two areas.

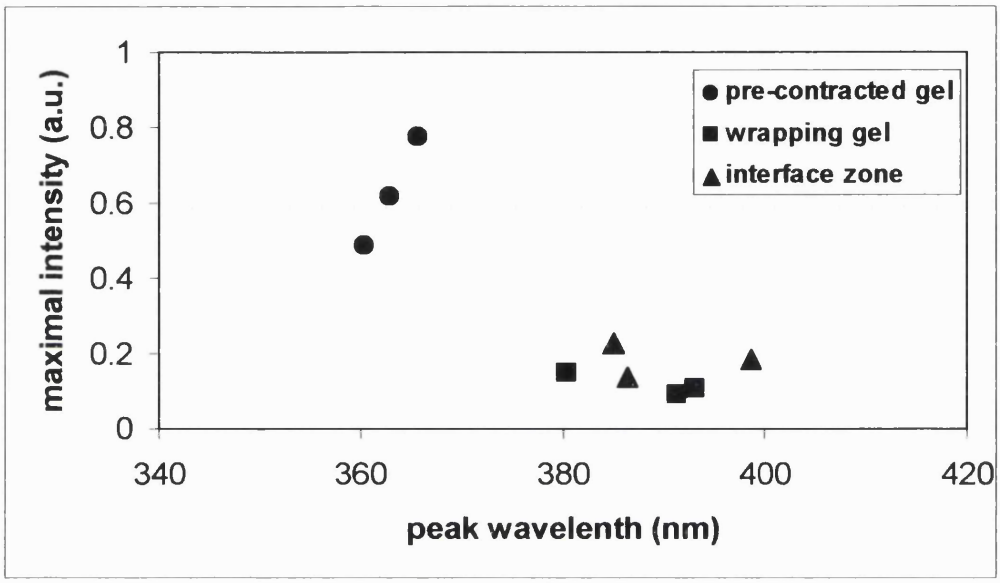

Figure 7-11 Scatter plot of the parameters deduced from the characteristic peaks in Figure 7-10, i.e. wavelength and maximal intensity. The cluster of values derived from the spectra taken from the pre-contracted gel area occupied a completely separated and unique domain. However the other 2 groups (i.e. wrapping gel and interface area) did not form separate clusters.

c) Identification of specific wavelengths that correlate with structural changes

The same wavelength (500 nm) used to monitor collagen gel contraction was also used to assess the ability of ESS to discriminate between different areas of the interface constructs. Again the intensity of the selected wavelength was ratioed to the intensity and slope of the spectrum in the IR region (615-810) in order to take other spectral features into account.

Owing to the similarity of spectra for culture medium and wrapping gel (Figure 7-9), an additional parameter was inserted into the analysis: the proximity of the probe to the surface of the construct. The optical probe was

positioned on each area of the interface construct (i.e. wrapping gel, interface and pre-contracted gel zone) and moved at different vertical positions (stepping 1 mm) by a manual rack pinion microscope stage, from just above the surface to just touching and with increasing depression into the gel along the z axis (total of 5 positions). The first 3 vertical positions were used in the analysis: 1) above surface (~1mm) 2) just touching surface 3) pressed into surface. Deeper positions were discarded due to large distortion of the spectra, probably caused by structural matrix deformation due to the effect of compression. The values for the normalised intensity at 500nm are shown in the scatter, Figure 7-12.

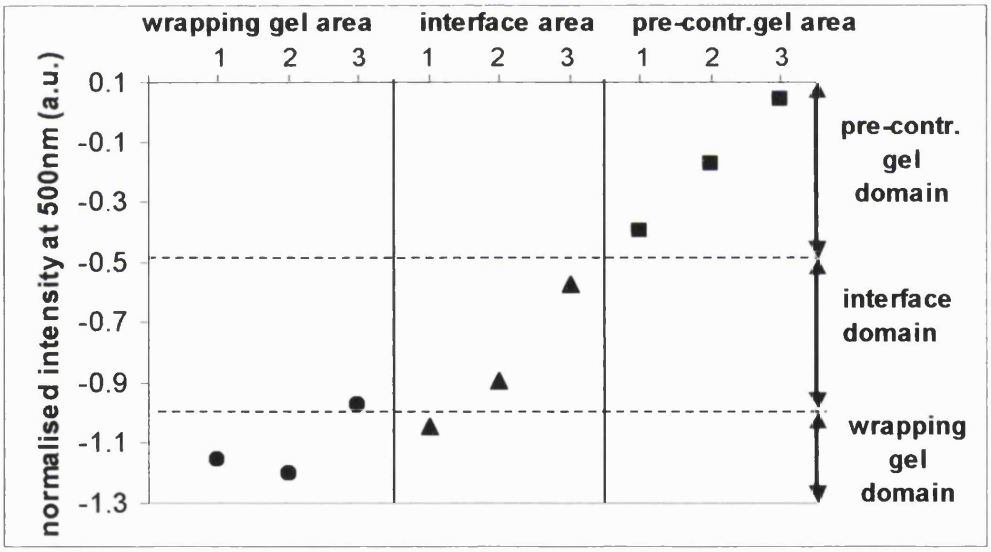

Figure 7-12 Scatter plot of the normalised intensity at 500nm. The optical probe was positioned on each area of the interface construct (i.e. wrapping gel, interface and pre-contracted gel zone) and moved at different vertical positions (stepping 1 mm) by a manual rack pinion microscope stage, from just above the surface (position 1) to just touching (position 2) to pressed into surface (position 3). Normalised spectral values at 500nm clustered into generally separated domains. Wrapping gel and interface area groups had a small overlap in their domains between the most pressured point of the wrap gel and the least pressured point of the interface area, but not between values taken at the same depth.

From left to right, values in each area (numbered 1,2,3) corresponded to progressive movement of the probe in the z-axis, into the gel surface. In this way the first values at the beginning of each area sector had the same probe position (vertically). In all cases there was a progressive increase in normalised intensity as the probe was depressed into the construct. The clusters of values taken at the same depth occupied completely separated domains. Generally the selected wavelength was able to identify completely separated domains for the different areas examined apart from one point overlap. This was between the most pressured point of the wrap gel and the least pressured point of the interface area.

Figure 7-13 summarises the results of the use of the selected wavelength to discriminate different interface areas of the interface construct (model I, assembly for mechanical testing). Mean values of the normalised intensity at 500nm for each area were obtained from three distinct interface constructs. Positions on the z-axis (Figure 7-12) were not considered (were averaged together) in this analysis due to their relative uniformity within each area.

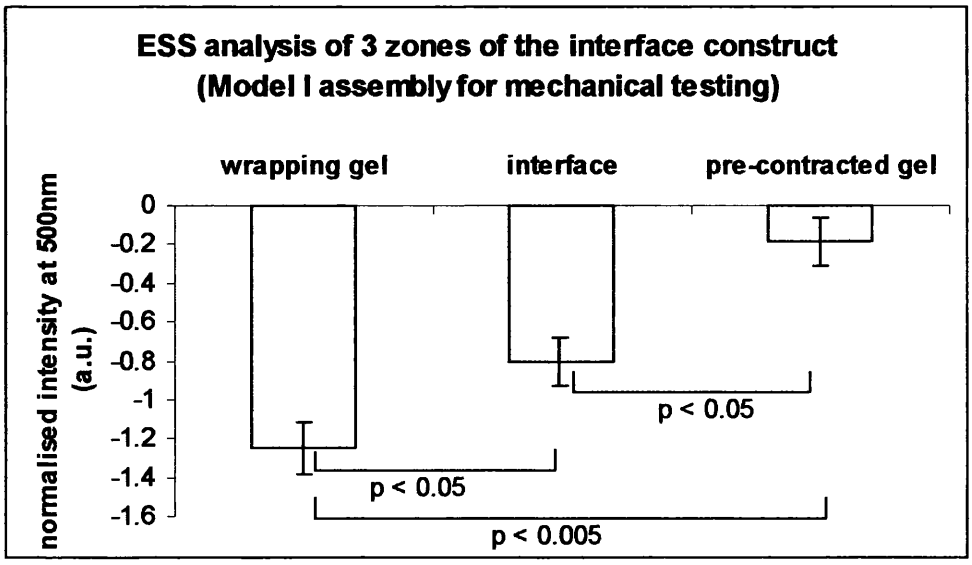

Figure 7-13 Mean normalised intensity at 500nm collected from different areas of the interface construct (Model I). Bars indicate SE. Each area resulted spectrally significantly different from the others. P-values, resulting from t-test, are indicated below the brackets joining the columns (n > 3).

The trend shown in Figure 7-12 was followed, with values of the normalised intensity at 500nm increasing from the wrapping gel area towards the pre-contracted gel area. Intensity values from area wrapping gel area were significantly lower than the values from both the interface area (1.5 fold) and the pre-contracted gel area (6.7 fold). Values of spectra from the interface area were significantly lower (4.3 fold) than values from the pre-contracted gel area.

In conclusion, the normalised intensity at 500nm showed to be correlated to structural changes of the three different areas of the interface construct. This added statistical relevance to the previous cluster analysis (Figure 7-12) in which the same normalised intensity was used (only one interface construct was analysed in it). Therefore spectral features contained in the composite ESS spectra have the potential to identify relative differences in cultured collagen gel interface constructs.

7.2.3.3 ESS of model II interface construct (assembly for microscopy imaging)

Circular interface constructs (model II, assembly for microscopy imaging) were cultured for 10 days prior fixation (chapter 6).

An unexpected remarkable lysis of the gel in the construct was observed (chapter 6), which triggered the interest in analysing this second version of the wrapping interface model by ESS. The central part of the interface area (i.e. area of overlapping between the circular pre-contracted gel and wrapping gel) was completely lysed (chapter 6). This reduced the interface area to a ring with an almost empty hole in the centre (filled with the medium with some gel fragments). Spectral acquisitions were performed after fixation in this set of experiments; therefore the surrounding fluid was the fixative solution. Although comparison could not be made with the previous set of experiments on model I, the aim here was to investigate the

potential of ESS to discriminate between areas of the interface construct (i.e. wrapping gel area, interface area, lysed area). In this case the lysed area represented a new area to be tested by ESS (not present in model I). An additional difference from the previous interface construct (i.e. model I) was that the pre-contracted gel was completely embedded into the wrapping gel. Therefore, in the circular interface constructs (i.e. model II) no spectra could be acquired from the pre-contracted gel alone.

Figure 7-14 shows the changes in the ESS spectra as the probe moved along the interface construct from the wrapping gel area (side) towards the interface area located in the centre (as diagrammatically drawn). The spectral signatures from both the wrapping cell-free gel area (spectral signatures 1,2 and 3) and the lysed area (spectral signatures 5 and 6) appeared distinct. Shifts in intensity were observed within each area although characteristic profiles were maintained. These shifts are likely to be due to the proximity of edges of each of these areas.

Clearly the fixative introduced specific spectral features, which could be observed as oscillations between 300 and 600. However these were not present in the other areas. Generally the three areas of the interface construct produced distinct spectral patterns in both intensity and shape.

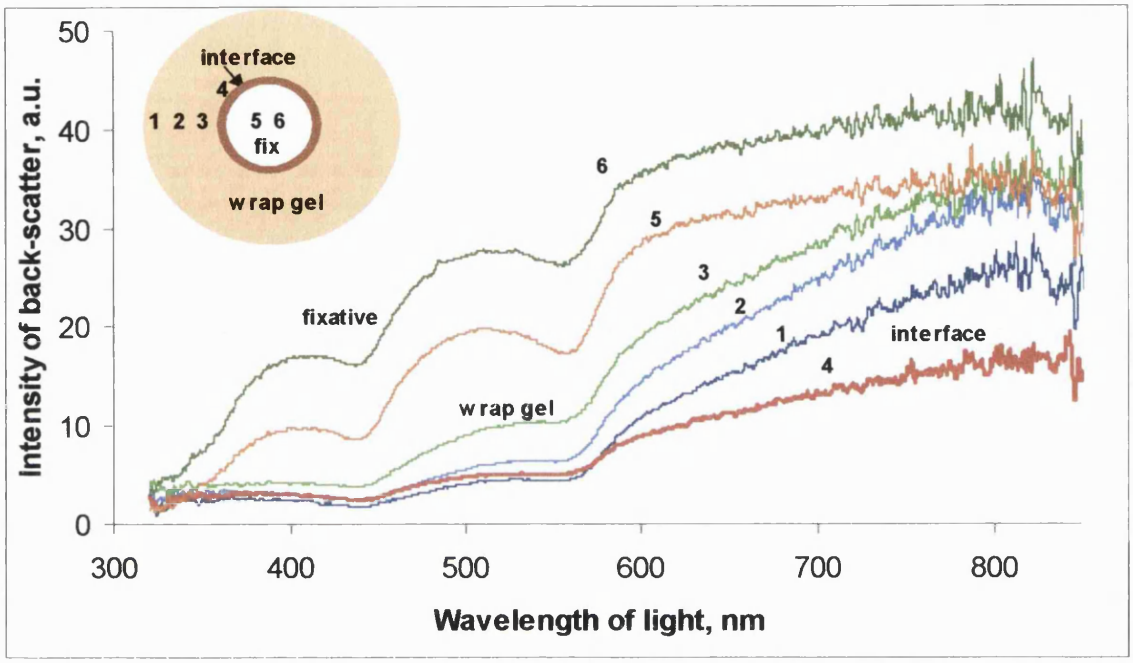

Figure 7-14 ESS spectra taken from different zones, shown in the set, over the surface of interface constructs (model II, assembly for microscopy imaging) moving from the wrapping cell-free gel towards the centre of the interface area. In this case the centre zone (5 and 6) had been lysed leaving a visibly degraded area resembling an empty hole filled with the fixative in which the interface construct was floating.

Again the normalised intensity at 500nm was analyses to test if this parameter, consistently with the result of the previous section, was able to identify relative differences between the distinct structural elements composing the interface construct. Again the optical probe was positioned on each area of the interface construct (i.e. wrapping gel, interface and lysed area) and moved at different vertical positions (stepping 1 mm) from just above the surface to just touching and with increasing depression into the gel along the z axis (total of 5 positions). The first 3 vertical positions were used in the analysis: 1) above surface (~1mm) 2) just touching surface 3) pressed into surface. Figure 7-15 shows the values of the normalised intensity at 500nm on a scatter graph. From left to right, values in each

area (numbered 1,2,3) corresponded to progressive movement of the probe in the z-axis, into the gel surface. In this way the first values at the beginning of each area sector had the same probe position (vertically). Differently from the previous result (Figure 7-12), the values of the normalised intensity did not increase as the probe was depressed into the construct. The pressure of the probe into the construct surface did not seem to cause a defined trend in the spectra under this analysis. However intensity values from different areas clustered in completely separated domains with no overlapping. This showed that, again, the selected wavelength was able to identify completely separated domains for the different areas examined.

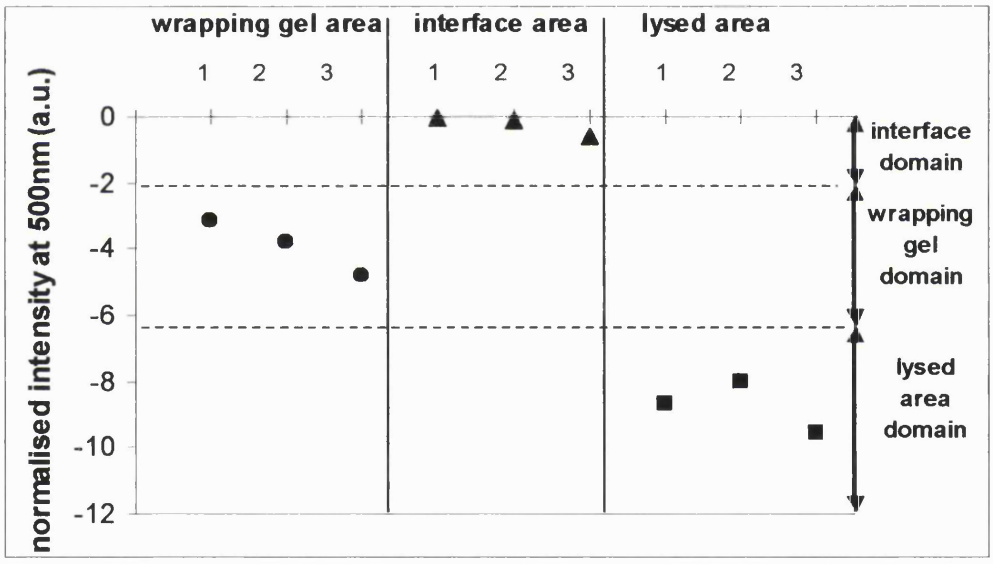

Figure 7-15 Scatter plot of the normalised intensity at 500nm. The optical probe was positioned on each area of the interface construct (i.e. wrapping gel, interface and pre-contracted gel zone) and moved at different vertical positions (stepping 1 mm) by a manual rack pinion microscope stage, from just above the surface (position 1) to just touching (position 2) to pressed into surface (position 3). Normalised spectral values at 500nm clustered into completely separated domains.

Figure 7-16 summarises the results of the use of the selected wavelength to discriminate different interface areas of the interface

construct (model I, assembly for mechanical testing). Mean values of the normalised intensity at 500nm for each area were calculated from three distinct interface constructs. Positions on the z-axis (Figure 7-15) were not considered in this analysis due to their relative uniformity within each area.

The trend shown in Figure 7-16 was followed, with the lowest values of the normalised intensity at 500nm registered for the lysed area. Values from the wrapping gel area and the interface area were increasingly higher. Intensity values from area wrapping gel area were significantly lower than the values from both the interface area (1.5 fold) and the pre-contracted gel area (6.7 fold). Mean normalised intensity for the lysed area was significantly lower than for both the interface area (2.7 fold) and the wrapping gel area (1.8 fold). Finally spectral intensity for the wrapping gel area was lower (1.5 fold) than for the interface area, but not significantly.

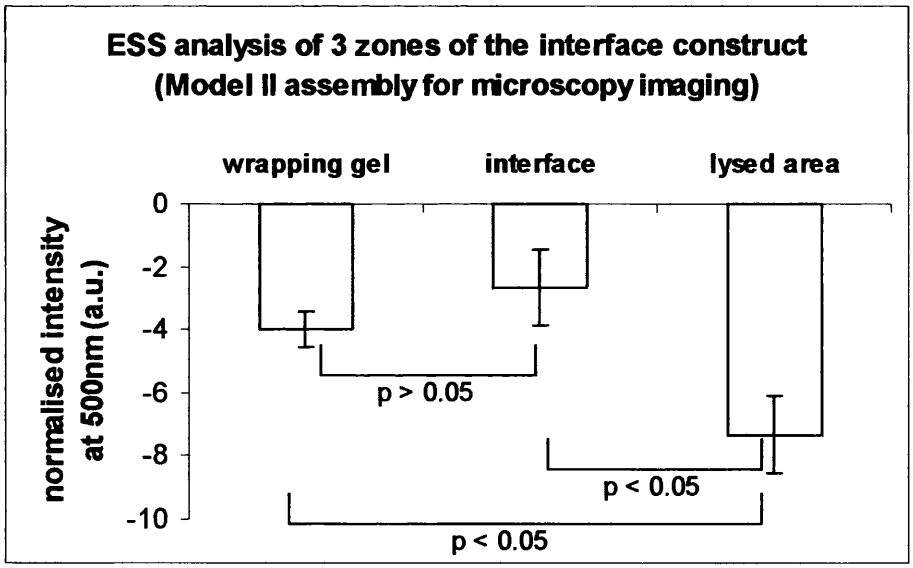

Figure 7-16 Mean normalised intensity at 500nm collected from different areas of the interface construct (Model II). Bars indicate SE. Mean intensity value from the lysed area was significantly different from the other areas. The difference between the mean intensity from the wrapping gel area and the interface area was not statistically different. P-values, resulting from t-test, are indicated below the brackets joining the columns (n > 3).

In conclusion, using the normalised intensity at 500nm, the lysed area could be identified as distinct from the other 2 areas. However the wrapping gel area and the interface area were not significantly different between them by the same parameter. These 2 areas were successfully identified in the previous set of experiment using the normalised intensity at 500nm. This might be due to the change of the medium in which the construct was floating from standard culture medium to fixative.

Despite the lack of statistical significance the normalised intensity at 500nm was distributed in completely separated domains for each area of the construct in the scatter plot derived from a single construct Figure 7-15.

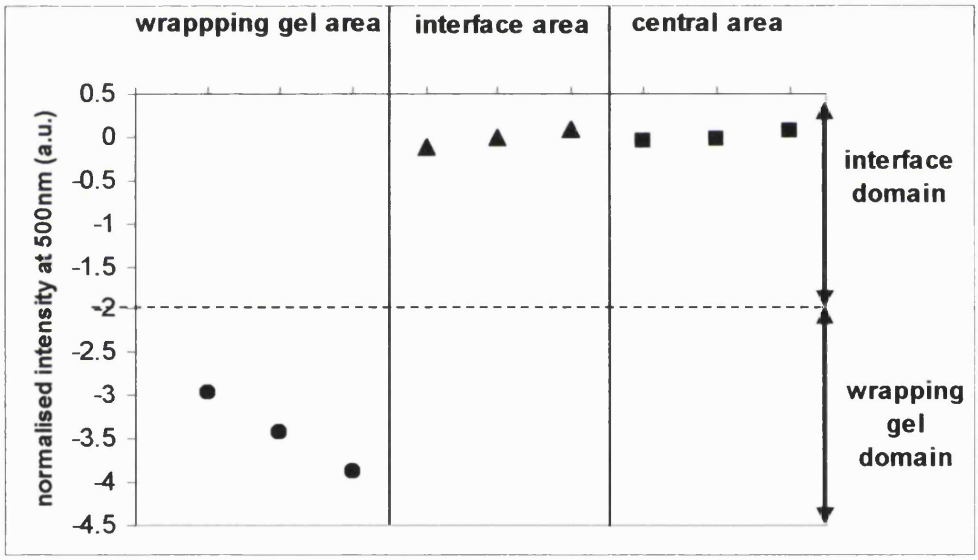

Figure 7-17 Scatter plot of the normalised intensity at 500nm. The optical probe was positioned on each area of the interface construct (i.e. wrapping gel area, interface area and non-lysed central area of the interface) and moved at 3 different vertical positions as above (Figure 7-15). Normalised spectral values at 500nm clustered into separated domains.

In order to test whether the same parameter was able to discriminate between wrapping gel area and interface area in interface constructs were

lysis was absent, the experment was repeated on non-lysed construct. Lysis was cell-mediated since the non lysed construct were generated using a different cell type seeded in the pre-contracted gel (chapter 6). The graph displayed in Figure 7-17 is analogous to the graph in Figure 7-15 but shows that in the spectral values derived from centre of the interface area, where no cell-mediated lyses was present, resulted in the same domain of the intensity values of the interface area (almost superimposed). This showed, lysed area was previously identified as a distinct area. When lyses was not present in the construct, the spectral values across the interface zone did not differ.

7.2.4 Contribution of isolated factors to the spectral signatures of fibroblast-populated collagen lattices

The experiments presented in this section aimed at isolating single physical contributions to the spectral signature of fibroblast-populated collagen lattices. In particular the contribution of cell concentration and gel thickness was investigated. Characteristic wavelengths, which are known to be related to the optical properties of the single biochemical components, were used for the analysis of the spectra.

Collagen gels were cast and floated in multiwell plates and ESS spectra were taken within 1 hour after gels were set. This early time point allowed exclusion other effects on the spectra due to maturation of the constructs such as cell-mediated contraction, pH changes, collagen gel matrix intrinsic contraction. Two series were studied, either (1) constant volume gels were seeded with different concentration of cells or (2) cell-free gels with variable volumes were prepared, depending on the parameter investigated.

The probe was positioned on the surface of the gels around the centre to avoid possible edge effects described previously in section 7.2.3.1.

Again spectral intensity was normalised by the number of pulses from the xenon lamp and ratioed to the raw spectrum from the Spectralon (reference spectrum).

7.2.4.1 Contribution of gel thickness to ESS spectra

Collagen gel of volumes ranging from 0.5 to 5 ml were cast in wells of constant volume (i.e. 12 multiwell plates) to obtain gels with different thickness (from 1.31 mm to 13.15 mm). ESS spectra were taken within 1 hour of the gel setting (gels were fully set and floated within 30 minutes of casting).

Figure 7-18 shows the ESS spectra between 320 and 800 acquired from cell-free gels with different thickness floated in standard culture medium. No correlation between the volume variable and the spectral signatures was evident from the composite spectral signatures. However a common local minimum could be identified at a constant wavelength (560nm) for all curves. This was caused by phenol red contained in the culture medium.

Spectral signatures were normalised to assume a unit value at the absorption peak at 560 nm which was invariant for all curves. Then curves were inverted to obtain the corresponding absorption (Figure 7-19). This transformation reordered the spectral signatures it appeared evident a consistent shift down of each curve at each increase in gel thickness (particularly in the region between 320nm and the peak at 560nm).

Local peaks in absorption centred in the region 385-390nm were found to decrease in amplitude as the thickness of the gel increased.

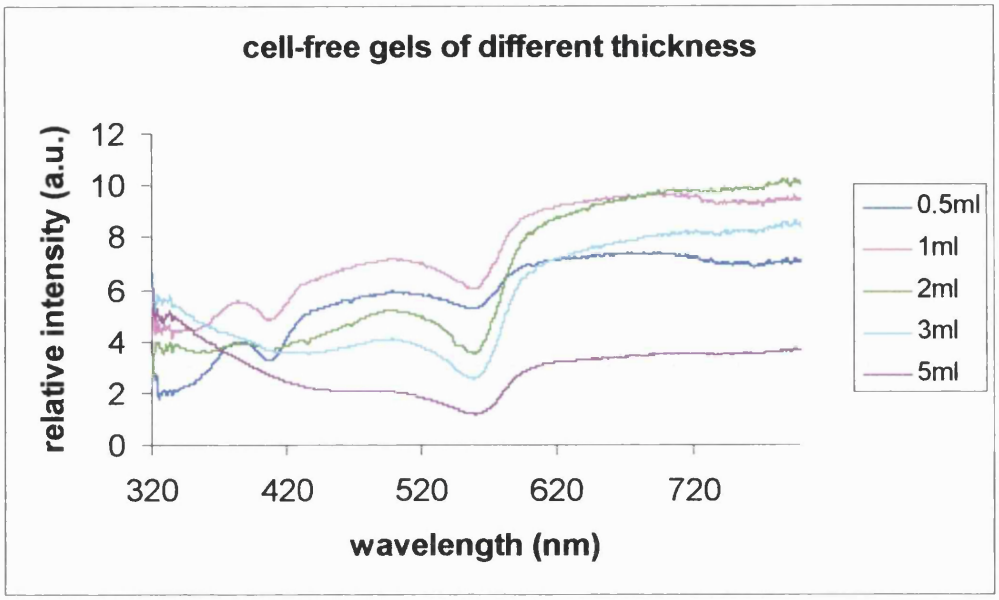

Figure 7-18 ESS spectra taken from cell-free gel having increasing thickness (from 1.31 mm to 13.15 mm). Different thickness was obtained by casting different gel volumes (from 0.5 to 5 ml) in a constant volume space (i.e. multiwell plates). Minima at 560nm correspond to phenol red in the medium.

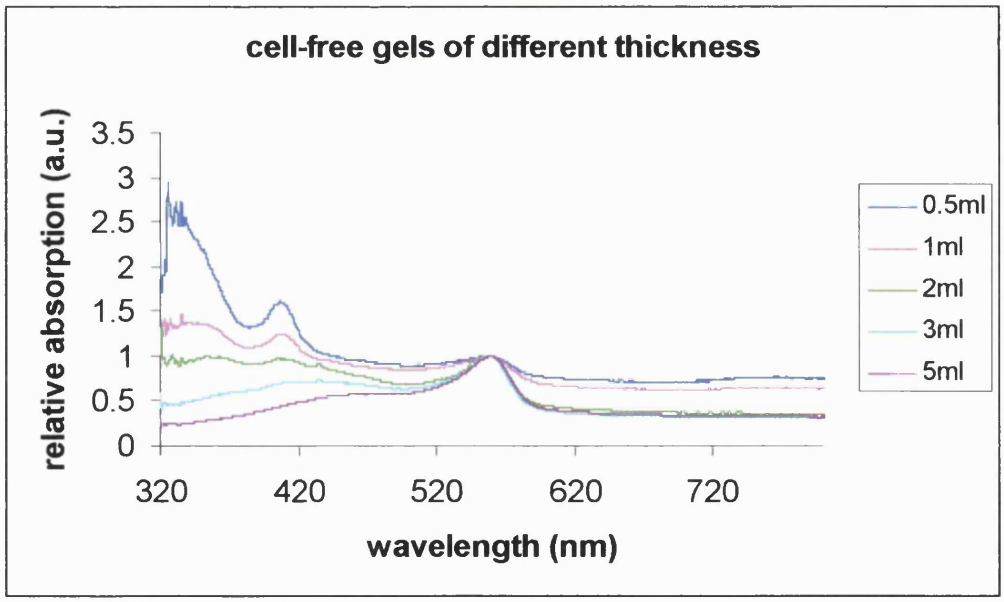

Figure 7-19 Spectral signatures in absorption derived from graph in Figure 7-19 (which represented intensity signatures) by normalising to unity around the local minimum in 560nm and inverting.

Interestingly the spectral region 385-390 nm has been reported to be the spectral window of light-induced autofluorescence emission for collagen (Glassman et al., 1995; Sady et al., 1995). Assuming that the light can travel through the full thickness of the gel, increased thickness corresponds to increased amount of collagen (along the whole thickness) in which the light travels before being scattered back. This fact in combination with peaks observed in the collagen autofluorescence spectral window suggested that the collagen content might be the main contributor to the spectral changes in the region 385-390nm.

Figure 7-20 shows the values of the area under the spectral signatures (i.e. the absorbed energy) in the region 385-390nm plotted over gel thickness. The amount of absorption was inversely proportional to gel thickness for all the levels of thickness examined (up to 13 mm). This showed that spectra were modified by all the levels of thickness, implicating that the penetration depth of light in cell-free collagen gel was much larger than the values reported in literature, i.e. ~1 mm (Mourant et al., 1996a).

Since all cell-free gels had the same collagen concentration, increased gel thickness corresponded to an increase of collagen material along the axis of thickness. The maintained sensitivity of ESS spectra to all thickness levels has also the implication that as light absorption decreased (or also backscattered intensity increased) the amount of collagen increased. This implication is supported by the fact that the chosen spectral window has been previously used to selectively determine the total amount of collagen through its intrinsic fluorescence (Glassman et al., 1995; Sady et al., 1995).

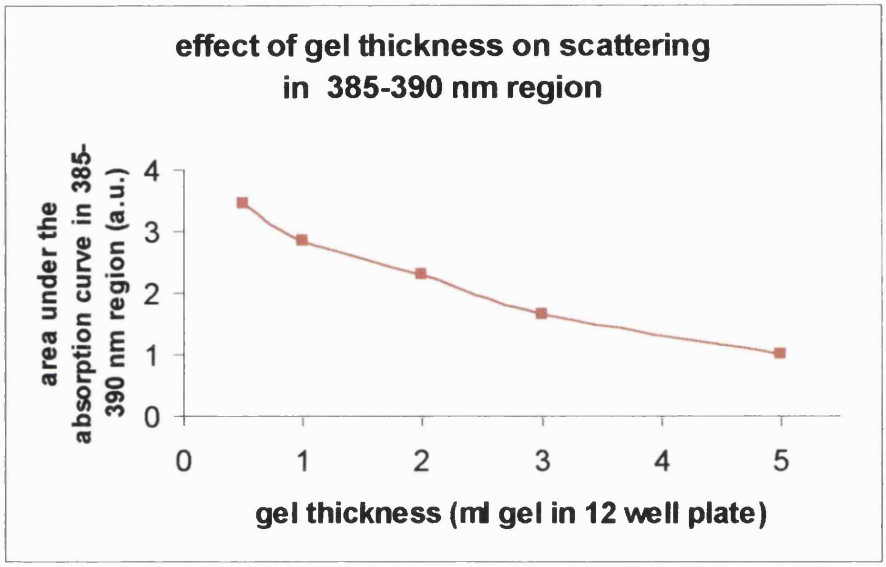

Figure 7-20 Changes in the absorption of backscattered spectra in the region 385-390nm (i.e. the area under the transformed spectral signatures plotted in Figure 7-19) showed inverse correlation to changes in gel thickness.

In summary this experiment showed that changes in thickness of cell-free gel were correlated to changes in the ESS spectrum in the collagen autofluorescence region of the spectrum, i.e. 385-390 nm. In the chosen spectral window and experimental condition (i.e. cell-free collagen gel) increase of backscattered intensity was correlated to the increase in the amount of collagen along the gel thickness. Therefore the collagen autofluorescence region might be useful for spectral monitoring of the amount of collagen material contained in collagen gels.

Additionally the penetration depth of light in cell-free collagen gel was over 13 mm, much larger than the values reported, i.e. ~ 1 mm (Mourant et al., 1996a).

7.2.4.2 Contribution of cell concentration to the spectral signatures of fibroblast-populated collagen gels

Gels of constant volumes (2 ml) were seeded with cell concentration ranging from 0 to 10 million cells per ml and ESS spectra were taken within 1 hour after gels set (gels were fully set and floated within 30 minutes after casting).

Figure 7-21 shows the ESS spectra between 320 and 800 acquired from cell-seeded collagen gels floated in standard culture medium. No correlation between the volume variable and the spectral signatures was evident from the composite spectral signatures. The common local minimum at 560nm, due to phenol red absorption, was less evident than in the previous experiment (Figure 7-18) and not present for all curves.

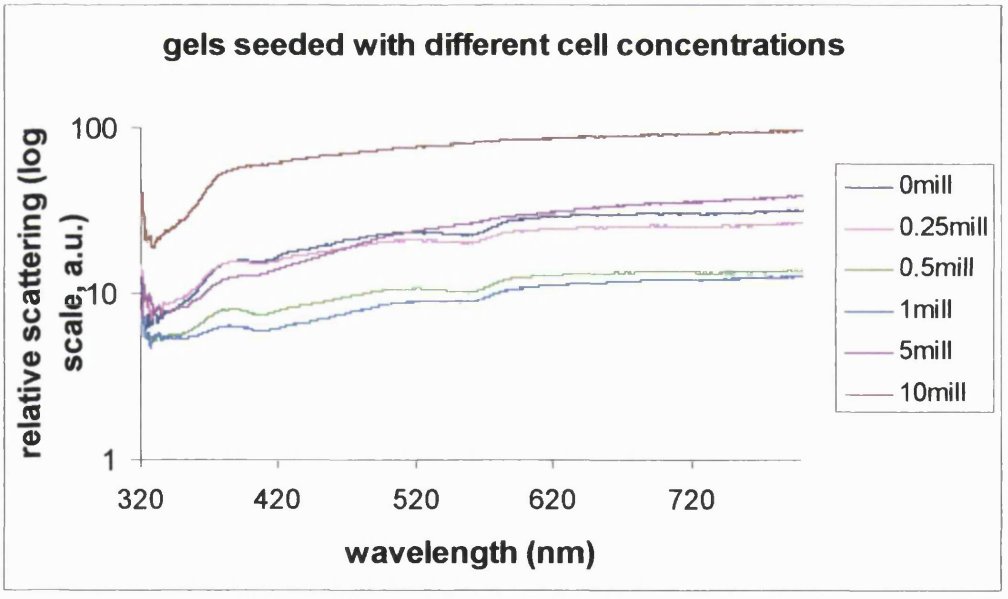

Figure 7-21 ESS spectra taken from collagen gels having constant volumes seeded with increasing cell concentrations from 0 to 10 million/ml. The scattering intensity has been plotted in logarithmic scale to allow a better distribution of the curves on the graph.

The previous experiment (7.2.4.1) suggested that the spectral window of intrinsic fluorescence might be useful to identify spectral contributions of specific gel components. Hence the spectral region of light-induced cell autofluorescence emission, i.e. 520-560nm (Stamenovic & Wang, 2000) Dellinger-Monti-1998, was used to analyse the spectral contribution of cell concentration.

Figure 7-22 shows that the slope of the ESS spectra in the region 520-560 nm was directly correlated to increases in cell concentration in the gels.

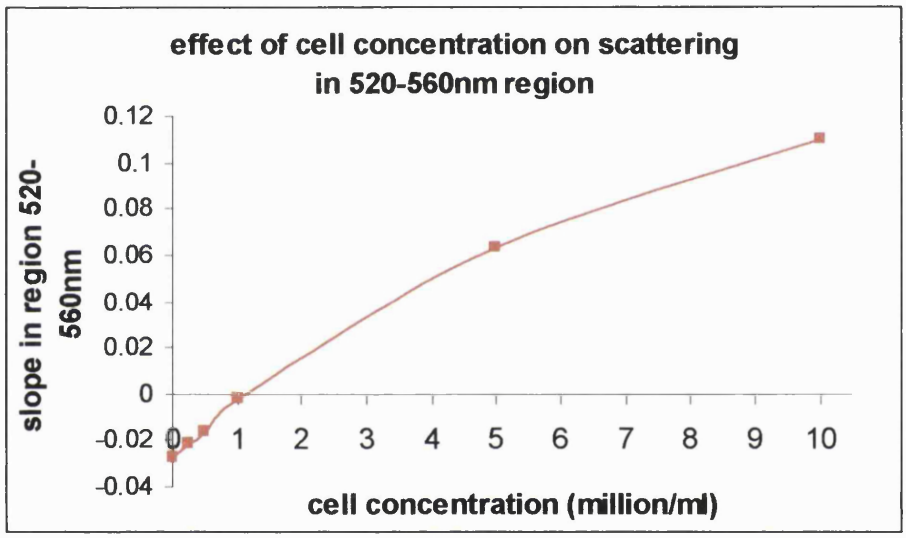

Figure 7-22 Changes in the slope of ESS spectra in the region 520-560nm plotted against changes in cell concentration in collagen lattices having constant volume.

In summary this experiment showed that changes in the spectral slopes in the region 520-560nm were well correlated to changes in cells concentration. Therefore the cell autofluorescence region of the spectrum might be useful for spectral monitoring of cell concentration in collagen gel constructs.

7.3 Discussion

A novel optical method based on elastic scattering spectroscopy (ESS) was developed with the potential to monitor structural and biochemical changes in cultured fibroblast-populated collagen lattices (FPCLs). Changes in ESS spectra were successfully correlated with temporal changes in collagen gel structures and composition due to cell-mediated contraction. Known different collagen-gel-based elements in the interface constructs (chapter 6) were also correlated to distinct spectral features.

For all the experiments, it can be argued that the optical probe only monitors structural changes of a small volume only (estimated ~1 mm^3) (Mourant et al., 1996a) even if the spectral changes recorded have been postulated to have correlation with changes in dimension / structure measured for the whole collagen gel construct. However, the highly isotropic nature of the collagen gel construct allows for an extension of the properties of a small area to most of the sample (see FE model, chapter 5). In addition, the volume analysed is considerably bigger than that of other optical measurement techniques such as small angle scattering (Bowes et al., 1999; Ferdman & Yannas, 1993; Sacks et al., 1997) and polarized light microscopy (Guido & Tranquillo, 1993). The technique used in this study is also not invasive or disrupting, requiring no specific preparation of the sample to analyse other than surface contact.

The elastic scattered spectrum acquired covered a wide range of wavelength (320 to 900 nm), and previous works (de Vries et al., 2000; Mourant et al., 1995; Mourant et al., 1996a; Mourant et al., 1996b; Osawa & Niwa, 1993; Perelman et al., 1998; Wallace et al., 2000) have shown that it contains information on the wavelength dependencies of both scattering structures (e.g. cells and other matrix components) and absorption by chromophores. Changes in the composite spectra appeared to correlate with changes in the collagen dimension, organisation and condition, which, in turn, depend on culture duration and biomechanical conditioning. We have

been able to determine a strong correlation between gel contraction and spectral intensity by isolating the 500nm wavelength, and ratioing it to the intensity and slope of the spectrum in the near IR region (615-810nm) in order to take other spectral features into account. However this is only one among numerous spectral changes recorded, as it was found to correlate to the global compaction of the gel. It is not yet clear which are the contributions of the single components of the gel to the multiple temporal spectral changes. Variations in other wavelengths might take account for other events like the increase in collagen fibril diameter and density, cell morphology, density and spreading, preferred orientations.

The normalised intensity at 500nm was also used to successfully discriminate between the different elements composing the interface constructs. Structural changes between the different areas of the interface constructs were followed by significant differences in levels of the normalised intensity. The same parameter, however, did not yield a significant discrimination between the areas of circular interface constructs after fixation. Fixation processes are known to change internal crosslinking of collagen gels and therefore induce structural changes at molecular level which are likely to be responsible for the altered ability to discriminate between the areas of the interface construct. Additionally the spectrum of the fixative had distinct oscillations in the spectral region 300-600nm that might overlap with the structural information. Therefore further studies are needed to characterise ESS spectra from FPCLs which were subject to fixation processes.

The other two methods used to analyse the ESS spectrum acquired from the elements of the interface constructs were: 1) ratioing the acquired spectrum with scattering components independent from structural changes (such as the culture medium) and 2) identification of local peaks. Neither method was as efficient as the normalised intensity at 500nm in the discrimination between the different areas of the interface construct. However, the first revealed a limit in the absolute sensitivity of the ESS technique, i.e. the spectrum of culture medium and cell-free gel (called "wrapping gel" in the

interface constructs) were not significantly different. Relative differences were evident in the slopes of the ratioed spectra (in the region 320-500nm). The second, i.e. identification of local peaks in the spectral region 320-420nm, was useful in discriminating gross structural differences distinct elements of the interface construct such as between wrapping gel and pre-contracted gel.

It is important to point out that *relative* changes in collagen-based structures were correlated to changes in ESS spectra and further work is needed to determine whether this technique can produce absolute measurements of the gel condition. Absolute spectral measurements would require a precise knowledge of the spectral contribution of the single components of cell-seeded collagen gels to the acquired backscattered light. Additionally well-established relationship must be known between gel thickness, light penetration depth and spectral contributions of culture media and background material used as a container for the gel. In ESS measurements of cell-free gels with different thickness, the light was able to penetrate long distances (over 13 mm) inside the near transparent low absorbing lattices. This implies that in many experiments in which gel thickness is less than 13 mm the light can travel through the sample and reach the layers underneath it. These layers (i.e. culture medium and the bottom of the container in which the gel was cast) would play a role in the absolute changes observed in the backscattered spectrum. The finding of light penetration depth appears to contradict the previous reports, in which white light penetration depth, for an optical setup similar to the one used in the current study, was estimated around ~ 1 mm (Bigio et al., 1993; Mourant et al., 1996a). This value, calculated through Monte Carlo simulations, was derived with the assumption that the light would travel through dense opaque tissue, while in the current experiment the collagen gel had low density (98% water) and was near transparent.

The spectral contributions of two isolated elements of FPCL (i.e. thickness of cell-free gels and cell concentration) showed to be correlated to specific distinct regions of the ESS spectrum. These were the light-induced

autofluorescence regions of cells (Gorgidze et al., 1998) and collagen (Glassman et al., 1995; Sady et al., 1995). In a recent study the ESS spectra were combined to fluorescence spectra to remove the distortions by absorption and scattering from intrinsic tissue fluorescence (measured simultaneously) through a complicated photon migration-based model (Muller et al., 2001). Through that approach collagen fluorescence could be quantified in vivo and showed potential as biomarker for epithelial precancerous changes. In the current study a simple direct correlation between the amount of collagen (increasing with collagen gel thickness) and the intensity of backscattered light in the collagen autofluorescence region was determined.

ESS measurements of the spectral contributions of single components in FPCLs (i.e. cell concentration and collagen amount) were highly simplified in such a way that all the simultaneous structural changes, which are normally occurring during cell-mediated contraction, could be excluded. Further analysis should be carried out to ensure that these correlations will be still present in standard experimental conditions in which complex collagen packing is combined with simultaneous changes in intracellular structures and cell concentration. Besides, the amount of collagen and cell concentration might not be the actual basic components contributing to the spectra of FPCLs. The increased spectral intensity due to increased cell concentration, for example, is thought be determined principally by intracellular structures such as mitochondria and nuclei (Hielscher et al., 1997; Mourant et al., 1998). The main contributions to the collagen autofluorescence have been attributed to crosslinking submolecules such as hydroxypyridinium (Sady et al., 1995) and pyridinoline.

Another important aspect in monitoring the formation of engineered collagen-based constructs is the assessment of spatial organisation of the collagen network. This is remodelled by the cells to different degrees of fibrillar collagen packing and alignment (Grinnell & Lamke, 1984; Porter et al., 1998). In the current study structural spatial information was combined in the ESS spectra with other biochemical information in a complex way.

Imaging techniques using forward scattering of light have been employed for spatial quantification of tissue collagenous structures (Bowes et al., 1999; de Vries et al., 2000; Ferdman & Yannas, 1993; Sacks et al., 1997; Waldman et al., 1999). However, forward scattering methods are not suitable for an endoscopic backscattering setup such as the one used in this study. Additionally only spectral analysis but not imaging can be performed in the current setup.

Diffuse reflectance of backscattered polarized light combined to imaging techniques has been shown to be correlated to the size of the scatterers contained in a turbid media (Hielscher et al., 1997; Mourant et al., 1998). However polarised light imaging of skin has been shown to yield images based only on photons backscattered from the superficial epidermal and initial papillary dermis because the birefringent dermal collagen rapidly randomises the light (Jacques et al., 2000). Therefore backscattered polarised light techniques appear to be more suitable for measurement of structures on the surface rather than internal to the tissue (Guzelsu et al., 2003).

A method using the analysis of wavelength-dependent periodic oscillations in ESS spectra (also called diffuse reflectance) has been shown to be able to determine the distribution and density of cell nuclei in the epithelial layers (Perelman et al., 1998; Wallace et al., 2000; Backman et al., 1999). This information was shown to be useful for early detection of epithelium malignancy. A similar method based on the analysis of the maxima and minima in ESS spectra led to the determination of particle size in bilayered tissue phantoms (Canpolat & Mourant, 2001). However these methods were focussed on the determination of the size of scatters a thin superficial tissue layer (up to 500 μm), i.e. the epithelial layer, in which malignancy is known to develop. Hence they would not be suitable for the analysis of thicker 3D samples. Furthermore these methods were based on the Van de Hulst approximation of Mie's scattering theory in the visible range which can be used if $\lambda << d$, where λ is the light wavelength and d is

the diameter of the scattering particle (van de Hulst, 1981). This assumption limits the use of these techniques to small structures in the order of 100 nm, such as collagen fibrils.

Simple variable clustering has been used in this study to classify spectral features in relation to the distinct structures of engineered interface constructs. More complex classification methods of ESS spectral signatures such as artificial neural networks and hierarchical cluster analysis has shown to be useful in the clinical use for the diagnosis of breast cancer (Bigio et al., 2000). Similar classification techniques could be applied to find correlation between ESS spectra and architectural organisation of collagen networks.

Monte Carlo simulations have been computed in order to estimate collagen fibre diameter for contracting FPCLs from the ESS spectra (Bixio et al., 2002). Although this model needs further validation, it has potential to be developed as a viable method to derive important structural parameters.

Finally a recently published method using a linear array of detectors demonstrated that the ESS principle can be used to identify spatial anisotropy in human skin (Nickell et al., 2000). Without some modification to the current system this method might be used to determine the degree or anisotropy and alignment of structures in FPCLs. The drawback of this technique is that the fine minimally invasive optical fibre would be replaced by a large sensor. Although this might be acceptable for the optical measurement of engineered tissue, it would not be suitable for in vivo endoscopic applications.

In conclusion elastic scattering spectroscopy offers promises for a "real time" non-invasive tool for monitoring structure and density of tissue engineered constructs.

Chapter 8

Conclusions

8.1 A mechanistic model for cell-matrix interaction during the cell-matrix remodelling process.

In the present study different aspects of cell-mediated structural matrix remodelling in collagen gel based matrices have been investigated under two different approaches. The first approach tested the ability of the cells to lock tension in the matrix by spatially/structurally remodelling, through cell mediated matrix contraction. The second approach tested the ability of the cells to strengthen the interface between collagen lattices by structurally remodelling the interface zone, possibly through cellular migration.

The results obtained by the two models appear to converge to a unique consistent model for the cell-mediated matrix remodelling process. This is a fundamentally iterative process which occurs at interstitial ultrastructural level by the continuous local interaction between cell and matrix. This interaction is regulated by many factors including:

- Mechanical configuration (i.e. distribution of mechanical properties through specific system geometries)
- Matrix stiffness
- Cell force generation
- Growth factors

In this study, simple, mechanical conditions (i.e. uniaxial tension) have been used to study the ability of the cell to remodel a random fibrillar network into an ordered aligned system of packed fibril bundles. It is increasingly clear, and confirmed in this work, that it is the force generated by the cells that causes aligned reorganisation. And it emerges also that only under specific macroscopic constraints and defined geometries this aligned reorganisation occurs. However, it was not clear how macroscopic constraints were perceived at microscopic level and how these were translated into local regulatory signals for the cells which lead them to produce specific matrix spatial reorganisation. Additionally it was not fully understood how cell-matrix remodelling could lead to a stably spatially organised matrix whose final mechanical and structural properties are radically different from the starting properties.

A working model which attempts to connect the microscopic to the macroscopic level in the cell-matrix remodelling process of collagen lattices is proposed.

Fibroblasts are attachment-based cells, therefore they are conditioned by the mechanical properties of the matrix to which they adhere and perceive mechanical loading through the matrix. Cell spreading and locomotion generates forces at the adhesion sites to which the matrix reacts. In a 3D fibrillar collagen network, cellular forces are applied to local fibrils to which cells adhere. Collagen fibrils are intrinsically anisotropic due to their molecular structure. This structure is stiffer along the longitudinal axis of the fibre than in the other transverse directions. An additional degree of local anisotropy is given by the uniaxial isometric tension. Since deformation is not permitted in one direction, a gradient of stress is generated along that direction (i.e. local stiffness increases in reaction to cell tractional forces). When cells apply forces to the fibrillar network they would experience a greater resistance when pulling along the axis of fibres rather than transversally to the axis. Therefore cells would tend either to be pulled by their traction forces towards stiffness gradients (such as along fibres) or deform the matrix around them without moving in the case of

more compliant area (such as transversally to fibres axes). Additionally due to axial isometric tension, the cells can easily compress and compact the collagen network along the orthogonal directions to the axis but not along the axis.

As fibres deformed in random directions by cells reach a state of local alignment they will become the stiffest local points because the two anisotropies (i.e. the macroscopic isometric tension and the intrinsic fibre anisotropy) are acting conjunctly. Tension applied along the axis of fibres reduces also the transverse deformability by a tension-strengthening mechanism.

These aligned fibres with the least deformability become attractors for the surrounding fibres which can be easily deformed until they align to the attractors. Fibroblasts keep exerting forces that deform their substrate until the stiffness of the substrate is able to resist them. This stiffness balance is likely to happen along aligned fibres which are the locally stiffest points. When this local stiffness balance is reached cells alignment is likely to occur since cells are known to move towards stiffer substrates (Stamenovic & Wang, 2000) and then to align to spatial features through contact guidance mechanisms (Tranquillo, 1999).

Iterating this process leads to increasingly higher stability as cells and fibres keep aligning. Eventually lattices becomes thin strings of condensed fibres aligned along the axis of load. Increased force generation by cells, stimulated by TGF-β1 treatment can accelerate this process (Wilson-Jones 2002, MSc Thesis UCL).

Cyclic mechanical loading, on the other hand, has been shown to increase alignment by helping reorientation of fibres along the axis of load (Eastwood et al., 1998; Parsons, 2000). This process suggests a mechanism by which, even under lower cellular forces, alignment attractors are rapidly generated. Cellular forces are still necessary to stabilise fibril alignment around these attractors as it is demonstrated by cyclically loaded cell-free lattices in which no clear sign of alignment could be detected.

A mechanism using the analogy with the internal stretching of a piece of fabric has been proposed to explain the formation of aligned straps in collagen gels (Sawhney & Howard, 2002). This explains the alignment of fibres composing the fabric along the line of stretching between 2 points, by showing how fibres in the interconnected network are compressed along that line aligning to it. A similar mechanism might act locally between single cells exerting forces on the interconnected network of fibres. However the alignment is not given by the two focal points, where force is applied, but by the complex system of anisotropy described above.

The FE model proposed in this study was a preliminary attempt to validate this working hypothesis by computer simulation. The model indicated that cell interstitial traction in a uniaxially clamped matrix leads to alignment of the local matrix stiffness. Stiffness gradients are known to attract cell migration (Lo et al., 2000) and alignment to topographical cues has been also demonstrated in previous studies (Clark et al., 1987; Guido & Tranquillo, 1993).

Notably, the proposed model, which explains macroscopic remodelling through local mechanical interaction between cells and matrix, is consistent with the results on the permanent shortening of the collagen lattices.

The matrix reorganisation obtained through cellular forces and mechanical constraints is consolidated by new interfibrillar bonds which have shown to consolidate the remodelled structure even when the cells, initially holding it together, had been removed. The results on stable structural matrix remodelling, therefore, add to the model the concept that the stability of the increasingly aligned conformation is consolidated by new bonds between fibrils which strengthen the structure of the new architecture. These new bonds depend on many factors including compression of fibrils due to cellular forces, induced aligned packing by mechanical loading and collagen production and lyses by cells.

Whatever the process of consolidation is, this consolidation adds a new important feedback process into the proposed mechanical model. This is given by the matrix feedback which gradually stabilises and stiffens,

accumulating tension in itself rather than being held entirely by cell generated tension. Therefore not only matrix becomes stiffer in reaction to cellular forces but also as a result of the stabilisation process described above.

A similar cell-matrix interactions can be hypothesised to be at the base of the formation and strengthening of tissue interfaces. Cellular migration, involving tractional forces, might be responsible for the structural remodelling of the matrix in the interface zone. Then this reorganisation might be then stabilises by cell collagen deposition.

In summary two central concepts can be deduced from this study:

1. Stable structural remodelling of collagen matrices depends on the coordinated action of cell force generation and collagen deposition.
2. The remodelling process is iterative and leads to a gradual stable reorganisation of the matrix internal architecture which no longer needs cellular forces.

The cell-mediated remodelling process has been implicated in many fundamental biological processes including morphogenesis, growth, adaptation and repair. Abnormal regulation of these processes results in important tissue pathologies including contractures, scars, adhesions and fibrosis.

Understanding the mechanisms which regulate the cell-matrix remodelling process can indicate strategies to tackle these pathologies. For instance, in the treatment of tissue contractures, strategies should involve the blocking of cell force generation at early stages, since at later stages the remodelled the matrix becomes consolidated and cellular forces are no longer needed to sustain the developed abnormal tension. For the treatment of adhesion/poor-integration conditions, it appears that particular attention should be given to the control of cellular migration.

The distribution of tensile forces and the mechanical properties of the matrix have been shown to play a key role in the regulation of the cellular remodelling process via a feedback loop mechanism. This suggests that intervening early at a mechanical level on the pathological tissue, i.e. altering tension and/or geometry of the tissue area, might be useful to block further development of tissue contractures or undesired tissue adhesions.

8.2 A model platform study

It is increasingly recognised that there is a need for new models and approaches to deal with the complexity of the remodelling processes, as an orchestration of interdependent factors including of biochemical interactions, cellular architecture, micromechanics and structural complexity (Huang-Ingberg 1999, Cowin 2000, Tomasek 2002, Shreiber-Tranquillo 2002, Silver 2000, Wakatsuki-Elson 2003, Guilak, 1999). Further, new evidence from the relatively new field of tissue engineering has highlighted the importance of designing new optimised bioreactors. Similarly, evidence accumulated in the field of tissue engineering have highlighted the importance of controlling multiple cell regulatory signals (physical and chemical in the culture environment in order to achieve controlled tissue formation (Brown, 2002; Vunjak-Novakovic et al., 1999).

In this sense, this study can be viewed as a model platform, with the aim of proposing new methodological approaches to the study of 3D cell-matrix remodelling.

Mechanical aspects have been accurately characterised in two collagen-bases tissue models. These models were useful to identify basic factors involved in the cell-matrix structural remodelling process.

The first model showed that the tension developed in the collagen matrices during the cell-mediated contraction is gradually locked in the

matrix which no longer requires cell forces. This mechanism is thought to be based on a continuous feedback between mechanical stresses and strains in the matrix and cellular responses as force generation and collagen deposition.

The second model showed that fibroblasts in collagen lattices contracted for 2 days in culture were able to strengthen the adhesions of the contracted lattice with a cell-free collagen matrix. This mechanism was correlated to cell migration across the tissue interface, leading to remodelling of the interface zone.

It should be noted that the two proposed models can be correlated by using FPCLs, pre-cultured under different treatments, as building components for the generation of interface constructs. In this way, the degree of stable structural remodelling (i.e. RMT previously measured) could be correlated to the interface integration and strengthening process. At present the correlation of such parameters has never been considered, but it might provide important new knowledge about how the degree of tissue maturation influencing the development of tissue integration or adhesions.

In order to monitor the evolution of spatial remodelling in 3D collagen matrices, while in culture, an optical method, based on elastic scattering spectroscopy has been developed. This technique showed that ESS-based optical methods have the potential for real-time, minimally-invasive measurement of cell-mediated structural remodelling of tissue models in bioreactor cultures.

The well-defined geometries and mechanical conditions of the model used in this study allowed to generate computer models of the biological systems under investigation. This allowed us not only to define in detail the distribution of stresses and strains, but also to produce predictions concerning critical failure points where stresses were concentrated (chapter 6). Additionally it permitted the modelling of cell-mediated remodelling process via a bottom-up approach, that is from local random cell-matrix interactions to higher level of structural reorganisation (e.g. involving global

alignment of cells and fibrils). The huge amount of discrete, interdependent, interactions involved in cell-matrix interactions in a 3D environment cannot be treated intuitively or analytically, but it needs a numerical approach.

In conclusion this study has used an interdisciplinary approach to investigate cell-matrix remodelling process, involving a parallel use of mechanical and biochemical control, real-time minimally-invasive optical monitoring and computer modelling for analysis of stresses and predictive computation of cell-matrix interactions.

Although most of the models and methods proposed are still in their initial experimental stage, this study has produced a model platform which can be used for the development of a new generation of complex bioreactors in which tissue morphogenesis would be analysed under different simultaneous parameters (e.g. biochemical, mechanical and structural).

Reference List

Alberts, B., Johnson, A., Lewis, J., Raff, M., Roberts, K., and Walter, P. (2002) Molecular biology of the cell. Garland Science, New York.

Altman, G.H., Horan, R.L., Martin, I., Farhadi, J., Stark, P.R., Volloch, V., Richmond, J.C., Vunjak-Novakovic, G., and Kaplan, D.L. (2002) Cell differentiation by mechanical stress. *FASEB J,* **16**:270-2.

Anderson, R.R. (1991) Polarized light examination and photography of the skin. *Arch Dermatol,* **127**:1000-5.

Andersson-Engels, S., Johansson, J., Svanberg, K., and Svanberg, S. Laser induced fluorescence in medical diagnostics. Proc. SPIE. 1203. **1990.**

Arora, P.D., Narani, N., and McCulloch, C.A. (1999) The compliance of collagen gels regulates transforming growth factor- beta induction of alpha-smooth muscle actin in fibroblasts. *Am J Pathol,* **154**:871-82.

Arup Corporate. Arup Corporate. What caused the Bridge to move? **2003.** Arup Corporate. 2003.

Awad, H.A., Butler, D.L., Harris, M.T., Ibrahim, R.E., Wu, Y., Young, R.G., Kadiyala, S., and Boivin, G.P. (2000) In vitro characterization of mesenchymal stem cell-seeded collagen scaffolds for tendon repair: effects of initial seeding density on contraction kinetics. *J Biomed Mater Res,* **51**:233-40.

Backman, V., Gujar, R., Badizadegan, K., Itzkan, I., Dasari, R.R., Perelman, L.T., and Feld, M.S. (1999) Polarized light scattering spectroscopy for quantitative measurement of epithelial structures in situ. *IEEE J. Seleceted Topics in Q. Electronics,* **5**:1019-26.

Barocas, V.H., Moon, A.G., and Tranquillo, R.T. (1995) The fibroblast-populated collagen microsphere assay of cell traction force - Part 2: measurement of the cell traction parameter. *J Biomech Eng,* **117**:161-169.

Barocas, V.H. and Tranquillo, R.T. (1997a) An anisotropic biphasic theory of tissue-equivalent mechanics: the interplay among cell traction, fibrillar network deformation, fibril alignment, and cell contact guidance. *J Biomech Eng,* **119**:137-145.

Barocas, V.H. and Tranquillo, R.T. (1997b) A finite element solution for the anisotropic biphasic theory of tissue-equivalent mechanics: the effect of contact guidance on isometric cell traction measurement. *J. Biomech. Eng.,* **119**:261-7.

Bell, E., Ehrlich, H.P., Buttle, D.J., and Nakatsuji, T. (1981a) Living tissue formed in vitro and accepted as skin-equivalent tissue of full thickness. *Science,* **211**:1052-4.

Bell, E., Ehrlich, H.P., Sher, S., Merrill, C., Sarber, R., Hull, B., Nakatsuji, T., Church, D., and Buttle, D.J. (1981b) Development and use of a living skin equivalent. *Plast Reconstr Surg,* **67**:386-92.

Bell, E., Ivarsson, B., and Merrill, C. (1979) Production of a tissue-like structure by contraction of collagen lattices by human fibroblasts of different proliferative potential in vitro. *Proc Natl Acad Sci U S A,* **76**:1274-8.

Bell, E. (1991) Tissue Engineering: A Perspective. *Journal of Cellular Biochemistry,* **45**:239-41.
Notes: viewpoint section .

Bellows, C.G., Melcher, A.H., and Aubin, J.E. (1982) Association between tension and orientation of periodontal ligament fibroblasts and exogenous collagen fibres in collagen gels in vitro. *J Cell Sci,* **58**:125-38.

Berry, C.C., Cacou, C., Lee, D.A., Bader, D.L., and Shelton, J.C. (2003) Dermal fibroblasts respond to mechanical conditioning in a strain profile dependent manner. *Biorheology,* **40**:337-45.

Bigio, I.J., Bown, S.G., Briggs, G., Kelley, C., Lakhani, S., Pickard, D., Ripley, P.M., Rose, I.G., and Saunders, C. (2000) Diagnosis of breast cancer using elastic-scattering spectroscopy: preliminary clinical results. *J Biomed Optics,* **5(2)**:221-8.

Bigio, I.J., Loree, T.R., Mourant, J., Shimada, T., Story-Held, K., Glickman, R.D., and Conn, R. (1993) Optical diagnostics based on elastic scattering: recent clinical demonstrations with Los Alamos Optical Biopsy System. *Proc. SPIE,* **2081**:174-184.

Bixio, L., Caria, A., Brown, R. A., and Ruggiero, C. Modelling elastic scattering spectroscopy and light transport in 3D collagen gel constructs. Proceedings of the IEEE-EMBS Special Topic Conference on Molecular, Cellular and Tissue Engineering. **2002.**

Bohren, C.F. and Huffman, D.R. (1983) Absorption and scattering of light by small particles. Wiley, New York; Chichester.

Borsi, L., Castellani, P., Risso, A.M., Leprini, A., and Zardi, L. (1990) Transforming growth factor-beta regulates the splicing pattern of fibronectin messenger RNA precursor. *FEBS Lett,* **261**:175-8.

Bottiroli, G., Croce, A.C., Locatelli, D., Marchesini, R., Pignoli, E., Tomatis, S., Cuzzoni, C., Di Palma, S., Dalfante, M., and Spinelli, P. (1995) Natural fluorescence of normal and neoplastic human colon: a comprehensive "ex vivo" study. *Lasers Surg Med,* **16**:48-60.

Boukhalfa, G., Desmouliere, A., Rondeau, E., Gabbiani, G., and Sraer, J.D. (1996) Relationship between alpha-smooth muscle actin expression and fibrotic changes in human kidney. *Exp Nephrol,* 4:241-7.

Bowes, L.E., Jimenez, M.C., Hiester, E.D., Sacks, M.S., Brahmatewari, J., Mertz, P., and Eaglstein, W.H. (1999) Collagen fiber orientation as quantified by small angle light scattering in wounds treated with transforming growth factor-beta2 and its neutalizing antibody. *Wound Repair Regen,* **7**:179-86.

Brett, J.G. and Godman, G.C. (1984) Macrovacuolation induced by cytochalasin: its relation to the cytoskeleton; morphological and cytochemical observations. *Tissue Cell,* **16(3)**:311-24.

Brown, R.A. (2002) Tissue Engineering: Clinical Applications and Mechanical Control. In: Future Strategies for Tissue and Organ Replacement. J.M. Polak, L.L. Hench, and P. Kemp, eds. Imperial College Press, London, pp. 51-78.

Brown, R.A. and Byers, P.D. (1989) Swelling of cartilage and expansion of the collagen network. *Calcif Tissue Int,* **45**:260-1.

Brown, R.A., Prajapati, R., McGrouther, D.A., Yannas, I.V., and Eastwood, M. (1998) Tensional homeostasis in dermal fibroblasts: mechanical responses to mechanical loading in three-dimensional substrates. *J Cell Physiol,* **175**:323-32.

Brown, R.A., Sethi, K.K., Gwanmesia, I., Raemdonck, D., Eastwood, M., and Mudera, V. (2002) Enhanced fibroblast contraction of 3D collagen lattices and integrin expression by TGF-beta1 and -beta3: mechanoregulatory growth factors? *Exp Cell Res,* **274**:310-22.

Brown, R.A., Talas, G., Porter, R.A., McGrouther, D.A., and Eastwood, M. (1996) Balanced mechanical forces and microtubulecontribution to fibroblast contraction. *J. Cell. Phys.*, **169**:439-447.

Brown, R.A. (2000) Bioartificial Implants: Design and Tissue Engineering. In: Structural biological material. Design and structure-property relationships. M. Elices, ed. Pergamon, Amsterdam. Oxford, pp. 105-160.

Cacou, C., Eastwood, M., McGrouther, D.A., and Brown, R.A. (1996) Culture force monitor for investigating the formation of adhesion between tissue interfaces *in vitro* . *Cell. Eng.*, **1**:109-114.

Cacou, C., Palmer, D., Lee, D.A., Bader, D.L., and Shelton, J.C. (2000) A system for monitoring the response of uniaxial strain on cell seeded collagen gels. *Med Eng Phys,* **22**:327-33.

Callister, W.D.Jr. (2003) Material science and engineering. An introduction. John Wiley & Sons, Inc., New York, USA.

Canpolat, M. and Mourant, J.R. (2000) High-angle scattering events strongly affect light collection in clinically relevant measurement geometries for light transport through tissue. *Phys Med Biol,* **45**:1127-40.

Canpolat, M. and Mourant, J.R. (2001) Particle size analysis of turbid media with single optical fiber in contact with medium to deliver and detect white light. *Appl. Opt.*, **40**:3792-99.

Case, K.M. and Zwefel, P.F. (1967) Linear transport theory. Addison-Wesley, Reading, Mass.

Cheema, U., Yang, S.Y., Mudera, V., Goldspink, G.G., and Brown, R.A. (2003) 3-D in vitro model of early skeletal muscle development. *Cell Motil Cytoskeleton,* **54**:226-36.

Chegini, N. (1997) The role of growth factors in peritoneal healing: transforming growth factor beta (TGF-beta). *Eur J Surg Suppl,*17-23.

Christiansen, D.L., Huang, E.K., and Silver, F.H. (2000) Assembly of type I collagen: fusion of fibril subunits and the influence of fibril diameter on mechanical properties. *Matrix Biol,* **19**:409-20.

Cima, L.G., Vacanti, J.P., Vacanti, C., Ingber, D., Mooney, D., and Langer, R. (1991) Tissue engineering by cell transplantation using degradable polymer substrates. *J Biomech Eng,* **113**:143-51.

Clark, P., Connolly, P., Curtis, A.S., Dow, J.A., and Wilkinson, C.D. (1987) Topographical control of cell behaviour. I. Simple step cues. *Development,* **99**:439-48.

Clark, R.A., Folkvord, J.M., Hart, C.E., Murray, M.J., and McPherson, J.M. (1989) Platelet isoforms of platelet-derived growth factor stimulate fibroblasts to contract collagen matrices. *J Clin Invest,* **84** :1036-40.

Clark, R.A.F. (1996) The Molecular and Cellular Biology of Wound Repair. Plenum, New York.

Cohen, E.P. (1995) Fibrosis causes progressive kidney failure. *Med Hypotheses,* **45**:459-62.

Cope, M. and Delpy, D.T. (1988) System for long-term measurement of cerebral blood and tissue oxygenation on newborn infants by near infra-red transillumination. *Med Biol Eng Comput,* **26**:289-94.

Cowin, S.C. (2000) How is a tissue built? *J Biomech Eng,* **122**:553-69.

Cox, H.L. (1952) The leasticity and strength of paper and other fibrous materials. *Br. J. App. Phys.,* **3**:72-79.

Cusick, R.A., Lee, H., Sano, K., Pollok, J.M., Utsunomiya, H., Ma, P.X., Langer, R., and Vacanti, J.P. (1997) The effect of donor and recipient age on engraftment of tissue- engineered liver. *J Pediatr Surg,* **32**:357-60.

Dallon, J.C. (2000) Numerical aspects of discrete and continuum hybrid models in cell biology. *App. Num. Math.,* **32**.

Dallon, J.C., Sherratt, J.A., and Maini, P.K. (1999) Mathematical modelling of extracellular matrix dynamics using discrete cells: fiber orientation and tissue regeneration. *J Theor Biol,* **199**:449-71.

Darby, I., Skalli, O., and Gabbiani, G. (1990) Alpha-smooth muscle actin is transiently expressed by myofibroblasts during experimental wound healing. *Lab Invest,* **63**:21-9.

de Vries, H.J., Enomoto, D.N., van Marle, J., van Zuijlen, P.P., Mekkes, J.R., and Bos, J.D. (2000) Dermal organization in scleroderma: the fast Fourier transform and the laser scatter method objectify fibrosis in nonlesional as well as lesional skin. *Lab Invest,* **80**:1281-9.

Delvoye, P., Wiliquet, P., Leveque, J.L., Nusgens, B.V., and Lapiere, C.M. (1991) Measurement of mechanical forces generated by skin fibroblasts embedded in a three-dimensional collagen gel. *J Invest Dermatol,* **97**:898-902.

Dembo, M. and Wang, Y. (1999) Stresses at the cell-to-substrate interface during locomotion of fibroblasts. *Biophys. J.,* **76**:2307-16.

Desmouliere, A. and Gabbiani, G. (1994) Modulation of fibroblastic cytoskeletal features during pathological situations: the role of extracellular matrix and cytokines. *Cell Motil Cytoskeleton,* **29**:195-203.

Desmouliere, A. and Gabbiani, G. (1995) Myofibroblast differentiation during fibrosis. *Exp Nephrol,* **3**:134-9.

Desmouliere, A., Geinoz, A., Gabbiani, F., and Gabbiani, G. (1993) Transforming growth factor-beta 1 induces alpha-smooth muscle actin expression in granulation tissue myofibroblasts and in quiescent and growing cultured fibroblasts. *J Cell Biol,* **122**:103-11.

Dickey, J.P., Hewlett, B.R., Dumas, G.A., and Bednar, D.A. (1998) Measuring collagen fiber orientation: a two-dimensional quantitative macroscopic technique. *J Biomech Eng,* **120**:537-40.

DiMicco, M.A. and Sah, R.L. (2001) Integrative cartilage repair: adhesive strength is correlated with collagen deposition. *J Orthop Res,* **19**:1105-12.

DiMilla, P.A., Barbee, K., and Lauffenburger, D.A. (1991) Mathematical model for the effects of adhesion and mechanics on cell migration speed. *Biophys J,* **60**:15-37.

Drezek, R., Durn, A., and Richards-Kortum, R. (1999) Light scattering from cells: finite-difference time-domain simulations and goniometric measurements. *Appl. Opt.,* **38**:3651-61.

Dry, C. M. Smart multiphase composite materials that repair themselves by a release of liquids that become solids. Varadan, V. K. SPIE Proceedings : Smart Structures and Materials 1994: Smart Materials. 2189. **1994**. The Pennsylvania State Univ., University Park, PA, USA.

Dunn, M.G., Liesch, J.B., Tiku, M.L., and Zawadsky, J.P. (1995) Development of fibroblast-seeded ligament analogs for ACL reconstruction. *J Biomed Mater Res,* **29**:1363-71.

Eaglestein, W.H. and Falanga, V. (1998) Tissue engineering and the development of Apligraft, a human skin equivalent. *Cutis,* **62**:1-8.

Eastwood, M. Mechatronic devices for the investigation of fibroblast populated collagen gel contraction and the effects of mechanical loading. PhD Thesis, University College London Library. **1996**.

Eastwood, M., McGrouther, D.A., and Brown, R.A. (1994) A culture force monitor for measurement of contraction forces generated in human dermal fibroblast cultures: evidence for cell-matrix mechanical signalling. *Biochim Biophys*

Acta, **1201**:186-92.

Eastwood, M., McGrouther, D.A., and Brown, R.A. (1998a) Fibroblast responses to mechanical forces. *Proc Inst Mech Eng [H],* **212**:85-92.

Eastwood, M., Mudera, V.C., McGrouther, D.A., and Brown, R.A. (1998b) Effect of precise mechanical loading on fibroblast populated collagen lattices: morphological changes. *Cell Motil Cytoskeleton,* **40**:13-21.

Eastwood, M., Porter, R., Khan, U., McGrouther, G., and Brown, R. (1996) Quantitative analysis of collagen gel contractile forces generated by dermal fibroblasts and the relationship to cell morphology. *J Cell Physiol,* **166**:33-42.

Eddy, R.J., Petro, J.A., and Tomasek, J.J. (1988) Evidence for the nonmuscle nature of the "myofibroblast" of granulation tissue and hypertropic scar. An immunofluorescence study. *Am J Pathol,* **130**:252-60.

Edwards, A.D., Richardson, C., van der Zee, P., Elwell, C., Wyatt, J.S., Cope, M., Delpy, D.T., and Reynolds, E.O. (1993) Measurement of hemoglobin flow and blood flow by near-infrared spectroscopy. *J Appl Physiol,* **75**:1884-9.

Edwards, J.C. (2000) Fibroblast biology. Development and differentiation of synovial fibroblasts in arthritis. *Arthritis Res,* **2**:344-7.

Efrat, S. (1998) Development of engineered pancreatic beta-cell lines for cell therapy of diabetes. *Adv Drug Deliv Rev,* **33**:45-52.

Ehrlich, H.P. (1988) Wound closure: evidence of cooperation between fibroblasts and collagen matrix. *Eye,* **2 (Pt 2)**:149-57.

Elsdale, T. and Bard, J. (1972) Collagen substrata for studies on cell behavior. *J Cell Biol,* **54**:626-37.

Farrell, T.J., Patterson, M.S., and Wilson, B. (1992) A diffusion theory model of spatially resolved, steady-state diffuse reflectance for the noninvasive determination of tissue optical properties in vivo. *Med Phys,* **19**:879-88.

Ferdman, A.G. and Yannas, I.V. (1993) Scattering of light from histologic sections: a new method for the analysis of connective tissue. *J Invest Dermatol,* **100**:710-6.

Fluck, J., Querfeld, C., Cremer, A., Niland, S., Krieg, T., and Sollberg, S. (1998) Normal human primary fibroblasts undergo apoptosis in three-dimensional contractile collagen gels. *J Invest Dermatol,* **110**:153-7.

Frank, C.J., Redd, D.C., Gansler, T.S., and McCreery, R.L. (1994) Characterization of human breast biopsy specimens with near-IR Raman spectroscopy. *Anal Chem,* **66**:319-26.

Freyman, T.M., Yannas, I.V., Yokoo, R., and Gibson, L.J. (2001) Fibroblast contraction of a collagen-GAG matrix. *Biomaterials,* **22**:2883-91.

Freyman, T.M., Yannas, I.V., Yokoo, R., and Gibson, L.J. (2002) Fibroblast contractile force is independent of the stiffness which resists the contraction. *Exp Cell Res,* **272**:153-62.

Fu, S. and Lauke, B. (1998) The elastic modulus of misaligned short-fibre-reinforced polymers. *Comp. Sci Technol.* **58**:389-400.

Gabbiani, G., Ryan, G.B., and Majne, G. (1971) Presence of modified fibroblasts in granulation tissue and their possible role in wound contraction. *Experientia,* **27**:549-50.

Gailit, J. and Clark, R.A. (1996) Studies in vitro on the role of alpha v and beta 1 integrins in the adhesion of human dermal fibroblasts to provisional matrix proteins fibronectin, vitronectin, and fibrinogen. *J Invest Dermatol,* **106**:102-8.

Gandjbakhche, A.H., Bonner, R.F., Arai, A.E., and Balaban, R.S. (1999) Visible-light photon migration through myocardium in vivo. *Am J Physiol,* **277**:H698-704.

Gao, J., Dennis, J.E., Solchaga, L.A., Awadallah, A.S., Goldberg, V.M., and Caplan, A.I. (2001) Tissue-engineered fabrication of an osteochondral composite graft using rat bone marrow-derived mesenchymal stem cells. *Tissue Eng,* **7**:363-71.

Germain, L., Jean, A., Auger, F.A., and Garrel, D.R. (1994) Human wound healing fibroblasts have greater contractile properties than dermal fibroblasts. *J Surg Res,* **57**:268-273.

Glassman, W., Byam-Smith, M., and Garfield, R.E. (1995) Changes in rat cervical collagen during gestation and after antiprogesterone treatment as measured in vivo with light-induced autofluorescence. *Am. J. Obstet. Gynecol.,* **173(5)**:1550-6.

Gonzalez, M., Bell, W.H., Guerrero, C.A., Buschang, P.H., and Samchukov, M.L. (2001) Positional changes and stability of bone segments during simultaneous bilateral mandibular lengthening and widening by distraction. *Br J Oral Maxillofac Surg,* **39**:169-78.

Gorgidze, L.A., Oshemkova, S.A., and Vorobjev, I.A. (1998) Blue light inhibits mitosis in tissue culture cells. *Biosci Rep,* **18**:215-24.

Gosiewska, A., Rezania, A., Dhanaraj, S., Vyakarnam, M., Zhou, J., Burtis, D., Brown, L., Kong, W., Zimmerman, M., and Geesin, J.C. (2001) Development of a three-dimensional transmigration assay for testing cell-polymer interactions for tissue engineering applications. *Tissue Eng,* **7**:267-77.

Goulet, F., Rancourt, D., Cloutier, R., Germain, L., Poole, A.R., and Auger, F.A. (2000) Tendons and ligaments. In: Principles of Tissue Engineering . R. Lanza, R. Langer, and K. Vacanti, eds. Academic Press, San Diego; London., pp. 711-21.

Greiling, D. and Clark, R.A. (1997) Fibronectin provides a conduit for fibroblast transmigration from collagenous stroma into fibrin clot provisional matrix. *J Cell Sci,* **110 (Pt 7)**:861-70.

Griffith, L.G. and Naughton, G. (2002) Tissue engineering--current challenges and expanding opportunities. *Science,* **295**:1009-14.

Grinnell, F. (1994) Fibroblasts, myofibroblasts, and wound contraction. *J Cell Biol,* **124**:401-4.

Grinnell, F. (1999) Signal transduction pathways activated during fibroblast contraction of collagen matrices. *Curr Top Pathol,* **93**:61-73.

Grinnell, F. (2000) Fibroblast-collagen-matrix contraction: growth-factor signalling and mechanical loading. *Trends Cell Biol,* **10**:362-5.

Grinnell, F. (2003) Fibroblast biology in three-dimensional collagen matrices. *Trends Cell Biol,* **13**:264-9.

Grinnell, F., Fukamizu, H., Pawelek, P., and Nakagawa, S. (1989) Collagen processing, crosslinking, and fibril bundle assembly in matrix produced by fibroblasts in long-term cultures supplemented with ascorbic acid. *Exp Cell Res,* **181**:483-91.

Grinnell, F. and Ho, C.H. (2002) Transforming growth factor beta stimulates fibroblast-collagen matrix contraction by different mechanisms in mechanically loaded and unloaded matrices. *Exp Cell Res,* **273**:248-55.

Grinnell, F., Ho, C.H., Lin, Y.C., and Skuta, G. (1999) Differences in the regulation of fibroblast contraction of floating versus stressed collagen matrices. *J Biol Chem,* **274**:918-23.

Grinnell, F., Ho, C.H., Tamariz, E., Lee, D.J., and Skuta, G. (2003) Dendritic Fibroblasts in Three-dimensional Collagen Matrices. *Mol Biol Cell,* **14**:384-95.

Grinnell, F. and Lamke, C.R. (1984) Reorganization of hydrated collagen lattices by human skin fibroblasts. *J Cell Sci,* **66**:51-63.

Grinnell, F., Zhu, M., Carlson, M.A., and Abrams, J.M. (1999) Release of mechanical tension triggers apoptosis of human fibroblasts in a model of regressing granulation tissue. *Exp Cell Res,* **248**:608-19.

Groenhuis, R.A.J., Berwerda, H.A., and Ten Bosh, J.J. (1983) Scattering and absorption of turbid materials determined from reflection measurements. *Theory Appl. Opt.,* **22**:2456-2462.

Gruber, R.P. and Jones, H.W. (1981) Review of closed capsulotomy complications. *Ann Plast Surg,* **6**:271-6.

Guido, S. and Tranquillo, R.T. (1993) A methodology for the systematic and quantitative study of cell contact guidance in oriented collagen gels. Correlation of fibroblast orientation and gel birefringence. *J Cell Sci,* **105 (Pt 2)**:317-31.

Guidry, C., Bradley, K.M., and King, J.L. (2003) Tractional force generation by human muller cells: growth factor responsiveness and integrin receptor involvement. *Invest Ophthalmol Vis Sci,* **44**:1355-63.

Guidry, C. and Grinnell, F. (1985) Studies on the mechanism of hydrated collagen gel reorganization by human skin fibroblasts. *J Cell Sci,* **79**:67-81.

Guidry, C. and Grinnell, F. (1986) Contraction of hydrated collagen gels by fibroblasts: Evidence for two mechanisms by which collagen fibrils are stabilised. *Collagen Rel. Res.,* **6**:515-529.

Gullberg, D., Tingstrom, A., Thuresson, A.C., Olsson, L., Terracio, L., Borg, T.K., and Rubin, K. (1990) Beta 1 integrin-mediated collagen gel contraction is stimulated by PDGF. *Exp Cell Res,* **186**:264-72.

Guzelsu, N., Federici, J.F., Lim, H.C., Chauhdry, H.R., Ritter, A.B., and Findley, T. (2003) Measurement of skin stretch via light reflection. *J. Biomed. Opt.,* **8(1)**:80-6.

Halliday, D. and Resnick, R. (1978) Physics: Parts I & II combined 3rd ed.. Wiley, New York ; London.

Halliday, N.L. and Tomasek, J.J. (1995) Mechanical properties of the extracellular matrix influence fibronectin fibril assembly in vitro. *Exp Cell Res,* **217**:109-17.

Hansen, K.A., Weiss, J.A., and Barton, J.K. (2002) Recruitment of tendon crimp with applied tensile strain. *J Biomech Eng,* **124**:72-7.

Harris, A.K., Stopak, D., and Wild, P. (1981) Fibroblast traction as a mechanism for collagen morphogenesis. *Nature,* **290** :249-51.

Harris, A.K., Wild, P., and Stopak, D. (1980) Silicone rubber substrata: a new wrinkle in the study of cell locomotion. *Science,* **208**:177-9.

Haskell, R.C., Svaasand, L.O., Tsay, T.T., Feng, T.C., McAdams, M.S., and Tromberg, B.J. (1994) Boundary conditions for the diffusion equation in radiative transfer. *J Opt Soc Am A,* 11:2727-41.

Hielscher, A.H., Mourant, J.R., and Bigio, I.J. (1997) Influence of particle size and concentration on the diffuse backscattering of polarized light from tissue phantoms and biological cell suspensions. *Applied Optics,* **36(1)**:125-135.

Hinz, B., Celetta, G., Tomasek, J.J., Gabbiani, G., and Chaponnier, C. (2001) Alpha-smooth muscle actin expression upregulates fibroblast contractile activity. *Mol Biol Cell,* **12**:2730-41.

Huang, D., Chang, T.R., Aggarwal, A., Lee, R.C., and Ehrlich, H.P. (1993) Mechanisms and dynamics of mechanical strengthening in ligament- equivalent fibroblast-populated collagen matrices. *Ann Biomed Eng,* **21**:289-305.

Huang, S. and Ingber, D.E. (1999) The structural and mechanical complexity of cell-growth control. *Nat Cell Biol,* 1:E131-8.

Huttenlocher, A., Sandborg, R.R., and Horwitz, A.F. (1995) Adhesion in cell migration. *Curr Opin Cell Biol,* **7**:697-706.

Hynes, R.O. (1992) Integrins: versatility, modulation, and signaling in cell adhesion. *Cell,* **69**:11-25.

Ingber, D.E. (2002) Cancer as a disease of epithelial-mesenchymal interactions and extracellular matrix regulation. *Differentiation,* **70**:547-60.

Isogai, N., Landis, W., Kim, T.H., Gerstenfeld, L.C., Upton, J., and Vacanti, J.P. (1999) Formation of phalanges and small joints by tissue-engineering. *J Bone Joint Surg Am,* **81**:306-16.

Jacques, S.L., Roman, J.R., and Lee, K. (2000) Imaging superficial tissues with polarized light. *Lasers Surg Med,* **26**:119-29.

Jeronimidis, G. (2000a) (b) Design and Function of Structural Biological Materials. In: Structural biological material. Design and structure-property relationships. M. Elices, ed. Pergamon, Amsterdam. Oxford, pp. 19-29.

Jeronimidis, G. (2000b) (a) Structure-Property Relashionships in Biological Materials. In: Structural biological material. Design and structure-property relationships. M. Elices, ed. Pergamon, Amsterdam. Oxford, pp. 3-15.

Jester, J.V., Barry-Lane, P.A., Cavanagh, H.D., and Petroll, W.M. (1996) Induction of alpha-smooth muscle actin expression and myofibroblast transformation in cultured corneal keratocytes. *Cornea,* **15**:505-16.

Jones, M.E., Ladhani, K., Mudera, V., Grobbelaar, A.O., McGrouther, D.A., and Sanders, R. (2000) Flexor tendon blood vessels. *J Hand Surg [Br],* **25(6)**:552-9.

Kastelic, J. and Baer, E. Society of Experimental Biology, Symp. XXXIV. p. 397. **1980.**

Kasugai, S., Suzuki, S., Shibata, S., Yasui, S., Amano, H., and Ogura, H. (1990) Measurements of the isometric contractile forces generated by dog periodontal ligament fibroblasts in vitro. *Arch Oral Biol,* **35**:597-601.

Kessler, D., Dethlefsen, S., Haase, I., Plomann, M., Hirche, F., Krieg, T., and Eckes, B. (2001) Fibroblasts in mechanically stressed collagen lattices assume a "synthetic" phenotype. *J Biol Chem,* **276**:36575-85.

Kim, A.C. and Spector, M. (2000) Distribution of chondrocytes containing alpha-smooth muscle actin in human articular cartilage. *J Orthop Res,* **18**:749-55.

Kinner, B. and Spector, M. (2002) Expression of smooth muscle actin in osteoblasts in human bone. *J Orthop Res,* **20**:622-32.

Kinner, B., Zaleskas, J.M., and Spector, M. (2002) Regulation of smooth muscle actin expression and contraction in adult human mesenchymal stem cells. *Exp Cell Res,* **278**:72-83.

Klein, M.B., Yalamanchi, N., Pham, H., Longaker, M.T., and Chang, J. (2002) Flexor tendon healing in vitro: effects of TGF-beta on tendon cell collagen production. *J Hand Surg [Am],* **27**:615-20.

Knapp, D.M., Helou, E.F., and Tranquillo, R.T. (1999) A fibrin or collagen gel assay for tissue cell chemotaxis: assessment of fibroblast chemotaxis to GRGDSP. *Exp Cell Res,* **247**:543-53.

Kolodney, M.S. and Elson, E.L. (1993) Correlation of myosin light chain phosphorylation with isometric contraction of fibroblasts. *J Biol Chem,* **268**:23850-5.

Kolodney, M.S. and Wysolmerski, R.B. (1992) Isometric contraction by fibroblasts and endothelial cells in tissue culture: a quantitative study. *J Cell Biol,* **117**:73-82.

Kubota, K., Okazaki, J., Louie, O., Kent, K.C., and Liu, B. (2003) TGF-beta stimulates collagen (I) in vascular smooth muscle cells via a short element in the proximal collagen promoter. *J Surg Res,* **109**:43-50.

Kupper, T.S. and Ferguson, T.A. (1993) A potential pathophysiologic role for alpha 2 beta 1 integrin in human eye diseases involving vitreoretinal traction. *FASEB J,* **7**:1401-6.

Lambert, C.A., Colige, A.C., Munaut, C., Lapiere, C.M., and Nusgens, B.V. (2001) Distinct pathways in the over-expression of matrix metalloproteinases in human fibroblasts by relaxation of mechanical tension. *Matrix Biol,* **20(7)**:397-408.

Lamberti, P.M. and Wezeman, F.H. (2002) Biologic behavior of an in vitro hydrated collagen gel-human tenocyte tendon model. *Clin Orthop,*414-23.

Langelier, E., Rancourt, D., Bouchard, S., Lord, C., Stevens, P.P., Germain, L., and Auger, F.A. (1999) Cyclic traction machine for long-term culture of fibroblast-populated collagen gels. *Ann Biomed Eng,* **27**:67-72.

Lauffenburger, D.A. and Horwitz, A.F. (1996) Cell migration: a physically integrated molecular process. *Cell,* **84**:359-69.

Liakakos, T., Thomakos, N., Fine, P.M., Dervenis, C., and Young, R.L. (2001) Peritoneal adhesions: etiology, pathophysiology, and clinical significance. Recent advances in prevention and management. *Dig Surg* , **18**:260-73.

Lijnen, P. and Petrov, V. (2002) Transforming growth factor-beta 1-induced collagen production in cultures of cardiac fibroblasts is the result of the appearance of myofibroblasts. *Methods Find Exp Clin Pharmacol,* **24**:333-44.

Lo, C.M., Wang, H.B., Dembo, M., and Wang, Y.L. (2000) Cell movement is guided by the rigidity of the substrate. *Biophys J,* **79**:144-52.

Lorenz, H.P., Hedrick, M.H., Chang, J., Mehrara, B.J., and Longaker, M.T. (2000) The impact of biomolecular medicine and tissue engineering on plastic surgery in the 21st century. *Plast Reconstr Surg,* **105**:2467-81.

Marenzana, M. and Brown, R. A. Development of an Interface Model for the Generation amd Engineering of Tissue Interfaces in Vitro. Proceedings of the IEEE-EMBS Special Topic Conference on Molecular, Cellular and Tissue Engineering. **2002**.

Marenzana, M., Pickard, D., MacRobert, A.J., and Brown, R.A. (2002) Optical measurement of three-dimensional collagen gel constructs by elastic scattering spectroscopy. *Tissue Eng,* 8:409-18.

Martelli-Junior, H., Cotrim, P., Graner, E., Sauk, J.J., and Coletta, R.D. (2003) Effect of transforming growth factor-beta1, interleukin-6, and interferon-gamma on the expression of type I collagen, heat shock protein 47, matrix metalloproteinase (MMP)-1 and MMP-2 by fibroblasts from normal gingiva and hereditary gingival fibromatosis. *J Periodontol,* **74**:296-306.

Martin, P. (1997) Wound healing--aiming for perfect skin regeneration. *Science,* **276**:75-81.

Martin, R., Farjanel, J., Eichenberger, D., Colige, A., Kessler, E., Hulmes, D.J., and Giraud-Guille, M.M. (2000) Liquid crystalline ordering of procollagen as a determinant of three- dimensional extracellular matrix architecture. *J Mol Biol,* **301**:11-7.

Masur, S.K., Dewal, H.S., Dinh, T.T., Erenburg, I., and Petridou, S. (1996) Myofibroblasts differentiate from fibroblasts when plated at low density. *Proc Natl Acad Sci U S A,* **93**:4219-23.

McFarlane, R.M. (2002) On the origin and spread of Dupuytren's disease. *J Hand Surg [Am],* **27**:385-90.

Meglinsky, I.V. and Matcher, S.J. (2001) Modelling the sampling volume for skin blood oxygenation measurements. *Med Biol Eng Comput,* **39**:44-50.

Mochitate, K., Pawelek, P., and Grinnell, F. (1991) Stress relaxation of contracted collagen gels: disruption of actin filament bundles, release of cell surface fibronectin, and down- regulation of DNA and protein synthesis. *Exp Cell Res,* **193**:198-207.

Montesano, R. and Orci, L. (1988) Transforming growth factor beta stimulates collagen-matrix contraction by fibroblasts: implications for wound healing. *Proc Natl Acad Sci U S A,* **85**:4894-7.

Moon, A.G. and Tranquillo, R.T. (1993) Fibroblast-populated collagen microsphere assay of cell traction force: Part 1. Continuum model. *AIChE J,* **39(1)**:163-177.

Mooney, D., Hansen, L., Vacanti, J., Langer, R., Farmer, S., and Ingber, D. (1992) Switching from differentiation to growth in hepatocytes: control by extracellular matrix. *J Cell Physiol,* **151**:497-505.

Moulin, V., Castilloux, G., Jean, A., Garrel, D.R., Auger, F.A., and Germain, L. (1996) In vitro models to study wound healing fibroblasts. *Burns,* **22**:359-62.

Mourant, J.R., Bigio, I.J., Boyer, J., Conn, R.L., Johnson, T., and Shimada, T. (1995) Spectroscopic diagnosis of bladder cancer with elastic light scattering. *Lasers Surg Med,* 17:350-7.

Mourant, J.R., Bigio, I.J., Boyer, J., Johnson, T.M., Lacey, J., Bohorfoush, G., and Mellow, M. (1996) Elastic scattering spectroscopy as a diagnostic tool for differentiating pathologies in the gastrointestinal tract: preliminary testing. *Journal of Biomedical Optics* , 1:192-199.

Mourant, J.R., Bigio, I.J., Jack, D.A., Johnson, T., and Miller, H.D. (1997) Measuring absorption coefficients in small volumes of high scattering media: source-detector separation for which path lengths do not depend on scattering properties. *Appl. Opt.,* **36**:5655-61.

Mourant, J.R., Boyer, J., Hielscher, A., and Bigio, I. (1996) Influence of the scattering phase function on light transport measurements in turbid media performed with small source-detector separations. *Optics Letters,* **21**:546-548.

Mourant, J.R., Canpolat, M., Brocker, C., Esponda-Ramos, O., Johnson, T.M., Matanock, A., Stetter, K., and Freyer, J.P. (2000) Light scattering from cells: the contribution of the nucleus and the effects of proliferative status. *J Biomed Opt,* **5**:131-7.

Mourant, J.R., Hielscher, A.H., Eick, A.A., Johnson, T.M., and Freyer, J.P. (1998) Evidence of intrinsic differences in the light scattering properties of tumorigenic and nontumorigenic cells. *Cancer,* **84**:366-74.

Mourant, J.R., Johnson, T.M., Carpenter, S., Guerra, A., Aida, T., and Freyer, J.P. (2002) Polarized angular dependent spectroscopy of epithelial cells and epithelial cell nuclei to determine the size scale of scattering structures. *J Biomed Opt,* **7**:378-87.

Mudera, V., Eastwood, M., McFarland, C., and Brown, R.A. (2002) Evidence for sequential utilization of fibronectin, vitronectin, and collagen during fibroblast-mediated collagen contraction. *Wound Repair Regen,* **10**:397-408.

Mudera, V.C., Pleass, R., Eastwood, M., Tarnuzzer, R., Schultz, G., Khaw, P., McGrouther, D.A., and Brown, R.A. (2000) Molecular responses of human dermal fibroblasts to dual cues: contact guidance and mechanical load. *Cell Motil Cytoskeleton,* **45**:1-9.

Murray, J.D. and Oster, G.F. (1984) Cell traction models for generating pattern and form in morphogenesis. *J Math Biol,* **19**:265-79.

Murray, J.D., Oster, G.F., and Harris, A.K. (1983) A mechanical model for mesenchymal morphogenesis. *J Math Biol,* **17**:125-9.

Murray, M.M. and Spector, M. (2001) The migration of cells from the ruptured human anterior cruciate ligament into collagen-glycosaminoglycan regeneration templates in vitro. *Biomaterials,* **22**:2393-402.

Mutsaers, S.E., Bishop, J.E., McGrouther, G., and Laurent, G.J. (1997) Mechanisms of tissue repair: from wound healing to fibrosis. *Int J Biochem Cell Biol,* **29**:5-17.

Nakatani, T., Marui, T., Hitora, T., Doita, M., Nishida, K., and Kurosaka, M. (2002) Mechanical stretching force promotes collagen synthesis by cultured cells from human ligamentum flavum via transforming growth factor-beta1. *J Orthop Res,* **20**:1380-6.

Nerem, R.M. (2000a) Tissue engineering: confronting the transplantation crisis. *Proc Inst Mech Eng [H],* **214**:95-9.

Nerem, R.M. (2000b) Tissue engineering a blood vessel substitute: the role of biomechanics. *Yonsei Med J,* **41**:735-9.

Nickell, S., Hermann, M., Essenpreis, M., Farrell, T.J., Kramer, U., and Patterson, M.S. (2000) Anisotropy of light propagation in human skin. *Phys Med Biol,* **45**:2873-86.

Nijssen, A., Bakker Schut, T.C., Heule, F., Caspers, P.J., Hayes, D.P., Neumann, M.H., and Puppels, G.J. (2002) Discriminating basal cell carcinoma from its surrounding tissue by Raman spectroscopy. *J Invest Dermatol,* **119**:64-9.

Niklason, L.E. and Langer, R. (2001) Prospects for organ and tissue replacement. *JAMA,* **285**:573-6.

Nilsson, A.M., Heinrich, D., Olajos, J., and Andersson-Engels, S. (1997) Near infrared diffuse reflection and laser-induced fluorescence spectroscopy for myocardial tissue characterisation. *Spectrochim Acta A Mol Biomol Spectrosc,* **53A**:1901-12.

Obradovic, B., Martin, I., Padera, R.F., Treppo, S., Freed, L.E., and Vunjak-Novakovic, G. (2001) Integration of engineered cartilage. *J Orthop Res,* **19**:1089-97.

Odell, G.M., Oster, G.F., Alberch, P., and Burnside, B. (1981) The mechanical basis of morphogenesis. I. Epithelial folding and invagination. *Biophys. J.* **85**:446-462.

Osawa, M. and Niwa, S. (1993) A portable diffusive reflectance spectrophotometer for rapid and automatic measurement of tissue. *Measurements in Science and Technology* , 4:668-676.

Ozerdem, B. and Tozeren, A. (1995) Physical response of collagen gels to tensile strain. *J Biomech Eng,* **117**:397-401.

Pap, T., Muller-Ladner, U., Gay, R.E., and Gay, S. (2000) Fibroblast biology. Role of synovial fibroblasts in the pathogenesis of rheumatoid arthritis. *Arthritis Res,* **2**:361-7.

Parizi, M., Howard, E.W., and Tomasek, J.J. (2000) Regulation of LPA-promoted myofibroblast contraction: role of Rho, myosin light chain kinase, and myosin light chain phosphatase. *Exp Cell Res,* **254**:210-20.

Parsons, M. The effect of mechanical load on dermal fibroblast collagen deposition and organisation. PhD Thesis, University College London Library. **2000.**

Parsons, M., Kessler, E., Laurent, G.J., Brown, R.A., and Bishop, J.E. (1999) Mechanical load enhances procollagen processing in dermal fibroblasts by regulating levels of procollagen C-proteinase. *Exp Cell Res,* **252**:319-31.

Pelham, R.J.Jr. and Wang, Y. (1999) High resolution detection of mechanical forces exerted by locomoting fibroblasts on the substrate. *Mol Biol Cell,* **10**:935-45.

Pelham, R.J. Jr and Wang, Y.L. (1998) Cell locomotion and focal adhesions are regulated by the mechanical properties of the substrate. *Biol Bull,* **194**:348-9; discussion 349-50.

Perelman, L.T., Backman, V., Wallace, M., Zonios, G., Manoharan, R., Nusrat, A., Shields, S., Seiler, M., Lima, C., Hamano, T., Itzkan, I., Van Dam, J., Crawford, J.M., and Feld, M. (1998) Observation of periodic fine structure in reflectance from biological tissue: a new technique for measuring nuclear size distribution. *Physical Review Letters,* **80**:627-630.

Peretti, G.M., Bonassar, L.J., Caruso, E.M., Randolph, M.A., Trahan, C.A., and Zaleske, D.J. (1999) Biomechanical analysis of a chondrocyte-based repair model of articular cartilage. *Tissue Eng,* **5**:317-26.

Peretti, G.M., Randolph, M.A., Caruso, E.M., Rossetti, F., and Zaleske, D.J. (1998) Bonding of cartilage matrices with cultured chondrocytes: an experimental model. *J Orthop Res,* **16**:89-95.

Peskin, C.S. and McQueen, D.M. (1995) A general method for the computer simulation of biological systems interacting with fluids. In: Biological fluid dynamics. C.P. Ellington and T.J. Pedley, eds. Cambridge Press, Cambridge.

Petri, J.B., Konig, S., Haupt, B., Haustein, U.F., and Herrmann, K. (1997) Molecular analysis of different phases in human wound healing. *Exp Dermatol,* **6**:133-9.

Porter, R.A., Brown, R.A., Eastwood, M., Occleston, N.L., and Khaw, P.T. (1998) Ultrastructural changes during contraction of collagen lattices by ocular fibroblasts. *Wound Repair Regen,* **6**:157-66.

Prajapati, R.T., Chavally-Mis, B., Herbage, D., Eastwood, M., and Brown, R.A. (2000a) Mechanical loading regulates protease production by fibroblasts in three-dimensional collagen substrates. *Wound Repair Regen,* 8:226-37.

Prajapati, R.T., Eastwood, M., and Brown, R.A. (2000b) Duration and orientation of mechanical loads determine fibroblast cyto- mechanical activation: monitored by protease release. *Wound Repair Regen,* 8:238-46.

Reed, M.J., Vernon, R.B., Abrass, I.B., and Sage, E.H. (1994) TGF-beta 1 induces the expression of type I collagen and SPARC, and enhances contraction of collagen gels, by fibroblasts from young and aged donors. *J Cell Physiol,* **158**:169-79.

Reindel, E.S., Ayroso, A.M., Chen, A.C., Chun, D.M., Schinagl, R.M., and Sah, R.L. (1995) Integrative repair of articular cartilage in vitro: adhesive strength of the interface region. *J Orthop Res,* **13**:751-60.

Riikonen, T., Koivisto, L., Vihinen, P., and Heino, J. (1995) Transforming growth factor-beta regulates collagen gel contraction by increasing alpha 2 beta 1 integrin expression in osteogenic cells. *J Biol Chem,* **270**:376-82.

Roberts, A.B., Sporn, M.B., Assoian, R.K., Smith, J.M., Roche, N.S., Wakefield, L.M., Heine, U.I., Liotta, L.A., Falanga, V., Kehrl, J.H., and et, a.l. (1986) Transforming growth factor type beta: rapid induction of fibrosis and angiogenesis in vivo and stimulation of collagen formation in vitro. *Proc Natl Acad Sci U S A,* **83**:4167-71.

Rodriguez, E.K., Hoger, A., and McCulloch, A.D. (1994) Stress-dependent finite growth in soft elastic tissues. *J Biomech,* **27**:455-67.

Romer, T.J., Fitzmaurice, M., Cothren, R.M., Richards-Kortum, R., Petras, R., Sivak, M.V. Jr, and Kramer, J.R. Jr (1995) Laser-induced fluorescence microscopy of normal colon and dysplasia in colonic adenomas: implications for spectroscopic diagnosis. *Am J Gastroenterol,* **90**:81-7.

Roy, P., Petroll, W.M., Cavanagh, H.D., Chuong, C.J., and Jester, J.V. (1997) An in vitro force measurement assay to study the early mechanical interaction between corneal fibroblasts and collagen matrix. *Exp Cell Res,* **232**:106-17.

Roy, P., Petroll, W.M., Cavanagh, H.D., and Jester, J.V. (1999a) Exertion of tractional force requires the coordinated up-regulation of cell contractility and adhesion. *Cell Motil Cytoskeleton,* **43**:23-34.

Roy, P., Petroll, W.M., Chuong, C.J., Cavanagh, H.D., and Jester, J.V. (1999b) Effect of cell migration on the maintenance of tension on a collagen matrix. *Ann Biomed Eng,* **27**:721-30.

Sacks, M.S., Chuong, C.J., Petroll, W.M., Kwan, M., and Halberstadt, C. (1997) Collagen fiber architecture of a cultured dermal tissue. *J Biomech Eng,* **119**:124-7.

Sady, C., Khosrof, S., and Nagaraj, R. (1995) Advanced maillard reaction and crosslinking of corneal collagen in diabetes. *Biochem. Biophys. Res. Comm.,* **214(3)**:793-7.

Saidi, I.S. and Jaques, S.L. (1995) Mie and Rayleigh modelling of visible-light scattering in neonatal skin. *Appl. Opt.,* **34**:7410-18.

Sankaran, V. and Walsh, J.T. Jr (1998) Birefringence measurement of rapid structural changes during collagen denaturation. *Photochem Photobiol,* **68**:846-51.

Sarkissian, M. and Lafyatis, R. (1998) Transforming growth factor-beta and platelet derived growth factor regulation of fibrillar fibronectin matrix formation by synovial fibroblasts. *J Rheumatol,* **25**:613-22.

Sawer, P. The wobbly bridge is set to reopen? well, almost. **1911.**

Sawhney, R.K. and Howard, J. (2002) Slow local movements of collagen fibers by fibroblasts drive the rapid global self-organization of collagen gels. *J Cell Biol,* **157**:1083-91.

Schaefer, D., Martin, I., Jundt, G., Seidel, J., Heberer, M., Grodzinsky, A., Bergin, I., Vunjak-Novakovic, G., and Freed, L.E. (2002) Tissue-engineered composites for the repair of large osteochondral defects. *Arthritis Rheum,* **46**:2524-34.

Schaefer, D., Martin, I., Shastri, P., Padera, R.F., Langer, R., Freed, L.E., and Vunjak-Novakovic, G. (2000) In vitro generation of osteochondral composites. *Biomaterials,* **21**:2599-606.

Schmidt-Nielsen, K. (1983) Animal Physiology: Adaptation and Environment. Cambridge University Press, Cambridge ..

Schomacker, K.T., Frisoli, J.K., Compton, C.C., Flotte, T.J., Richter, J.M., Nishioka, N.S., and Deutsch, T.F. (1992) Ultraviolet laser-induced fluorescence of colonic tissue: basic biology and diagnostic potential. *Lasers Surg Med,* **12**:63-78.

Schreiber, R.E., Ilten-Kirby, B.M., Dunkelman, N.S., Symons, K.T., Rekettye, L.M., Willoughby, J., and Ratcliffe, A. (1999) Repair of osteochondral defects with allogeneic tissue engineered cartilage implants. *Clin Orthop,*S382-95.

Seliktar, D., Black, R.A., Vito, R.P., and Nerem, R.M. (2000) Dynamic mechanical conditioning of collagen-gel blood vessel constructs induces remodeling in vitro. *Ann Biomed Eng,* **28**:351-62.

Serini, G. and Gabbiani, G. (1999) Mechanisms of myofibroblast activity and phenotypic modulation. *Exp Cell Res,* **250**:273-83.

Sethi, K.K., Mudera, V., Sutterlin, R., Baschong, W., and Brown, R.A. (2002) Contraction-mediated pinocytosis of RGD-peptide by dermal fibroblasts: inhibition of matrix attachment blocks contraction and disrupts microfilament organisation. *Cell Motil Cytoskeleton,* **52**:231-41.

Sheetz, M.P. (1994) Cell migration by graded attachment to substrates and contraction. *Semin Cell Biol,* **5**:149-55.

Sherratt, J.A. and Dallon, J.C. (2002) Theoretical models of wound healing: past successes and future challenges. *C R Biol,* **325**:557-64.

Sherwood, J.K., Riley, S.L., Palazzolo, R., Brown, S.C., Monkhouse, D.C., Coates, M., Griffith, L.G., Landeen, L.K., and Ratcliffe, A. (2002) A three-dimensional osteochondral composite scaffold for articular cartilage repair. *Biomaterials,* **23**:4739-51.

Shreiber, D.I., Enever, P.A., and Tranquillo, R.T. (2001) Effects of pdgf-bb on rat dermal fibroblast behavior in mechanically stressed and unstressed collagen and fibrin gels. *Exp Cell Res,* **266**:155-66.

Shum-Tim, D., Stock, U., Hrkach, J., Shinoka, T., Lien, J., Moses, M.A., Stamp, A., Taylor, G., Moran, A.M., Landis, W., Langer, R., Vacanti, J.P., and Mayer, J.E. Jr (1999) Tissue engineering of autologous aorta using a new biodegradable polymer. *Ann Thorac Surg,* **68**:2298-304; discussion 2305.

Silver, F.H., Kato, Y.P., Ohno, M., and Wasserman, A.J. (1992) Analysis of mammalian connective tissue: relationship between hierarchical structures and mechanical properties. *J Long Term Eff Med Implants,* **2**:165-98.

Silver, F.H., Siperko, L.M., and Seehra, G.P. (2003) Mechanobiology of force transduction in dermal tissue. *Skin Res Technol,* **9**:3-23.

Silverman, R.P., Bonasser, L., Passaretti, D., Randolph, M.A., and Yaremchuk, M.J. (2000) Adhesion of tissue-engineered cartilate to native cartilage. *Plast Reconstr Surg,* **105**:1393-8.

Solchaga, L.A., Gao, J., Dennis, J.E., Awadallah, A., Lundberg, M., Caplan, A.I., and Goldberg, V.M. (2002) Treatment of osteochondral defects with autologous bone marrow in a hyaluronan-based delivery vehicle. *Tissue Eng,* **8**:333-47.

Spector, M. (2001) Musculoskeletal connective tissue cells with muscle: expression of muscle actin in and contraction of fibroblasts, chondrocytes, and osteoblasts. *Wound Repair Regen,* **9**:11-8.

Stamenovic, D. and Wang, N. (2000) Invited review: engineering approaches to cytoskeletal mechanics. *J Appl Physiol,* **89**:2085-90.

Stopak, D. and Harris, A.K. (1982) Connective tissue morphogenesis by fibroblast traction. I. Tissue culture observations. *Dev Biol,* **90**:383-98.

Stopak, D., Wessells, N.K., and Harris, A.K. (1985) Morphogenetic rearrangement of injected collagen in developing chicken limb buds. *Proc Natl Acad Sci U S A,* **82**:2804-8.

Sulaiman, H., Dawson, L., Laurent, G.J., Bellingan, G.J., and Herrick, S.E. (2002) Role of plasminogen activators in peritoneal adhesion formation. *Biochem Soc Trans,* **30**:126-31.

Tamariz, E. and Grinnell, F. (2002) Modulation of Fibroblast Morphology and Adhesion during Collagen Matrix Remodeling. *Mol Biol Cell,* **13**:3915-29.

Theodorou, S.J., Theodorou, D.J., and Sartoris, D.J. (2003) Osteoporosis and fractures: the size of the problem. *Hosp Med,* **64**:87-91.

Thoumine, O. and Ott, A. (1996) Influence of adhesion and cytoskeletal integrity on fibroblast traction. *Cell Motil Cytoskeleton,* **35**:269-80.

Tomasek, J.J. and Akiyama, S.K. (1992) Fibroblast-mediated collagen gel contraction does not require fibronectin-alpha 5 beta 1 integrin interaction. *Anat Rec,* **234**:153-60.

Tomasek, J.J., Gabbiani, G., Hinz, B., Chaponnier, C., and Brown, R.A. (2002) Myofibroblasts and mechano-regulation of connective tissue remodelling. *Nat Rev Mol Cell Biol,* **3**:349-63.

Tomasek, J.J., Haaksma, C.J., Eddy, R.J., and Vaughan, M.B. (1992) Fibroblast contraction occurs on release of tension in attached collagen lattices: dependency on an organized actin cytoskeleton and serum. *Anat Rec,* **232**:359-68.

Tomasek, J.J., Halliday, N.L., Updike, D.L., Ahern-Moore, J.S., Vu, T.K., Liu, R.W., and Howard, E.W. (1997) Gelatinase A activation is regulated by the organization of the polymerized actin cytoskeleton. *J Biol Chem,* **272**:7482-7.

Tomasek, J.J., Vaughan, M.B., and Haaksma, C.J. (1999) Cellular structure and biology of Dupuytren's disease. *Hand Clin,* **15**:21-34.

Torres, D.S., Freyman, T.M., Yannas, I.V., and Spector, M. (2000) Tendon cell contraction of collagen-GAG matrices in vitro: effect of cross-linking. *Biomaterials,* **21**:1607-19.

Tranquillo, R.T. (1999) Self-organization of tissue-equivalents: the nature and role of contact guidance. *Biochem Soc Symp,* **65**:27-42.

Trelstad, R.L. and Hayashi, K. (1979) Tendon collagen fibrillogenesis: intracellular subassemblies and cell surface changes associated with fibril growth. *Dev Biol,* **71**:228-42.

Tsai, C., Hata, K., Torii, S., Matsuyama, M., and Ueda, M. (1995) Contraction potency of hypertrophic scar-derived fibroblasts in a connective tissue model: in vitro analysis of wound contraction. *Ann Plast Surg,* **35**:638-46.

Tuchweber, B., Desmouliere, A., Costa, A.M., Yousef, I.M., and Gabbiani, G. (1999) Myofibroblastic differentiation and extracellular matrix deposition in early stages of cholestatic fibrosis in rat liver. *Curr Top Pathol,* **93**:103-9.

Tung, P.S. and Fritz, I.B. (1991) Transforming growth factor-beta and platelet-derived growth factor synergistically stimulate contraction by testicular peritubular cells in culture in serum-free medium. *J Cell Physiol,* **146**:386-93.

Uyama, S., Kaufmann, P.M., Takeda, T., and Vacanti, J.P. (1993) Delivery of whole liver-equivalent hepatocyte mass using polymer devices and hepatotrophic stimulation. *Transplantation,* **55**:932-5.

Vacanti, J.P. and Langer, R. (1999) Tissue engineering: the design and fabrication of living replacement devices for surgical reconstruction and transplantation. *Lancet,* **354 Suppl 1**:SI32-4.

Vacanti, J.P., Langer, R., Upton, J., and Marler, J.J. (1998) Transplantation of cells in matrices for tissue regeneration. *Adv Drug Deliv Rev,* **33**:165-182.

van de Hulst, H.C. (1981) Light scattering by small particles. Dover Publications, New York.

van Zuijlen, P.P., de Vries, H.J., Lamme, E.N., Coppens, J.E., van Marle, J., Kreis, R.W., and Middelkoop, E. (2002) Morphometry of dermal collagen orientation by Fourier analysis is superior to multi-observer assessment. *J Pathol,* **198**:284-91.

Vaughan, M.B., Howard, E.W., and Tomasek, J.J. (2000) Transforming growth factor-beta1 promotes the morphological and functional differentiation of the myofibroblast. *Exp Cell Res,* **257**:180-9.

Vunjak-Novakovic, G., Martin, I., Obradovic, B., Treppo, S., Grodzinsky, A.J., Langer, R., and Freed, L.E. (1999) Bioreactor cultivation conditions modulate the composition and mechanical properties of tissue-engineered cartilage. *J Orthop Res,* **17**:130-8.

Wakatsuki, T. and Elson, E.L. (2003) Reciprocal interactions between cells and extracellular matrix during remodeling of tissue constructs. *Biophys Chem,* **100**:593-605.

Wakatsuki, T., Kolodney, M.S., Zahalak, G.I., and Elson, E.L. (2000) Cell mechanics studied by a reconstituted model tissue. *Biophys J,* **79**:2353-68.

Wakatsuki, T., Schwab, B., Thompson, N.C., and Elson, E.L. (2001) Effects of cytochalasin D and latrunculin B on mechanical properties of cells. *J Cell Sci,* **114(Pt 5)**:1025-36.

Wakatsuki, T., Wysolmerski, R.B., and Elson, E.L. (2003) Mechanics of cell spreading: role of myosin II. *J Cell Sci,* **116**:1617-25.

Waldman, S.D., Sacks, M.S., and Lee, J.M. (1999) Imposed state of deformation determines local collagen fibre orientation but not apparent mechanical properties. *Biomed Sci Instrum,* **35**:51-6.

Wallace, M.B., Perelman, L.T., Backman, V., Crawford, J.M., Fitzmaurice, M., Seiler, M., Badizadegan, K., Shields, S.J., Itzkan, I., Dasari, R.R., Van Dam, J., and Feld, M.S. (2000) Endoscopic detection of dysplasia in patients with Barrett's esophagus using light-scattering spectroscopy. *Gastroenterology,* **119**:677-82.

Wang, L. and Jaques, S.L. (1995) Monte Carlo modeling of light transport in multi-layered tissues. *Comp. Meth. Progs. Biomed.,* **47**:131-146.

Wang, N. and Ingber, D.E. (1994) Control of cytoskeletal mechanics by extracellular matrix, cell shape, and mechanical tension. *Biophys J,* **66**:2181-9.

Wang, N., Naruse, K., Stamenovic, D., Fredberg, J.J., Mijailovich, S.M., Tolic-Norrelykke, I.M., Polte, T., Mannix, R., and Ingber, D.E. (2001) Mechanical behavior in living cells consistent with the tensegrity model. *Proc Natl Acad Sci U S A,* **98**:7765-70.

Wang, N., Tolic-Norrelykke, I.M., Chen, J., Mijailovich, S.M., Butler, J.P., Fredberg, J.J., and Stamenovic, D. (2002) Cell prestress. I. Stiffness and prestress are closely associated in adherent contractile cells. *Am J Physiol Cell*

Physiol, **282**:C606-16.

Wang, Y.N., Galiotis, C., and Bader, D.L. (2000) Determination of molecular changes in soft tissues under strain using laser Raman microscopy. *J Biomech,* **33**:483-6.

Wilkes, G.L. and Wilkes, P.H. (1974) Evidence for in vivo anisotropic rod structure in collagenous tissue as noted by small angle light scattering. *Biopolymers,* **13**:411-3.

Wolff, J. (1870) The law of bone remodelling.; translated . In: Wolff, Julius, 1836-1902: The law of bone remodelling. P.G.J. Maquet and R. Furlong, eds. Springer-Verlag , Berlin ; New York. (1986).

Wong, P.T., Goldstein, S.M., Grekin, R.C., Godwin, T.A., Pivik, C., and Rigas, B. (1993) Distinct infrared spectroscopic patterns of human basal cell carcinoma of the skin. *Cancer Res,* **53**:762-5.

Woo, S.L.-Y. and Buchwalter, J.A. (1988) Injury and repair of the musculoskeletal soft tissues. American Academy of Orthopaedic Surgeons, Savannah, Georgia.

Woodhead-Galloway, J. (1980) Collagen: The Anatomy of a Protein. Arnold, London.

Yamamoto, T., Noble, N.A., Miller, D.E., and Border, W.A. (1994) Sustained expression of TGF-beta 1 underlies development of progressive kidney fibrosis. *Kidney Int,* **45**:916-27.

Young, R.G., Butler, D.L., Weber, W., Caplan, A.I., Gordon, S.L., and Fink, D.J. (1998) Use of mesenchymal stem cells in a collagen matrix for Achilles tendon repair. *J Orthop Res,* **16**:406-13.

Zahalak, G.I., Wagenseil, J.E., Wakatsuki, T., and Elson, E.L. (2000) A cell-based constitutive relation for bio-artificial tissues. *Biophys J,* **79**:2369-81.

Zaleskas, J.M., Kinner, B., Freyman, T.M., Yannas, I.V., Gibson, L.J., and Spector, M. (2001) Growth factor regulation of smooth muscle actin expression and contraction of human articular chondrocytes and meniscal cells in a collagen-GAG matrix. *Exp Cell Res,* **270**:21-31.

Zavahir, F., McGrouther, D.A., Misra, A., Smith, K., Brown, R.A., and Mudera, V. (2001) A study of the cellular response to orientated fibronectin material in healing extensor rat tendon. *J. Mat Sci: Mat Med,* **12**:1005-1011.

Appendix 1

Real Time CFM User Interface: Frontend Panel

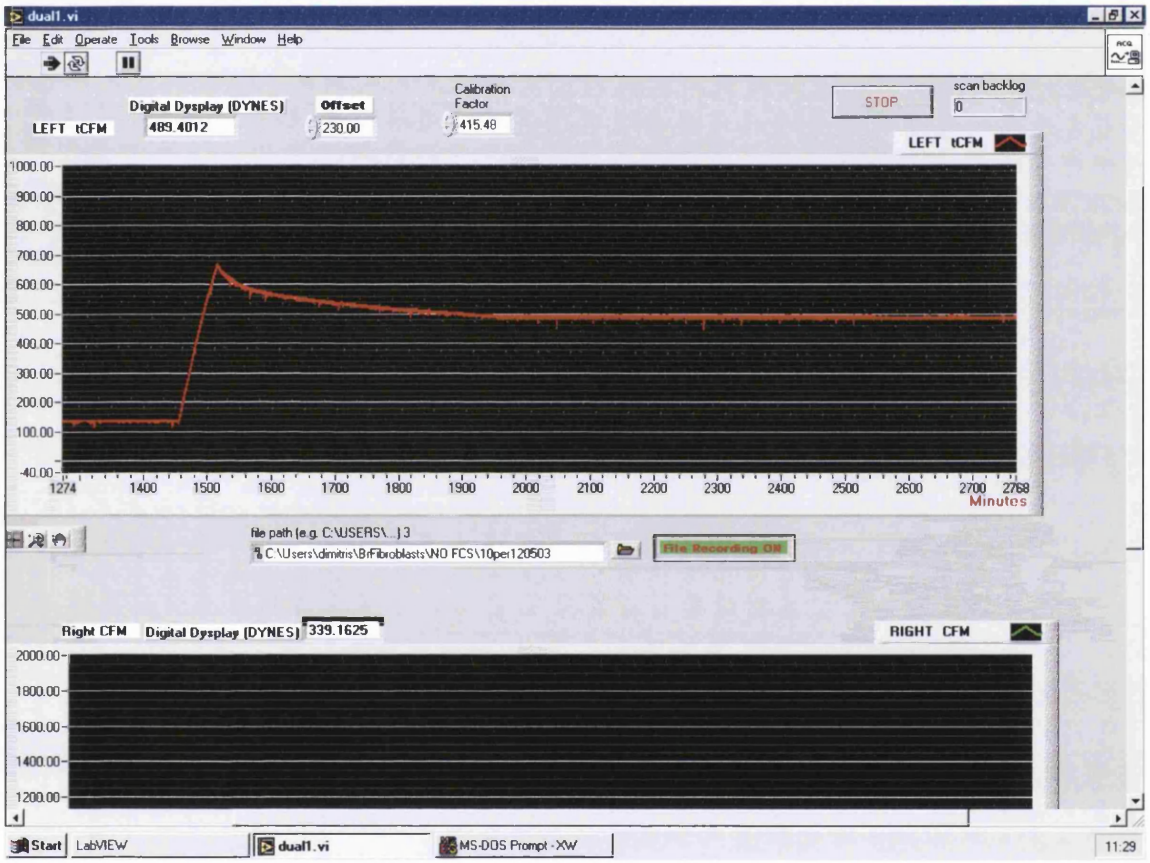

Real Time CFM User Interface: Programming Code

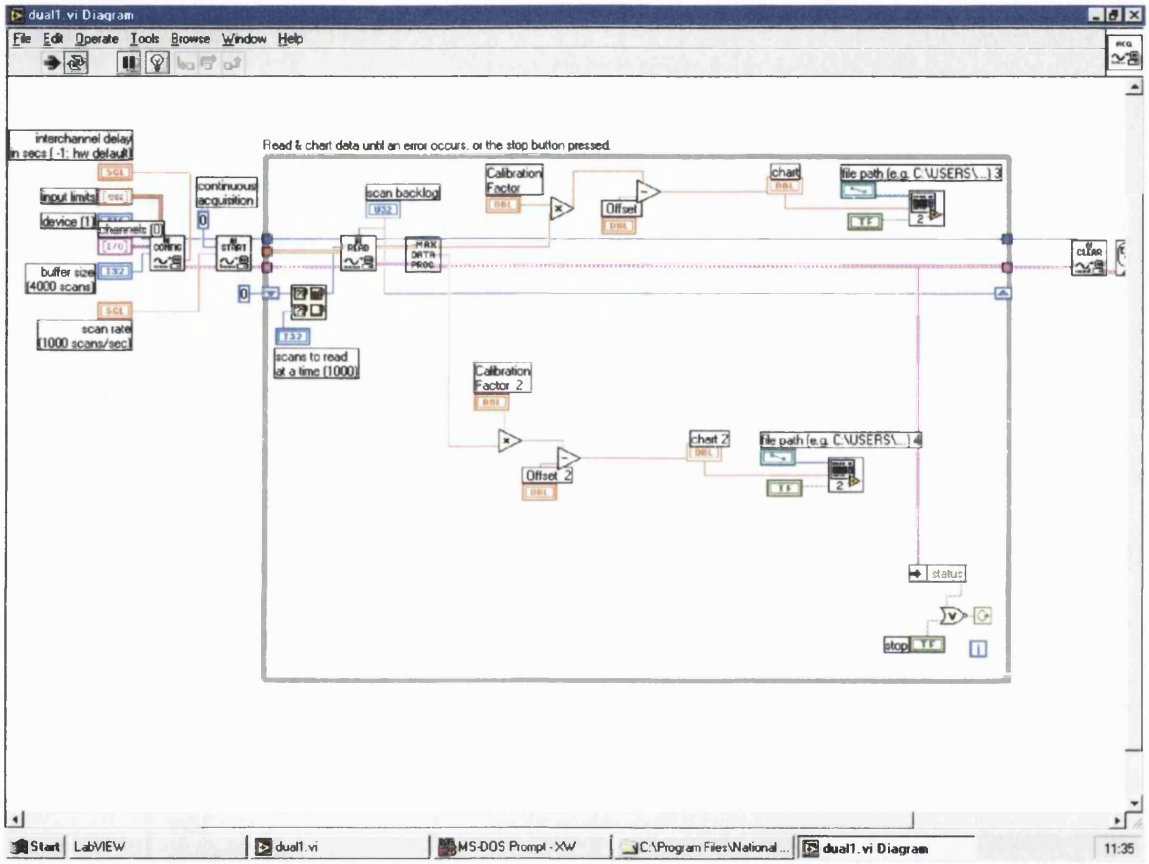

Appendix 2

Image analysis code for NIH-Image macro: Automated determination of gel area

```
macro 'DrawSelection [F1]';
var
n1:integer;
n:integer;
str:string;
begin
NewTextWindow('Result window');
ResetCounter;
{SelecTool('drawline');}
Measure;
n1 := rLength[1];
KillROI;
n:=GetNumber('ROI diameter:',n1);}
MakeOvalRoi(280,60,n,n);
{SelecTool('oval');}
End;

macro 'SelectArea [F2]';
var
str:string;
n:integer;
begin
str:=GetString('Selection OK?','yes');
if (str = 'yes') then begin
  copy;
  SetNewSize(400,400);
  MakeNewWindow('bis');
  paste;
  SetDensitySlice(125,188);
end Else begin
  n:=GetNumber('ROI diameter:',288);
  MakeOvalRoi(280,60,n,n);
end;
End;
```

```
macro 'MeasureArea [F3]';
var
area:integer;
begin
ResetCounter;
Measure;
area:=rArea[1];
PutMessage('Area=',area);
SelectWindow('bis');
Dispose;
SelectWindow('Result window');
writeln('area gel:',area)
End;
```

Appendix 3

Image analysis code for NIH-Image macro: Automatic determination of the orientation index

```
macro 'Newset';
begin
NewTextWindow('Result window');
End;

macro 'ProcessImage [F1]';
var
n1:integer;
n:integer;
str:string;
begin
ResetCounter;
Measure;
n1 := rLength[1];
KillROI;
FFT('foreward');
Filter('smooth');
Filter('smooth');
{SetDensitySlice(138,255);}
SetThreshold(135);
{AutoThreshold;}
Filter('min');
End;
```